

Sensitive Skins and Somatic Processing for Affective and Sociable Robots based upon a Somatic Alphabet Approach

by

Walter Dan Stiehl
Bachelor of Science, Mechanical Engineering
Bachelor of Science, Brain and Cognitive Science
Massachusetts Institute of Technology, 2003

Submitted to the Program in Media Arts and Sciences,
School of Architecture and Planning,
in partial fulfillment of the requirements for the degree of

Master of Science in Media Arts and Sciences

at the

MASSACHUSETTS INSTITUTE OF TECHNOLOGY

June 2005

© Massachusetts Institute of Technology, 2005. All Rights Reserved.

Signature of author: _____

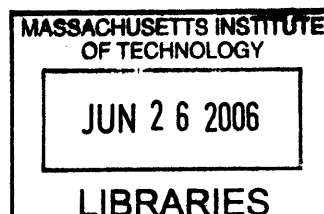
Walter Dan Stiehl
Program in Media Arts and Sciences
May 6, 2005

Certified by: _____

Dr. Cynthia Breazeal
LG Group Career Development Professor
Assistant Professor of Media Arts and Sciences
MIT Media Laboratory

Accepted by: _____

Dr. Andrew Lippman
Chair, Departmental Committee on Graduate Students
Program in Media Arts and Sciences



ROTCH

Sensitive Skins and Somatic Processing for Affective and Sociable Robots based upon a Somatic Alphabet Approach

by

Walter Dan Stiehl

Submitted to the Program in Media Arts and Sciences,
School of Architecture and Planning on May 6, 2005
in partial fulfillment of the requirements for the degree of
Master of Science in Media Arts and Sciences

Abstract

The sense of touch is one of the most important senses of the human body. This thesis describes the biologically inspired design of “sensitive skins” for two different robotic platforms: Leonardo, a high degree-of-freedom, sociable robot and the Huggable, a portable therapeutic robotic companion for relational, affective touch.

The first step in the design of the “sensitive skin” for Leonardo: a set of hands featuring 40 force-sensing resistors (FSRs) and embedded processing was created. Somatosensory inspired algorithms for calculating the location, direction of motion, and orientation with a set of these sensors forms the first stage in the design of a “Virtual Somatosensory Cortex.”

A multi-modal (temperature, electric field sensors, and Quantum Tunneling Composite (QTC) based force sensors) three dimensional sensor array was created as the first step in the design of the “sensitive skin” for the Huggable. A soft silicone skin was placed over this array. Preliminary results using neural networks show that the affective content of touch can be determined.

This work was sponsored in part by the NSF Center for Bits and Atoms Contract No.CCR-0122419, a Microsoft iCampus grant, and the MIT Media Lab Things That Think and Digital Life Consortia.

Thesis Supervisor: Cynthia Breazeal
Title: Assistant Professor of Media Arts and Sciences

Sensitive Skins and Somatic Processing for Affective and Sociable Robots based upon a Somatic Alphabet Approach

by

Walter Dan Stiehl

Thesis Advisor: _____

Dr. Cynthia Breazeal
LG Group Career Development Professor
Assistant Professor of Media Arts and Sciences
MIT Media Laboratory

Thesis Reader: _____

Dr. Christopher Moore
Assistant Professor of Brain and Cognitive Science
MIT Department of Brain and Cognitive Science
MIT McGovern Institute

Thesis Reader: _____

Dr. Joseph A. Paradiso
Sony Career Development Professor
Associate Professor of Media Arts and Sciences
MIT Media Lab

Acknowledgements

I have been incredibly fortunate to have the opportunity to work with and know the collection of people listed below. This thesis would not have been possible without them.

To my parents, Alan and Elaine Stiehl, who continue to provide me with support whenever I need it. To Papa and Nana, for letting me first experiment with the tools of the special effects trade in their basement. To the rest of the Stiehl and Vaccaro family, for always showing an interest in my work and helping out in any way they could. To Lindsay, this thesis would never have happened without you. You kept me going even in the most stressful of time you could always get me to smile and relax. I am incredibly lucky to have you as a part of my life.

I have had the great opportunity to work and learn from a great many talented people in the special effects industry. Their instruction has changed the way in which I approach art and design, and their influence is seen throughout this thesis. To Tate Holland, John Bailey, Paul Thompson, Karl Zundel and the other instructors and staff of mud – the Make-Up Designory in Burbank, California. Karl, I am truly grateful for your instruction and guidance not only during the months of class but afterwards as well. I will always consider you a mentor and a friend. To Tom McLaughlin, whose Silicone Art Seminar and Workshop taught me a great deal about silicone and began to generate some of the ideas and applications demonstrated in this thesis. To Stan Winston, Richard Landon, Lindsay MacGowan, Alan Scott, Jon Dawe, Al Sousa, Keith Marbory, and the other members of the Leonardo team at Stan Winston Studio. Their guidance both during my time at the studio while Leonardo was being constructed and through phone calls and e-mail afterwards was incredibly beneficial. Without the mechanical design and materials help provided by Richard, Lindsay, Alan, Keith, and J.D. this thesis would not have been possible. I am truly grateful to be part of collaboration with such a talented group of artists and engineers.

To Professor Steve Benton for first opening the world of the Media Lab to me when he answered my father's request for a tour of the Media Lab while I was deciding between MIT and other colleges. I am very happy to say that my decision to come to MIT was made practically on the spot. To Bill Tomlinson, whose first enthusiastic words to me while on that tour were "You know how to do latex? We could use someone to make us a latex chicken..." And thus began my entry into the Media Lab. To Professor Bruce Blumberg who took a chance by giving a 17-year-old high school graduate the task of creating a series of chickens for the Swamp! SIGGRAPH '98 Demo. Now as I look back, I realize how much faith he and Bill must have had in me; for this I am truly grateful. To Robert Burke, Marc Downie, Scott Eaton, Damian Isla, Yuri Ivanov, Michael Patrick Johnson, Ben Resner, Matt Berlin, Michal Hlavac, Chris Kline, Ken Russell, Jed Wahl, Andrew Wilson, Song-Yee Yoon, Delphine Nain, Aileen Kawabe and the other members of the Synthetic Characters Group with whom I have had the privilege to work. Daphna Buchsbaum knows where I live. Special thanks goes to Rob and Scott who worked together with me to bring to life Rufus,

the first computer controlled animatronic character I worked on. Many of the ideas in this thesis first began to gel from the desires of wanting to “touch” Rufus and scratch his head and have him respond.

To Professor Joe Paradiso and the other members of the Responsive Environments Group, especially Mark Feldmeier, Josh Lifton, Hong Ma, Stacy Morris, and Ari Benbasat, who each provided helpful answers to various questions during the design and construction of this thesis. It was Joe who first introduced me to the wonders of electric field sensing.

To Professor Christopher Moore and the members of his research lab. Without their knowledge of human skin, much of the focus of this thesis and a large portion of Chapter 2 would not have been possible. I look forward to many more discussions on skin as my work continues. To the faculty and staff of MIT, especially those at the Media Lab for making MIT such a wonderful place to spend a decade of my life.

Finally, to Professor Cynthia Breazeal for believing in me and in the importance of a sense of touch for robotics and allowing me the incredible opportunities I have had so far working with her. To the other members of the Robotic Life Group, both past and present. To Matt Hancher, for teaching me about board design and fabrication. To John McBean who made life at the lab fun while still sharing his knowledge. To Josh Strickon for his guidance in the initial software design of this thesis. To Matthew Berlin and Jesse Grey who were always willing to help. To Jeff Lieberman who is one of the most talented people I have ever met. To the other members of the group - Corey Kidd, Andrew ‘Zoz’ Brooks, Andrea Lockerd, Guy Hoffman, Heather Knight, Hans Lee, Blake Brasher, Dan McAnulty. They make work fun.

I have also had a group of amazingly talented undergraduates who have assisted with this project. Levi Lalla, Danny Hilton, Louis Basel, Derik Thomann, and Michael Wolf were always willing to help out the project and devote many hours to it when required.

“So Dan, now that you have completed your Master’s Thesis, what are you going to do now?”

I’M GOING TO DISNEYWORLD!!!!

Table of Contents

1 Motivation 21

Section I: Nature and Robots 25

2 Nature’s “Sensitive Skin” – Lessons from Neuroscience 27

- 2.1 Introduction 27
- 2.2 Essential Terminology and Concepts 28
- 2.3 Skin – The Largest Sensory Organ 32
- 2.4 Receptor Types of Somatic Sensation 34
- 2.5 Properties of the Stimulus Encoded at the Periphery 43
- 2.6 Pathway from Receptor to Cortex 46
- 2.7 The Somatosensory Cortex 55
- 2.8 Other Findings from Studies of Humans 66

3 The Healing Power of Touch: Companion Animals and Pet Therapy 69

- 3.1 Benefits of a Relationship with Animals 69
- 3.2 Populations that can Benefit from Pet Therapy 70

4 Previous Robotic Implementations 73

- 4.1 Touch Sensing and “Sensitive Skins” 73
- 4.2 Companion Robots 74

5 The “Somatic Alphabet” Approach towards the Design of “Sensitive Skins”: An Overview 79

- 5.1 The “Letters” of the “Alphabet” 79
- 5.2 The “Words” of the “Alphabet” 80
- 5.3 The “Sentences” of the “Alphabet” 80
- 5.4 Current Implementation 81

Section II: Leonardo 83

6 Leonardo’s New Hands: An Overview 85

- 6.1 Leonardo, A Sociable Robot 85
- 6.2 Design Constraints and Challenges 86
- 6.3 Previous Work – the “Pixel” Platform 90

7 New Hand: Electromechanical Design 95

- 7.1 Modifications to the Original Hand Design 95
 - 7.1.1 Dual Layer Approach 95

- 7.1.2 New Finger Design 96
- 7.1.3 New Hand Design 97
- 7.2 Sensor Mounting 100
 - 7.2.1 Sensor Selection and Modification 100
 - 7.2.2 Sensor Circuit Board Mechanical Design 101
 - 7.2.3 Fingertip Mounting 104
 - 7.2.4 Mechanical Design Considerations of the Mid-Hand Circuit Board 105
- 7.3 Assembly 106

8 Electronics Design 113

- 8.1 Sensor Performance 113
- 8.2 Mid-Hand Processing Board 116
- 8.3 Somatic Communication Board 118

9 Virtual Somatosensory Cortex 121

- 9.1 Organization 121
- 9.2 Peripheral Sensor Signal 123
- 9.3 Low Level “Cortical Processing” of Centroid Location, Direction of Motion, and Orientation 126
 - 9.3.1 Centroid Location 126
 - 9.3.2 Direction of Motion 126
 - 9.3.3 Orientation 127
 - 9.3.4 Results 129

Section III: The Huggable 133

10 The Huggable: An Overview 135

- 10.1 The Huggable, a Therapeutic Robotic Companion for Relational, Affective Touch 135
- 10.2 Design Constraints and Challenges 137
- 10.3 Lessons from Leonardo 137

11 Electromechanical Design 139

- 11.1 Working within the Bear Envelope 139
- 11.2 Sensor Selection, Attachment, and Wiring 141
 - 11.2.1 Sensor Selection: Mechanical Considerations 141
 - 11.2.2 Sensor Circuit Board: Mechanical Design 142
 - 11.2.3 QTC Sensor Mounting 145
 - 11.2.4 Thermistor Sensor Mounting 148
 - 11.2.5 Shielding 148
- 11.3 Mid-Plane Circuit Board: Mechanical Design 149
- 11.4 Mechanical Structure Design and Assembly 150

12 Electronic Design 157

- 12.1 Multi-layered Approach 157
 - 12.1.1 Division Into Body Regions 157
 - 12.1.2 Flow of Information 158
- 12.2 Sensor Performance 161
 - 12.2.1 QTC Sensor 161
 - 12.2.2 Electric Field Sensor 162
 - 12.2.3 Temperature Sensor 164
- 12.3 Arm Circuit Boards 165
- 12.4 Mid-plane Circuit Boards 168
 - 12.4.1 Wire Reduction 169
 - 12.4.2 Electric Field Sensor Isolation 171
- 12.5 Huggable Somatic Processing Circuit Board 173
 - 12.5.1 Electric Field Sensing Pathway 175
 - 12.5.2 QTC Light Touch Pathway 176
 - 12.5.3 QTC Moderate Touch Pathway 177
 - 12.5.4 QTC Hard Touch Pathway 177
 - 12.5.5 Temperature Pathway 178
 - 12.5.6 Auto Calibration Function 178

13 Synthetic Silicone Skin 183

- 13.1 Why give a robot skin? 183
- 13.2 Types of Silicone 187
- 13.3 Silicone Selection 189
 - 13.3.1 Sample Preparation 189
 - 13.3.2 Hardness Measurement 192
 - 13.3.3 Silicone Mass Considerations 196
 - 13.3.4 Sensor Performance 197
 - 13.3.5 Viscosity 201
 - 13.3.6 Sensor Selection 201
- 13.4 Silicone Mold Design 202

14 Affective Processing 209

- 14.1 Overview 209
- 14.2 Peripheral Sensory Output 209
 - 14.2.1 Response of Electric Field Sensor to touch by a human and inanimate objects 210
 - 14.2.2 Performance of three levels of QTC processing 213
 - 14.2.3 Temperature Sensor Response 215
 - 14.2.4 Combined Response across multiple sensors 216
- 14.3 Feature Extraction 221
- 14.4 Neural Network 223
 - 14.4.1 Data Collection Methods 223
 - 14.4.2 Training of the Neural Network 225
 - 14.4.3 Results 226
 - 14.4.4 Discussion of Results 236

Section IV: Conclusion 237

15 Conclusions and Future Work 239

- 15.1 Conclusions 239
- 15.2 Future Work: Leonardo 239
- 15.3 Future Work: The Huggable 240

References 244

List of Figures

Figure 2-1: The Views of the Brain and Body.....	29
Figure 2-2: Divisions of the Central Nervous System.	30
Figure 2-3: Three Views of the Human Brain.	31
Figure 2-4: Brodmann's Areas.....	32
Figure 2-5: Sectional View of the Skin.....	33
Figure 2-6: Sectional View of Hairy and Glaborous Skin with Mechanoreceptors Highlighted.	34
Figure 2-7: Responses of Slowly Adapting (SA) and Rapidly Adapting (RA) Receptors to an Indented Probe	38
Figure 2-8: Measures of Spatial Acuity on Different Body Sites.	42
Figure 2-9: Response of Single Human Mechanoreceptors to Scanned Braille Characters	43
Figure 2-10: Responses of an SA Fiber to a Flat Plate and to Selected Cylindrical Bars of Different Radii of Curvature Indented in the Skin	44
Figure 2-11: The Response of an RA Fiber to a Flat Plate and to Selected Cylindrical Bars of Different Radii of Curvature Indented into the Skin	45
Figure 2-12: The Morphology of a Dorsal Root Ganglion Cell ...	47
Figure 2-13: Types of Peripheral Nerve Fibers through which Somatic Information can Travel	48
Figure 2-14: The Segments of the Spinal Cord	49
Figure 2-15: The Dermatome Map of the Human Body.....	50
Figure 2-16: The Overlap of Dermatomes.....	51
Figure 2-17: The Dorsal Column Medial Lemniscal and Anterolateral Systems	52
Figure 2-18: The Reflex Arc.....	54
Figure 2-19: The 3 Divisions of the Somatosensory Cortex.....	55
Figure 2-20: The Flow of Information through the Primary Somatosensory Cortex	56
Figure 2-21: The Somatotopic Map of the Primary Somatosensory Cortex.....	57
Figure 2-22: The Homunculus.....	58
Figure 2-23: Cortical Columns in the Primary Somatosensory Cortex.....	59
Figure 2-24: Combinations of Lower Order Neurons to Form Higher Order Neurons.....	61
Figure 2-25: The Increase in Receptive Field Size in Higher Cortical Areas.	62

Figure 2-26: Response of a Motion-Sensitive Neuron in Area 1..	63
Figure 2-27: The Response of an Orientation-Sensitive Neuron in Area 2.....	63
Figure 2-28: Response of a Direction Sensitive Neuron in Area 1.	64
Figure 2-29: Creation of a Direction-Sensitive Neuron from the Spatial Arrangement of Presynaptic Inputs.	65
Figure 4-1: Sony AIBO ERS-7.	75
Figure 4-2: Omron NeCoRo	75
Figure 4-3: Paro	76
Figure 4-4: NearMe.....	76
Figure 5-1: Diagram of the “Somatic Alphabet” Approach	81
Figure 6-1: Leonardo.	85
Figure 6-2: Mechanical Design of Leonardo’s Hand	87
Figure 6-3: Images of Robotic Hands.....	88
Figure 6-4: Unfinished, Unpainted Foam Latex Hand Coverings. Design.	89
Figure 6-5: Leonardo and his buttons.	90
Figure 6-6: The “Pixel” Hand	91
Figure 6-7: The 64 Channel Analog-to-Digital Processing Circuit Board for the Pixel Hand.	93
Figure 7-1: The Internal Cable Routing of the Original Leonardo Hands..	95
Figure 7-2: Dual Layer Approach for sensate Hands.	96
Figure 7-3: Closeup of the Finger Design of the New Leonardo Hands.	97
Figure 7-4: Two Images of the New Hand Solid Model.	98
Figure 7-5: New Leonardo Hands prior to attachment of circuit boards.....	99
Figure 7-6: Dimensions of the Interlink Part #400 Force Sensing Resistor (FSR).....	100
Figure 7-7: The Use of Spacers in the “Pixel” Hand.	101
Figure 7-8: The Back of Hand Circuit Board with sensors and circuitry attached.....	103
Figure 7-9: The Side circuit board.	104
Figure 7-10: The Fingertip with mounted sensors.....	105
Figure 7-11: The Mid-Hand Circuit Board.	106
Figure 7-12: The Mechanical Cable Routing.....	107
Figure 7-13: The kapton film which divides the mechanical spring housing from the mid-hand circuit board.....	108
Figure 7-14: The mounted mid-hand circuit board.....	108

Figure 7-15: The Assembled New Leonardo Left Hand – Back of Hand View.	109
Figure 7-16: The Assembled Leonardo Left Hand – Side and Back of Hand shown.	110
Figure 7-17: The Assembled Left and Right Hands.	110
Figure 7-18: The Stretch Fabric Glove for the New Leonardo Hands.	111
Figure 7-19: The Mounted Left Hand of Leonardo with Foam Latex Glove.	112
Figure 8-1: The Construction of the FSR Sensor.	114
Figure 8-2: The Response of a Model #402 (0.5” diameter circular sensing area) to Applied Loads.	115
Figure 8-3: The Flow of Information in the Mid-Hand Circuit Board.	116
Figure 8-4: Voltage Divider circuit used for the FSRs.	117
Figure 8-5: The Somatic Communication Circuit Board.	119
Figure 9-1: The Reflex Arc.	121
Figure 9-2: The Theoretical Location of the “Virtual Somatosensory Cortex”	122
Figure 9-3: The Hierarchical Organization from Sensor Level to “Virtual Somatosensory Cortex”	123
Figure 9-4: Responses of Slowly Adapting (SA) and Rapidly Adapting (RA) Receptors to an Indented Probe.	124
Figure 9-5: The Response of a Single FSR to Finger Taps.	125
Figure 9-6: Diagram of Orientation Calculation.	128
Figure 9-7: “Cortical Level” processing results.	130
Figure 9-8: Direction of Motion and Orientation	131
Figure 10-1: The Huggable.	135
Figure 10-2: The Neck Mechanism of the Huggable.	136
Figure 11-1: The Solid Model of the Teddy Bear Arm based upon physical measurement.	139
Figure 11-2: The 3D Printed Teddy Bear Arm.	140
Figure 11-3: The QTC Switch Substrate	141
Figure 11-4: The Initial Solid Model Used for Sizing of the Sensor Circuit Boards.	143
Figure 11-5: The Huggable Arm Sensor Circuit Board.	144
Figure 11-6: The QTC Sensor Cutting Jig and Cut Sensor	145
Figure 11-7: The QTC Gluing Template.	146
Figure 11-8: The QTC Clamping Jig.	146
Figure 11-9: The QTC Cutting Template.	147

Figure 11-10: The Arm Sensor Circuit Board with QTC and Multiplexers Attached.	148
Figure 11-11: The Arm Sensor Circuit Board with Thermistors Mounted	148
Figure 11-12: The Sensor Circuit Board with Copper Shield Attached.	149
Figure 11-13: The Mid-Plane Circuit Board.....	150
Figure 11-14: The Detailed Arm Assembly Solid Model.....	151
Figure 11-15: The Arm Rib Drilling Jig	152
Figure 11-16: The Mechanical Understructure with Mid-Plane Circuit Board Mounted.	153
Figure 11-17: The Mounted Sensor Circuit Boards – Internal Shielding View.....	154
Figure 11-18: The Mounted Sensor Circuit Boards and Mid-Plane Circuit Boards – Internal Shielding View.....	154
Figure 11-19: The Completed Arm Assembly – Front View.	155
Figure 11-20: The Completed Arm Assembly – Side View.....	155
Figure 11-21: The Completed Arm Assembly – Perspective View	156
Figure 12-1: The Numbered Sensor Circuit Boards.	157
Figure 12-2: The Division of the Huggable into Somatic Processing Board Sections.....	159
Figure 12-3: The Flow of Sensor Information Within One Somatic Processing Section	160
Figure 12-4: The Plot of the Resistance vs. Force for the QTC Switch Substrate.....	162
Figure 12-5: Resistance-Ratio vs. Temperature Characteristics for Thermistors and RTDs.....	164
Figure 12-6: The Bottom of the Arm Sensor Circuit Board.	165
Figure 12-7: The Assembled Top and Left Side Arm Sensor Circuit Boards.	167
Figure 12-8: The Bottom of the Mid-Plane Circuit Board.	169
Figure 12-9: The Huggable Somatic Processing Circuit Board..	174
Figure 13-1: Examples of Realistic Prostheses.....	184
Figure 13-2: Three Different Facial Expressions of Hiroshi Kobayashi’s Face Robots.....	185
Figure 13-3: Public Anemone shown at SIGGRAPH 2002 in San Antonio Texas.....	186
Figure 13-4: The Acylic Silicone Sample Molds.	191
Figure 13-5: The Measurement of the Durometer of the Silicone Samples.....	192

Figure 13-6: The Plot of Durometer as a Function of Silicone Fluid Percentage.	193
Figure 13-7: Common Medical Grade Silicones Used in Prosthetic Work.	195
Figure 13-8: The QTC 5x5 Sensor Array for Silicone Sample Testing.....	198
Figure 13-9: The XY-Stage with the 25 Sensor QTC Array Attached.	199
Figure 13-10: The Plot of Applied Force vs Sensor reading.	200
Figure 13-11: The Rippling of Very Soft Silicones with Large Applied Forces.	201
Figure 13-12: The Solid Model of the Silicone Arm Molds.....	203
Figure 13-13: The Printing of the Silicone Arm Molds on a Z Corporation Z510 3D printer.	204
Figure 13-14: The Finished Silicone Arm Molds.	204
Figure 13-15: Injecting the Silicone into the Arm Silicone Molds	205
Figure 13-16: The Arm Silicone Skin.....	206
Figure 13-17: Closeup of the Holes in the Silicone Skin to allow the Thermistors to Pass Through.	206
Figure 13-18: The Completed Arm Assembly with Silicone Skin	207
Figure 13-19: The Completed Arm Assemble with Silicone and Fur	207
Figure 13-20: The Layered Structure of the Huggable “Sensitive Skin.”	208
Figure 14-1: The Response of the Electric Field Sensor to the Human Hand Moving towards and Away from the Electrode.	210
Figure 14-2: Top Region Electrode in Contact with Three Objects and a Human Hand.....	211
Figure 14-3: The Electric Field Sensor Signal in Contact with the Objects of Figure 14-2.	211
Figure 14-4: The Contact Points for the Shielding Experiment.	212
Figure 14-5: The Electric Field Sensor Signal from the Top and Left Electrode for Contact with the Top and Left Electrode and the Bottom and Right Electrode.	213
Figure 14-6: The Processing of the QTC Signal for Light, Moderate, and Hard Touch.	214
Figure 14-7: The Response of the Temperature Signal	215

Figure 14-8: The Response of the Electric Field, QTC, and Temperature Sensors to Patting.	217
Figure 14-9: The Response of the Electric Field, QTC, and Temperature Sensors to Squeezing.	218
Figure 14-10: The Response of the Electric Field, QTC, and Temperature Sensors to Petting.	220
Figure 14-11: The Specificity of the Classification of Type.	227
Figure 14-12: The Negative Predictive Value of Type Classification.	228
Figure 14-13: The Sensitivity of Type Classification.	228
Figure 14-14: The Positive Predictive Value of Type Classification.	229
Figure 14-15: The Specificity of Class Classification.	230
Figure 14-16: The Negative Predictive Value of Class Classification.	231
Figure 14-17: The Sensitivity of Class Classification.	231
Figure 14-18: The Positive Predictive Value of Class Classification.	232
Figure 14-19: The Specificity of the Response Classification.	233
Figure 14-20: The Negative Predictive Value of Response Classification.	234
Figure 14-21: The Sensitivity of Response Classification.	234
Figure 14-22: The Positive Predictive Value of Response Classification.	235

List of Tables

Table 2-1: Somatic Sensation Receptor Types	36
Table 2-2: Mechanoreceptors in Glaborous Skin.	37
Table 6-1: The Number of Sensors Per Region of the “Pixel” Hand.....	93
Table 7-1: The Number of Sensors per Region of the New Leonardo Hands.	102
Table 12-1: The Pin Assignment for the Common Throughput of the Mid-Plane Circuit Board.	170
Table 13-1: Silicone Formulas used in Experiments.	190
Table 13-2: The Durometer Conversion Chart	194
Table 13-3: The Density of Each of the Twelve Silicone Samples	197
Table 14-1: The Data Sets Used for the Classification of Affective Touch	224

1 Motivation

The sense of touch is the earliest sensory system to become fully functional in all species (Montagu 1986). When we can't see in a dark room, our sense of touch helps to guide us. Our sense of touch helps to protect by allowing us to feel pain so we don't damage our bodies. Our sense of touch also allows us to communicate with one another through handshakes, hugs, or even a reassuring pat on the back. With all these wonderful things that touch provides, it is remarkable that this sensory system is lacking in many robotic platforms.

For many robots, the sense of touch is limited to grippers or other manipulators. While a small number of robots do exist with a full body sense of touch, the majority of these systems use the sense of touch to protect the robot from damage, or to keep the robot from injuring humans in a shared workspace (Kanda, Ishiguro et al. 2002). More recently new types of robotic companions, such as Sony's AIBO robotic dog, have been developed. These robots only feature a small number of localized tactile sensors. Is this the extent that touch should exist in robotics? If so, why is touch so important to all living creatures?

The sense of touch can provide a robot with a way to function in the ever-changing complex world of human life. Vision alone is not sufficient to function in unstructured environments due to problems of occlusion (Lumelsky, Shur et al. 2001). Tactile and visual information can be combined to form stronger percepts such as distinguishing between similarly colored objects based upon softness, or surface texture. Full body touch can help to convey the "illusion of life." No matter how lifelike the movement of a robot may appear, if it is touched and does not respond, the illusion is instantly broken. In the context of human robot interaction, touch can be used to help guide the robots body into new positions. For example, a sense of touch can help distinguish between when a person places his or her hand around the robot's arm to guide it to an object and the impact felt by the arm bumping into a wall or an object.

Touch also can provide affective content which a robot could use for learning or interaction. As robots become more sociable in their behavior and organic in their appearance, the sense of touch can hold a much greater emotional meaning.

Robots which are soft, expressive, and lovable begged to be touched by people, especially children. This touch can be used for reward, such as patting the robot on the head much like a pet, for play, such as tickling the robot to get a response, or to illicit a reaction, for example tapping the robot on the shoulder to get its attention. Additionally the robot can convey emotions based on its sense of touch. For example, if the robot is “sad,” touch can be used to cheer it up through hugs, tickles, or pats on the head. These are only a few of the many examples in which a full body sense of touch can be beneficial to the field of robotics.

This thesis describes the design of “sensitive skins” for two different robotic platforms – Leonardo, a sociable robot, and the Huggable, a therapeutic robotic companion. At the center of this discussion is the notion that the human and animal somatosensory system can provide a wonderful design framework for exploring the “mother of all senses.”

The thesis is divided into four sections, of which the last is the conclusion. The first section provides background information for the implementation sections which follow. Chapter 2 provides an in depth description of the human and animal somatosensory system. Chapter 3 provides insight from a wide body of literature on pet therapy. Much of our interaction with pets is through touch and thus, provides an interesting study of how touch can carry affective information to help people relax. Chapter 4 describes a few robotic implementations of both robotic touch sensing systems as well as robotic companions. Finally, Chapter 5 proposes the “Somatic Alphabet Approach” which is one way of thinking about the design of robotic sensor skins.

Section II is focused on the “sensitive skin” design for Leonardo. Chapter 6 provides an overview of Leonardo, as well the design challenges for a new set of sensate hands. Chapter 7 describes the electromechanical design of these new hands. Chapter 8 provides a description of the electronics for this sensing system. Finally, Chapter 9 discusses the “Virtual Somatosensory Cortex,” a software system inspired by the somatosensory system of humans and animals.

Section III is focused on the “sensitive skin” design for the Huggable. Chapter 10 provides an overview of the project, as well as the design challenges for the first section of what will be a full body sensitive skin. Chapter 11 provides the electromechanical

design description. Chapter 12 details the electronics of the sensory system. The synthetic silicone skin formulation and fabrication is described in Chapter 13. Some initial work in classifying the affective content of touch is discussed in Chapter 14. Finally Chapter 15 provides a conclusion to this thesis.

Section I: Nature and Robots

2 Nature’s “Sensitive Skin” – Lessons from Neuroscience

2.1 Introduction

Our skin is the largest sensory organ of our body. It acts as a shield, protecting us from bacteria and infection. It is capable of detecting skin indentations as small as $1\mu\text{m}$ (Nolte 2002). Layers of skin are constantly being regrown and replaced, yet there are no changes in our perception. Throughout the body, skin has a rich variety of different properties including stiffness, texture, sensory innervation and color to name a few. But most importantly, the sense of touch, so intimately linked to our skin, is the first of the sensory systems to develop. Before a human embryo is less than 6 weeks old and has not yet formed eyes to see or ears to hear, the sense of touch is highly developed. Even as early as nine weeks in the womb, the fetus will close its fingers in a gripping motion if its palm is touched. (Montagu 1986). Clearly skin and the sense of touch are an engineering marvel of nature.

In order to design a biologically inspired sense of touch system for robots it is important to first understand how humans and animals are able to perceive the world around them through a sense of touch. In this chapter, the biological sensors, the mechanoreceptors, which transduce the physical world into information that the brain can understand, will be described. Next, the wiring from sensor to somatosensory cortex, the processing center of touch in the brain, will be illustrated. After this discussion, the focus will be placed on the somatosensory cortex and its organization and processing. Finally, experiments in haptics and other fields which shed light onto how different modalities are combined will be discussed.

Central to this discussion is the notion that there is not one single “somatic” sensor, but rather our perception of the world around us through touch is due to the combinations of many different types of sensors, each specially designed for a specific function. In many ways, one can imagine each sensor and way of processing the information from each sensor as letters in an alphabet. While each letter may convey some information, the combination of each letter into words and sentences can have much greater meaning. Thus percepts can be formed from the

arrangements of these “letters.” A further discussion of this “Somatic Alphabet Approach” is in Chapter 5. The majority of this chapter originally appeared in (Stiehl 2003).

2.2 Essential Terminology and Concepts

Before entering into a discussion of the brain, it is important to describe a few key concepts and terms which will be used throughout the chapter. This section is intended to help those who have never studied neuroscience or neuroanatomy.

There are a series of terms which provide a way to visualize the three-dimensional structure of the brain and the body through a series of two-dimensional slices as shown in Figure 2-1. The three planes are the **sagittal** (dividing the body into left and right sides), the **coronal** (dividing the body into front and back), and the **horizontal** (dividing the body into top and bottom) planes. In addition to these slices there are also a series of terms used for orientation in the brain. To determine where with respect to the middle of the plane one is looking the terms **medial** (towards the middle) and **lateral** (towards the side) are used. For example, a mid-sagittal slice would cut the brain directly down the center as shown in Figure 2-1. Other orientation terms differentiate between the head end (either **anterior**, **cephalic**, or **rostral** can be used) and the tail end (either **caudal** or **posterior**) of the body. For example, the caudate equina is the collection of spinal nerve roots at the base of the spinal cord. Along the midline of the body, i.e., the trunk of the body, is referred to as **proximal** and the periphery, i.e., moving towards the fingers or toes, is referred to as **distal**. The terms **dorsal** (toward or at the back) and **ventral** (toward or at the belly or front) are used to describe both four- and two-legged animals. However, because of the original usage in animals, and to allow for consistency across species to humans, the terms dorsal and ventral are also used to describe the top of the brain, dorsal, and the bottom of the brain, ventral. This makes sense if one thinks of placing a human on all fours with head forward like an animal; thus now the back of the body and top of the brain are parallel to each other.

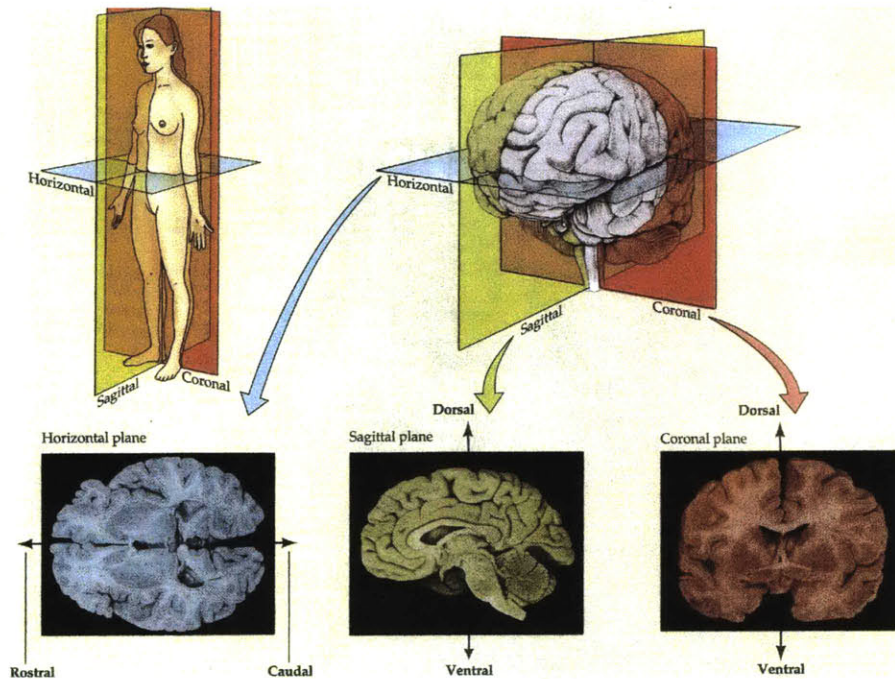


Figure 2-1: The Views of the Brain and Body. (Rosenzweig, Breedlove et al. 2002, pg 37)

There are two major divisions of the nervous system – the central and peripheral nervous system. The central nervous system (CNS) consists of the brain and the spinal cord. The peripheral nervous system (PNS) consists of the cranial nerves (a series of nerves which originate in the head and as such bypass the spinal cord and connect directly to the brain), the spinal nerves (the series of nerves which connect to the spinal cord at its different levels), and the autonomic nervous system. A visual depiction of the division between the systems appears in Figure 2-2.

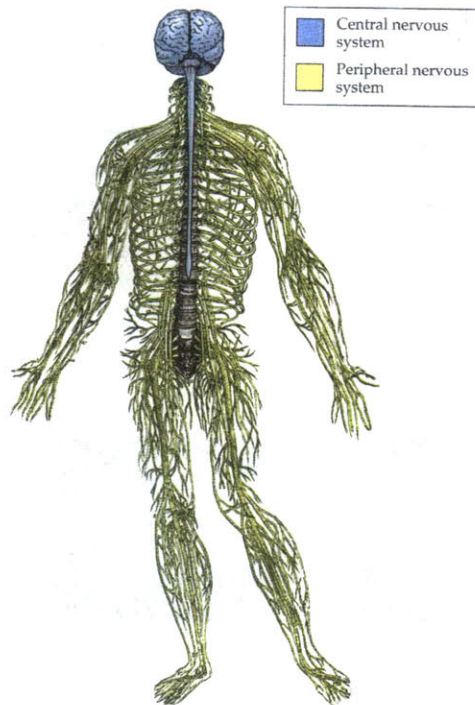


Figure 2-2: Divisions of the Central Nervous System. The Central Nervous System (CNS) is shown in blue, the Peripheral Nervous System (PNS) is shown in yellow. (Rosenzweig, Breedlove et al. 2002, pg 36)

While the majority of this discussion of the sense of touch in humans will deal primarily with one brain region, the somatosensory cortex also referred to as the postcentral gyrus, for purposes of orientation and relationship to other major structures of the brain it is worthwhile to spend some focus on the major regions of the brain. The cerebral hemispheres (the two halves of the brain) can be divided into 4 regions or lobes as indicated in Figure 2-3.

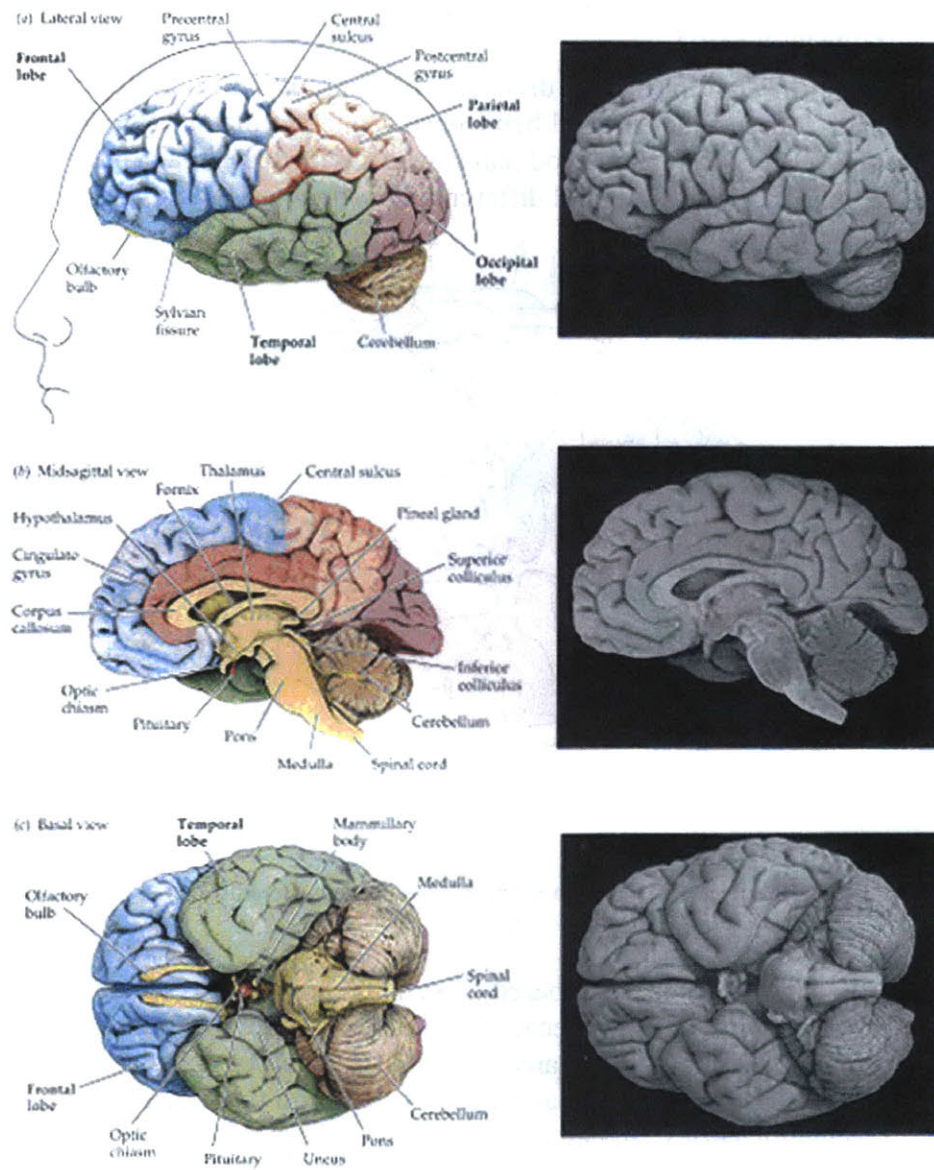


Figure 2-3: Three Views of the Human Brain. The postcentral gyrus is located in (a). (Rosenzweig, Breedlove et al. 2002, pg 42)

The four lobes consist of the temporal lobe, the occipital lobe, the parietal lobe, and the frontal lobe. The postcentral gyrus can be clearly seen in (a) of at the top of the brain caudal to the central sulcus. Of other special note, the primary motor cortex (the

postcentral gyrus) sits directly across the central sulcus from the postcentral gyrus.

In addition to the division of the brain based on the four major lobes of the cerebral hemispheres, another method was done in 1909 by Korbinian Brodmann, who divided the brain into 46 regions based on structural differences as shown in Figure 2-4.

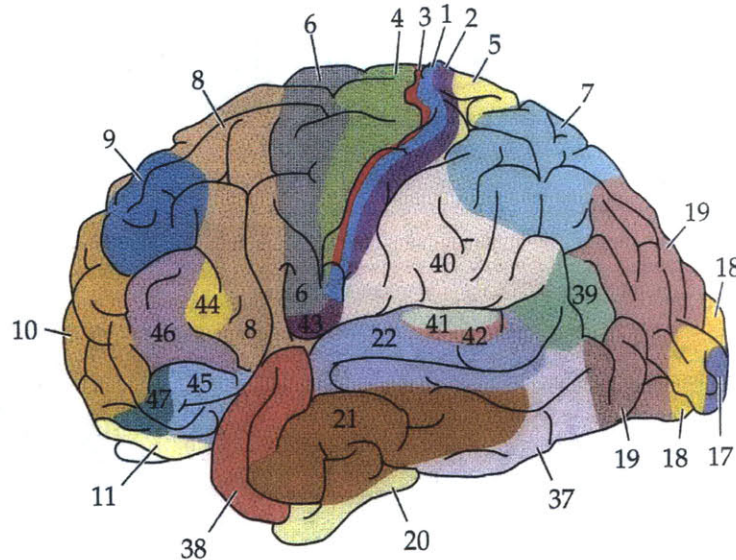


Figure 2-4: Brodmann's Areas. (Rosenzweig, Breedlove et al. 2002, pg 49)

While the divisions were based on structure, many researchers use his numbering schemes because they also correlate with function. Of particular mention are areas 3, 1, and 2 which form the somatosensory cortex, areas 5 and 7 which form the somatosensory association cortex, and area 4 which forms the motor cortex.

2.3 Skin – The Largest Sensory Organ

The skin is by far the largest sensory organ of the body. An average-sized adult human has a total skin surface area of 1.8 square meters, which is almost 1000 times the size of the area of the two retinas of the eyes, a density of 1250 kg/m³ and weighs approximately 5 kg (Sherrick and Cholewiak 1986). It varies in thickness from 1/10th of a millimeter to 3 or 4 millimeters in

sections, with the thickest regions being the palms of the hands and the soles of the feet and thinnest on the eyelids (Montagu 1986). There are two major types of skin in the body of humans and other animals – glabrous, found on the palm of the hand and sole of the foot, and hairy, found on almost every other part of the body.

The skin itself consists of a series of layers as shown in Figure 2-5.

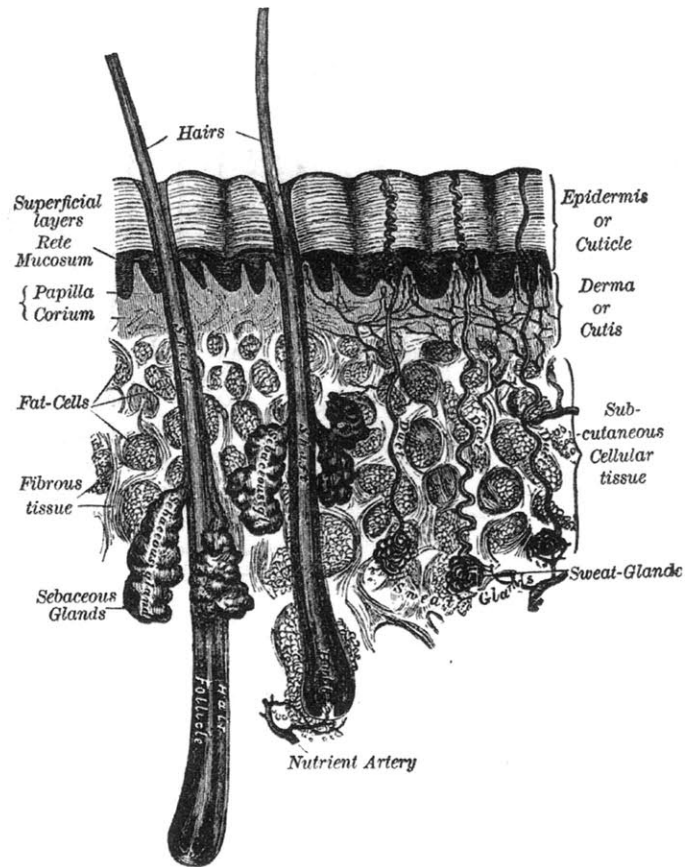


Figure 2-5: Sectional View of the Skin. (Gray 1977, pg 1136)

The epidermis or cuticle consists of two layers. The upper layer is the corneum, which consists of tough anuclear cells that are lost through friction and natural growth. Below this layer in the epidermis is the germinative layer which replaces the lost corneum cells. Below the epidermis is the dermis, also referred to as the cutis or corium. In the dermis are found the papillae, which are the irregularities which are responsible for the fingerprint

patterns of the hands and feet. Beneath the dermis are found the sweat glands, hair follicles, and sebaceous glands.

The layered structure of the skin shown in Figure 2-5 highlights the physical makeup of the skin, but does not indicate the types of sensors found in the skin that respond to touch and other stimuli. Figure 2-6 shows another view of the skin, this time with an emphasis placed on the location of the mechanoreceptors.

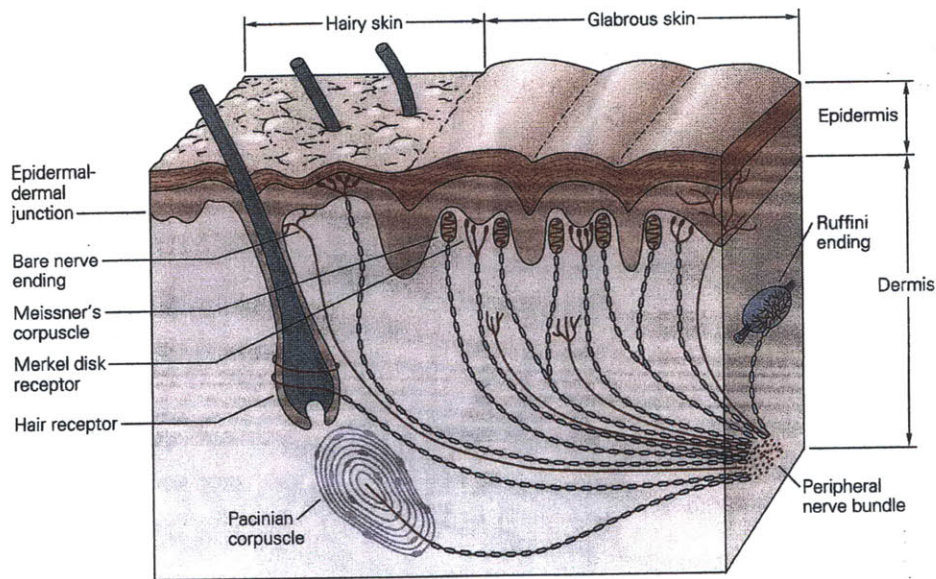


Figure 2-6: Sectional View of Hairy and Glabrous Skin with Mechanoreceptors Highlighted. (Kandel, Schwartz et al. 2000, pg 433)

As can be clearly seen from this figure, there are a wide variety of mechanoreceptors in the skin, each with a different location and preferred stimulus. Thus, by analyzing the outputs of each type of sensor an accurate depiction of the stimulus can be determined. In the next section, an in-depth discussion of the types of mechanoreceptors and what information they encode will be provided.

2.4 Receptor Types of Somatic Sensation

Our perception of the world around us through the somatic senses is due to the wide variety of receptors in our skin. Thus

there is not one solitary “somatic sensor” but rather a collection of different sensors each encoding a specific type of stimulus. Each type of sensor can be classified as one of four types, each responding to a different modality. The first class of sensors are the discriminative touch sensors, which are used to recognize the properties of objects such as size, shape, and texture as well as the movement of these objects across the skin. It is this class of objects that the discussion of this section will largely focus on as it most closely correlates to the sensors used for the robotic hand that is the subject of this thesis. Another class of receptors is those that deal with proprioception, the sense of limb and body movement and static position. The third class of receptors are those that deal with pain or itch, the nociceptive receptors. The final class are those that deal with temperature, a sensation of either warmth or cold. Table 2-1 shows a summary of the receptor types responsible for somatic sensations.

Another common grouping is based upon the two classes of somatic sensation. The first class, epicritic sensations, concerns the fine aspects of touch such as topognosis (detecting a gentle touch and determining where on the body it occurred), discerns the frequency and amplitude of vibration, resolving spatial details such as texture and two-point discrimination (the distance between two simultaneously touched points on the skin) and stereognosis (recognizing the shape of objects grasped in the hand). This class uses the encapsulated mechanoreceptors. The second class are the protopathic sensations, which are mediated by bare nerve ending receptors. This class of sensation involves pain and temperature. It is also important to note that pain also includes the sensations of itch and tickling. For a further discussion of pain see (Rollman 1991; Kandel, Schwartz et al. 2000 ch. 24). For a further discussion of temperature sensing see (Stevens 1991; Craig and Rollman 1999). For a further discussion of muscle and skeletal mechanoreceptors see (Clark and Horch 1986).

Table 2-1: Somatic Sensation Receptor Types adapted from
(Kandel, Schwartz et al. 2000, pg 432)

Receptor Type	Fiber Name	Modality
Cutaneous and subcutaneous mechanoreceptors		Touch
Meissner's corpuscle	RA	Stroking, fluttering
Merkel disc receptor	SAI	Pressure, texture
Pacinian corpuscle	PC	Vibration
Ruffini ending	SAII	Skin Stretch
Hair-tylotrich, hair-guard	G1, G2	Stroking, fluttering
Hair-down	D	Light Stroking
Field	F	Skin Stretch
Thermal Receptors		Temperature
Cool receptors	III	Skin cooling (25°C)
Warm receptors	IV	Skin warming (41°C)
Heat nociceptors	III	Hot temperatures (>45°C)
Cold nociceptors	IV	Cold temperatures (<5°C)
Nociceptors		Pain
Mechanical	III	Sharp, pricking pain
Thermal-mechanical	III	Burning pain
Thermal-mechanical	IV	Freezing pain
Polymodal	IV	Slow, burning pain
Muscle and skeletal mechanoreceptors		Limb proprioception
Muscle spindle primary	Ia	Muscle length and speed
Muscle spindle secondary	II	Muscle stretch
Golgi tendon organ	Ib	Muscle contraction
Joint capsule mechanoreceptors	II	Joint angle
Stretch-sensitive free endings	III	Excess stretch or force

There are four main types of mechanoreceptors which have been found in glabrous skin. These receptors can be arranged in a grid along two different axes as shown in Table 2-2. One axis corresponds to adaption, which is how a receptor responds to a sustained stimulus. The second axis refers to the receptive field size, or how large of an area on the skin a receptor will be sensitive to.

Table 2-2: Mechanoreceptors in Glabrous Skin. Adapted from (Kandel, Schwartz et al. 2000)

	Slowly Adapting (SA)	Rapidly Adapting (RA)
Small Receptive Field (Superficial Layers)	Merkel disk receptors	Meissner's corpuscles
Large Receptive Field (Deep Layers)	Ruffini endings	Pacinian corpuscles

There are two types of adaption – rapidly and slowly adapting. Rapidly adapting, or RA, receptors respond primarily to the changes in a stimulus, thus in many ways one can think of such receptors as functioning as a derivative indicating the changes in or movement of a stimulus. They fire at a rate proportional to the speed of motion and their duration of activity corresponds to the duration of motion (Kandel, Schwartz et al. 2000 pg 438). Slowly adapting, or SA, receptors encode a static position and are capable of doing so continuously over a period of several minutes. However there is some gradual decay, which is obvious from everyday experience, as you don't feel your clothing on your body after a while. In fact, the amount that a slowly adapting receptor fires has been shown to indicate how rapidly the pressure is applied to the skin (initially) and then in steady-state shows a level proportional to skin indentation (Kandel, Schwartz et al. 2000 pg 438). The responses of both rapidly and slowly adapting receptors to a probe touching the skin are shown in Figure 2-7.

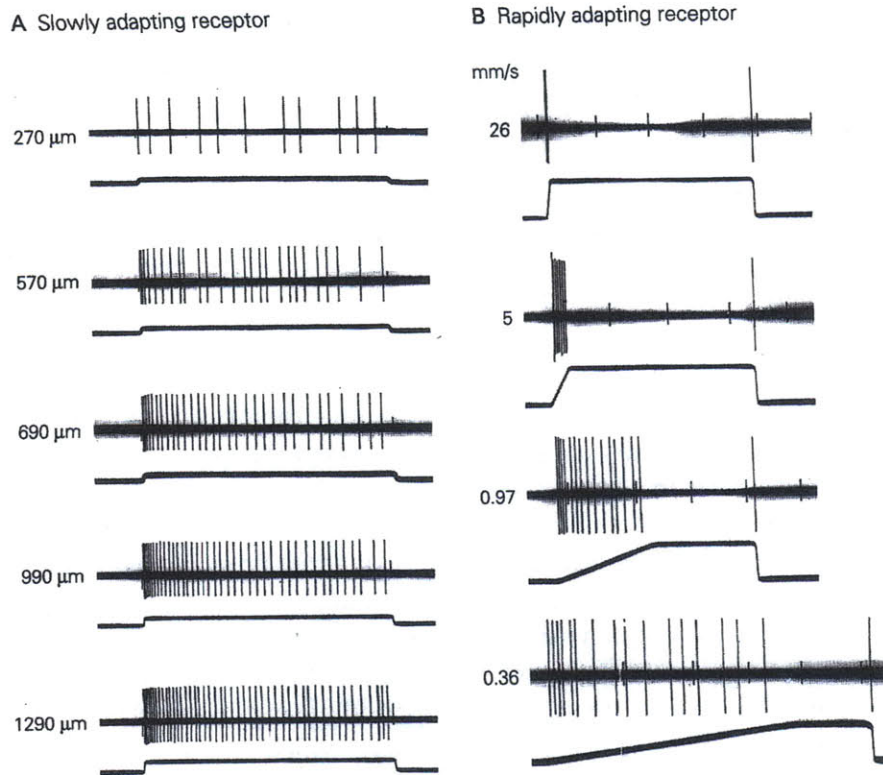


Figure 2-7: Responses of Slowly Adapting (SA) and Rapidly Adapting (RA) Receptors to an Indented Probe from (Kandel, Schwartz et al. 2000, pg. 424). In each image the response of the receptor is shown by a series of vertical bars (spikes) corresponding to each time that cell fires in response to the presented stimulus. Beneath the spike train is the time profile of the stimulus, with a step increase indicating that the probe was indented into the skin and a step decrease indicating that the probe was removed. In A, the response of a slowly adapting receptor is shown. As can be seen clearly from the figure, as indentation increases (indicated by a depth in μm) the firing rate (indicated by the number of vertical bars per interval) increases. It is also important to note that there is a greater density of spikes, i.e., a faster firing rate as the stimulus is applied. In B, the response of a rapidly adapting receptor is shown. As can be shown, the cell responds to changes in stimulus, as indicated by the ramp. The cell fires only while the skin is indented and finally when the stimulus is removed. It is silent otherwise.

The location and depth of a mechanoreceptor in the skin influence the receptive field size, which can be characterized as punctate for a small receptive field with a sharply defined boundary and diffuse for a larger field with less definition of boundary (Sekuler and Blake 2002). While the act of pressing into the skin with a probe, as shown in Figure 2-7, may seem like a simple stimulus, the complexity of the skin causes very different reactions in different locations in the skin. This is due to the fact that the deforming skin layers are “viscoelastic.” Thus due to the viscous nature of the skin, when it is touched energy from the contact point will be transmitted through the skin. However, the elastic nature of the skin means that some of this energy will be stored and then used to return the skin to its original shape (Cholewiak and Collins 1991). In addition the path from stimulus to receptor is often filled with obstacles such as blood vessels, bone, fat cells or other types of obstructions as shown in Figure 2-5. Each obstacle may actually distort the signal before it reaches the receptor (Cholewiak and Collins 1991). Thus the “image” that each sensor “sees” may be very different from the original “image” of the stimulus. The receptors closer to the skin surface, in the papillary ridges of the superficial layers of the skin, such as the Meissner corpuscle and Merkel disk receptor, shown in Figure 2-6, have a small receptive field which is more finely tuned. In contrast, those deep in the skin, such as the Pacinian corpuscle and the Ruffini endings, also shown in Figure 2-6, have a much wider receptive field, but have less spatial sensitivity. Often such receptors will have a region directly above them in which sensitivity is greatest.

The physical properties of each receptor also dictate how it responds to a stimulus. The Meissner’s corpuscle, RA, is actually mechanically coupled to the papillary ridge edge as shown in Figure 2-6, which allows for a high degree of sensitivity. It has a layered structure, in which the sensory nerve terminal is wrapped around and in between layers of stacked epithelial cells, each oriented in the direction perpendicular to the long axis of the cell. A thin outer capsule surrounds the stack. When vertical pressure is applied to a dermal papilla, the nerve endings are compressed between the stack and thus, the pressure is “sensed.” Pressure applied to nearby papilla are not as effective to the pressure applied directly over the cell, thus it has a small receptive field as mentioned previously (Nolte 2002).

The Merkel disk receptor, SAI, is non-encapsulated. These receptors are usually found in clusters, often at the center of a papillary ridge. The Merkel ending, a disk-shaped expansion of the terminal of a sensory fiber, inserts into the base of a Merkel cell to create this receptor. One fiber may branch to connect to many of these cells (Nolte 2002). Compressing strain from the skin is passed to the sensory nerve due to the fact that the cell encloses a semi-rigid structure (Kandel, Schwartz et al. 2000). This receptor is found in both hairy and glabrous skin.

The Ruffini ending, SAII, is found in the dermis, subcutaneous, and other connective tissue sites. It functions as a skin stretch receptor. Strands of collagenous connective tissue cross a thin, cigar-shaped capsule. The sensory fiber enters and branches, thus interspersing between the collagenous strands. Thus when the skin is stretched, tension is applied to one or both ends of the cell and squeezes the sensory fiber terminals between the strands. Because of the property of the strands (collagen is not very elastic) the deformation can be held for a long time thus creating the slowly adapting response (Nolte 2002). This receptor helps to detect the shape of grasped objects (Kandel, Schwartz et al. 2000).

The final glabrous skin mechanoreceptor is the Pacinian corpuscle, PC, also shown in Figure 2-6. These receptors are very widespread and found subcutaneously. The onion-like structure, due to the many concentric layers, of this encapsulated cell contribute to its rapidly adapting response. Between the thin layers of epithelial cells are fluid-filled spaces. In the center of the cell is the nerve ending. Because of the mechanical structure of this receptor and the elasticity of the layers, only fast acting forces are transmitted through the layers of the cell to reach the nerve ending. Any sustained forces simply deform each successive layer slightly less than the previous one and as a result do not reach the nerve ending in the center of the receptor. Because of their speed in detecting changes they have been linked to vibration detection (Nolte 2002).

The number and type of mechanoreceptors in the skin vary throughout the body. As a result the ability to discriminate different properties of the stimulus varies as well. This organization can be determined through the use of psychophysical tests of spatial perception such as the two-point limen and the error

of localization test (Cholewiak and Collins 1991). In the two-point limen test a subject is presented with either one or two points pressed into the skin. The experimenter then instructs the subject to determine whether he or she feels a single point or a set of two distinct points. The distance between the points when the subject first perceives them as two distinct locations is recorded. This measurement, shown in Figure 2-8 as a solid line, correlates well with receptor density. It is important to note though that, with practice, subjects show an improvement on this task (Cholewiak and Collins 1991). The error of localization test, indicated by dots in Figure 2-8, presents a subject with an initial stimulus, a touch presented at a specific point on the body. Then at some time later, a second stimulus is presented either at the same location or a different one. The subject is asked to indicate whether the second touch was in the same location or a different one. Again the spacing between points when a single location becomes two locations is the variable being measured (Cholewiak and Collins 1991). It is important to note that this test involves some form of spatial memory. The differences between the two tests as shown in the figure are indicative of the fact that other variables, such as the difference in neural activity invoked by each test, can have an effect on the results.

Even with the differences between the two tests, there are general trends which are shown in the data. First, there is a wide difference between the spatial perception of the fingertips, as small as 2 mm on the pad, and the back, as large as 70 mm (Sekuler and Blake 2002). Second, there is a general trend of finer spatial perception, increased receptor density, as one moves from the trunk of the body to the extremities. In many ways this organization makes sense, as a greater spatial perception is required in the fingertips and hand for manipulation of objects than in the arm or back. This spatial resolution also reflects the types of mechanoreceptors present. In the fingertips, there are an abundance of Meissner corpuscles and Merkel disks. These small receptive fields, or punctate, receptors allow for very fine spatial resolution in the fingertips because the diameters of these receptors are smaller than the ridges of the fingerprints in glabrous skin.

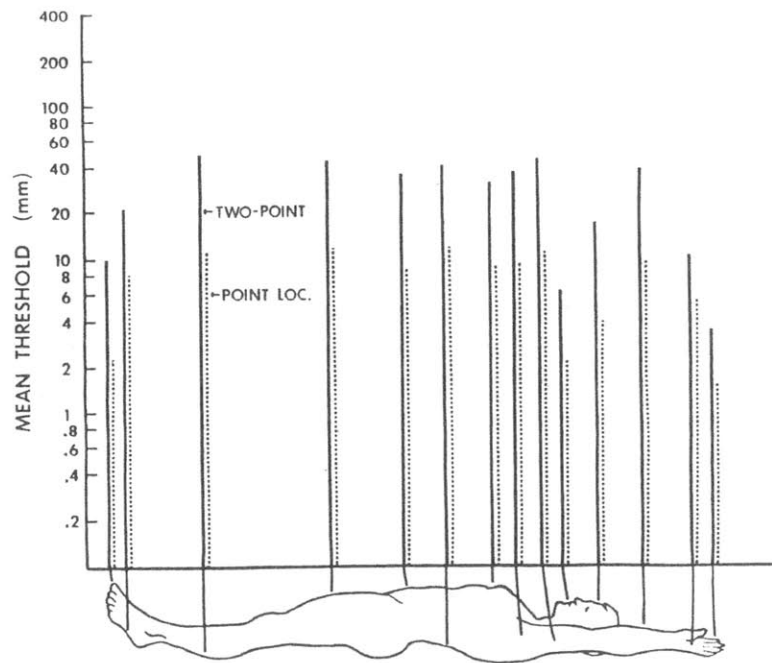


Figure 2-8: Measures of Spatial Acuity on Different Body Sites (Cholewiak and Collins 1991 pg 52). The solid lines indicate the spacing between points in the two-point limen at which the two points are perceived as being separate. The dotted lines correspond to the results of the error localization test

In addition to spatial perception, touch has a temporal aspect as well. Studies of the temporal properties of touch have compared touch to the senses of hearing and vision (Pohja 1996). It was found that the limit at which tactile stimuli can be perceived as two separate events if spaced in time was 5ms or more. Any lower temporal difference and the two stimuli will be perceived as one. This was slower than hearing, 0.1 ms, but faster than vision, 25 ms (Pohja 1996). If a sequence of events are presented, it was found that 20 ms was required by all three senses to determine the order in which the stimuli were presented (Pohja 1996).

A much more in-depth discussion of other psychophysical studies to determine the limits of tactile perception appears in (Cholewiak and Collins 1991) In the next section, the ways the mechanoreceptors can combine to encode different stimuli will be presented and the “alphabet” will begin to be discussed.

2.5 Properties of the Stimulus Encoded at the Periphery

As discussed in Section 2.4, the four main types of mechanoreceptors found in glabrous skin respond to stimuli differently. It is as a result of these differences that researchers have shown that certain properties of the stimulus can be encoded at the level of the receptors themselves. In many ways one can think of each mechanoreceptor as part of an alphabet for object detection.

One major area of research involves the encoding of texture and roughness. In the majority of these studies a stimulus is stroked across the finger pad of a monkey and responses from the nerve are recorded. Some examples of stimuli presented have been dot patterns (Johnson and Lamb 1981; Lamb 1983; Connor, Hsiao et al. 1990; Johnson, Phillips et al. 1991; Connor and Johnson 1992; Johnson and Hsiao 1992; Johnson and Hsiao 1994), raised letters (Vega-Bermudez, Johnson et al. 1991), and grooved surfaces (Lederman 1974). The responses to Braille of the four mechanoreceptors of glabrous skin appear in Figure 2-9.

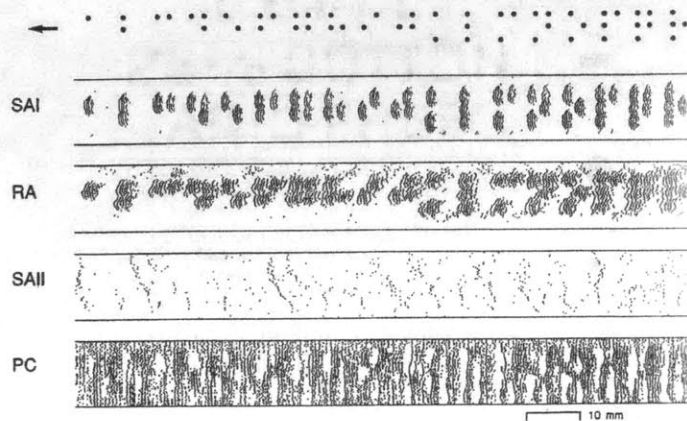


Figure 2-9: Response of Single Human Mechanoreceptors to Scanned Braille Characters from (Johnson and Hsiao 1992, pg 229). At top is the original Braille stimulus, a pattern of embossed dots 0.43 mm high. Below are the responses of the four mechanoreceptors, SAI – Merkel disc receptor, RA – Meissner's corpuscle, SAII Ruffini endings, and PC – Pacinian corpuscle. Each dot corresponds to one action potential.

In the above figure, responses from a single afferent fiber were recorded, and the plot was created by scanning the finger pad across a row of dots, then moving the row vertically up and repeating until the whole Braille pattern was scanned. From this figure, it becomes clear that the candidates for the encoding of form/texture appear to be primarily the SAI afferents with the possibility of some encoding by RA afferents (Johnson and Hsiao 1992).

Another area of research involves the encoding of shape (LaMotte and Srinivasan 1993) and curvature (LaMotte and Srinivasan 1987; LaMotte and Srinivasan 1987; Srinivasan and LaMotte 1987) by the mechanoreceptors in the periphery. In one set of experiments, a series of cylinders of varying diameter from 1/32 to 1/2 of an inch were placed into the distal finger pad of an anesthetized monkey (LaMotte and Srinivasan 1993). The responses of SAI, i.e., Merkel disc, and RA, i.e., Meissner corpuscle, fibers were recorded from single mechanoreceptive peripheral nerve fibers. A summary of their findings appears in Figure 2-10, the SA fiber, and Figure 2-11, the RA fiber.

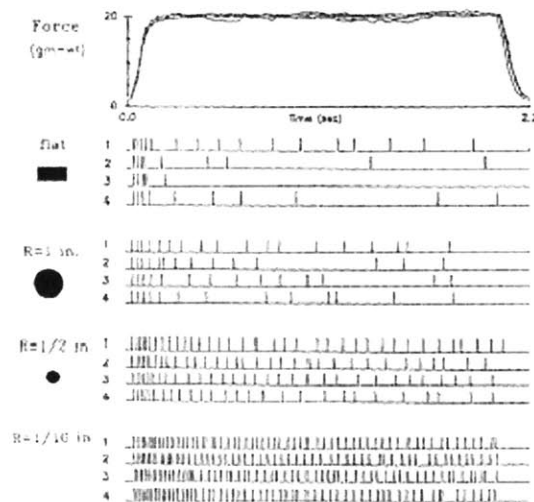


Figure 2-10: Responses of an SA Fiber to a Flat Plate and to Selected Cylindrical Bars of Different Radii of Curvature Indented in the Skin from (LaMotte and Srinivasan 1993, pg 45). The vertical tick marks show an action potential.

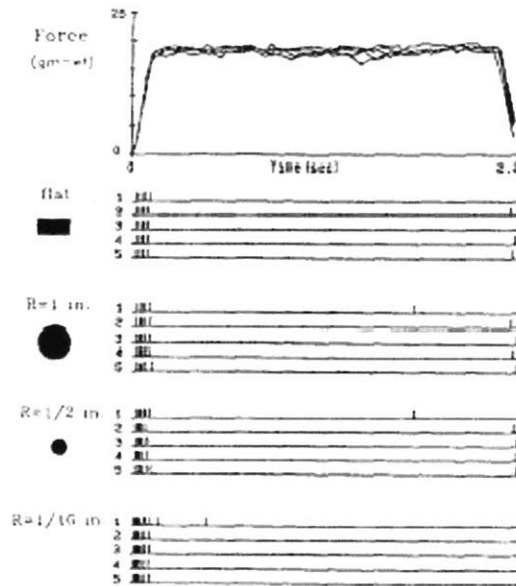


Figure 2-11: The Response of an RA Fiber to a Flat Plate and to Selected Cylindrical Bars of Different Radii of Curvature Indented into the Skin from (LaMotte and Srinivasan 1993, pg 46). The vertical bars indicate an action potential.

As can be seen from the above figures, the SA fibers first had an initial higher discharge rate during the indentation of the probe. Once the probe was indented, the firing rate of the SA fiber increased as the curvature, the reciprocal of the radius of the cylinder, increased. The response of the RA fiber was initial firing as the probe was indented into the skin, which reflected the motion of the probe, and no or very little firing in steady state. However, curvature did not seem to have a large effect on this firing rate.

These findings can be explained as a result of the number of Merkel disks receptors that fire when a probe of some radius of curvature is indented into the skin. A probe with a small radius has a small surface area and thus will activate only a small number of Merkel disk receptors in a population. But because this force is concentrated on a small number of these receptors, the firing rate will be high since each receptor receives a large portion of the force. However, as the diameter increases, the area, i.e., the number of Merkel disks activated, increases as well. But now the response of each individual Merkel disk is lower because the force is distributed across more receptors in the population (Kandel,

Schwartz et al. 2000). Thus one can infer that the firing rate of an individual receptor can be related to the pressure, the total force divided by the surface area, it feels.

These are only two examples from studies that observe the responses of single fibers in the periphery. Other work in the realm of vibration has shown that the oscillations of a sinusoidal signal presented to skin will be reflected in a pulse code in which the mechanoreceptor fires an action potential at a rate of one spike per cycle of the sinusoidal wave (Kandel, Schwartz et al. 2000). It has been shown that the three mechanoreceptors which show this response are “tuned” to different frequencies – the Merkel disc receptors respond best between 5-15 Hz, the Meissner’s corpuscles prefer the range of 20-50 Hz, and the Pacinian corpuscles are active for 60-400 Hz (Kandel, Schwartz et al. 2000). These results presented deal only with the realm of touch. Other similar types of peripheral encoding can be seen in temperature, pain, and proprioception as well. Thus it becomes clear that much information is encoded by the receptors at the periphery, and the “alphabet” of somatic sensation begins here. In the next section, the path a signal travels from receptor to the somatosensory cortex for higher level processing will be traced.

2.6 Pathway from Receptor to Cortex

As was previously mentioned in Sections 2.4 and 2.5, a single nerve fiber will receive input from a cluster of Merkel disc receptors or Meissner’s corpuscles. In contrast, the mechanoreceptors with a larger receptive field such as the Pacinian corpuscle and Ruffini ending will be connected to a single nerve fiber. Regardless of what type the somatic receptor is, all somatosensory information, except for the face and part of the head, is carried by dorsal root ganglion neurons as shown in Figure 2-12. Information from the head and face is carried by the trigeminal sensory neurons, which are similar in both morphology and function to the dorsal root ganglion cells (Kandel, Schwartz et al. 2000).

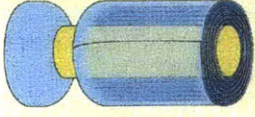
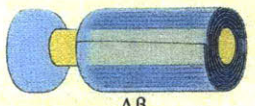


Receptor type	Axon type	Diameter (μm)	Conduction speed (m/s)
Proprioceptors of skeletal muscles	 A α	13–20	80–120
Mechanoreceptors of skin	 A β	6–12	35–75
Pain, temperature	 A δ	1–5	5–30
Temperature, pain, itch	 C	0.02–1.5	0.5–2

Figure 2-13: Types of Peripheral Nerve Fibers through which Somatic Information can Travel from (Rosenzweig, Breedlove et al. 2002, pg 237)

Both the diameter and the myelination of the fiber affect the conduction speed of the information. A larger diameter of the axon will increase the conduction rate. The myelin sheath, indicated in the figure by the larger diameter tubes surrounding the smaller diameter nerve fibers in the top three fibers, is made up of fat cells and acts as an insulator to the axon thus increasing the speed of conduction. The conduction of an action potential along a nerve fiber has been mathematically modeled; for a further discussion of this see chapter 6 in (Dayan and Abbott 2001). All the mechanoreceptive axons are A-alpha,-beta except for the hair down receptor which is A-delta (Kandel, Schwartz et al. 2000, pg 432).

There is an organizational level as to how the sensory information from each type of somatic receptor enters into the central nervous system through the spinal cord. The spinal cord is divided into a series of layers as shown in Figure 2-14. Each section has nerves that correspond to a specific section of the body.

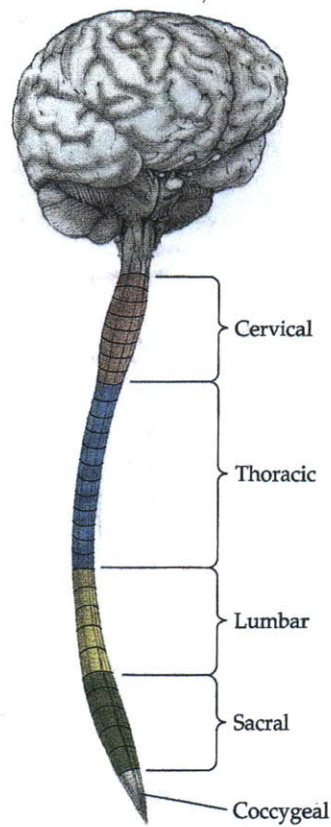


Figure 2-14: The Segments of the Spinal Cord from
(Rosenzweig, Breedlove et al. 2002, pg 232)

There are 8 cervical (neck), 12 thoracic (trunk), 5 lumbar (lower back), 5 sacral (pelvic), and 1 coccygeal (bottom) sections (Rosenzweig, Breedlove et al. 2002, pg 39). The way in which regions of skin on the body are innervated by spinal nerves also shows a similar map to the division of the spinal cord. Each region of skin innervated by a specific spinal root is called a dermatome. The dermatome map of the body is shown in Figure 2-15.

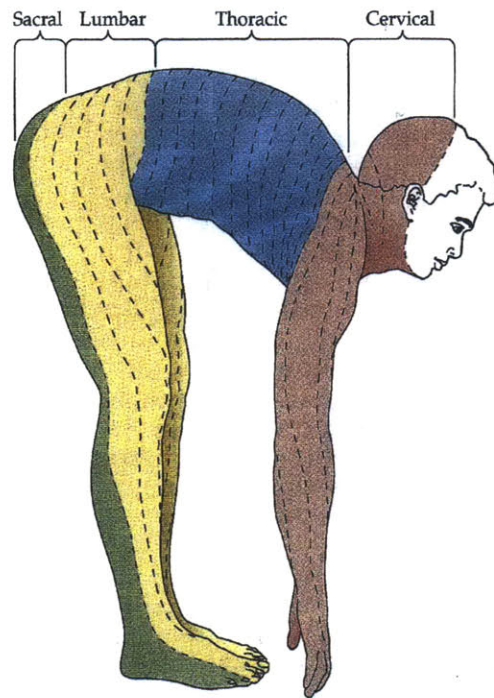


Figure 2-15: The Dermatome Map of the Human Body from (Rosenzweig, Breedlove et al. 2002, pg 232).

The reason for the 4-legged posture shown in the figure is due to the convention described previously in Section 2.1. From a comparison between Figure 2-14 and Figure 2-15, the regions of the skin and the sections of spinal map very closely to one another. The region of the face that is not marked corresponds to the skin that is innervated by the trigeminal sensory neurons that do not connect to the spinal cord but rather connect directly to the brain. Patients with spinal cord injuries will lose sensation in all regions below their injury in the dermatome map, due to the fact that sensory information from those regions of skin cannot make it up the spinal cord and into the brain.

In reality, there is not a clear division between the dermatomes as shown in Figure 2-15. The dermatomes actually overlap as shown in Figure 2-16.

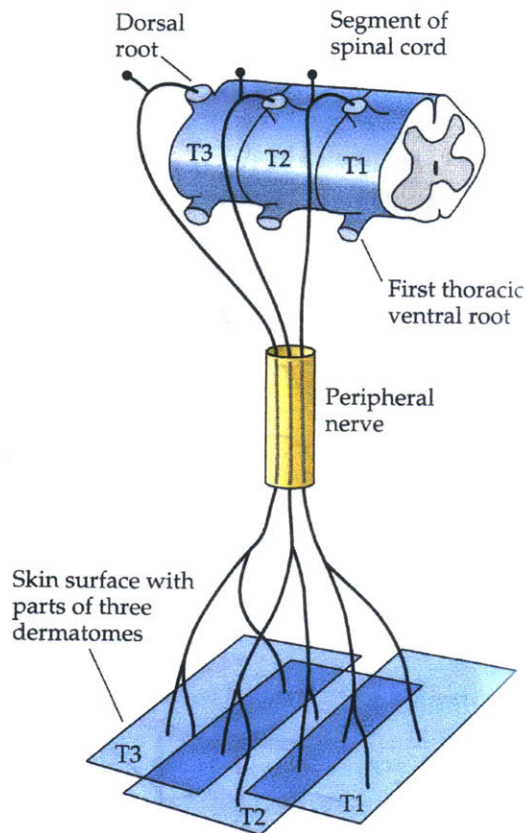


Figure 2-16: The Overlap of Dermatomes from (Rosenzweig, Breedlove et al. 2002, pg 232).

This overlap helps in higher level processing as will be discussed in the next section.

Once inside the spinal cord, there are two paths which somatic information can take on its path to the brain. The first pathway, the dorsal column-medial lemniscal system, is the primary path for touch and proprioception information. The second pathway, the anterolateral system, is the primary pathway for pain and temperature sensation. Both pathways are shown in Figure 2-17.

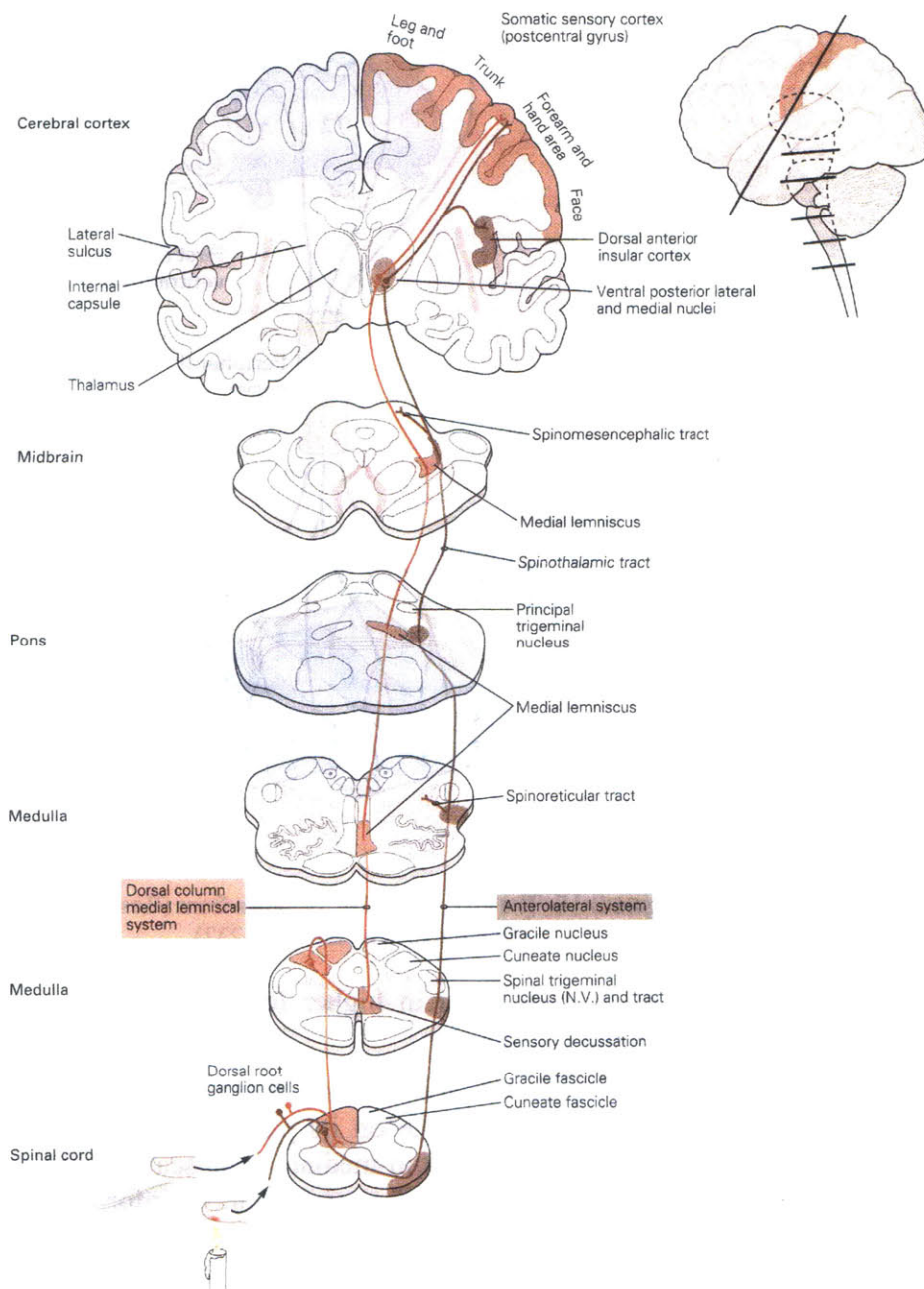


Figure 2-17: The Dorsal Column Medial Lemniscal and Anterolateral Systems from (Kandel, Schwartz et al. 2000, pg 447).

While it appears from the figure that there is a single route in which a specific type of sensory information will travel to the thalamus, this is really not the case. Most sensory information will travel by more than one route (Nolte 2002). But for the sake of simplicity in this discussion, the focus will be on the single primary pathway for touch.

Upon entry into the spinal cord, there is segregation into medial or lateral division based on type of fiber in this pathway. The large diameter, myelinated fibers are contained in the medial division while the smaller, finely myelinated or unmyelinated fibers are contained in the lateral division (Nolte 2002). In addition to this segregation by fiber type, there is an additional segregation based on entry level. Fibers which enter caudal to T6, i.e., to the left of the 6th Thoracic section in Figure 2-15, are grouped in a bundle called the fasciculus gracilis. Those fibers rostral to T6 are grouped in another bundle referred to as the fasciculus cuneatus (Nolte 2002). Each successive layer of fibers adds laterally to the columns already present. Thus a somatotopic map is developed at the level of the spinal cord in which fibers corresponding to the sacral dermatomes are more medial and cervical layer fibers are most lateral (Nolte 2002). Another division occurs based on the type of information. Proprioceptive axons are more ventral than the axons of tactile receptors that are more dorsal in the dorsal column nuclei. In the gracile and cuneate nuclei, the proprioceptive fibers terminate more rostrally than the tactile axons (Kandel, Schwartz et al. 2000).

At the brainstem (the medulla), these primary afferents synapse for the first time in the nucleus gracilis for those fibers grouped in the fasciculus gracilis and the nucleus cuneatus for those fibers bundled in the fasciculus cuneatus. It is here, as shown in Figure 2-17, that sensory decussation occurs – the fibers cross the midline and form the medial lemniscus. Below this point fibers from the right side of the body traveled up the right side of the spinal cord. Above this point, regions in the left side of the brain that deal with somatic sensation correspond to the sensory receptors in the right side of the body. This reversal is seen in other modalities as well. The medial lemniscus continues through the brain and finally synapses in the ventral posterolateral nucleus (VPL) of the thalamus. From here, the third-order fibers continue

on into the postcentral gyrus, otherwise known as to primary somatosensory cortex (Nolte 2002).

At this point before moving onto the somatosensory cortex, a discussion of spinal reflexes, specifically those that pertain to tactile information seems appropriate. Reflexes are involuntary, stereotyped responses to sensory inputs (Nolte 2002, pg 234). All reflexes are contained to the level of the spinal cord and as such do not require higher forms of processing. In most cases, the reflex loop consists of a sensory neuron which synapses onto an interneuron which in turn synapses onto a motor neuron which results in a response. A diagram of a reflex arc based on touch is shown in

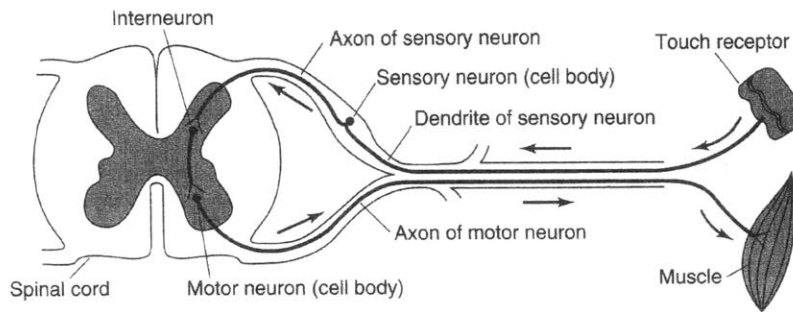


Figure 2-18: The Reflex Arc from (Sekuler and Blake 2002, pg 519).

Because the entire system occurs within the level of the spinal cord, usually with only a single interneuron, the response can be very fast. More complicated reflexes also involve coordination between limbs, such as with crossed effects, in which an opposite limb must counteract the motion. For example, when you step on a tack and pull one leg away suddenly the opposite leg counteracts and prevents you from falling down (Nolte 2002). A further discussion of reflexes can be found in Chapter 10 of (Nolte 2002) and Chapter 36 of (Kandel, Schwartz et al. 2000).

The entire path from mechanoreceptor to primary somatosensory cortex consists of only 3 synapses. The first occurs when the axon of the dorsal root ganglion cell synapses at either the gracile or cuneate nucleus in the medulla just prior to decussation. The second synapse occurs when the medial lemniscus synapses at the VPL. The final synapse occurs when a fiber from the VPL synapses at the postcentral gyrus. At each

level of the CNS, the somatotopic map is preserved. In the next section, the processing and organization of the somatosensory cortex will be discussed.

2.7 The Somatosensory Cortex

The somatosensory cortex can be thought of as having three major divisions – the primary somatosensory cortex (SI), the secondary somatosensory cortex (SII), and the posterior parietal cortex (Kandel, Schwartz et al. 2000). Figure 2-19 illustrates these divisions in relation to the rest of the brain.

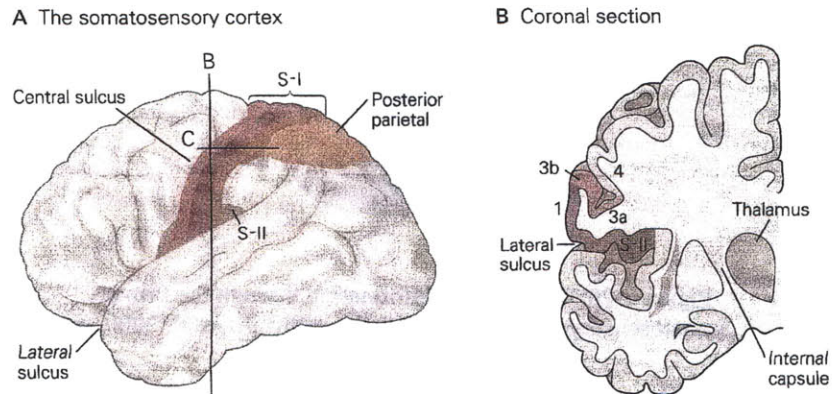


Figure 2-19: The 3 Divisions of the Somatosensory Cortex from (Kandel, Schwartz et al. 2000, pg 453).

The primary somatosensory cortex (SI) consists of Brodmann's areas 3a, 3b, 1, and 2. Touch information is sent to areas 3b and 1, while proprioception is sent to areas 3a and 2. The majority of fibers ascending from the VPL in the thalamus terminate in 3a and 3b, while a small percentage terminate in areas 1 and 2. Areas 1 and 2 also receive information from areas 3a and 3b. It is also possible for processing to occur both serially and in parallel due to the nature of the interconnections between the regions as shown in Figure 2-20 (Kandel, Schwartz et al. 2000).

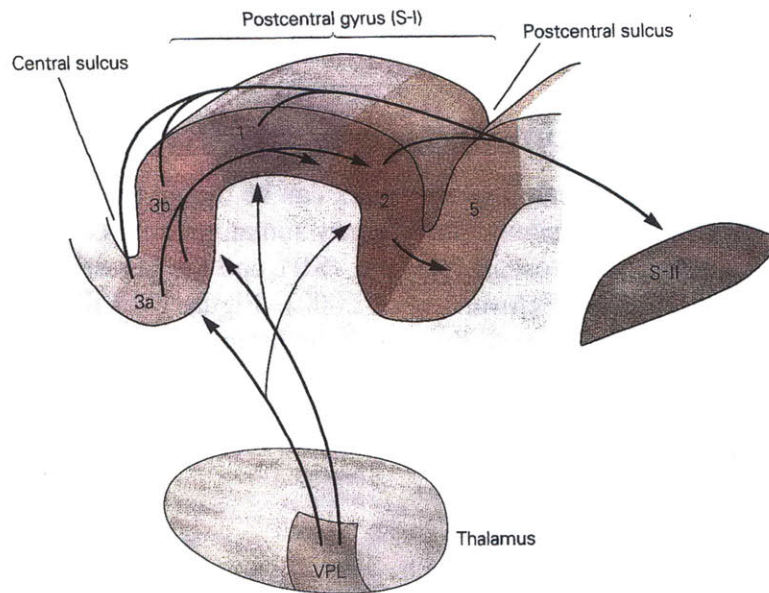


Figure 2-20: The Flow of Information through the Primary Somatosensory Cortex from (Kandel, Schwartz et al. 2000, pg 453).

The secondary somatosensory cortex (SII) receives input from the primary somatosensory cortex and projects to the insular cortex, which then passes information to the temporal lobe for tactile memory (Kandel, Schwartz et al. 2000). The posterior parietal cortex consists of Brodmann's areas 5 and 7. In this region, both sides of the brain are connected through the corpus callosum, the bundle of axons which cross from one hemisphere to the other shown in . Thus this is the first point in which somatic information from both sides of the body is integrated. The posterior parietal cortex receives input from SI as well as the pulvinar and projects to the motor areas of the frontal lobe, and thus is an important part in both sensory initiation and the guidance of movement (Kandel, Schwartz et al. 2000, pg 453). Proprioceptive and tactile information, as well information from the two hands are integrated in Area 5. Visual, tactile, and proprioceptive inputs are integrated to combine visual and stereognosis (the detection of the shape of objects grasped in the hand) information together in area 7 (Kandel, Schwartz et al. 2000).

The somatotopic map continues in each region of the primary somatosensory cortex (3a, 3b, 1, and 2). However, as can be shown in Figure 2-21, this map does not reflect the body surface but rather the number of receptors in each region.

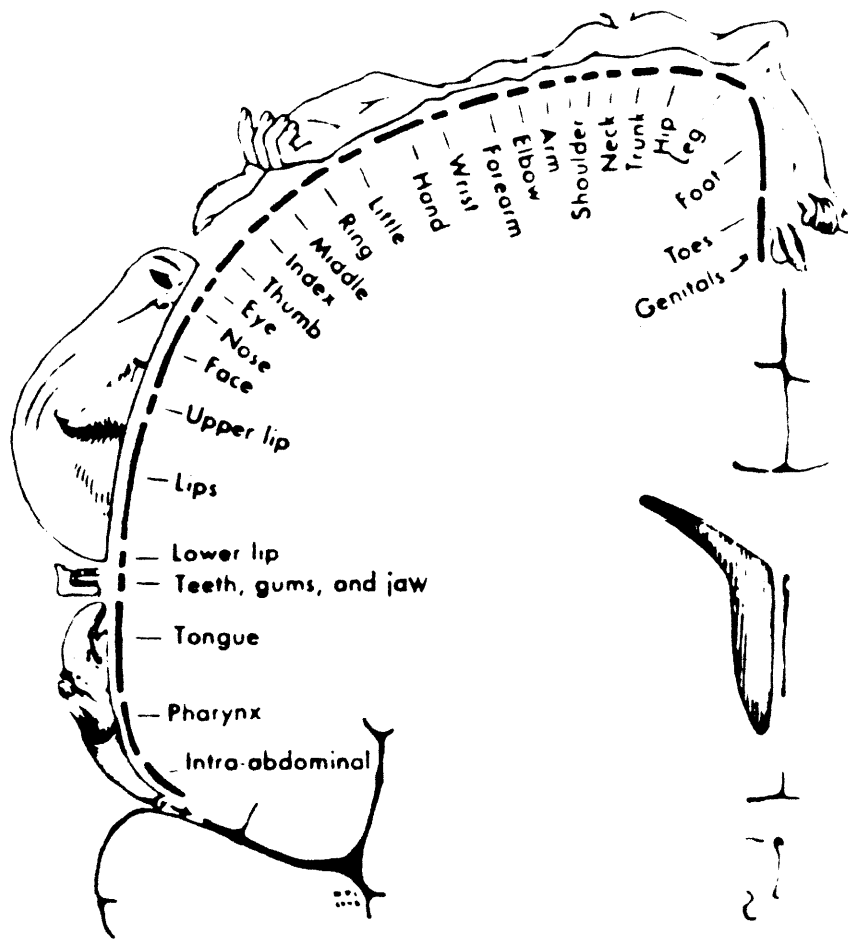


Figure 2-21: The Somatotopic Map of the Primary Somatosensory Cortex from (Penfield and Rasmussen 1950/1978).

Regions such as the fingers, lips, and tongue, which have a high density of receptors, are devoted to a larger area of cortex than regions such as the trunk which have a much lower density. This map has also been referred to as the Homunculus, or “little man,” which is shown in Figure 2-22. In this image, the size of each

body region reflects the number of receptors present in that location.

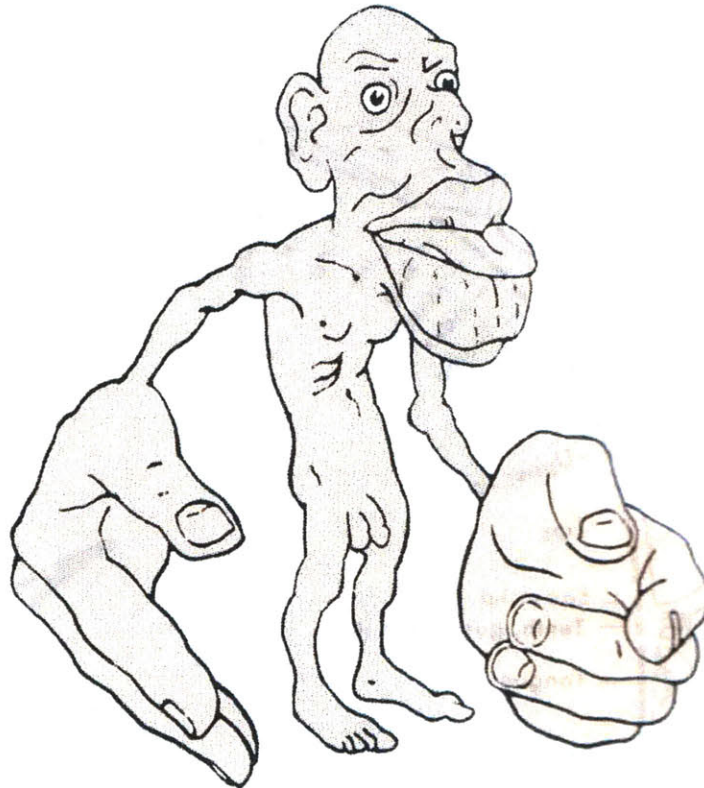


Figure 2-22: The Homunculus from (Rosenzweig, Breedlove et al. 2002, pg 233).

Another further division occurs in the cortical columns. The cortex consists of six layers, with each layer corresponding to a specific communication or processing pathway. A section from area 3b is shown in Figure 2-23.

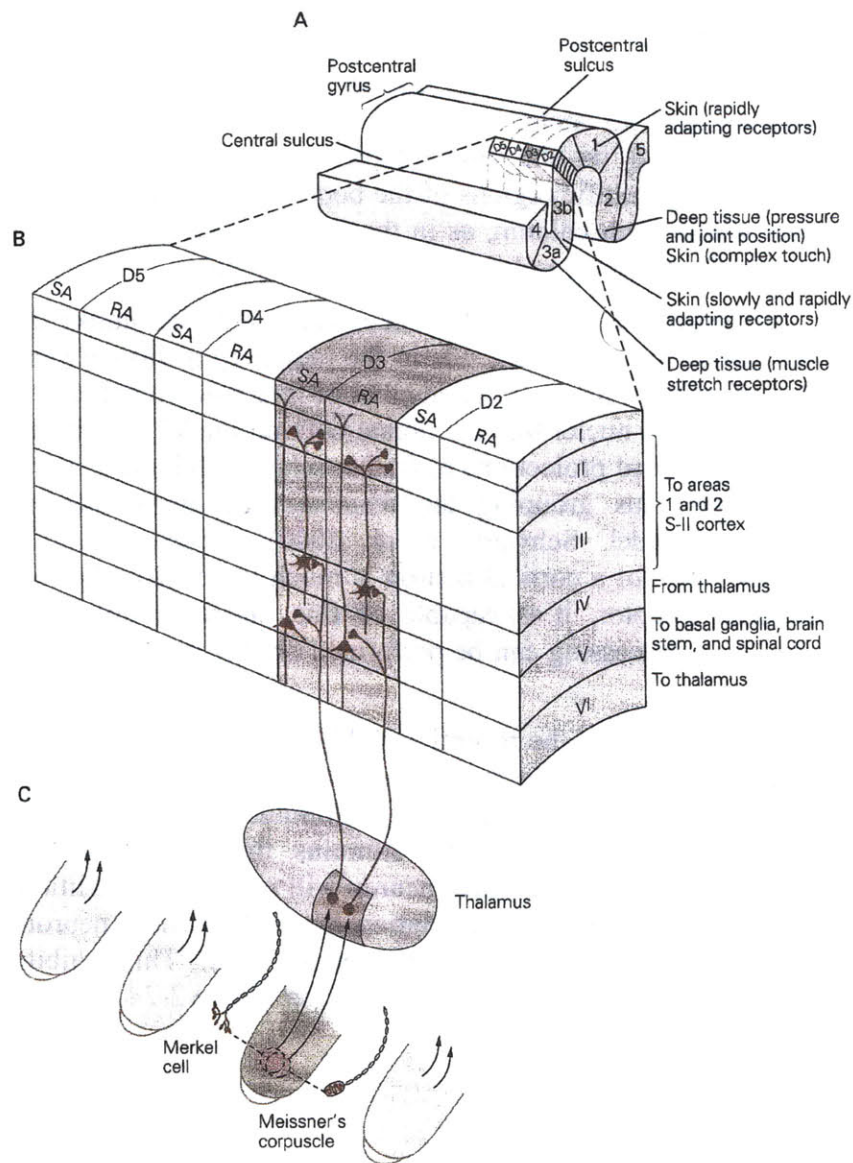


Figure 2-23: Cortical Columns in the Primary Somatosensory Cortex from (Kandel, Schwartz et al. 2000, pg 459). In A, the location of the section of Area 3b chosen for detail in B is shown. B shows the columnal organization. C shows the input, overlapping receptive fields from RA and SA receptors in the fingertip.

Input to the cortex from the thalamus enters through cortical layer IV. Layers V and VI are used for communication to other regions of the CNS. Layers II and III are used for communication to areas 1, 2, and SII. Each column is first organized based on the somatotopic map; columns of cortex correspond to specific regions of the body. A second organization occurs within each column, as in the case of Area 3b, into inputs from rapidly adapting and slowly adapting receptors.

Cortical neurons also have receptive fields, but unlike those of the dorsal root ganglion cells in the periphery a cortical neuron will receive input from a large number of mechanoreceptive fibers, due to the relay nuclei like the dorsal column nuclei and thalamic nuclei which send projections to further relay nuclei and inhibitory interneurons thus grouping the responses of many individual receptors (Kandel, Schwartz et al. 2000). Even though the receptive field for a cortical neuron is much larger than that of an individual receptor, it is capable of fine discrimination. Thus higher level processing can be performed on this larger number of cells.

The center of the receptive field has a region of maximum sensitivity. As a stimulus moves closer to the center of a receptive field, the response increases. As a stimulus moves toward the periphery from the center of the stimulus, the response becomes weaker until finally the cortical neuron will not fire. In addition to this preferred location of stimulation for each cortical neuron, a region of inhibition surrounds the receptive field. This inhibitory surround allows for finer acuity as shown in Figure 2-24.

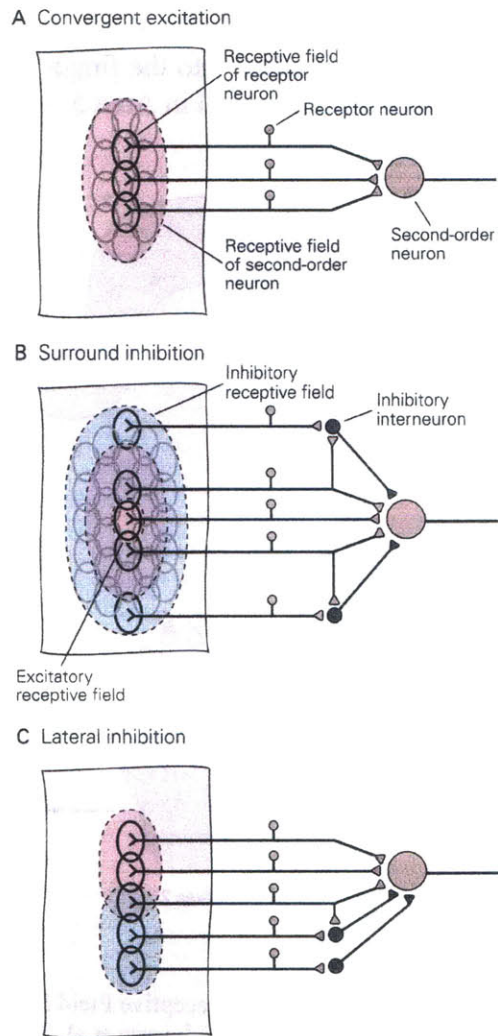


Figure 2-24: Combinations of Lower Order Neurons to Form Higher Order Neurons from (Kandel, Schwartz et al. 2000, pg 463).

Lateral inhibition helps with feature detection as it can be used to help discriminate edges.

As information from lower level cortical regions, such as 3a and 3b, is projected to higher-level cortical regions, such as 1, 2, 5, and 7, the size of the receptive field increases, but the processing becomes more complex as shown in Figure 2-25. The receptive fields of lower cortical areas combine into the fields

of the higher levels as shown below – a single region on one fingertip in Area 3b is combined with those of the other fingertips in Area 1 then further combined into the finger pads in Area 2, and finally the two hands are integrated in Area 5.

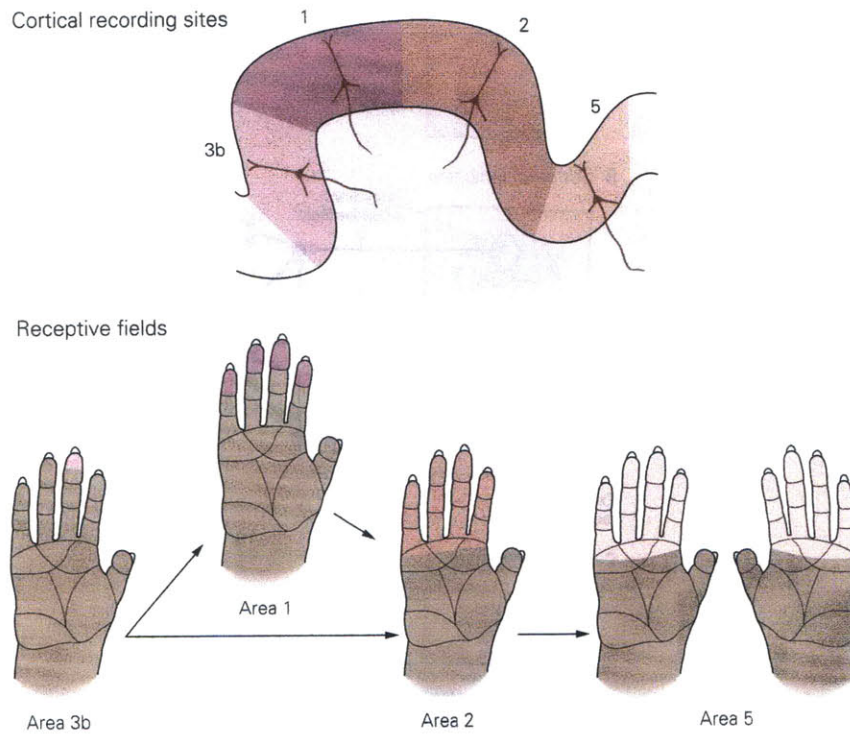


Figure 2-25: The Increase in Receptive Field Size in Higher Cortical Areas from (Kandel, Schwartz et al. 2000, pg 455).

The higher-level cortical regions have more complex neurons. For example, there are motion-sensitive (Areas 3b, 1, and 2), direction-sensitive (Areas 1 and 2), and orientation-sensitive neurons (Area 2) (Hyvarinen and Poranen 1978; Kandel, Schwartz et al. 2000). Motion-sensitive neurons do not respond to skin indentation but rather prefer motion in any direction, as shown in Figure 2-26.

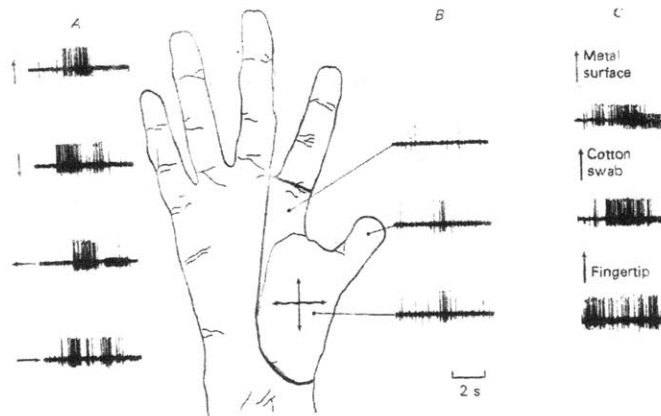


Figure 2-26: Response of a Motion-Sensitive Neuron in Area 1 from (Hyvarinen and Poranen 1978, pg 526). The dark lines on the hand indicate the size of the receptive field. A shows the response of the motion-sensitive neuron to motion in four orthogonal directions. B shows the lack of response to punctate stimuli at each of the 3 indicated locations. C shows that a similar response was produced for distally moving stimuli regardless of type.

Orientation-sensitive neurons are capable of determining the angle of an object placed on the skin as shown in Figure 2-27.

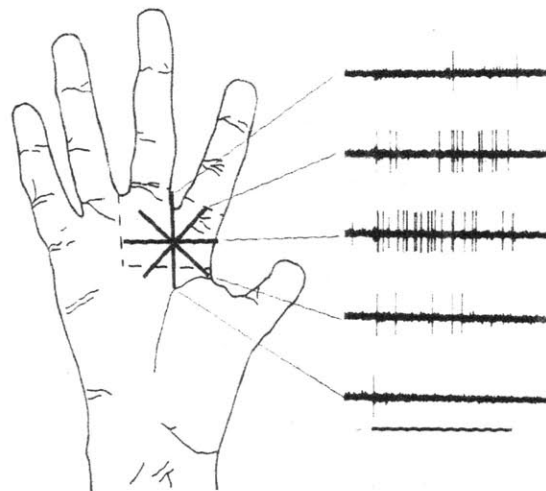


Figure 2-27: The Response of an Orientation-Sensitive Neuron in Area 2 from (Hyvarinen and Poranen 1978, pg 531). The Receptive field is indicated by the dotted lines. The solid lines indicate the orientation of a 0.7 mm wide metal bar indented into the skin. The best performance was seen at an orientation perpendicular to the axis of the hand.

Direction-sensitive neurons, shown in **Error! Reference source not found.**, are capable of determining the direction of the object and fire when an object is moved across the skin in a preferred direction and are silent otherwise.

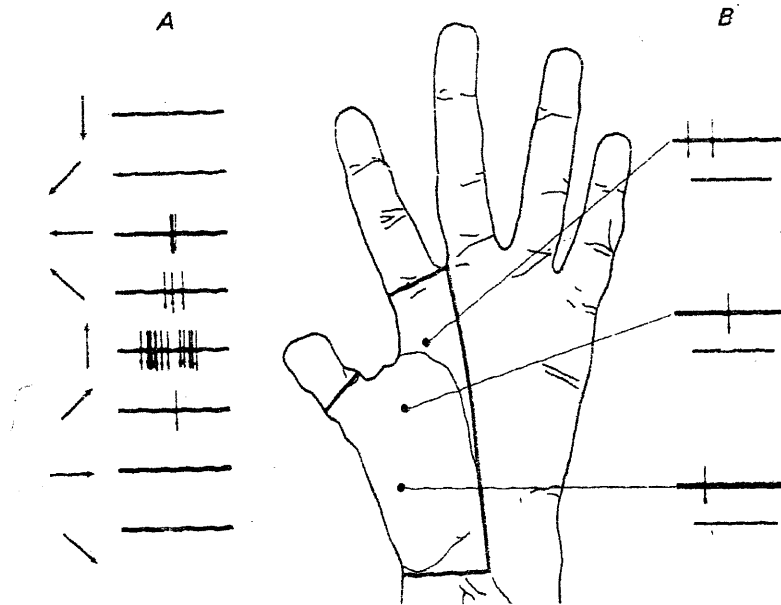


Figure 2-28: Response of a Direction Sensitive Neuron in Area 1 from (Hyvarinen and Poranen 1978, pg 526). The outlined region on the palm corresponds to the receptive field of this cell. A shows the response of the neuron to moving punctate stimuli in the indicated direction. B shows the response of punctate stimuli indented into the skin at each indicated point.

One possible way a direction-sensitive neuron can be assembled from a collection of lower level relay neurons is shown in Figure 2-29. By the spatial orientation and lateral inhibition of these relay neurons, direction can be inferred from the response. Thus a bar moving through a region of excitation then inhibition, or vice versa, will imply movement in one direction. However, movement that passes through both excitatory and inhibitory regions simultaneously will not show a direction sensitivity.

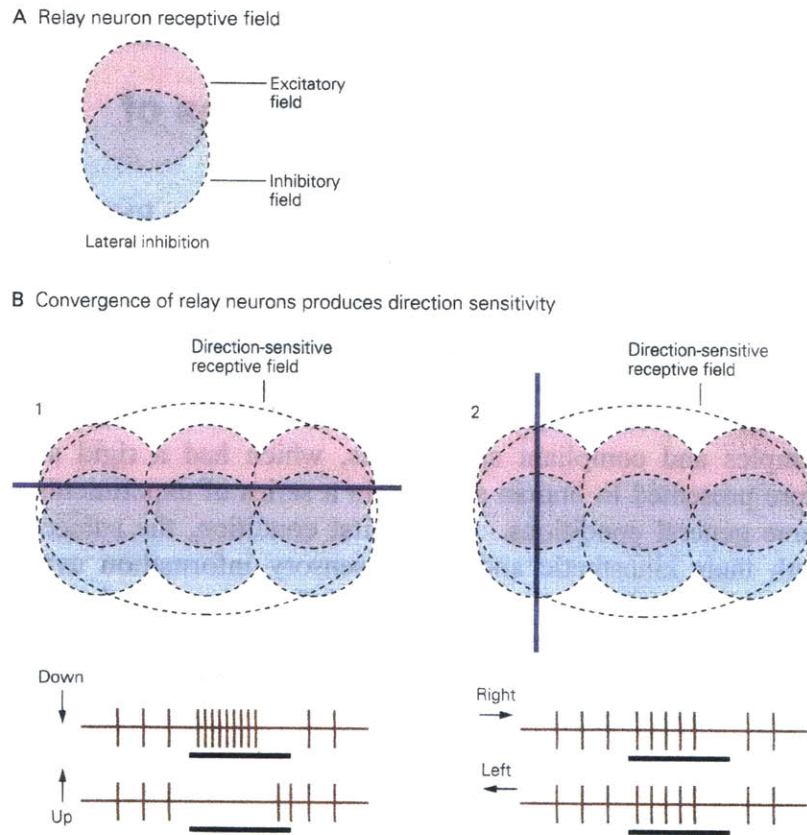


Figure 2-29: Creation of a Direction-Sensitive Neuron from the Spatial Arrangement of Presynaptic Inputs (Kandel, Schwartz et al. 2000, pg 467). A shows the lateral inhibition of a relay neuron's receptive field. B shows how groupings of these relay nuclei can be combined to produce a direction-sensitive cortical neuron. In B1, the bar moves perpendicular to the excitatory and inhibitory fields, thus a downward movement will first cross a region of excitation and then inhibition as shown in the down spike train. In the up spike train, the bar first moves through a region of inhibition then excitation. If a bar moves parallel as shown in B2, there will not be a difference in response as a function of direction since both excitation and inhibition regions are activated simultaneously.

In addition, other cells and regions of the somatosensory cortex as well as other modalities of the somatic senses show a similar construction of higher order cortical neurons based on the combination of lower order neurons. Thus it becomes that the

“words” and “sentences” of perception through touch are formed by a combination of the alphabet of lower level processing.

2.8 Other Findings from Studies of Humans

In addition to the cell recordings in both the PNS and CNS, a series of other studies have been conducted which also shed light on the idea of an alphabet of somatic perception.

The detection of softness or hardness has been a realm of very little research. One study assessed the perception of softness in humans (Srinivasan and LaMotte 1995). In this study, rubber samples and compliant spring cells, which had a rigid surface, were presented to human subjects in a series of experiments, with three general conditions. In the first condition, the subjects had both their kinesthetic and tactile sensory information available, i.e., this was the case of “active touch.” In the second condition, the cutaneous information was removed through the use of local anesthesia on the finger pad, but kinesthetic information remained intact in this altered form of “active touch”. The final condition was passive touch, in which the stimulus was pushed into the finger pad under computer control; thus only cutaneous information was present.

While the subjects were able to discriminate the softness of the rubber samples using “active touch;” the discrimination of the compliance of the spring cells was poorer and required more applied force to do so. When cutaneous information was removed during the second condition, kinesthetic information alone was not enough to discriminate between the rubber samples or the spring cells. Under passive touch, in which the kinesthetic information was removed, subjects were capable of discriminating between the rubber samples, but not the spring cells. Thus for objects with rigid surfaces both kinesthetic and cutaneous information is required. Objects with deformable surfaces can be encoded by tactile information alone.

Another study used multi-dimensional scaling to group objects along three different axes (Hollins, Faldowski et al. 1993). In this study, a series of 17 objects, including wood, sandpaper, and velvet, were first placed beneath the index finger, then scanned across the fingertip from proximal to distal, and finally removed.

Subjects were allowed to assign the object a rating along 5 different scales, each pertaining to the object's texture. From the analysis of this experiment, the 3 dimensions were roughness-smoothness, hardness-softness, and elasticity or "springiness."

3 The Healing Power of Touch: Companion Animals and Pet Therapy

The relationship between humans and animals has existed for thousands of years. In 1976, a 12,000 year old human skeleton was uncovered in a tomb in holding the remains of a puppy. Simon Davis, the archaeologist who uncovered the find, was convinced the puppy was being held in an affectionate posed (Cusack 1988). In this chapter, some of the benefits of a relationship with animals will be described. The chapter will end with a discussion of the potential populations who can benefit from pet therapy.

3.1 Benefits of a Relationship with Animals

Prior to 1983, much of the published scientific literature contained little evidence of a documental association between pet contact and human health (Garrity and Stallones 1998). Much of this information lacked a strict scientific method and relied much on anecdotal evidence. However, since that time a large number of research studies have looked at the ways in which animals can provide benefit.

Karen Allen conducted an interesting study in which 45 adult women performed a standard experimental stress task in the presence of a female friend, a pet dog, or neither (Allen and Michelman 1990). A set of physiological measurements (skin conductance, systolic and diastolic blood pressure, and pulse rate) were recorded for each experimental case. The study showed that the presence of the pets lowered the stress in the subjects compared to a female friend. Allen argues that the reason for this result is that the pet acts as a buffer in the sense that it is non-evaluative in the way that the person's friend may be.

Other studies have shown that pet therapy works by the same biochemical ways of the relaxation response in acting on the adrenal and other corticosteroid or "stress hormones" resulting in a lowered blood pressure, heart, and respiratory rate (Ballarini

2003). Thus it appears that the animals are causing a real biological change which results in lowering stress.

Changes in the hormonal levels are seen in the animal as well. Odendaal performed a study in which the blood pressure and the hormonal levels of oxytocin, prolactin, dopamine, cortisol, β -endorphin, and β -phenylethylamine were monitored during the experiment. The experiment compared the before and after measurements of the above value for dog owners vs. people interaction with unfamiliar dogs, and dog interaction vs. quiet book reading (Odendaal 2000). This study showed significant increases in both humans and dogs for β -endorphin, oxytocin, prolactin, phenylacetic acid, and dopamine. Cortisol for the humans decreased significantly.

3.2 Populations that can Benefit from Pet Therapy

An entire branch of therapy has emerged from the studies of the benefits of the human and animal bond. The field is referred to as animal assisted therapy (AAT) or pet therapy. In many cases this therapy is performed in numerous settings such as education, prisons, nursing homes, hospices, people with developmental disabilities, and many other populations as well. A set of anecdotal evidence from interaction between humans and animals in a therapy situation can be found in chapter 7 of (Cusack 1988).

Many of the studies of animal assisted therapy look at the changes in the psychological state or mood of people when they are exposed to animals. Muschel conducted a pilot study with a series of terminally ill cancer patients and found that the exposure to animals reduced their anxiety and despair (Muschel 1984). Haughie studied the effects of animals and photographs on the interaction of elderly psychiatric patients and found that the dog intervention was the most effective (Haughie 1992). Kongable found that Alzheimer's patients increased their social behavior with staff as well as an increase in awareness when a dog was brought into a home for veterans (Kongable, Stolley et al. 1990). There are numerous other studies which show the positive benefits of companion animals.

The Eden Alternative is a new approach to the design of elder care facilities which was developed to address many of the

current problems with nursing homes. Dr. William H. Thomas, M.D. – the founder of this new approach – describes the current state of nursing homes as:

“Companionship is food and drink for the human spirit. All people, in all cultures, in all of recorded history, have sought the pleasures of companionship and have suffered when it was lacking. Current nursing home practice does not provide residents with the companionship they need. There are activities and treatments, not to mention nonstop ‘caregiving,’ but none of these offer real companionship.” (Thomas 1996)

The approach of the Eden Alternative involves a series of steps taken to bring nature into the nursing home. One part of this design is the use of animals in the nursing home. Many of these animals are allowed to roam from room to room of the facility. In addition, a series of song birds are located in cages throughout the building and the residents can help take care of these birds with the assistance of staff. Since employing this approach, of which companion animals are a large aspect, the number of prescribed medications in the facility has been reduced dramatically. In addition the general mood of the residents has improved.

In the next chapter, a discussion of a new form of therapy – robot therapy – will be described. This type of therapy is being employed in cases where animals are not available due to various reasons which will be discussed in the next chapter.

+

4 Previous Robotic Implementations

4.1 Touch Sensing and “Sensitive Skins”

Currently, much emphasis of the tactile processing for robots has been limited to grippers or other types of manipulators (Howe 1994; Martin, Ambrose et al. 2004). The manipulation of objects is a very difficult task but should not be the sole realm of tactile sensors. Portions of this section originally appeared in (Stiehl 2003).

The idea of a “sensitive skin” was first proposed in June of 2001 in the first issue of the IEEE Sensors Journal. In the abstract of this article the authors write:

“Sensitive skin is a large-area, flexible array of sensors with data processing capabilities, which can be used to cover the entire surface of a machine or even a part of the human body. Depending on the skin electronics, it endows its carrier with an ability to sense its surroundings via the skin’s proximity, touch, pressure, temperature, chemical/biological, or other sensors. Sensitive skin devices will make possible the use of unsupervised machines operating in unstructured, unpredictable surroundings—among people, among many obstacles, outdoors on a crowded street, undersea, or on faraway planets. Sensitive skin will make machines “cautious” and thus friendly to their environment. This will allow us to build machine helpers for the disabled and elderly, bring sensing to human prosthetics, and widen the scale of machines’ use in service industry...” (Lumelsky, Shur et al. 2001, pg 41).

The goal of a “sensitive skin” for robotics implies covering the entire surface area of the robot with a collection of sensors. In a similar idea to the alphabet of somatic perception, discussed in Chapter 2, a wide variety of sensors should be used. Such a design poses a series of design challenges which must be considered.

The first is the notion of flexibility. If the skin and the sensing system of the robot are to be the same entity, all of the wiring, sensing elements, and local processing, in addition to the material of the skin, itself must be able to bend around joints, conform to curvature, and stretch while still providing accurate sensor readings. One approach as to how this challenge may be met comes from the realm of conductive fabric sensors (DeRossi,

Carpi et al. 2002; Sergio, Manaresi et al. 2002). Another idea is to eliminate the wiring entirely through the use of inductive coupling (Hakozaki, Hatori et al. 2001) or optics (Yamada, Goto et al. 2002). The approach taken in this thesis is to decouple the skin from the sensor. Thus a silicone skin, which will be described in Chapter 7, covers the sensors which are rigidly mounted to the hand.

Another design challenge is the integration of processing elements into the skin. Some initial work has been done in this realm, combining both sensing and processing elements, for both a shear-stress sensor (Xu, Tai et al. 2002) and a fingerprint detector (Shigematsu, Morimura et al. 1999). How the skin processes information from a large number of sensors poses a similar problem to those researching wireless sensor networks, mainly how can a network of distributed sensing and processing elements communicate information to each other. Some approaches to this problem are discussed in (Paradiso, Lifton et al. 2004).

As robots become a part of daily life, giving them a “sensitive skin” will be necessary. Such a sensory system will promote social interaction between the robot and the humans who share its workspace, as the sense of touch could be another way in which training of the robot is conducted.

4.2 Companion Robots

Chapter 3 discussed the many benefits that pets can provide. Unfortunately, companion animals are not always available to everyone. There are numerous places where pets are not allowed due to health code restrictions, fear of bites, allergies, or other concerns. In addition, pet therapy in many nursing homes is a scheduled activity. The animal is brought into the nursing home for only a few hours each week and must be constantly supervised by a pet therapist. There also exist populations of people who would love to have a pet that they could care for, but can't due to mental or physical handicaps. Thus, there exists a real need for some form of pet surrogate. Out of this need a new type of robot – the robotic companion has emerged.

More so than in any other country, Japan has embraced the idea of using robots to care for its elder population which is rapidly growing. According to recent data from the National Institute of

Population and Social Security Research in Japan, currently 3.9 working adults support one senior citizen. This ratio is expected to decrease to 2:1 by 2030 and fall the 1.5:1 by 2050. Thus there has been a large emphasis placed upon the use of robots to help care for the elderly.

Four robotic companions have been developed in Japan. They are shown in Figures 4-1 through 4-4.



Figure 4-1: Sony AIBO ERS-7 (Sony Product Literature).

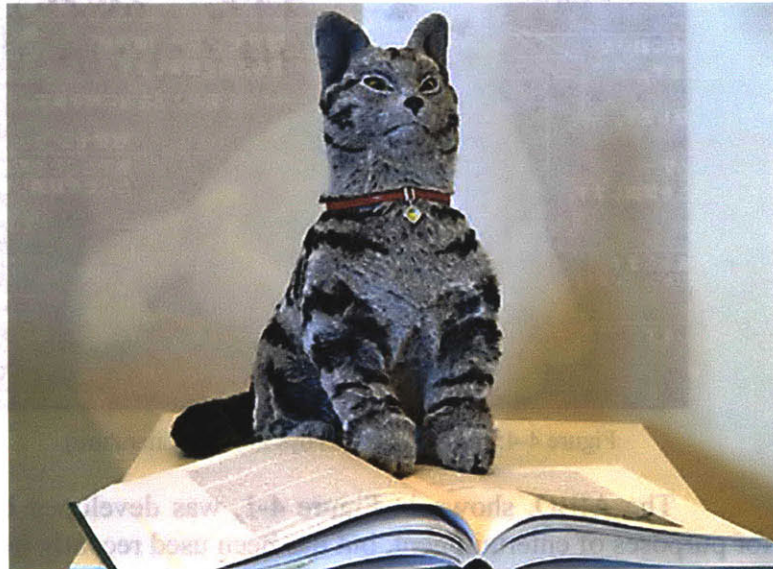


Figure 4-2: Omron NeCoRo (Omron Corporation Product Literature).



Figure 4-3: Paro (Paro Product Literature).

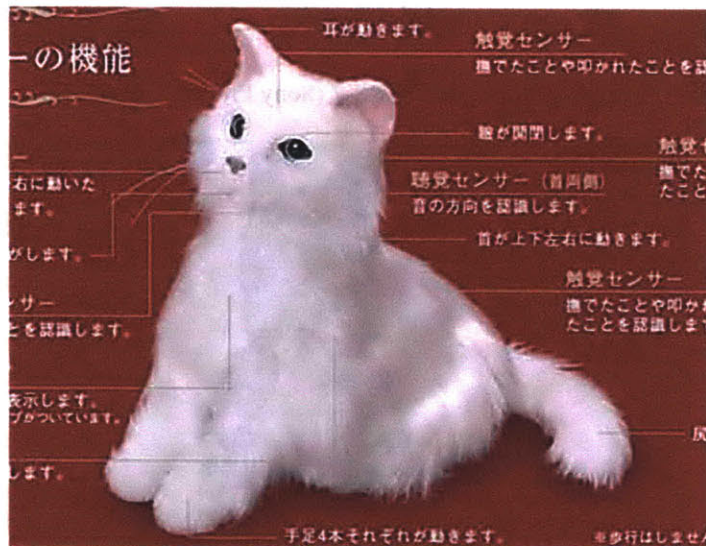


Figure 4-4: NearMe (Sega Toys Product Literature).

The AIBO, shown in Figure 4-1, was developed by Sony for purposes of entertainment, but has been used recently in robotic therapy applications as well (Tamura, Yonemitsu et al. 2004). In the Tamura study, an earlier version of the AIBO was shown to patients with dementia. A toy dog and a fur covering over the AIBO were also shown. The authors report that AIBO resulted in eliciting more interaction from the demented case. However, it is not clear from the study if this was due to novelty or due to another factor.

In contrast to the other robotic companions, AIBO is not furry. The robot also features the lowest number of tactile sensors

of the companion robots described in this chapter. The emphasis of AIBO's design is on the motion of the robot and the interaction. Thus AIBO is better suited for playing with on the floor than holding in one's arms.

The Omron NeCoRo, shown in Figure 4-2, and the NearMe, shown in Figure 4-4, are both of similar design, but differ in complexity. They each feature a fur covering over a hard plastic frame. There is no padding between the fur and the plastic, thus the robot feels hard to the touch. Each robot, like the AIBO, features a discrete set of touch sensors. These sensors are only located in specific regions of the body, and thus, there are large areas of the body which are not sensed. The NeCoRo has been used in a series of studies in person-robot communication (Libin and Libin 2004).

The Paro is currently the best implementation of a robotic companion. It features a soft hygienic fur. The robot also has sensors to detect light, posture, sound, and touch. The touch sensors are large patches all over the surface of the robot, under the fur. The total number of touch sensors is on the order of the NeCoRo and NearMe.

Many user studies have been conducted with the Paro involving elder adults (Wada, Shibata et al. 2002), young children (Shibata, Mitsui et al. 2001), and in other countries (Shibata, Wada et al. 2003). It is important to note that many of the studies feature largely subjective results and are usually reported from one or two interactions. It would be interesting to see how the long term interaction with a Paro develops.

In Section II, the Huggable, a therapeutic robotic companion for relational, affective touch will be described. Unlike the robot companions of this section, it was purposely designed to look like a fanciful creature – a teddy bear. In addition, the Huggable features a high density, full body “sensitive skin” unlike each of these robots which feature only a handful of sensors. With the large array of sensors, a greater repertoire of affective touch interactions can occur.

5 The “Somatic Alphabet” Approach towards the Design of “Sensitive Skins”: An Overview

In the first chapter of this section, the complexity of the somatosensory system in humans and animals was discussed. The vast number of sensory inputs has been engineered by evolution over millions of years so that we can quickly interpret that sensory information and respond appropriately. If the pen you are holding slightly slips in your grasp, you reflexively tighten your grip. The goal of this chapter is to outline one approach of abstracting a design methodology for the field of robotics in creating “sensitive skins.” We call this approach the “Somatic Alphabet” (Stiehl 2003; Stiehl and Breazeal 2004; Stiehl, Lalla et al. 2004).

5.1 The “Letters” of the “Alphabet”

The somatosensory system of humans and animals consists of four main modalities – temperature, touch, pain, and kinesthetic information. Within each of these modalities are a collection of sensors responsible for encoding some region of that sensory stimulus. In many cases there are well established differences between sensor types for a given stimulus. More intuitively, the temperature information of an object you are touching is not encoded by the receptors responsible for muscle tension in your hand. Thus nature has designed a system that uses various peripheral sensors to divide up a complicated world into distinct features, or primitives. In the “Somatic Alphabet” approach these primitives are the “letters” of the alphabet.

As there is not a single “somatic” sensor in our skin, thus we should not build “sensitive skins” for robots relying on only one sensor to encode all the properties of the world encountered through touch. Currently there exist a wide variety of commercially available sensors which function in similar ways to receptors in our skin. Thermistors, RTDs, and thermocouples measure temperature. Potentiometers measure the kinesthetic property of joint angle position. Force sensitive resistors, load cells, or vibration sensors measure touch information. Finally, pain can be encoded as the extremes of temperature or touch. Additionally within each of these modalities, sensors can be

selected or processed differently to encode different regions of the modality. For example the same force sensor can be paired with different resistor values in a voltage divider to detect sensitivity to different ranges of applied force. Thus, as was originally described in (Lumelsky, Shur et al. 2001), a “sensitive skin” must feature a collection of different sensors, or “letters” in our approach.

5.2 The “Words” of the “Alphabet”

In the biological somatosensory system, the receptors in the skin travel from the periphery, up the spinal cord, and into the brain. In the somatosensory cortex, these receptors are combined into receptive fields for higher order processing, such as direction of motion or orientation as was previously described in Chapter 2. This cortical level processing forms the “words” of the “Somatic Alphabet” by combining the “letters” of sensory information to convey meaning.

In the robotic “sensitive skin” the location and type of sensors used is known. The information from these sensors must travel from the periphery of the robot into a central processing computer and be combined to ascertain a snapshot of the world in time. Direction of motion, centroid location, and other “words” created by combining the sensor outputs into meaningful receptive fields help to allow the robot to perceive and react to the ever-changing complex human world.

5.3 The “Sentences” of the “Alphabet”

Our perception of the world doesn’t consist of only the sense of touch, but rather we combine all our senses to create a much richer understanding. For example the surface texture, the weight, the color, and the scent all combine to tell you that the object you are holding is an orange and not a pineapple. Thus we combine the “words” of the “somatic alphabet” with our other senses to form the “sentences” of perception.

In many robotic systems visual and auditory information are processed. By combining these senses with tactile information to form “sentences” much richer interactions can occur. For example, one such interaction could consist of the robot being told to pick up the soft red ball. Auditory processing is used to parse

the speech. Visual processing is used to find the ball and distinguish it from the other colored objects. Finally, tactile processing combined with motor control is used to grasp the ball and distinguish it from the hard red ball sitting on the table. Additionally, the motion of the ball in the robot's hand is calculated using the "words" of object location and direction of motion to keep it from falling out of its grip. Softness, direction of motion, and location in the hand are calculated from combining the individual sensors, or "letters," of the hand into receptive fields. Figure 5-1 shows a diagram of the "Somatic Alphabet" approach for this case.

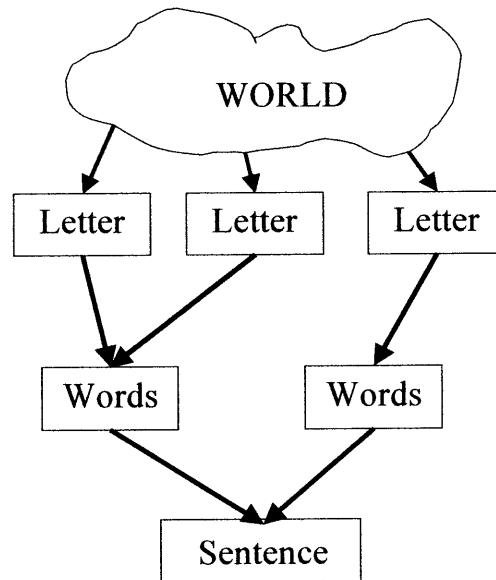


Figure 5-1: Diagram of the "Somatic Alphabet" Approach

5.4 Current Implementation

The next sections describe the implementations of the "Somatic Alphabet" for two different robots – Leonardo, a many degree-of-freedom, highly complex, sociable, humanoid robot (described in Section II), and the Huggable, a low degree-of-freedom, portable, therapeutic, relational robotic companion for affective touch (described in Section III). While an entire "sensitive skin" has not been implemented in either case, the sensate regions allow for an initial exploration.

In Section II, a new pair of sensate hands for Leonardo will be described. These hands combine a series of force sensing resistors, the “letters,” into different receptive fields, the “words.” Each receptive field is then processed to determine the centroid location, direction of motion, and orientation of an object. In Section III, a section of the arm of the Huggable will be described. This section features three types of sensors, or “letters,” – quantum tunneling composite (QTC) force sensors, temperature sensing thermistors, and electric field sensors. These sensors are then combined in a similar fashion as the hands of Section II to form the “words” of centroid location and motion. Finally affective processing is done using these “words” to determine the type of affective interaction, such as petting or slapping.

Section II: Leonardo

6 Leonardo's New Hands: An Overview

6.1 Leonardo, A Sociable Robot

The goal of the Robotic Life Group at the MIT Media Lab is to build capable and appealing robot creatures inspired from the science of animal and human behavior which are engaging to humans and as such encourage social interaction between humans and robots. Leonardo, shown in Figure 6-1, was created through a collaboration with Stan Winston Studio, the four-time Academy Award-winning special effects studio responsible for such characters as "Teddy" in A.I. and the animatronic dinosaurs of Jurassic Park.



Figure 6-1: Leonardo. Photo copyright Sam Ogden. Leonardo character design copyright Stan Winston Studio

As can be seen from Figure 6-1, Leonardo was designed to look like a creature. Unlike traditional humanoid robots, which usually have a hard exterior and low facial movement, Leonardo was designed to have an organic look and feel. In addition to its furry exterior, foam latex hands, and silicone face, over 60 degrees of freedom allow for a very lifelike range of movement with an emphasis on expression and communication. Currently, Leonardo is the most expressive robot in the world today.

In addition to serving as a research platform for lifelike, organic movement, Leonardo also is a test bed for work in sociable robots and Human Robot Interaction (HRI). A sociable robot is defined in Professor Cynthia Breazeal's "Designing Sociable Robots" (Breazeal 2002) as:

"... a sociable robot is able to communicate and interact with us, understand and even relate to us, in a personal way. It should be able to understand us and itself in social terms. We, in turn, should be able to understand it in the same social terms – to be able to relate to it and to empathize with it. Such a robot must be able to adapt and learn throughout its lifetime, incorporating shared experiences with other individuals into its understanding of self, of others, and of the relationships they share. In short, a sociable robot is socially intelligent in a human-like way, and interacting with it is like interacting with another person."

Leonardo, to be truly a sociable robot, must be able to interact with people as if it were another living creature itself. Thus it must be capable of displaying some intentions and the ability to learn. It must have a set of behaviors. It must be able to express emotion. It must be able to react to the world around it in a convincing way. One of the ways in which Leonardo will be able to react and interact to the world around it is through a sense of touch, not only on the hands, but truly over its entire body. This is the ultimate goal for the initial work described in this thesis.

6.2 Design Constraints and Challenges

The new hands needed to be designed so as to easily replace the current hands shown in Figure 6-2. As shown in Figure 6-1, Leonardo in his final furry form has a foam latex glove which surrounds the mechanical hands. This glove is based upon the original character sculpture from which a set of molds were

created. Thus, while it would be nice to lengthen Leonardo's fingers this would require a very time-consuming change as a new sculpture would need to be created, new molds would have to be made, and finally new foam hands would have to be poured and painted.

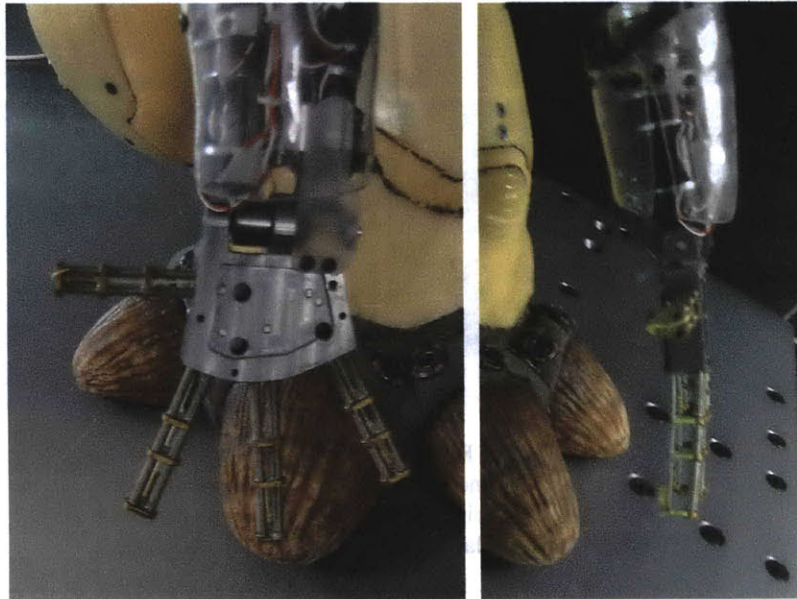


Figure 6-2: Mechanical Design of Leonardo's Hand copyright Stan Winston Studio. At left is shown the back of the hand. At right is shown the side view.

The original design of the hands is very different from most other robotic hands designed for manipulation, shown in Figure 6-3. Even before the foam glove is attached, one can see that the fingers are not well constrained. Leonardo was designed for expression, not for manipulation. The fingers were designed as springs to protect the robot from damaging itself. In a manipulation task, there is no way to constrain the motion of the fingers, thus reaction forces will deflect the fingers. This deflection poses a problem for any force sensing system.

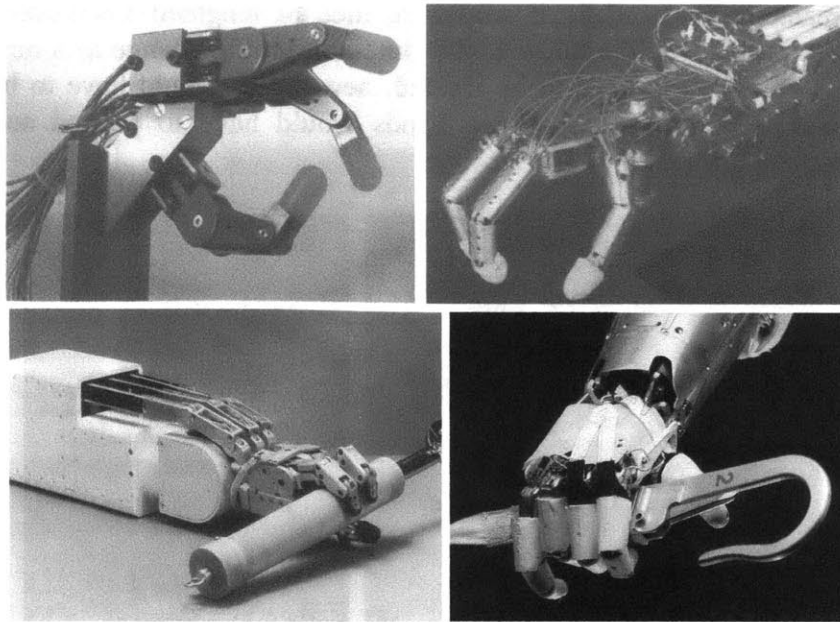


Figure 6-3: Images of Robotic Hands. Clockwise from top left: Stanford/JPL Hand (Salisbury hand) (Rosheim 1994), Hitachi Hand (Rosheim 1994), Jameson Hand (Rosheim 1994), Robonaut Hand (Menzel and D'Aluisio 2000)

The size of Leonardo's hands also poses a problem. The hands in Figure 6-3 are all human size or larger. Leonardo's hands are approximately one half the size of a human hand. The size of potential objects for manipulation must therefore be small, and that size would normally require a higher resolution of sensing.

Finally, once the foam hand glove is placed over the mechanism, the stubbiness of the actual fingers can clearly be seen in Figure 6-4. The organic look of a wrinkled palm with deep ridges results in variation in the thickness of the foam itself. Ideally whatever material is placed above an array of tactile sensors will be uniform not only in thickness but composition as well. The foam latex is formulated so as to be of very low weight, with many air cavities. Thus when force is applied to the surface of the foam, instead of the force going directly through the material some of that force compresses the foam, resulting in another sensing challenge.

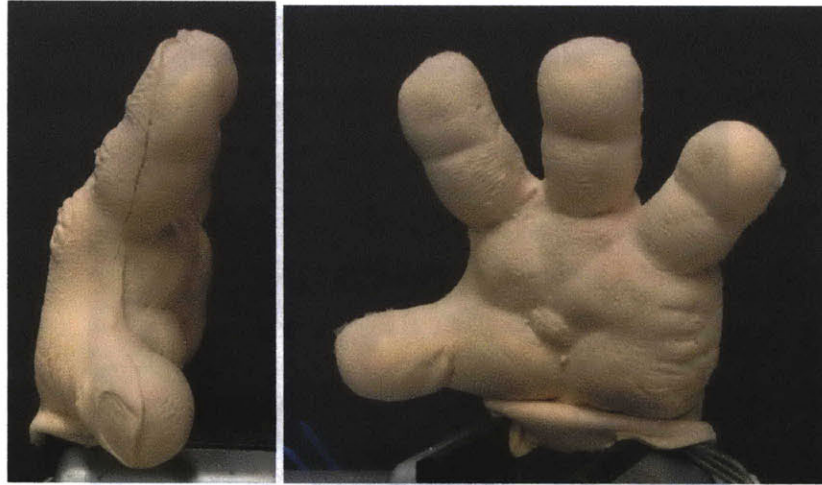


Figure 6-4: Unfinished, Unpainted Foam Latex Hand Coverings. Design copyright Stan Winston Studio. At left is the side of the left hand. At right is the palm section of the right hand.

In light of these many design challenges, the hands were chosen as the initial exploration into what would become a full-body sense of touch. While the hands could never be as manipulative as those in Figure 6-3, it would be possible through coordinated movement of both hands to move large objects. Additionally, many of the first tasks designed for Leonardo were simple pushing manipulations of buttons shown in Figure 6-5. (Breazeal, Brooks et al. 2003).

More than any other part of the robot, the hands are constantly moving within a workspace that includes objects, the buttons, as well as his own body, as shown in Figure 6-5. By instrumenting the hands with tactile sensors, accidental encounters with potential hazards can be avoided.

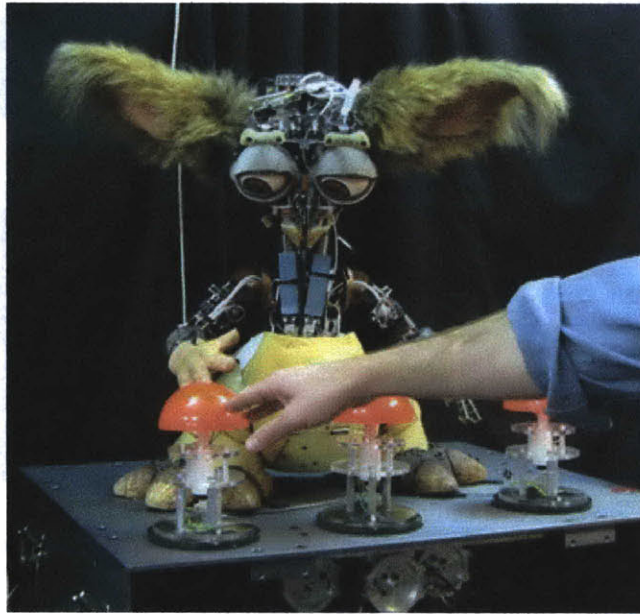


Figure 6-5: Leonardo and his Buttons.

6.3 Previous Work – the “Pixel” Platform

An initial test hand, the “Pixel” hand, was constructed prior to the design of the new hands (Stiehl 2003; Stiehl, Lalla et al. 2004). This hand was 1.5 times the size of Leonardo’s current hands. The goal of this first exploration was to develop a framework for tactile sensing without the need to immediately design for the complexities of integrating this framework with the complicated structure of Leonardo.

The “Pixel” platforms were a series of prototypes created by Stan Winston Studio to allow our lab to develop software and hardware for Leonardo while the robot was being constructed in California. These platforms replaced the higher precision Maxon motors with cheaper hobby servos. The arm “Pixel” platform was chosen for development of the “Pixel” hand as the design of the hand currently on the arm was similar to that of Leonardo, though smaller. Also the degrees of freedom in the arm mirrored the degrees of freedom of Leonardo’s arm.

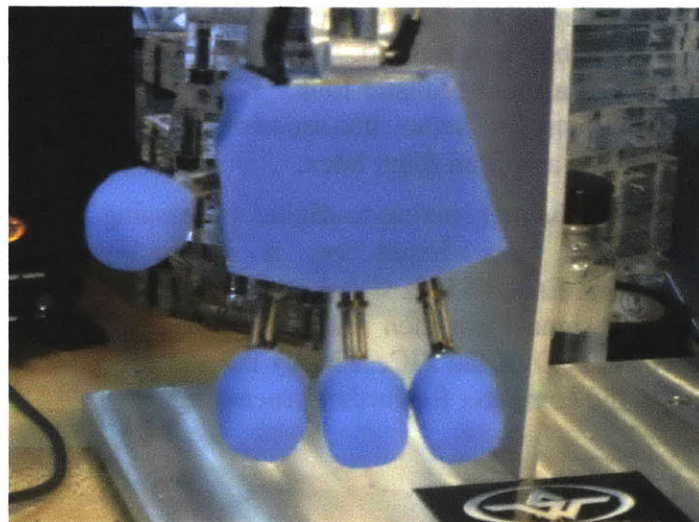
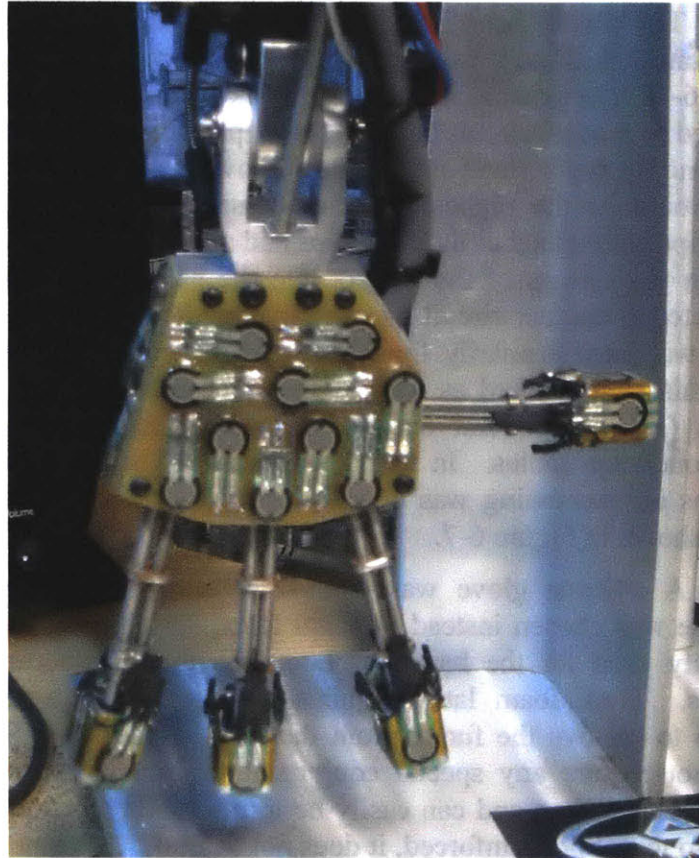


Figure 6-6: The "Pixel" Hand. Back of hand shown at top. At bottom is the silicone covering

The “Pixel” hand is shown in Figure 6-6. It featured a total of 43 Interlink force sensing resistors (FSR) arranged as shown in Table 6-1. The sensors of the palm, back of hand, and side were attached to printed circuit boards. Small plastic spacers were used to extend the top surface of the sensor above the solder tabs so that they would be the highest point of contact. The FSRs on the fingertips were glued to the fingertips and all the wires were routed through the springs of the fingers into the palm area where they connected to another circuit board. This middle of the hand circuit board was used primarily for cable management as all the wires from this circuit board as well as the three other sensing circuit boards (side, palm, and back of hand) left the hand via two multiconductor cables. In total there were 44 wires leaving the hand as all processing was done on a large development circuit board shown in Figure 6-7.

A silicone glove was created as shown in Figure 6-6. Silicone was chosen instead of foam latex, which is the material currently used for the hands of Leonardo for an assortment of reasons. First, foam latex requires an oven and a ventilation system to remove the fumes from the latex as it cures. Silicone does not require any special equipment. Secondly, foam latex degrades over time and can easily be torn. While silicone rubber can also tear if not reinforced, it does not degrade. Silicone rubber can also be formulated to have the softness of skin, as will be described in Chapter 13. The rubber does not wrinkle in the same way as foam when compressed. Additionally it can be colored intrinsically for a more realistic look. Finally the formulation of the rubber allows for better transmission of force through the material than the air-filled foam latex.

The 64-channel analog-to-digital processing circuit board of Figure 6-7 was based on a Microchip PIC16F877 microcontroller. Each FSR is signal conditioned through a voltage divider. The signals are then multiplexed and converted by the internal 10-bit A/D of the PIC. Finally the signals are transmitted via serial to the computer for further processing.

Table 6-1: The Number of Sensors Per Region of the “Pixel” Hand.

Region	Number of Sensors
Palm	10
Side	3
Back of Hand	10
Pinky Finger	5
Middle Finger	5
Index Finger	5
Thumb	5
Total	43

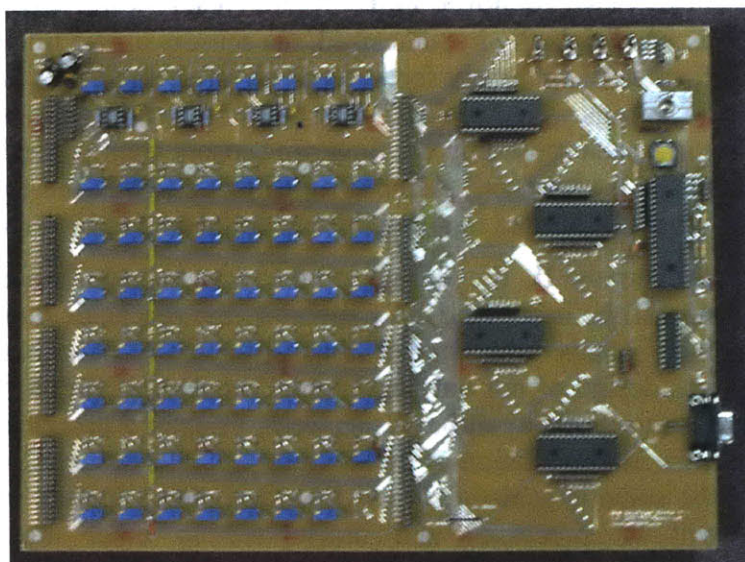


Figure 6-7: The 64-Channel Analog-to-Digital Processing Circuit Board for the Pixel Hand.

The “Pixel” hand was a great test platform to begin to explore the creation of a “sensitive skin” for Leonardo based upon a “Somatic Alphabet” approach. However, it did have a series of problems which needed to be solved for the final hand design. First, by mounting the sensors on spacers the actual thickness of the hands had increased. While this change was only a 1/4”, it was a significant increase in thickness and would cause the hands to no longer fit inside of the previously created latex gloves. The raised

sensors also changed the feel of the hands as the little bumps for each sensor could be detected.

Another problem with the “Pixel” hand design was the number of wires. As all the processing was done on a separate board outside of the hands, each sensor had its own distinct cable. For a robot with the potential for thousands of sensors on its surface this becomes unmanageable. Clearly, processing must happen as close to the sensors as possible.

Finally, the fingers needed a redesign. In the original design of Leonardo’s hands the fingers of one hand were all controlled by the same motor. Thus Leonardo could only open and close his hand. It was necessary to decouple the fingers to allow Leonardo to convey more expression such as pointing. The spring finger design, also employed in the “Pixel” hand, posed additional problems. As originally hypothesized, the sensors on the fingertips had difficulty detecting any forces because when the hands would close, the springs would deflect. Thus all the reaction force which should have been sensed by the fingertip sensors went towards the deflection of the springs. A more rigid, jointed structure for the fingers would be needed to allow for reaction forces to be sensed.

In Section II, the design of the new sensate hands for Leonardo will be described. In Chapter 7, the mechanical design of the new hands will be described. Chapter 8 describes the electronics design of not only an internal processing circuit board but communication circuit boards as well. Chapter 9 describes the initial work in the creation of the “Virtual Somatosensory Cortex” where the somatic sensory signals from the entire surface of the body will be processed and transmitted to other areas of Leonardo’s “Brain.”

7 New Hand: Electromechanical Design

7.1 Modifications to the Original Hand Design

In the previous chapter, the original hand design by Stan Winston Studio and an early prototype for the new sensate hands were described. The new sensate hands would need to be the exact size as the original hands to allow for them to fit inside the previously built foam latex hand gloves. Additionally, the fingers would need to be constrained to move in one degree of freedom. This chapter describes these changes.

7.1.1 Dual Layer Approach

The original hands featured 4 spring cable housings used to route the mechanical cables from the motors in the base of Leonardo to each finger as shown in Figure 7-1. Originally these fingers were driven by the same motor, but they were ultimately decoupled. The electrical wiring from the sensors would need to pass through the middle of the hand as well. A system to cleanly route both the mechanical and electrical cables inside the hand needed to be designed.

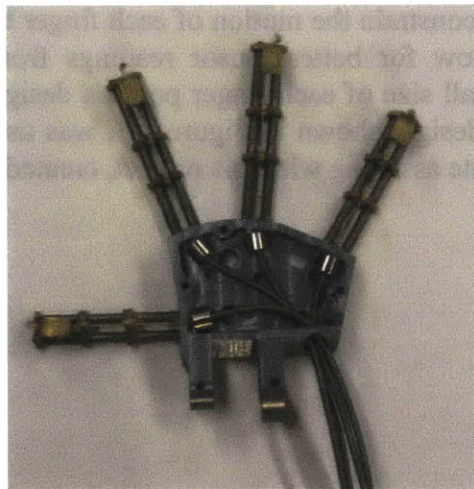


Figure 7-1: The Internal Cable Routing of the Original Leonardo Hands. Design copyright Stan Winston Studio.

The “Pixel” hand, described in the previous chapter, featured a dual layer approach, in which the electrical wiring ran below the mechanical cabling. An aluminum plate divided the two layers. This design would also be employed in the new Leonardo hands. However, an internal processing circuit board would be used instead of the aluminum dividing plate. Figure 7-2 shows a diagram of the dual layer approach for the new sensate hands.

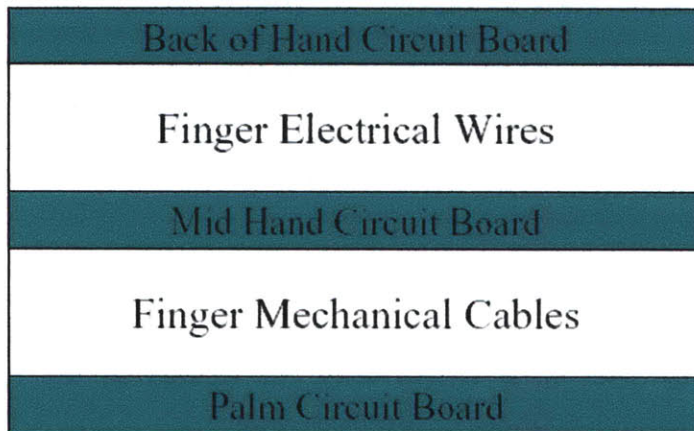


Figure 7-2: Dual Layer Approach for Sensate Hands.

7.1.2 New Finger Design

As shown in Figures 6-2 and 7-1, the original finger design featured a pair of springs for each finger. The new sensate hands would need to constrain the motion of each finger to one degree of freedom to allow for better sensor readings from the fingertip FSRs. The small size of each finger posed a design challenge. A jointed finger design, shown in Figure 7-3, was used. Levi Lalla, an undergraduate assisting with this project, created this design.

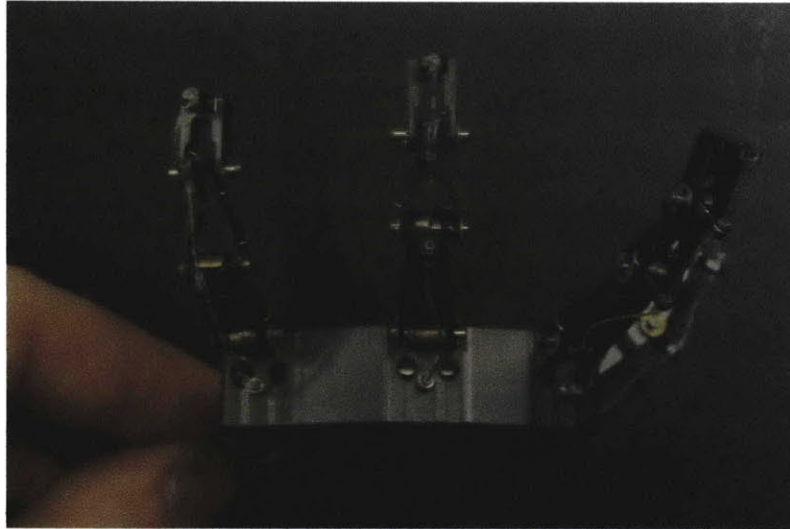


Figure 7-3: Close-up of the Finger Design of the New Leonardo Hands.

Each finger consists of three vertebrae sections, except for the thumb which has only two. Sections are connected to each other with pins and retaining rings. Torsion springs are used at the connection of each joint to provide a restoring force, as the cables are pull only. Teflon tubing is used at each section to protect the cables from damage. The tip of each finger is covered with a small square aluminum end cap, not shown in Figure 7-3. This end cap is used to attach the sensors. The fingers are machined from 7075 Aluminum for added strength.

7.1.3 New Hand Design

The hand is the most complicated part of the entire design. The fingers must attach to it. Mechanical cables must run through it to the fingers. Circuit boards for both sensing and processing must attach to it. Finally, electrical cables must exit the hand out to the rest of the robot. Due to the large number of interacting parts a highly detailed solid model was constructed to assess clearance issues as well as to optimize the placement of every hole. Figure 7-4 shows images of the solid model.

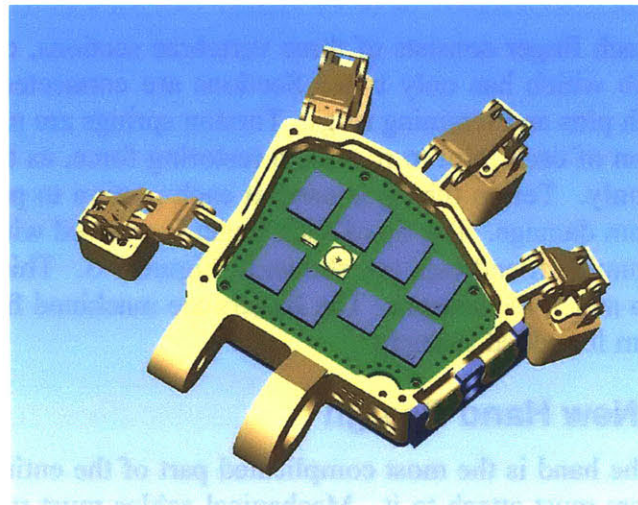
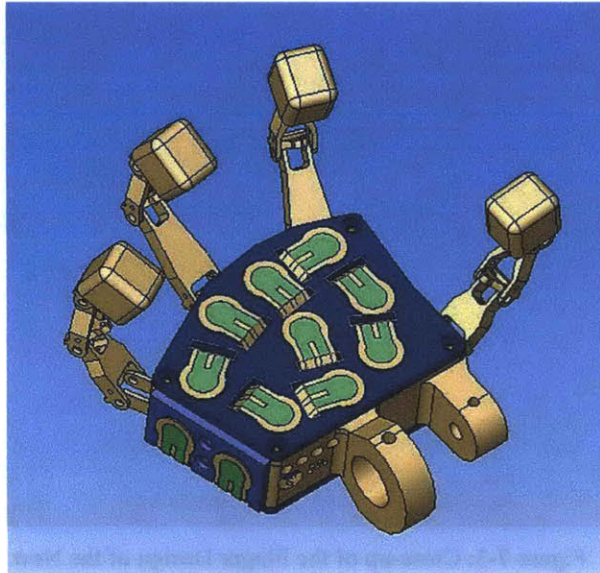


Figure 7-4: Two Images of the New Hand Solid Model. At top shows the Back of Hand and Side Circuit Boards. Below shows the hand with the Palm Circuit Board removed revealing the internal processing circuit board.

The external dimensions of the hand section were defined by the original hand design. Likewise the location of each finger as well as the holes for mounting the hand to the wrist had to remain the same.

At the base of each finger are two angled holes, shown in Figure 7-3. These holes are for the routing of the electrical wires

from the fingertip sensors to the mid-plane circuit board, shown in green in Figure 7-4. The angle of the holes was chosen so as to allow the wires to emerge just above the surface of the circuit board. The back of the hand also features a series of holes as shown in Figure 7-4. The four equal diameter holes are for the mechanical cable housing. The larger diameter hole is for a multi-conductor electrical cable which connects to the mid-hand processing board. The smaller angled holes were left available for future use. The angle of the holes was chosen so as to allow the cables to clear a pair of bevel gears used to rotate the hand at the wrist. Set screws, #0-80, are used to secure both the mechanical cables and electrical cables.

There are three sensor circuit boards (palm, side, and back of hand) and one internal mid-hand processing board that attach to the hand. These circuit boards will be described in the next section of this chapter, as well as in Chapter 8. #0-80 screws are used to attach the circuit boards to the hand. Cavities are cut out of the hand to provide clearance for the electrical components mounted to each board. Figure 7-5 is a photo of the hand and fingers prior to the mounting of the circuit boards. The hand is also made with 7075 Aluminum for added strength.

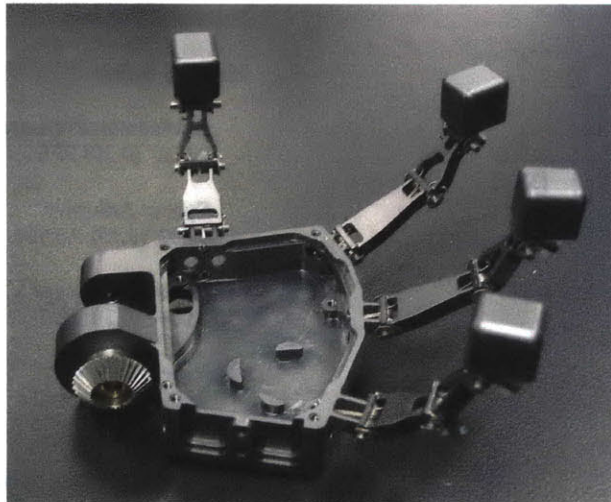


Figure 7-5: New Leonardo Hands Prior to Attachment of Circuit Boards

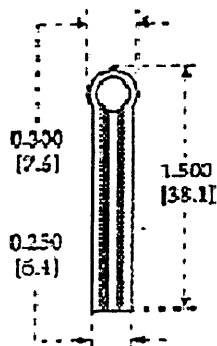
7.2 Sensor Mounting

The “Pixel” hand, described in Chapter 5, had three sensor circuit boards – the palm, the back of the hand, and the side of the hand. The new hand employs the same design. However, the sensor circuit boards of the new hand feature additional circuitry, described in Chapter 8, to multiplex the sensors. In this section, the mechanical design issues of the circuit boards will be described.

7.2.1 Sensor Selection and Modification

As in the original “Pixel” hand, Interlink part #400 force sensing resistors were selected for use in the new Leonardo hand (Interlink Electronics product literature.). Chapter 8 will describe the signal conditioning and performance of these sensors. Figure 7-6 shows the dimension of the sensor. The original long lead length was cut and new solder tabs were attached as described in (Stiehl 2003).

Part #400 (0.2" Circle)



Active Area 0.2" [5.0] diameter

Nominal Thickness 0.012 [0.30]

Material Build:

Semiconductive Layer
0.004" [0.10] PES

Spacer Adhesive
0.002" [0.05] Acrylic

Conductive Layer
0.004" [0.10] PES

Rear Adhesive
0.002" [0.05] Acrylic

Connectors
Solder Tabs (Not Shown)

Figure 7-6: Dimensions of the Interlink Part #400 Force Sensing Resistor (FSR) (Interlink Electronics product literature.)

These modified sensors were then placed onto the three sensing circuit boards. The size of each circuit board was defined by the original hand design. In the original “Pixel” hand, sensors were placed on the top surface of the board with spacers used to raise the active area of the sensor above the solder tabs, as shown in Figure 7-7. As described previously, the added thickness of the spacers would increase the total thickness of the hand to the point that it would not fit inside the foam glove. Also, because both the sensor active area and leads were mounted to the top surface of the circuit board, sensor density was not maximized. With the even smaller size of Leonardo’s hands this approach would result in fewer than 5 sensors for the palm and back of hand.

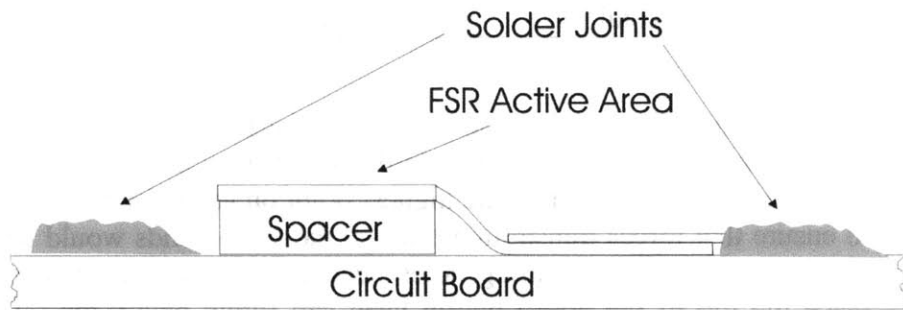


Figure 7-7: The Use of Spacers in the “Pixel” Hand.

7.2.2 Sensor Circuit Board Mechanical Design

To increase the sensor density of the new Leonardo hands, only the active areas of the FSRs would be glued to the top surface of the circuit boards. The solder tabs would pass through a slot at the base of the active sensor area and be soldered to pads on the underside of the circuit board, as shown in Figures 7-8 and 7-9. With this method employed, it was possible to have nearly the same number of sensors as in the “Pixel” hand. Table 7-1 shows the number of sensors for each region.

Table 7-1: The Number of Sensors per Region of the New Leonardo Hands.

Region	Number of Sensors
Palm	9
Side	2
Back of Hand	9
Pinky Finger	5
Middle Finger	5
Index Finger	5
Thumb	5
Total	40

Figures 7-8 and 7-9 show the palm, back of hand, and side circuit boards with sensors and additional circuitry attached. The sensor active area had to be the highest point on each circuit board to ensure that forces transmitted through the foam hands would be detected. Thus the mounting holes needed to be countersunk to place the top of the #0-80 button head cap screw below the top surface of the board. These holes were countersunk with 1/8"-end mill to a depth of roughly half the board thickness.

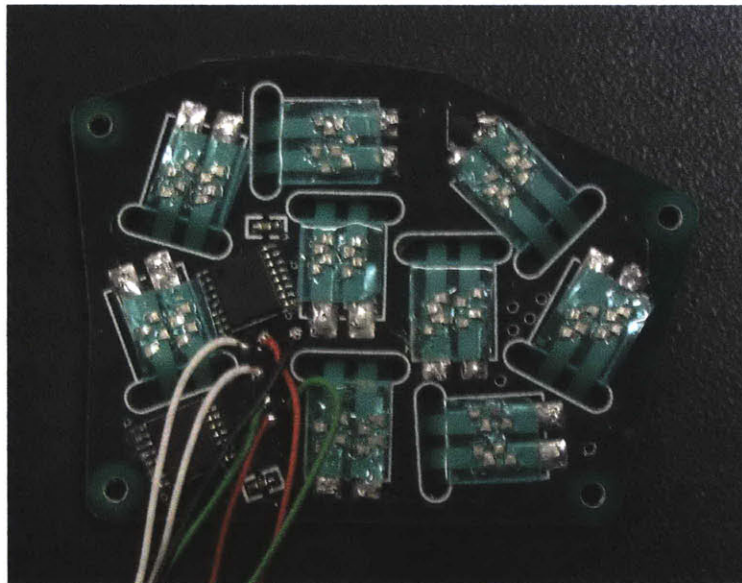
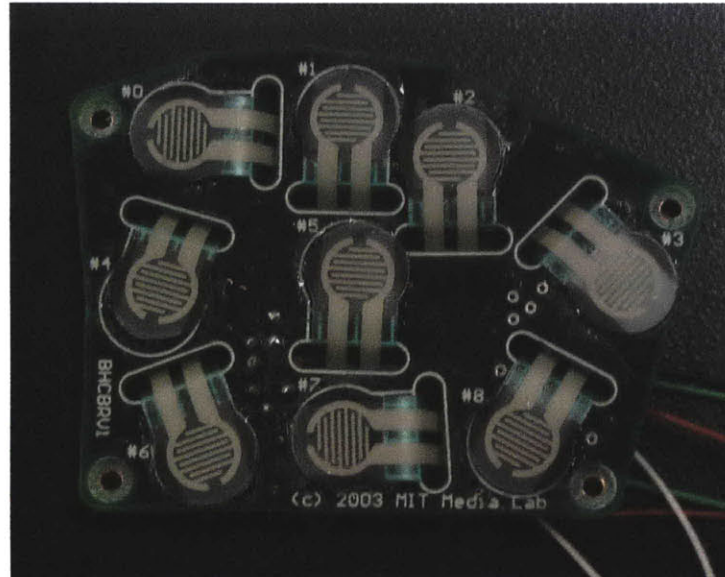


Figure 7-8: The Back of Hand Circuit Board with Sensors and Circuitry Attached. At top is the top view of the board. At bottom is the bottom view. The Palm circuit board is the mirror image of the Back of Hand circuit board.

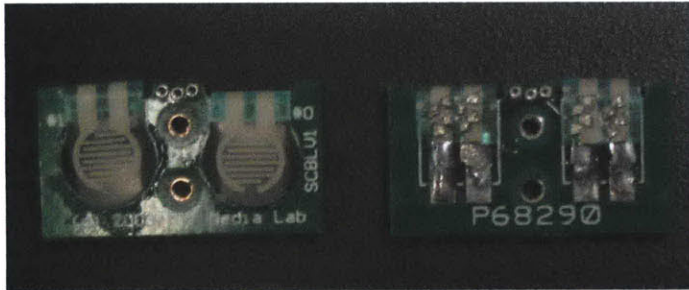


Figure 7-9: The Side circuit board. At left is the front of the circuit board. At right is back view of the circuit board.

The small size of the side circuit board caused the sensor leads to be bent a full 180 degrees as shown in Figure 7-9. While not ideal, this was the only way to allow for sensing on the side of the hand with the current FSRs. The three small holes above the mounting holes in Figure 7-9 are for 32-gauge electrical wires which transmit the sensor signal from each sensor, along with a shared ground, to the back of hand circuit board. The back of hand circuit board and the palm circuit board feature a pair of multiplexers which allow external input. Thus the sensor signals from the side circuit board pass through the multiplexer of the back of hand circuit board. The specifics of this circuit design will be discussed in Chapter 8.

7.2.3 Fingertip Mounting

Each fingertip, as shown in Figure 7-10, has a set of five sensors – front, side, left, back, and top. The four sensors around the sides of the fingertip are all the same length. The sensor mounted to the top of each fingertip has a longer lead length to allow it to pass over one of the side sensors. While not ideal, this was the only way to sense up the fingertip top with the current FSRs. All five sensors share a common ground, and this ground wire along with a wire from each sensor carrying signal runs down the entire length of the fingers into the hand and is finally connected to the mid-plane circuit board. Kapton tape is used to protect the sensor leads from damage. The fingertip is mounted to the fingers by a single #0-80 button head cap screw which fits through a hole in the top of the last finger vertebrae section. The tight tolerance as well as the clamping force of this screw keep the fingertip from rotating.

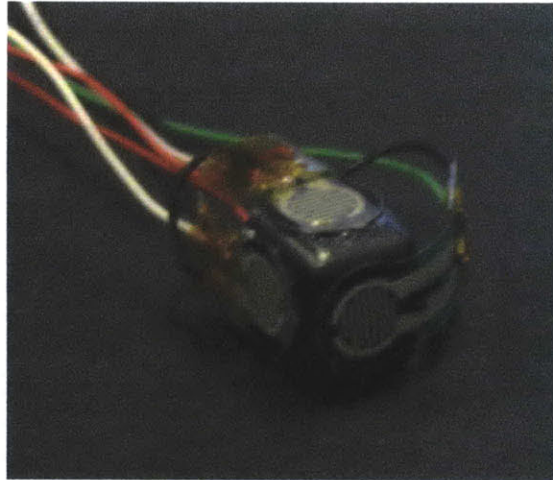


Figure 7-10: The Fingertip with Mounted Sensors.

7.2.4 Mechanical Design Considerations of the Mid-Hand Circuit Board

The new Leonardo hands would feature an internal processing board, the mid-hand circuit board. The circuit design of this board will be described in detail in Chapter 8. In this section the mechanical issues of the board design will be detailed. Figure 7-11 shows the mid-hand circuit board.

The non-rectangular geometry of the circuit board is due to the geometry of the hand. The numbered holes from 32 to 63 which span the edge of the circuit board are the connection points for the fingertip sensors. The back of hand and palm circuit boards connect to the row of holes along the bottom of the circuit board. The holes around the circular cutout in the lower right corner of the circuit board are for output. The circular cutout was designed to allow the multi-conductor cable, which is entering at a compound angle discussed previously, to emerge at the top surface of the mid hand circuit board.

The thickness of this circuit board was carefully designed so that it would fit within the small internal cavity of the hand. As such, the majority of components are on the top surface of the board. The smooth underside of the mid-hand circuit board sits directly above the mechanical cable housings for moving each finger. The four components on the bottom of the circuit board fit

inside an area protected from the cable housing, shown in Figure 7-12.

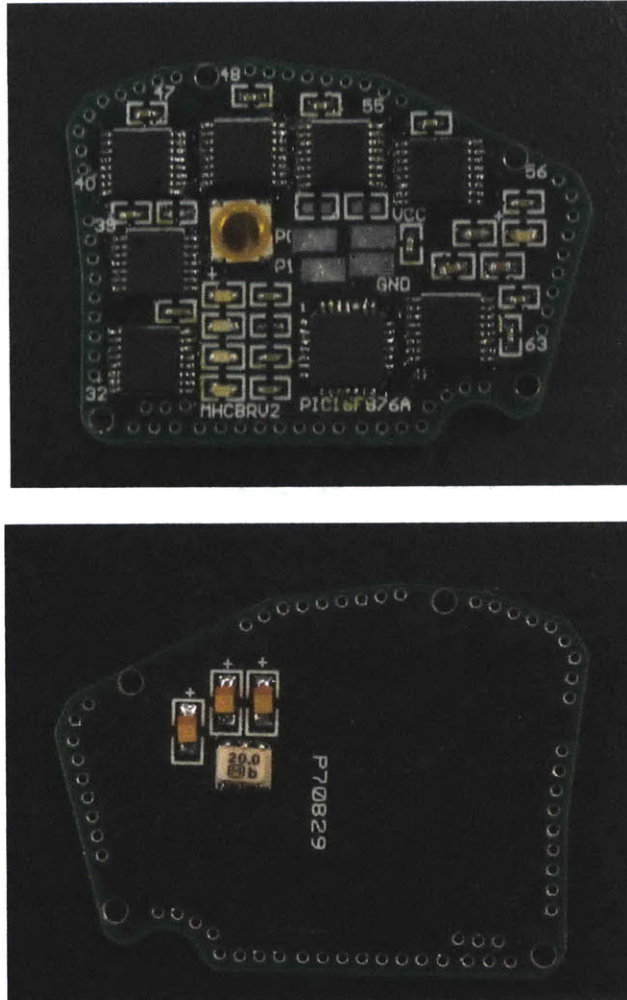


Figure 7-11: The Mid-Hand Circuit Board. The top of the circuit board is shown at top. The bottom of the circuit board is shown below.

7.3 Assembly

The complexity of the electromechanical design of the new hands requires that a specific order of assembly be followed. In this section this order will be described.

The mechanical cable spring housings are lined with Teflon tubing to prevent damage to the cable. Each cable is then routed

through the internal cavity as shown in Figure 7-12. The housings are secured at both ends with set screws to keep them from moving.

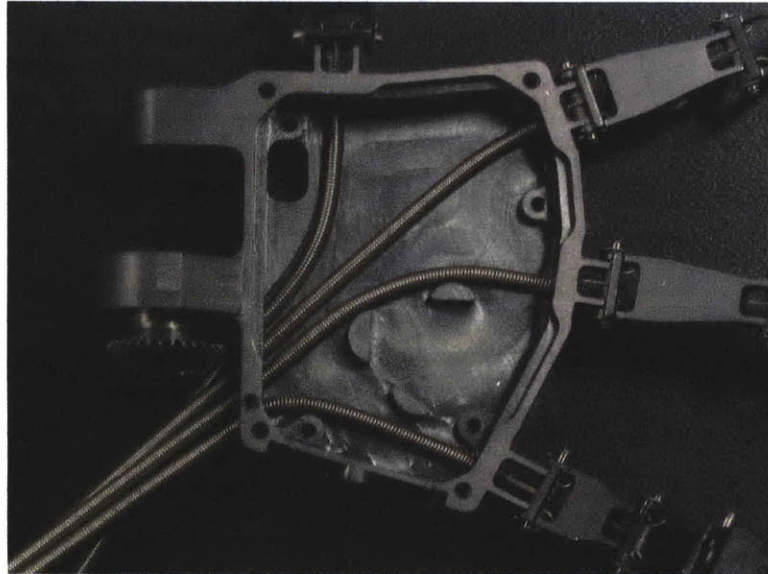


Figure 7-12: The Mechanical Cable Routing

A thin kapton sheet is used to separate the mid-hand circuit board from the mechanical cable housing to prevent accidental shorts. Figure 7-13 shows this kapton sheet. The mid-hand circuit board is then inserted with the multi-conductor output cable already attached. Figure 7-14 shows the mounted mid-hand circuit board.

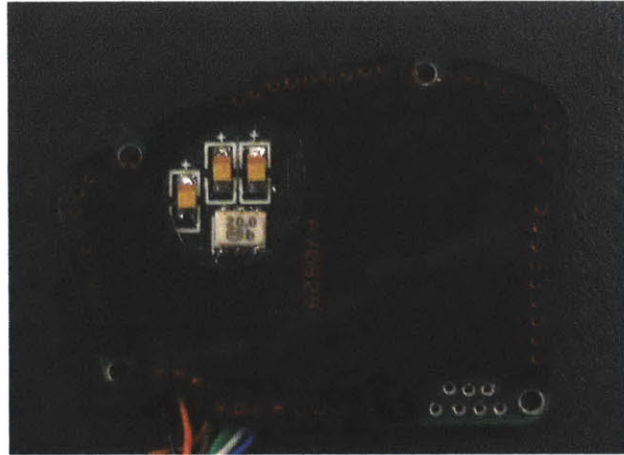


Figure 7-13: The Kapton Film which Divides the Mechanical Spring Housing from the Mid-Hand Circuit Board

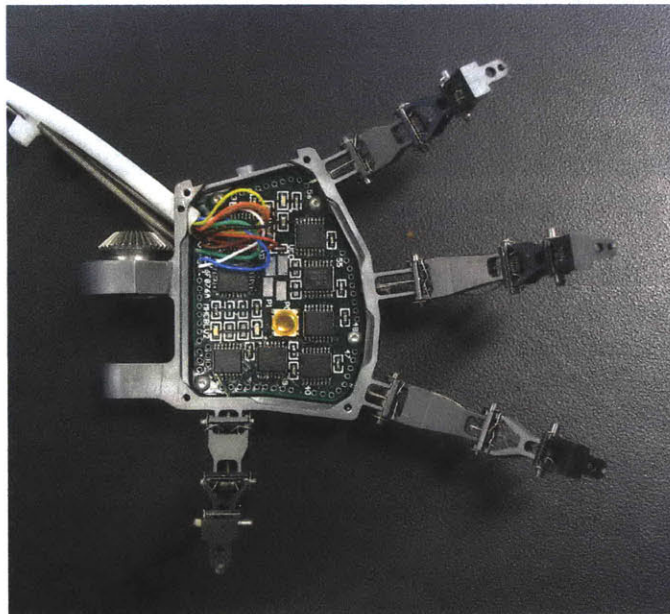


Figure 7-14: The Mounted Mid-Hand Circuit Board.

The sensor circuit boards are then attached and soldered to the mid hand-circuit board. While connectors would have been preferred to soldering each wire, the smallest connector which could have been used was still much too large to fit within the dimensions of Leonardo's small hands. Once the sensor circuit boards are in place, the fingertips are attached. The wires from each fingertip sensor are routed down the fingers and into the hand

where they are connected to the mid-hand circuit board. Figures 7-15 through 7-17 show photos of the completed assembly.

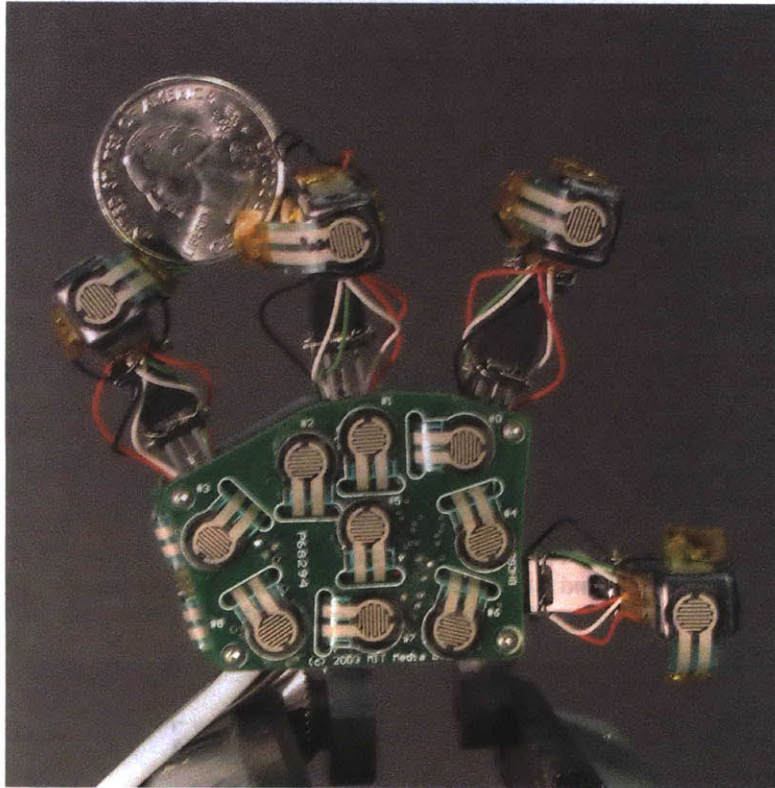


Figure 7-15: The Assembled New Leonardo Left Hand – Back of Hand View. A United States Quarter coin is shown for scale. Note that due to the torsional springs, the default position of the fingers is bent back.

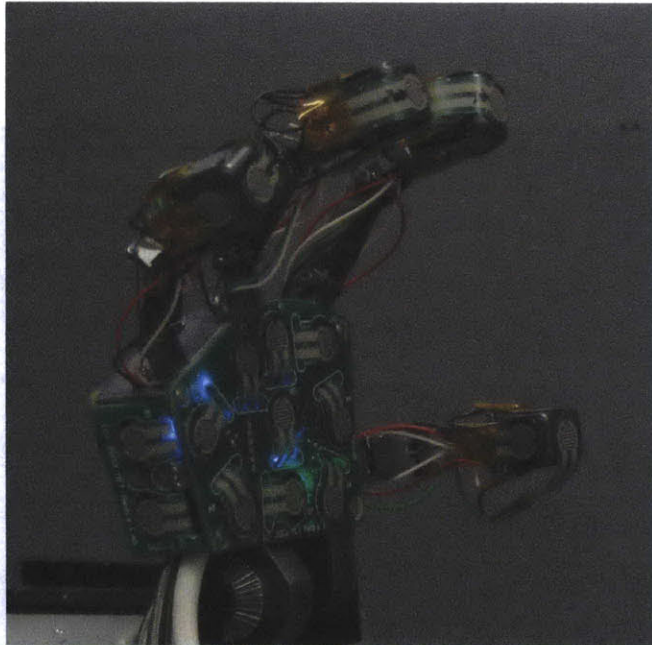


Figure 7-16: The Assembled Leonardo Left Hand – Side and Back of Hand is shown. The lights illuminating from inside the hand are from the powered mid-hand circuit board.



Figure 7-17: The Assembled Left and Right Hands.

From Figures 7-15 through 7-17 a potential problem can be clearly seen. The sensors and wires of the fingertips may be damaged as the foam latex glove is wrapped over the fingers. Additionally, the solder joints of the sensors and the torsional springs and pivot points of the finger vertebrae might catch and rip the delicate foam latex, which in the fingers is approximately an 1/8" thick. To remedy these problems a four-way stretch fabric glove was created as shown in Figure 7-18. This glove kept the wires of the fingers together and protected. The low friction of the fabric and its covering of all sharp points allowed the foam latex glove to roll smoothly over the new hands. Once the foam latex glove is attached the entire assembly can replace the original hand design. Figure 7-19 shows the mounted and completed assembly. The same process is repeated for the opposite hand.

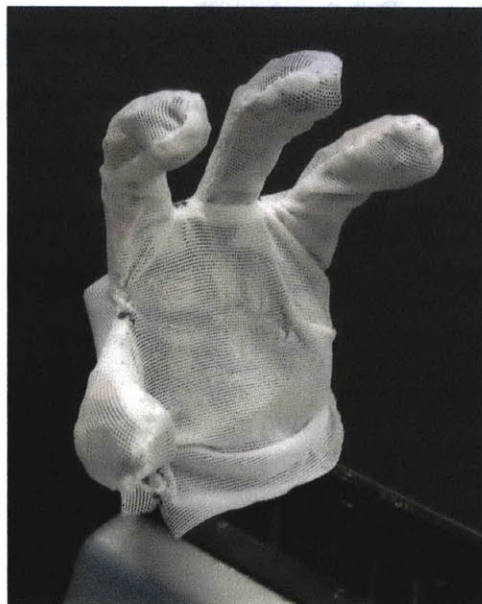


Figure 7-18: The Stretch Fabric Glove for the New Leonardo Hands.



Figure 7-19: The Mounted Left Hand of Leonardo with Foam Latex Glove.

8 Electronics Design

The human and animal somatosensory system has a very large number of sensors, yet within 15 milliseconds touch input reaches the primary somatosensory cortex. In our bodies this is done through an organization of nerves which synapse at the varying layers of the spinal cord as they ascend into the brain. As discussed in Chapter 2, this process occurs in a somatotopic fashion.

Leonardo's "sensitive skin" is heavily influenced by nature's design. Leonardo's skin can be broken out into its own somatotopic map. While our brain is highly parallelized, with multiple signals entering the brain at once, the realistic constraints of physical wiring and computation power prohibit such a massively parallelized system from being designed for a robotic platform.

One solution is to use the idea of a somatotopic map paired with local processing. Thus each body region of the robotic somatotopic map features its own low-level processor. For example, each hand features its own mid-hand circuit board which initially processes the data from all the sensors in the hand and outputs this information out to the "Virtual Somatosensory Cortex." This "Virtual Cortex" is a computer responsible for integration the information across multiple low-level processors and performing "cortical-level" processing such as orientation, direction, and formation of the other "words" of the "Somatic Alphabet."

In this chapter, the performance of the FSRs will be discussed. Next the mid-hand processing circuit boards will be detailed. Finally the somatic communication circuit boards, which act as a pass-through from collections of low-level processing boards to the main computer, will be described.

8.1 Sensor Performance

As discussed in Chapter 4, there are a wide variety of potential sensors from which to choose from in the design of a "sensitive skin." The design constraints of cost, responsiveness, low physical profile, small size, and sensitivity led to the choice of the Interlink FSRs for this application. A force-sensing resistor is

a polymer thick film (PTF) device which decreases in resistance as the force applied to the active area of the sensor increases. (Interlink Electronics product literature.)

The physical principle of how the sensor works is simple as shown in Figure 8-1. The top layer of the sensor contains a flexible substrate with a printed semiconductor. The bottom layer contains a flexible substrate with electrodes arranged in a finger-like pattern. The middle layer features a spacer. When force is applied to the top of the sensor, the semiconductor is pressed through the opening in the middle layer and connects the electrodes of the bottom layer increasing the conductance of the sensor. As more force is applied, more of the top layer comes in contact with the bottom layer and thus the resistance of the sensor will further decrease. This is very similar to the physical transduction of force of the Merkel disk receptor discussed in Chapter 2.

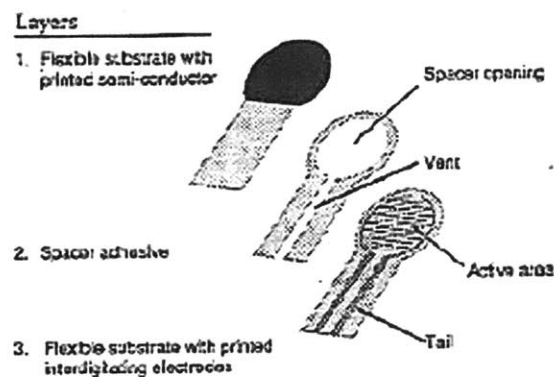


Figure 8-1: The Construction of the FSR Sensor (Interlink Electronics product literature.)

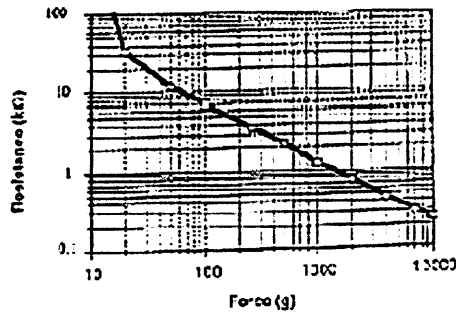


Figure 8-2: The Response of a Model #402 (0.5" diameter circular sensing area) to Applied Loads (Interlink Electronics product literature.) The actuator which applied the loads was made of stainless steel and had a 0.4" hemispherical diameter tip of polyurethane rubber with a value of 60 durometer.

The response of the sensor is shown in Figure 8-2. As can be shown clearly from the plot, the sensor exhibits a dual behavior. Initially the sensor functions like a switch until the "turn-on threshold" or "break force" which is shown by the change in slope. At this point (between 10 and 100 K-ohm), the resistance changes to below 10 K-ohm and a power law response is shown. Many factors will affect where this point occurs such as the size, thickness, substrate, and shape of the actuator and adhesive used. Because the area of the sensor determines the pressure applied, i.e., for the same size actuator under the same applied load, the smaller active area of the sensor will increase the pressure as shown in Equation 8-1.

$$P = \frac{F}{A} \quad (8-1)$$

In Equation 8-1, the pressure (P) is equal to the applied load (F) divided by the active area of the sensor (A). This equation assumes that the surface area of the actuator is a constant and is larger than the size of the sensor active area. A similar response can be shown for cases in which the actuator area varies and is smaller than the sensor active area. Thus (A) really indicates the area of contact, which is the area of the actuator when the actuator is smaller than sensor and the area of the sensor active area when the actuator is larger than the sensor. Using Equation 8-1, the

maximum saturation point of an FSR is calculated to be between 100 and 200 psi dependent on the sensor.

8.2 Mid-Hand Processing Board

In the original “Pixel” hand the processing of each sensory signal was done on a large external board. In the current implementation this large board has been replaced with a much smaller internal processing board based upon similar architecture. Figure 8-3 shows a diagram of the flow of information of the mid-hand circuit board.

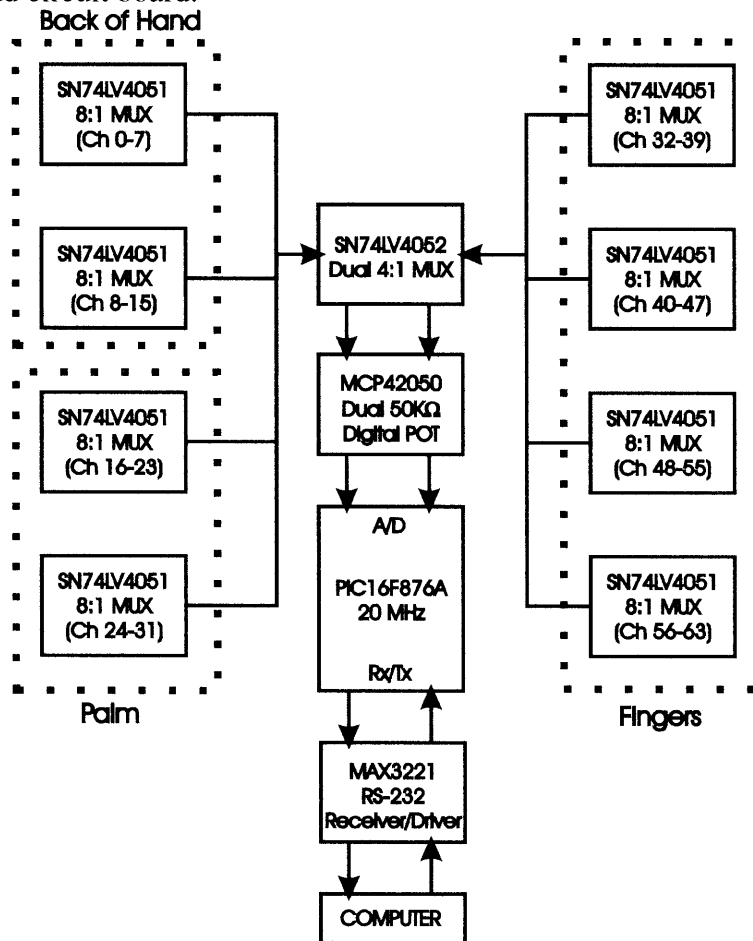


Figure 8-3: The Flow of Information in the Mid-Hand Circuit Board. The side circuit board is connected through the Back of Hand Circuit board channels 9 and 10.

The mid-hand circuit board, shown in Figure 7-11, is a 64-channel analog to digital processing board with RS-232 serial output. The selection of which sensor is read is made through a series of multiplexers across both the mid-hand circuit boards and the sensor circuit boards of the palm and back of the hand. The dotted lines in Figure 8-3 indicate the grouping of sensors into body region. The side circuit board sensors are connected to the multiplexers of the back of hand circuit board.

The palm and back of hand circuit boards each have a pair of Texas Instruments SN74LV4051 8:1 multiplexers. These multiplexers are controlled by the Microchip PIC16F876A 20 MHz microprocessor located on the mid-hand circuit board. The FSRs all share a common ground. The outputs of the multiplexer pair on each sensor circuit board pass through one side of a SN74LV4052 dual 4:1 multiplexer located on the mid-hand circuit board. Each finger has its own SN74LV4051 8:1 multiplexer located on the mid-hand circuit board. These multiplexers are connected to the second 4:1 multiplexer channel of the SN74LV4052.

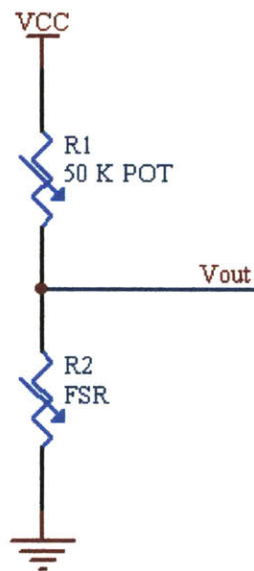


Figure 8-4: Voltage Divider circuit used for the FSRs

The FSRs are conditioned using a voltage divider shown in Figure 8-4. The sensor sits at the base of the voltage divider with a

potentiometer at the top. Equation 8-2 relates the output voltage to the resistive values.

$$V_{out} = \frac{R_2}{R_1 + R_2} V_{cc} \quad (8-2)$$

In the “Pixel” hand each sensor was matched with its own individual potentiometer to allow for individual adjustment of every sensor output value. Especially since every sensor is hand crimped and under a different thickness of foam latex in the glove, having the ability to adjust the potentiometer in the divider for each sensor becomes desirable. To maintain this ability without having 40 individual potentiometers, one for each sensor, a Microchip MCP42050 256-tap dual 50 K-ohm digital potentiometer is used. The PIC16F876A uses SPI communication to set the value of the digital potentiometer. The sensor circuit boards use the first channel of the digital potentiometer while the fingers are conditioned with the second channel.

The PIC16F876A uses the internal analog-to-digital converter to convert the analog sensor value. This conversion takes 50 μ s using the internal timer. Finally, the digital signal is output to the computer via a MAX3221 RS-232 serial driver/receiver at a baud rate of 57600. In circuit programming is used to program the PIC. This is a necessary feature as opening up the hands to reprogram the microcontroller is not feasible.

The microcontroller can do many more things than just switch between sensors and output the converted analog value. It can act as a low-level filter comparing the current sensor reading to a threshold. If the sensor value is below the threshold, the microcontroller can skip sending this value to the computer. This behavior may seem very simple, but it can have a large impact on the speed of processing an entire “sensitive skin.”

8.3 Somatic Communication Board

The output of each mid-hand processing board then connects to a Somatic Communications Board, shown in Figure 8-5. This circuit board is used for high-speed communication via USB through the Keyspan 4-port USB-to-Serial converter as well as in-circuit programming of each mid-

hand or other future processing board. This circuit board also functions as a regulated power for the set of processing boards.

Each board functions much like the levels of the spinal cord in the biological system. A set of four processing boards from each region of the body connect to a single communication board. For example, the hands and arms would share one board. This collection of communication boards begins to form the somatotopic map of Leonardo.



Figure 8-5: The Somatic Communication Circuit Board.

In the next chapter, the processing of sensory information from each mid-hand circuit board is described. Inspired by the biological somatosensory system, the “Virtual Somatosensory System” groups sets of sensors into receptive fields for processing.

9 Virtual Somatosensory Cortex

As was described in Chapter 2, the primary (SI) and secondary (SII) somatosensory cortexes contain cells which use population coding to arrive at higher levels of processing. Specifically, there are cells that respond to specific orientations of an applied stimulus within a receptive field. Others prefer specific directions of motion. These are only a few of the many “words” of the Somatosensory system.

In this Chapter I will discuss how the somatotopic map of Leonardo’s “Virtual Somatosensory Cortex” is created from the collection of processing circuit boards, such as the mid-hand circuit boards previously described. Using this framework allows for multiple levels of indexing and more efficient processing of sensory input. Finally, the actual “cortical level” processing of centroid location, direction of motion, and orientation will be described.

9.1 Organization

In the biological system tactile processing is done at two different levels. At the lowest level is the reflexive loop, shown in Figure 9-1, in which the sensory signal from each mechanoreceptor synapses on an interneuron, which in turn sends an action potential to a motor neuron resulting in movement. As the sensory signal never has to enter the brain for processing, movement can happen quickly.

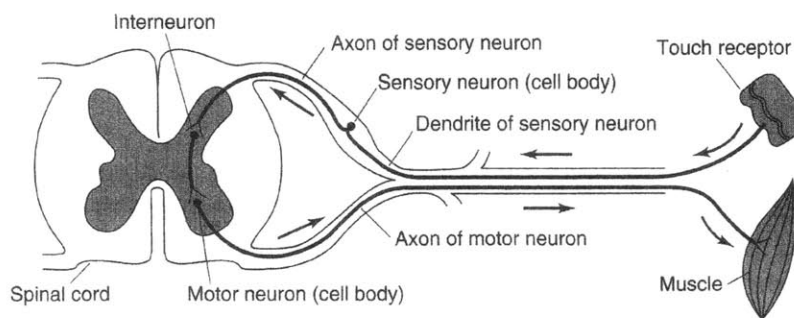


Figure 9-1: The Reflex Arc (Sekuler and Blake 2002)

Leonardo as well should have a similar high-speed processing loop to prevent injury. While currently not implemented, Figure 9-2 shows a diagram of how such a loop

could be created. Much like our own cortex, Leonardo has a high-level behavior system which receives sensory data, chooses the appropriate response, and outputs this response to the motors through a motor system. A distinct difference between the biological system and the robotic approach is that in biology, reflexes do not involve the somatosensory cortex. The robotic platform uses the processing power and networking capability of the rack-mounted computer running the “Virtual Somatosensory System” to ensure proper, fast communication with the motor system and motor drivers.

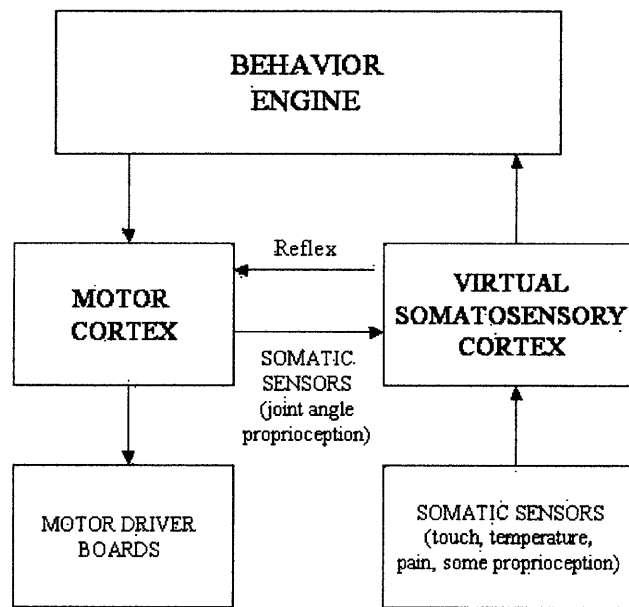


Figure 9-2: The Theoretical Location of the “Virtual Somatosensory Cortex”

The higher level of biological processing is done in the various portions of the somatosensory cortex. Each region of the cortex, as discussed earlier, is arranged in a somatotopic map. This somatotopy begins at the level of the spinal cord. Because of its organizational power, a somatotopic map is also implemented for Leonardo. Currently, this map includes only the hands, but the framework is in place for easy integration of other sensory areas as more and more of Leonardo’s “sensitive skin” is created. Figure 9-3 shows the hierarchical organization from sensor level to “Virtual Somatosensory Cortex” for Leonardo.

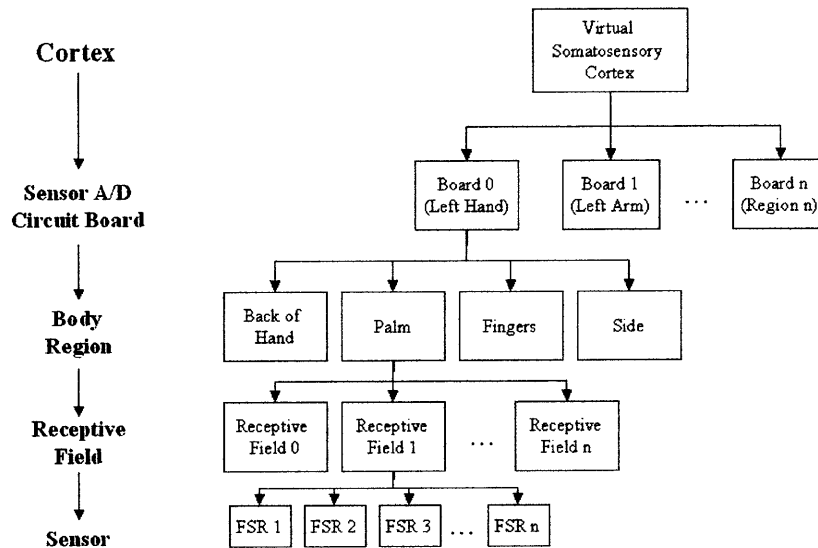


Figure 9-3: The Hierarchical Organization from Sensor Level to “Virtual Somatosensory Cortex”

The multiple levels of organization result in efficient processing. Sensor activity within a receptive field is carried up through each level all the way to the cortex. As mentioned previously different systems in the “brain” of Leonardo will need to have access to this information at varying levels depending on their function. Thus when Leonardo must look to see where he has been touched, the vision system needs access only to the sensor board level of somatic information. However, in the sense of reflexes where a motor must drive the limb in the opposite direction to the location of contact, the body region or receptive field level may be required.

9.2 Peripheral Sensor Signal

As discussed previously, our perception of touch is encoded by a variety of sensors, each encoding a specific type of stimulus. All processing done by the somatosensory cortex is based upon these initial input signals. In touch, one of the main divisions between the four mechanoreceptors in glabrous skin is based upon how quickly they adapt to changes in stimuli – either rapidly adapting or slowly adapting. Figure 9-4, repeated from Chapter 2, shows the response of a slowly adapting and quickly adapting mechanoreceptor to an indented probe.

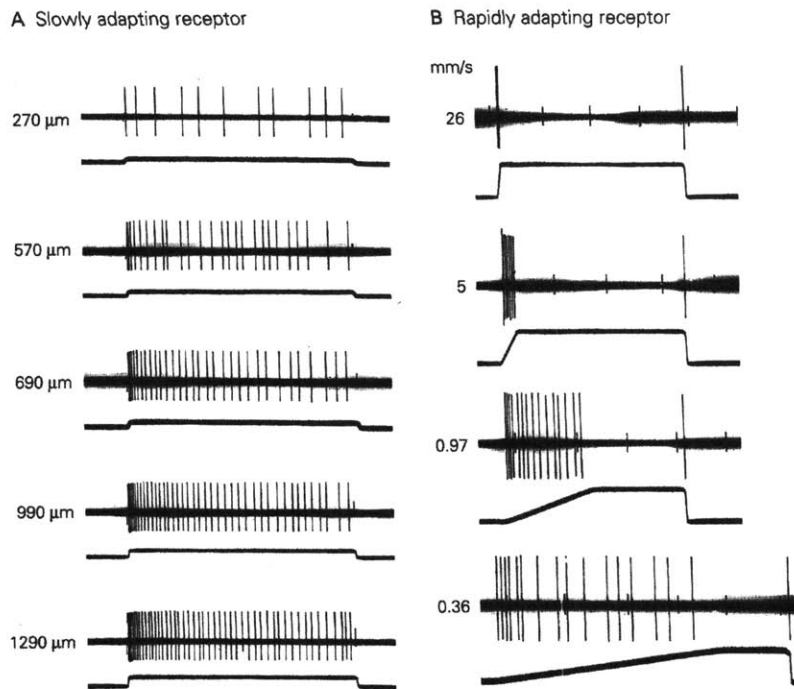


Figure 9-4: Responses of Slowly Adapting (SA) and Rapidly Adapting (RA) Receptors to an Indented Probe from (Kandel, Schwartz et al. 2000, pg. 424). In each image the response of the receptor is shown by a series of vertical bars (spikes) corresponding to each time that cell fires in response to the presented stimulus. Beneath the spike train is the time profile of the stimulus, with a step increase indicating that the probe was indented into the skin and a step decrease indicating that the probe was removed. In A, the response of a slowly adapting receptor is shown. As can be seen clearly from the figure, as indentation increases (indicated by a depth in μm) the firing rate (indicated by the number of vertical bars per interval) increases. It is also important to note that there is a greater density of spikes, i.e., a faster firing rate, as the stimulus is applied. In B, the response of a rapidly adapting receptor is shown. As can be shown, the cell responds to changes in stimulus, as indicated by the ramp. The cell fires only while the skin is indented and finally when the stimulus is removed. It is silent otherwise.

As shown in the figure, the slowly adapting mechanoreceptor encodes indentation by a spike count with more spikes indicating a greater indentation. Note indentation is related to the applied force. For a given material, the more applied force,

the greater the indentation. The rapidly adapting mechanoreceptor encodes changes in indentation.

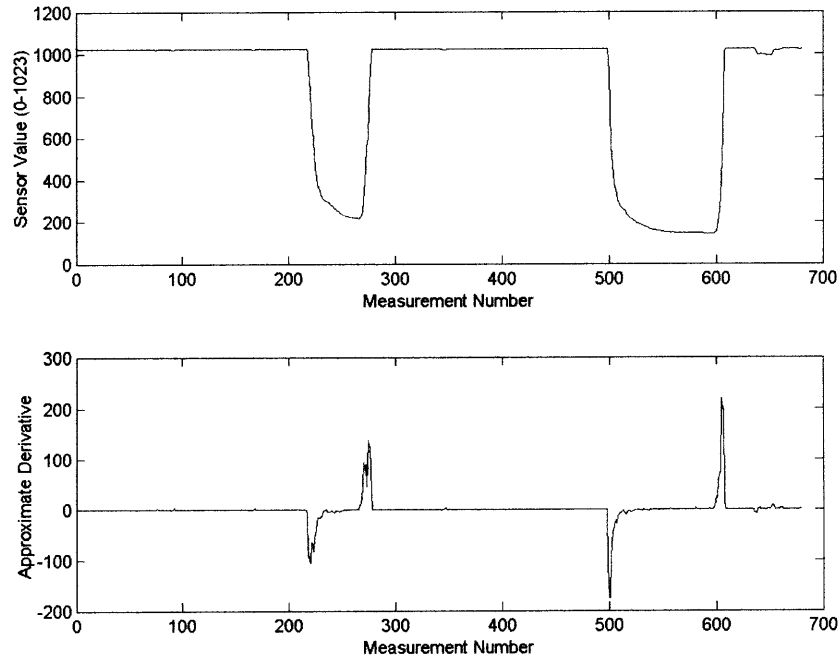


Figure 9-5: The Response of a Single FSR to Finger Taps. At top is the FSR 10-bit sensor value as converted from the analog signal. Below is the approximate derivative of this stimulus as calculated using the diff function in MATLAB.

Figure 9-5 shows the response of a single FSR used in the hand of Leonardo to a series of taps from a human finger applied to the top surface of the silicone. The similarities between the encoding of force data by the FSR and the encoding of indentation by the mechanoreceptors of Figure 9-4 can be seen. First, the raw sensor value is related the amount of force applied. When this number is subtracted from 1023, increasing force results in increasing sensor values similarly to how increasing indentation results in increasing spike count in the slowly adapting receptor. The derivative of the sensor signal also is similar to a rapidly adapting receptor, which fires to indicate changes in indentation.

9.3 Low Level “Cortical Processing” of Centroid Location, Direction of Motion, and Orientation

The “Virtual Somatosensory Cortex,” much like its biological counterpart, combines sensors together into receptive fields. Calculations are then performed within a receptive field on these populations of sensors. These equations and results originally appeared in (Stiehl and Breazeal 2004).

9.3.1 Centroid Location

The lowest level of processing is determines the centroid of a pressure profile within a receptive field. The location of each sensor in the receptive field, such as the palm of the hand, is known. Thus Equations 9-1 and 9-2 can be used to calculate the centroid position in the local coordinates of each receptive field. This location can later be transformed to global coordinates through forward kinematics. In these equations N represents the number of sensors in a receptive field, and P_i corresponds to the calibrated sensor output for the FSR.

$$X_{centroid}(t) = \frac{\sum_{i=0}^N (P_i(t) X_{sensor,i}(t))}{\sum_{i=0}^N P_i(t)} \quad (9-1)$$

$$Y_{centroid}(t) = \frac{\sum_{i=0}^N (P_i(t) Y_{sensor,i}(t))}{\sum_{i=0}^N P_i(t)} \quad (9-2)$$

9.3.2 Direction of Motion

Once the centroid location is known, motion can be calculated by comparing each calculated location to the previous one:

$$\Delta X_{centroid}(t) = X_{centroid}(t) - X_{centroid}(t - \Delta t) \quad (9-3)$$

$$\Delta Y_{centroid}(t) = Y_{centroid}(t) - Y_{centroid}(t - \Delta t) \quad (9-4)$$

where Δt is the time step between the current calculated centroid value and the previous one.

The direction of motion is calculated using Equation 9-5:

$$\theta_{direction}(t) = \arctan\left(\frac{\Delta Y_{centroid}(t)}{\Delta X_{centroid}(t)}\right) \quad (9-5)$$

The distance traveled by the centroid between time steps can be calculated using Equations 9-6 and 9-7:

$$R_{centroid}(t) = \sqrt{X_{centroid}^2(t) + Y_{centroid}^2(t)} \quad (9-6)$$

$$\Delta R_{centroid}(t) = R_{centroid}(t) - R_{centroid}(t - \Delta t) \quad (9-7)$$

This value can be used as a spatial filter, in which small perturbations in centroid position can be ignored if they fall outside the range of acceptable ΔR values.

Once the distance traveled per time step is known, the velocity can be calculated using Equation 9-8:

$$V_{centroid}(t) = \frac{\Delta R_{centroid}(t)}{\Delta t} \quad (9-8)$$

9.3.3 Orientation

Orientation-sensitive neurons have been shown to exist in both SI and SII as discussed previously. A “cortical level” algorithm can be used to determine the orientation as well. In this algorithm, each sensor can be thought of as a planetary body at a fixed location in 2-dimensional space where the gravitational pull of this body is proportional to the sensor value. A line is drawn from the centroid location to each of the sensors in the receptive field as shown in Figure 9-6. The length and angle of this line can be calculated using Equations 9-9 and 9-10:

$$R_{max,i}(t) = \sqrt{(X_{sensor,i}(t) - X_{centroid}(t))^2 + (Y_{sensor,i}(t) - Y_{centroid}(t))^2} \quad (9-9)$$

$$\theta_{max,i}(t) = \arctan\left(\frac{(Y_{sensor,i}(t) - Y_{centroid}(t))}{(X_{sensor,i}(t) - X_{centroid}(t))}\right) \quad (9-10)$$

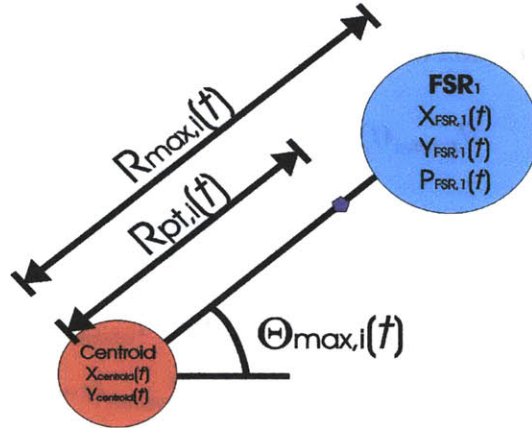


Figure 9-6: Diagram of Orientation Calculation

A point is then placed along each of these lines, and the length between the centroid and the point is a function of the sensor value, as described by Equation 9-11:

$$R_{pt,i}(t) = \frac{P_i(t)R_{max,i}(t)}{P_{max}} \quad (9-11)$$

where P_{max} is the maximum possible sensor value, i.e., 1023 in the raw 10-bit sensor case, and $P_i(t)$ is the individual sensor value. From this equation it becomes clear that non-active sensors, i.e., $P_i(t)=0$, will have $R_{pt,i}(t)$ values at the centroid location.

The maximum two lengths are used as endpoints to calculate the angle of orientation as described by Equations 9-12 and 9-13:

$$R_{orientation,1}(t) = \max(\{R_{pt,i}(t)\}) \quad (9-12)$$

$$R_{orientation,2}(t) = \max(\{R_{pt,i}(t)\} - \{R_{orientation,1}(t)\}) \quad (9-13)$$

Each endpoint is broken into its X and Y components as shown in Equations 9-14 and 9-15:

$$X_{orientation,i}(t) = R_{orientation,i}(t) \cos(\theta_{max,i}(t)) + X_{centroid}(t) \quad (9-14)$$

$$Y_{orientation,i}(t) = R_{orientation,i}(t) \sin(\theta_{max,i}(t)) + Y_{centroid}(t) \quad (9-15)$$

The equation of the line between these two endpoints is calculated using Equations 9-16 through 9-18:

$$m(t) = \left(\frac{Y_{orientation,1}(t) - Y_{orientation,2}(t)}{X_{orientation,1}(t) - X_{orientation,2}(t)} \right) \quad (9-16)$$

$$b(t) = Y_{orientation,1}(t) - m(t)X_{orientation,1}(t) \quad (9-17)$$

$$y = mx + b \quad (9-18)$$

The angle of orientation of this line about the centroid can be found using Equation 9-19:

$$\theta_{orientation}(t) = \arctan(m(t)) \quad (9-19)$$

9.3.4 Results

To test these algorithms a palm circuit board from the new right hand of Leonardo was mounted with spacers to a sheet of acrylic. A ¼” thick layer of Walco V-1082 silicone rubber with 20% silicone fluid was placed directly above. This silicone sample was previously used with the “Pixel” hands. Chapter 13 discusses the formulation of silicone rubber skins. A 1”-diameter delrin rod was rolled across the surface of the silicone rubber by hand. No measurements of the actual applied force or orientation of the objects were made. Figure 9-7 shows three snapshots of motion from three different time periods. Figure 9-8 shows a plot of the calculated direction of motion and orientation for this applied stimulus.

The calculations were done with both the linearized sensor value as well as the logarithmic sensor value. As Figure 8-2 shows, the normal response of the FSR is a logarithmic change in resistance with applied force.

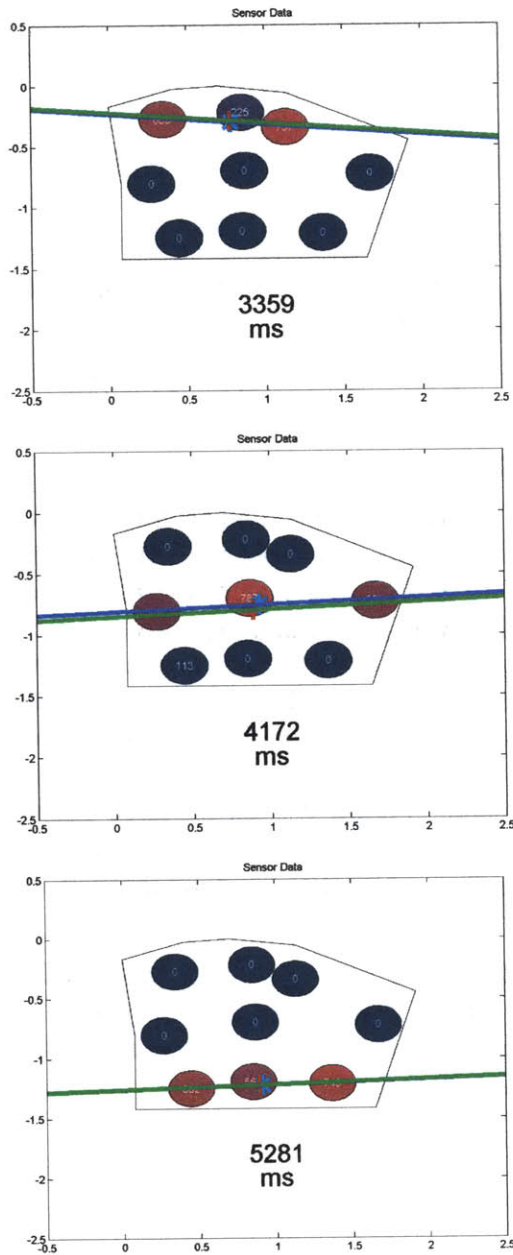


Figure 9-7: "Cortical Level" processing results. A delrin rod was rolled from the top of the circuit board down to the bottom (top to bottom). Each filled circle corresponds to the size and location of an FSR sensor on the right hand back sensor board. The color of the circle corresponds to the calibrated sensor value with black at 0 and bright red at 1000. The two lines indicate the orientation of the bar as calculated from Equation 9-19 using the logarithmic raw (green) and linearized (blue) sensor values. The calculated centroid of motion is shown as a red plus sign (logarithmic raw) and cyan asterisk (linearized).

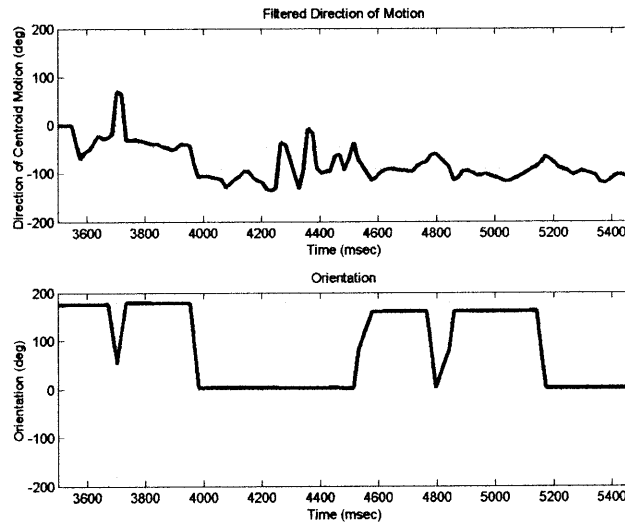


Figure 9-8: Direction of Motion and Orientation. Shown is the time response for Fig 9-7. At top is the filtered direction of motion information. At bottom is the orientation information. Note that in both plots, the dotted blue lines indicate 45 degree increments. Also note that in the orientation plot, an orientation of 0 degrees is equivalent to an orientation of 180.

A major limitation of the current sensor layout is displayed in Figure 9-8. The filtered orientation data does correspond well with the applied stimulus of rolling the delrin rod from the top of the palm to the bottom (0 degrees equivalent to 180 degrees). However the direction of motion is not as smooth. The spikes in the data which oscillate around -90 degrees which was the applied direction of motion are due to the fact that the sensors were not laid out in a uniform grid. As the rod moves from top to bottom, the next sensor is not located directly below the previous sensor, but is off to the left or right. However, even with this limitation, the calculated direction of motion does generally indicate a downward motion. With more sensors and the ability to space sensors closer together in a grid-like fashion these algorithms should produce better results.

As mentioned throughout this chapter, Leonardo was never designed to have a high degree of manipulation. Thus these failures due to the limitations of sensor placement and number of sensors are not a real hindrance. The majority of the objects, such as the buttons, with which Leonardo interacts, are larger than the active area of the hands.

In Section III, the Huggable, a relational robotic companion for therapeutic, affective touch will be described. The “sensitive skin” of this robot improves upon many of the problems with the current Leonardo design, such as sensor size and placement.

Section III: The Huggable

10 The Huggable: An Overview

10.1 The Huggable, a Therapeutic Robotic Companion for Relational, Affective Touch

In Chapter 3, the need for therapeutic robotic companions was discussed. Especially for those populations which do not have access to animals, a robotic pet surrogate can fill a basic human need to provide care and comfort.



Figure 10-1: The Huggable.

The Huggable is shown in Figure 10-1. Unlike other current robotic companions such as the NeCoRo (Omron Corporation Product Literature), AIBO (Sony Product Literature), Paro (Shibata and Tanie 2001), or the NearMe (Sega Toys Product Literature), the Huggable is not based upon a real animal. Instead the Huggable is a Teddy Bear, a comforting symbol from childhood.

The design of the Huggable is influenced by the study of companion animals, discussed in Chapter 3. As such the Huggable should be able to sense and interpret the type of touch interactions that are commonly given to pets. This affective content of touch is first sensed by a large array of hundreds of sensors in three

different modalities – electric field, temperature, and pressure. This “sensitive skin” encompasses the entire surface of the robot thus allowing the ability to convey the “illusion of life” described previously in this text. The design and layout of this skin, the subject of this thesis, is based upon the understanding of the human and animal somatosensory cortex, described in Chapter 2. This multi-modal, dense “sensitive skin” for the classification of affective touch distinguishes the Huggable from the other robotic companions of Chapter 4.

The Huggable also features silent, smooth voice coil actuators to move the neck and eyebrows to convey expression. A further discussion of these actuators can be found in (McBean 2004). Figure 10-2 is photo of the neck mechanism currently under development. Additional degrees of freedom will also be implemented in the future. Jeff Lieberman and Mike Wolf have been working on these designs.



Figure 10-2: The Neck Mechanism of the Huggable. The neck mechanism was designed and built by Jeff Lieberman.

The Huggable also features an embedded PC for sensor computation and to run the behavior system. Additionally, a data collection capability will be used to allow the hospital or nursing home to monitor the activity of the resident through the Huggable. This information can be communicated to doctors or other members of the staff via wireless. Thus the Huggable can become part of the team of patient and staff to promote the well being of the patient.

10.2 Design Constraints and Challenges

The Huggable is designed to be a portable platform able to be picked up and held by young children and the elderly. While the scope of this thesis is on the design of the “sensitive skin” for the Huggable, it is important to mention that this ultimate goal did impact the design.

The Huggable must feel soft and organic. It must be light enough so as to be picked up and held like a baby. The Huggable also must be able to detect a wide variety of tactile stimuli from light touches to hard squeezes. Additionally, the affective content of the touch should be classified regardless of how strong the person interacting with the bear is.

10.3 Lessons from Leonardo

As discussed in the previous section, the hands of Leonardo were designed using Interlink FSRs. These sensors were available only in four predefined geometries, of which the 0.2” diameter circle was the smallest. The long sensor lead also posed a problem in integration as it had to be trimmed and re-crimped, a time consuming process which would be impractical for a full body implementation of hundreds to thousands of sensors.

The performance of the Interlink FSRs was also not ideal. The sensors did not detect light pressures, such as gentle brushing across the palm, through the foam latex. This was due in part to the use of foam latex, which reduced the sensitivity of the sensors. The foam latex also degraded over time. For a platform which would be deployed to hospitals and other off-site locations and handled constantly, foam latex would not work.

Thus the Huggable must feature a new type of sensor and skin material. The Huggable must be able to detect very light

pressures, as the elderly and small children would not have as much strength as a healthy adult. The Huggable must also feature a soft skin that will not degrade over time.

In the next sections, a prototype arm section of the Huggable will be described. This arm section features three modalities of sensing chosen specifically for their ability to detect and differentiate human contact from inanimate objects. They are force sensors based upon Quantum Tunneling Composites (QTC) (Peratech Product Literature), electric field sensors (Motorola/Freescale Semiconductor.), and thermistors to measure temperature. While these sensors are different from those used in the new Leonardo hands, described in the previous section, they act as the “letters” of the “somatic alphabet” of the Huggable’s “sensitive skin.”

11 Electromechanical Design

11.1 Working within the Bear Envelope

The way that the Huggable feels when touched is an important part of the design. A commercial teddy bear, the Gund Butterscotch 20” large bear, was selected for prototyping purposes. This bear was selected for its large size and soft fur which was pleasant to touch.

Once the teddy bear was selected, it was 3-D scanned to create a virtual model. Unfortunately, even with the removal of the fur, the scanner was unable to cleanly scan the bear. Thus an alternative of measuring the external dimensions of the bear and modeling the envelope as a solid model was done. Figure 11-1 shows the solid model of the arm section based upon measurement. This solid model was created by Levi Lalla, an undergraduate in the Robotic Life Group assisting with the project.

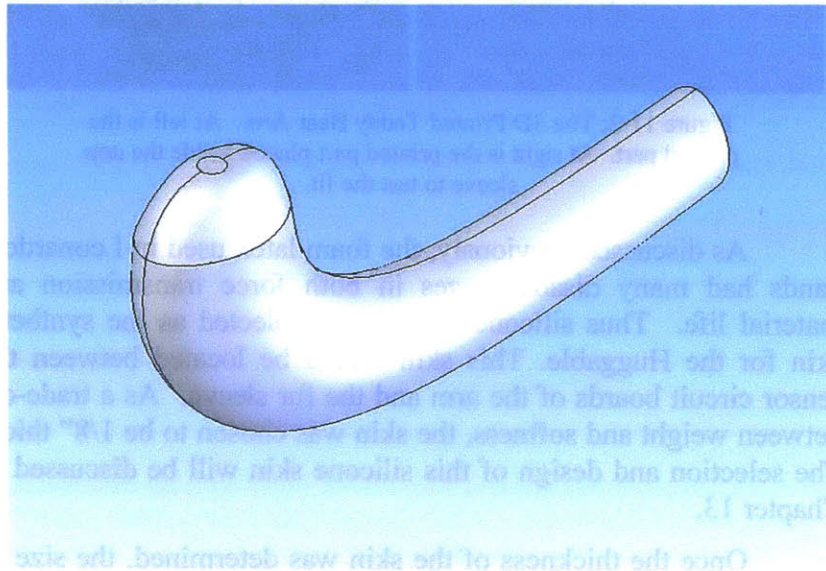


Figure 11-1: The Solid Model of the Teddy Bear Arm based upon physical measurement. This model was created by Levi Lalla.

The fit between the electromechanical understructure of the “sensitive skin” and the fur of the plush bear is important. Too loose of a fit and the fur will slide over the sensors creating bad

data. Additionally it would look unnatural for the fur to be so loose that it bunches together in sections. If too tight, the understructure will not fit inside the fur sleeve. In order to guarantee that the virtual model, which would be used in all stages of design was an exact copy of the internal structure of the fur sleeve the solid model of Figure 11-1 was 3D printed using a Z-Corporation 3D printer. To prevent the fragile printed part from breaking, super glue was applied to the entire surface. Once cured, the part was sanded until smooth. Figure 11-2 shows the 3D printed part inside the fur arm. Once the virtual model was confirmed to be accurate, the design of the sensor boards and underlying structure could begin.



Figure 11-2: The 3D Printed Teddy Bear Arm. At left is the printed part. At right is the printed part placed inside the arm sleeve to test the fit.

As discussed previously, the foam latex used in Leonardo's hands had many disadvantages in both force transmission and material life. Thus silicone rubber was selected as the synthetic skin for the Huggable. This skin would be located between the sensor circuit boards of the arm and the fur sleeve. As a trade-off between weight and softness, the skin was chosen to be 1/8" thick. The selection and design of this silicone skin will be discussed in Chapter 13.

Once the thickness of the skin was determined, the size of the cavity with which the sensor circuit boards and other electromechanical components was fixed. The solid model of Figure 11-1 was used to design the sensor circuit boards as well as the mechanical structure that would provide rigidity to the arm.

11.2 Sensor Selection, Attachment, and Wiring

11.2.1 Sensor Selection: Mechanical Considerations

Three modalities of sensing were chosen for the Huggable's "sensitive skin." In this chapter, the mechanical considerations of their integration within the arm section will be described. In Chapter 12, the sensor performance and processing will be discussed.

Quantum Tunneling Composites (QTC) were selected to replace the Interlink FSRs used previously in the Leonardo hand. These sensors are sold as A4 sheets and can be cut to any size. They are low cost compared to the FSRs and feature a much broader range of sensing, from over 10 M-ohms to less than 1 ohm (Peratech Product Literature). For these reasons these sensors have begun to be used in other robotic applications such as NASA's Robonaut (Martin, Ambrose et al. 2004) and the Shadow Robot Hand (Shadow Robot Company.; Ritter, Haschke et al. 2005) Figure 11-3 shows an image of the sheet of QTC switch substrate prior to creation of individual sensors.

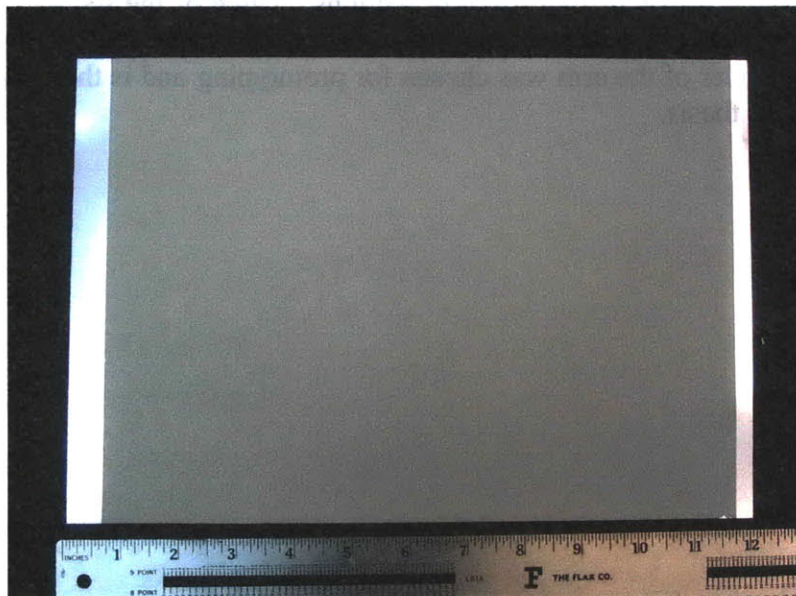


Figure 11-3: The QTC Switch Substrate

Electric field sensing was chosen for its ability to measure proximity. Thus it could detect light touches which would never be detected by the force sensors. This sensor consists of an electrode which is driven by the Motorola/Freescale Semiconductor 33794 electric field imaging device. Finally, thermistors were chosen to detect temperature. Because both the silicone and the fur were thermal insulators, the thermistors would need to be located just below the surface of the fur to ensure a good reading.

With the sensors selected, a layered structure for each sensor processing board emerged. The temperature sensors would be located above the QTC sensors which would be mounted directly to the sensor circuit boards. Below the QTC sensors would be a copper electrode used for the electric field sensor.

11.2.2 Sensor Circuit Board: Mechanical Design

The teddy bear arm has an ellipsoid cross-section. The initial prototype arm section would use rectangular sensing circuit boards. Eight circuit boards of equal dimensions would be arranged in an octagonal pattern 1/8" below the surface of the fur sleeve. Figure 11-4 shows the first solid model used for circuit board sizing. This solid model was designed by Levi Lalla. This model consists of four discrete sections. Three of the sections are identical to each other. The paw section, which is repeated in the remainder of the arm was chosen for prototyping and is the subject of this thesis.

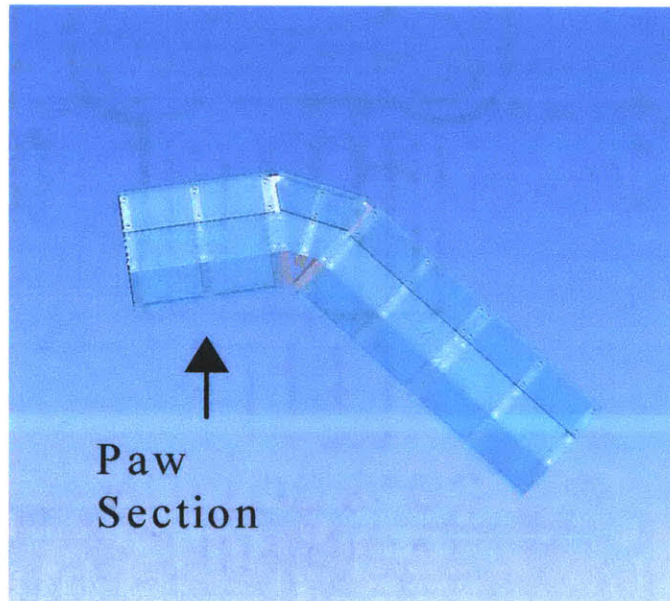


Figure 11-4: The Initial Solid Model Used for Sizing of the Sensor Circuit Boards. The paw section which is the subject of this thesis is indicated. This design was created by Levi Lalla.

From the solid model of Figure 11-4 the sensor circuit boards were designed to be 0.54" wide by 2.125" in length. The QTC sensors are formed by gluing cut sections of the switch substrate shown in Figure 11-3 to an electrode pattern. It was determined that 8 QTC electrodes could fit within the bounds of the sensor circuit board. The electrode for the electric field sensor would be located on the bottom of the board. Three pairs of holes for the thermistors were also placed in the middle of the board as well as at the two ends. Finally, multiplexers for both the temperature and QTC sensors would be placed on the bottom of the circuit board. Figure 11-5 shows the arm sensor circuit board prior to the placement of sensors and components.

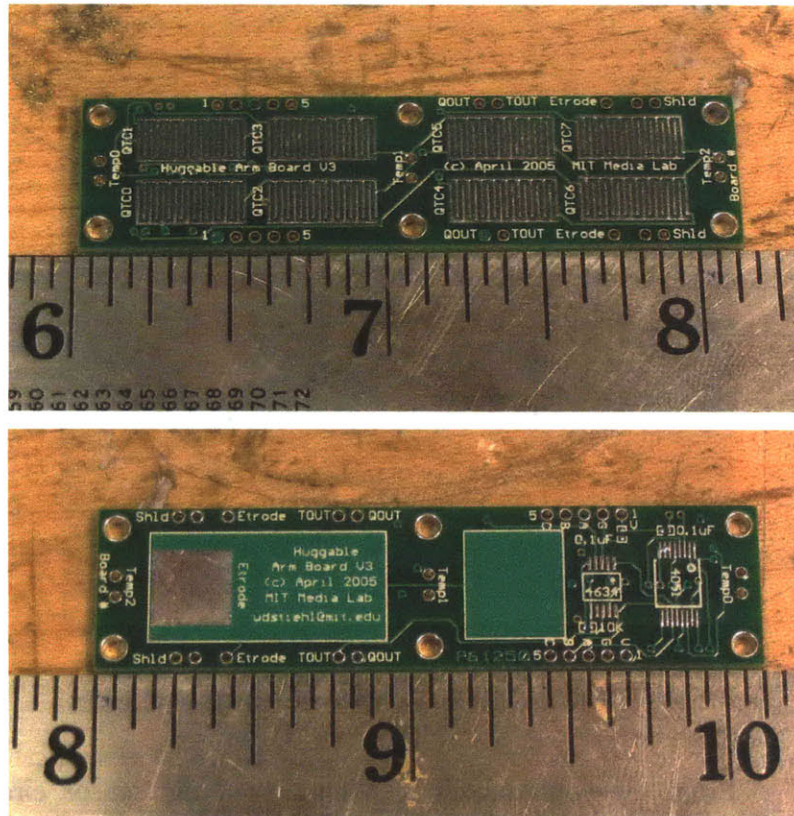


Figure 11-5: The Huggable Arm Sensor Circuit Board. At top is the top view of the circuit board. At bottom is the bottom view of the circuit board. The eight QTC electrodes are shown at the top. The small pairs of holes located between the mounting holes are for the mounting of the thermistors. The light green rectangles on the bottom of the circuit board are the solder masked electrode for the electric field sensor. The multiplexers for the temperature and QTC sensors are located to the right of the bottom image.

A few post-processing steps must be done to the circuit boards once they arrive from fabrication. First the holes on the top surface, even though they are solder masked, must be covered with kapton tape to prevent the possibility of shorting across the QTC sensors which will be glued to the top surface. This also helps during the wiring of the circuit boards as it prevents the solder from touching the QTC substrate and potentially damaging the sensor. Finally, the mounting holes must be countersunk with an 82 degree countersink. Instead of the #0-80 button head cap

screws used in the hands of Leonardo, #0-80 flat head cap screws will be used instead. These screws have an 82 degree taper.

11.2.3 QTC Sensor Mounting

A series of steps must be completed to mount the QTC sensors to the arm sensor circuit boards. A set of jigs were created to assist in the repeatability and accuracy of all sensor boards. This section describes the creation of the jigs as well as the steps to mount the QTC sensors.

Cutting the QTC Sensor Out of the A4 Sheet

A template was cut out of acrylic using a laser cutter. This template was placed over the QTC sheet, and the outline of this template was traced. The shape of the template was created using the solid model of the circuit board and the board layout. A paper cutter was used to cut out the QTC sensors, and scissors were used to trim away any excess substrate. Figure 11-6 shows the cutting jig as well as the cut sensor ready to be mounted.

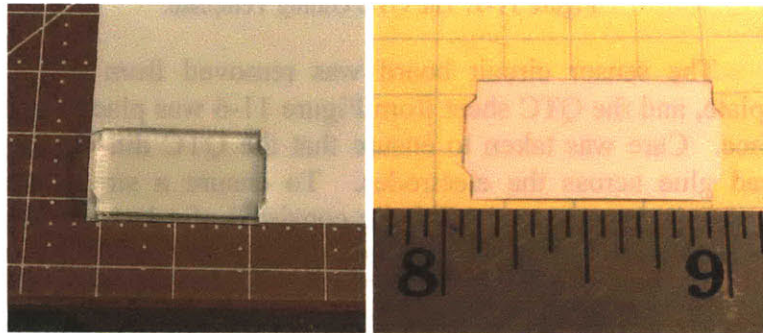


Figure 11-6: The QTC Sensor Cutting Jig and Cut Sensor. At Left is the acrylic jig. At Right is the finished sensor.

Gluing the QTC Sensor

After a series of experimentations with mounting the sensors using superglue or kapton tape, 3M Super 77 spray adhesive was recommended by Peratech. The spray adhesive offers many advantages over the other methods. First, with a template the glue can be applied to the same locations of every sensor board without accidentally covering the electrodes on the top surface of the sensor circuit board. Also with a spray it can be

quickly applied, which is important for the fabrication of multiple board for the entire “sensitive skin” of the Huggable.

A template was created from acrylic on the laser cutter. This template was designed from the solid model as well as the board layout. Figure 11-7 shows the template with a sensor circuit board ready for adhesive. The adhesive was allowed to dry for a period of 10 minutes or while the adhesive remained tacky. An additional coating was done if the adhesive had lost its tack so as to ensure a strong bond.

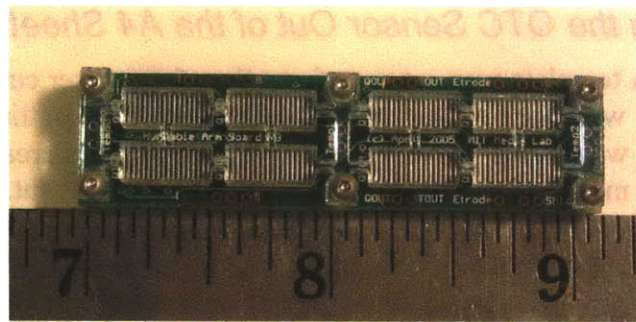


Figure 11-7: The QTC Gluing Template.

The sensor circuit board was removed from the gluing template, and the QTC sheet from Figure 11-6 was placed onto the surface. Care was taken to ensure that the QTC did not shift or spread glue across the electrodes. To ensure a strong bond a clamping jig was created. This jig consisted of a laser-cut acrylic plate with 1/8” adhesive-backed silicone rubber sheets that were cut to the same size as the QTC. The QTC was clamped overnight. Figure 11-8 shows the clamping jig with the sensor circuit board attached.

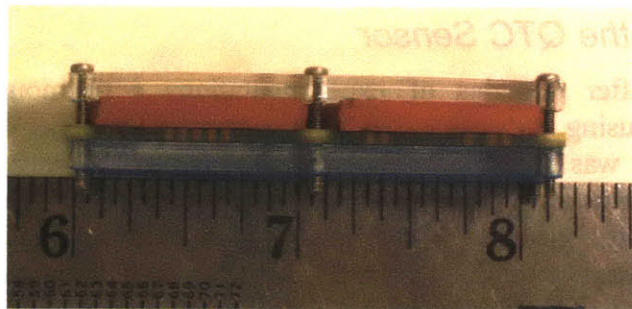


Figure 11-8: The QTC Clamping Jig

Cutting the QTC Sensor

The sensors were cut to prevent any unwanted signal transmission between adjacent sensors. The method of gluing an entire QTC sheet across four sensors was much less time intensive than cutting and gluing each of the four sensors individually. A cutting jig was created as shown in Figure 11-9. The sensor circuit board was placed inside this jig and an X-acto knife was used to carefully remove a thin line of sensor material between electrodes. The multiplexers for both the temperature and QTC sensors can be soldered in place once the QTC sensors have been cut. Figure 11-10 shows the sensor board with both QTC and multiplexers attached.

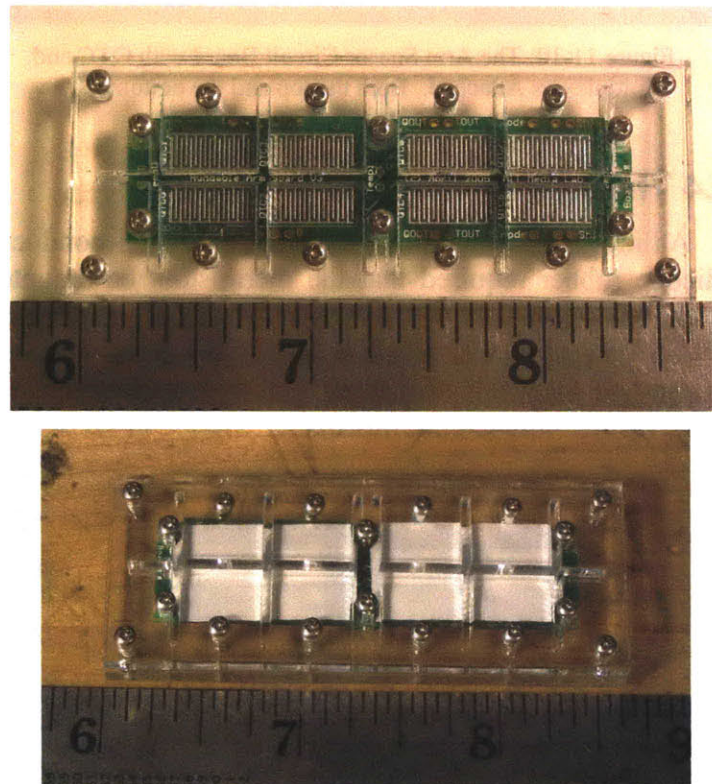


Figure 11-9: The QTC Cutting Template. At top shows the location of the cutting guides with respect to the electrodes. At bottom is the actual sensor board with QTC mounted prior to being cut.

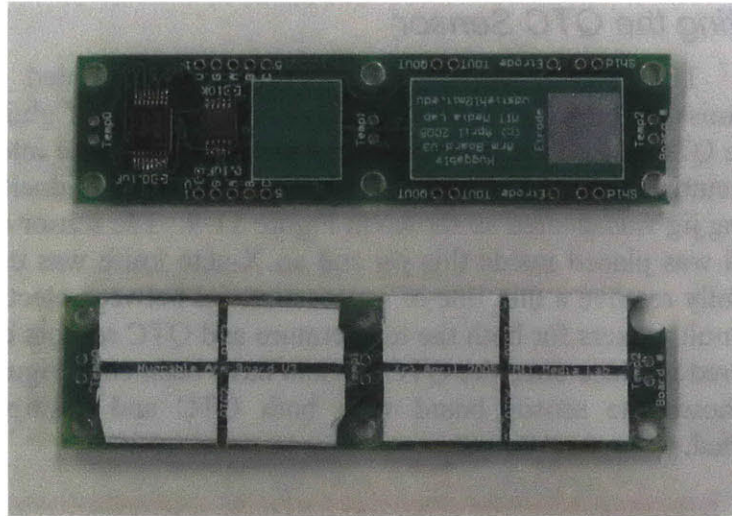


Figure 11-10: The Arm Sensor Circuit Board with QTC and Multiplexers Attached. Both the top and the bottom of the circuit board are shown.

11.2.4 Thermistor Sensor Mounting

As mentioned previously, the poor thermal conduction of the silicone rubber required that the thermistors be mounted just below the surface of the fur arm sleeve. Spacers were created using 3/64" diameter heat shrink tubing cut to 1/8" lengths. Each thermistor was then soldered to the sensor circuit board. Figure 11-11 shows the mounted thermistors.

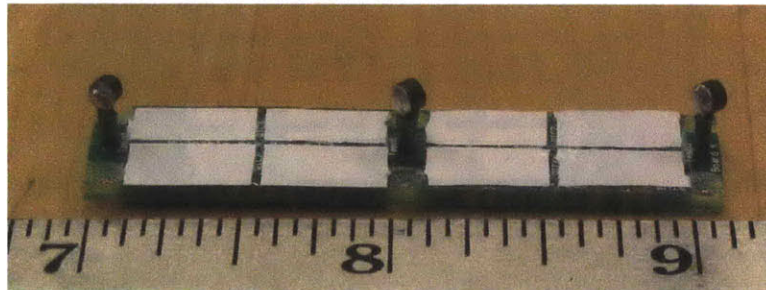


Figure 11-11: The Arm Sensor Circuit Board with Thermistors Mounted

11.2.5 Shielding

The electric field sensors must be shielded from the rest of the circuit and structure to prevent coupling. The method chosen to keep the electric field sensors separate from the rest of the

circuit will be described in Chapter 12. In this section, the creation of the shield will be detailed.

Each sensor board needs its own shield to allow for easy assembly of the arm section. The shield is cut from a sheet of copper using a template created from the solid model and board layout. A wire is soldered to the shield, and the shield is wrapped in kapton tape to prevent the shield from coming in contact with any exposed metal. The wire is connected to the shield of the sensor circuit board. Kapton tape is placed over the exposed copper electrode on the back of the circuit board to prevent shorting between shield and signal. Foam tape of 1/16" thickness is placed on the back of the circuit board. Foam tape of 1/32" thickness is placed over the multiplexers. The shield is then pressed onto the foam tape. Figure 11-12 shows the final circuit board with shield attached.

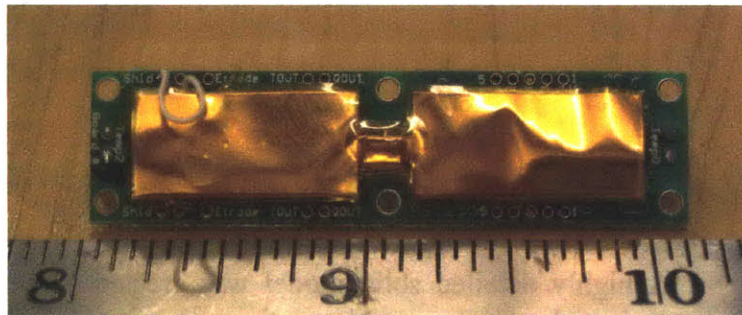


Figure 11-12: The Sensor Circuit Board with Copper Shield Attached.

11.3 Mid-Plane Circuit Board: Mechanical Design

A mid-plane circuit board was designed to act as a second level of multiplexing as well as to isolate the electric field sensors from the rest of the arm. The specifics of this sensor design will be described in Chapter 12. In this chapter, the mechanical design considerations will be discussed.

For easy assembly and disassembly a set of connectors are placed on the top surface of the circuit board. The integrated circuits (ICs) are mounted to the bottom of the board. Each mid-plane circuit board features a common multiconductor cable for power and control that passes from one board to the next.

Figure 11-13 shows the bottom of the mid-plane circuit board. The notch in the circuit board allows the board to be mounted closer to the center of the arm. The board is attached to a set of board mounts which are screwed into the outer two arm rib sections. The set of thirteen holes on the ends of the board is for connection of the common multiconductor cable.

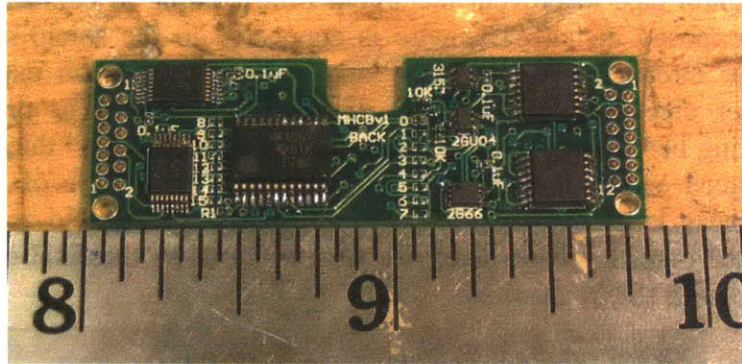


Figure 11-13: The Mid-Plane Circuit Board. In this image only the bottom is shown.

11.4 Mechanical Structure Design and Assembly

A highly detailed solid model was created to design the mechanical understructure underneath each circuit board. In addition to the eight arm sensor circuit boards an internal switching circuit board would have to fit. The specifics of the design of this internal switching circuit board will be discussed in the next chapter. Figure 11-14 shows a screen shot of the highly detailed solid model of the arm section.

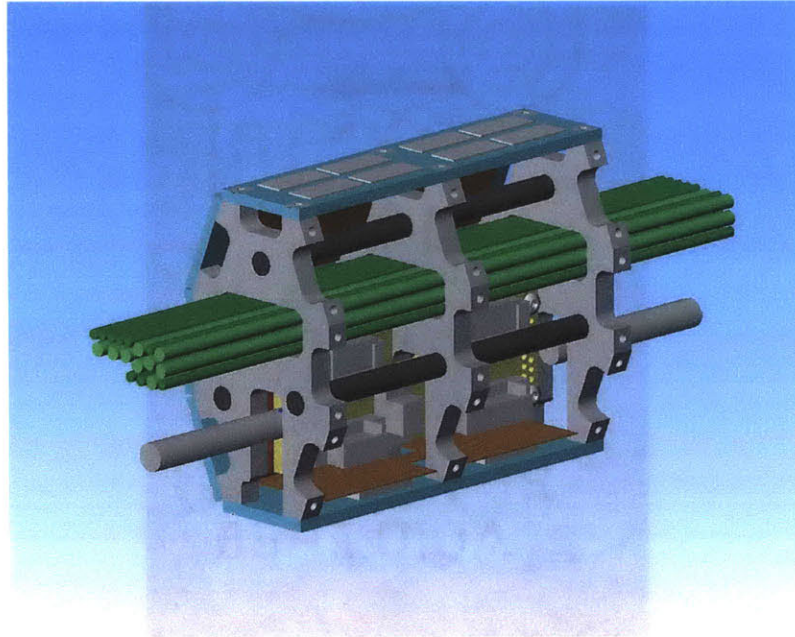


Figure 11-14: The Detailed Arm Assembly Solid Model

The mechanical understructure consists of three ribs (shown in grey). The ribs are connected through three press-fit rods (shown in black). The final mechanical section are two board mounts (not shown) for attaching the mid-level circuit board. All mechanical parts had to be made from non-conductive materials so as to not interfere with the electric field sensors. The ribs were water jet from 1/8" thick black delrin. The connecting rods were 1/8" diameter fiberglass rod. These materials were chosen for their high strength and machinability. The board mounts were water jet from 3/16" polycarbonate.

The sensor circuit board mounting holes in the rib structures were hand drilled in this prototype. A laser cut acrylic jig was created to easily drill out these holes. Figure 11-15 shows this jig. The holes were then tapped for the #0-80 flat head socket head cap screws used to mount the sensor circuit boards to the ribs.

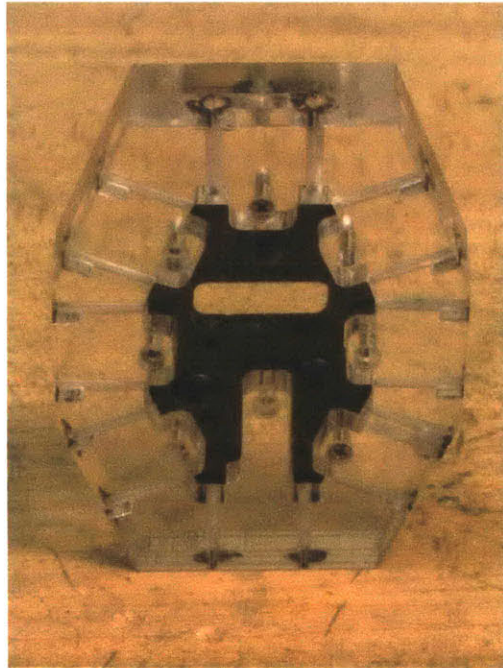


Figure 11-15: The Arm Rib Drilling Jig

The common multiconductor cable of the mid-plane circuit board slides into the slot at the bottom of the arm rib. A set screw is used to clamp this cable against the top corner of the slot. The large cutout at the top of the rib is for passing cables from each mid-plane circuit board output and each electric field sensor output. The cutouts on each face of the arm rib allow clearance for the copper shield.

Figure 11-16 shows the assembled mechanical understructure with the mid-plane circuit board attached. For clarity, the photo was taken before the wires were connected. The placement and orientation of the mid-plane connectors was carefully chosen to allow clearance for easy connection and disconnection.

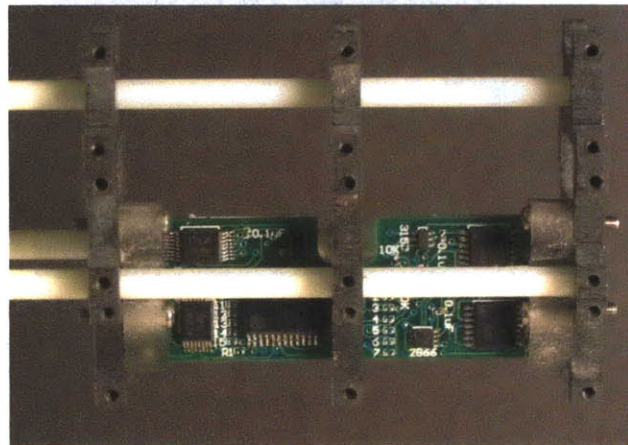
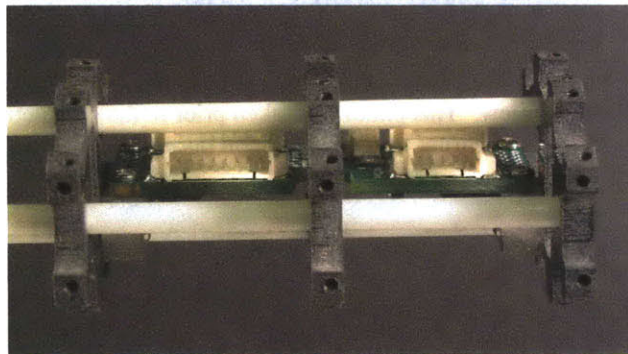
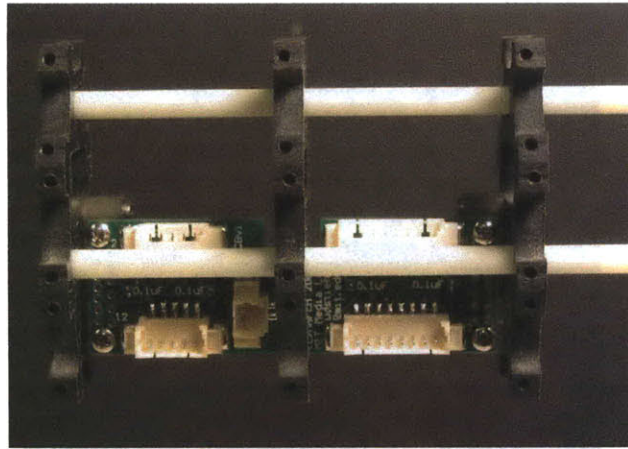


Figure 11-16: The Mechanical Understructure with Mid-Plane Circuit Board Mounted. At top is the front view showing the careful placement of connectors. In the middle is the top view showing the connectors for the top set of circuit boards. At bottom is the back of circuit board view.

Figures 11-17 through 11-21 show the completed assembly.

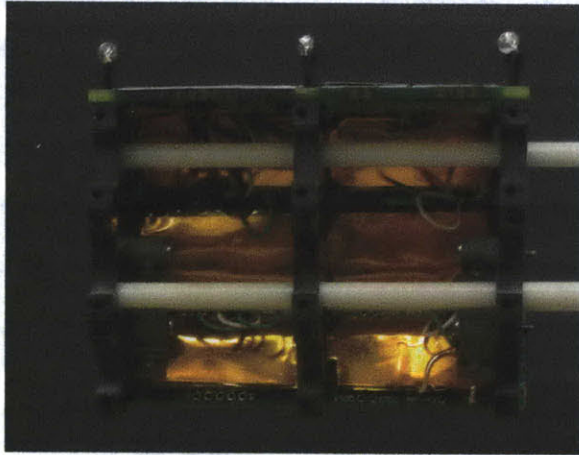


Figure 11-17: The Mounted Sensor Circuit Boards – Internal Shielding View. This photo was taken prior to the completion of wiring for demonstration purposes.

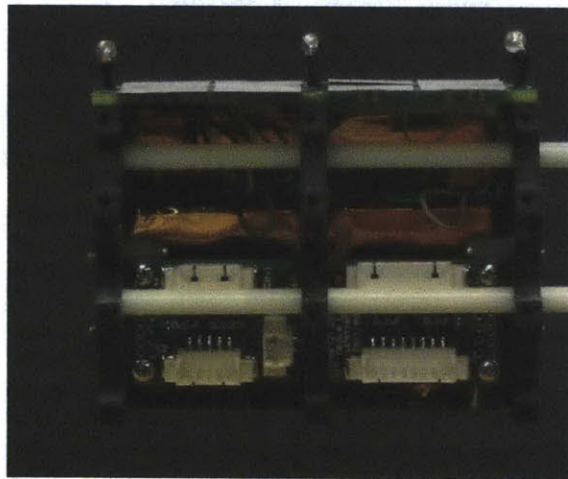


Figure 11-18: The Mounted Sensor Circuit Boards and Mid-Plane Circuit Boards – Internal Shielding View. As in Figure 11-17, this photo was taken prior to the completion of wiring for demonstration purposes.

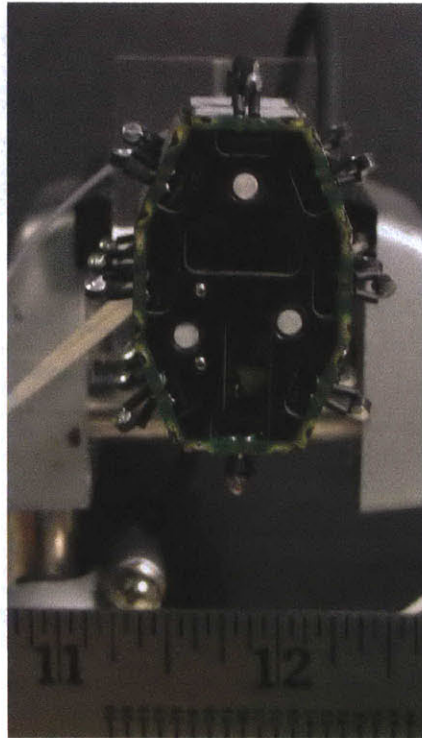


Figure 11-19: The Completed Arm Assembly – Front View.

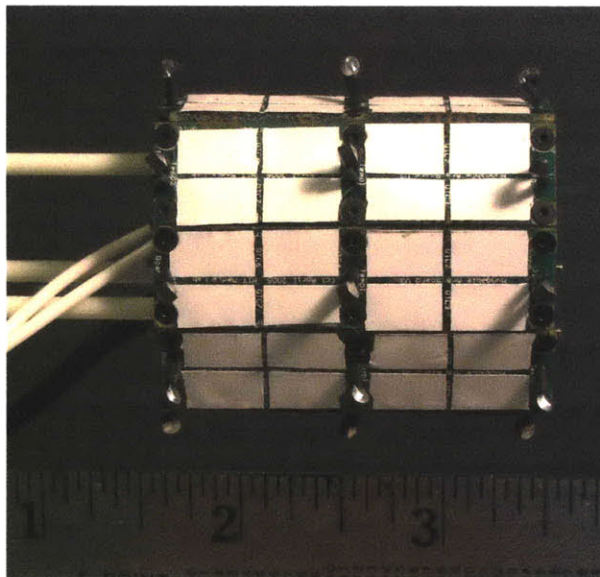


Figure 11-20: The Completed Arm Assembly – Side View

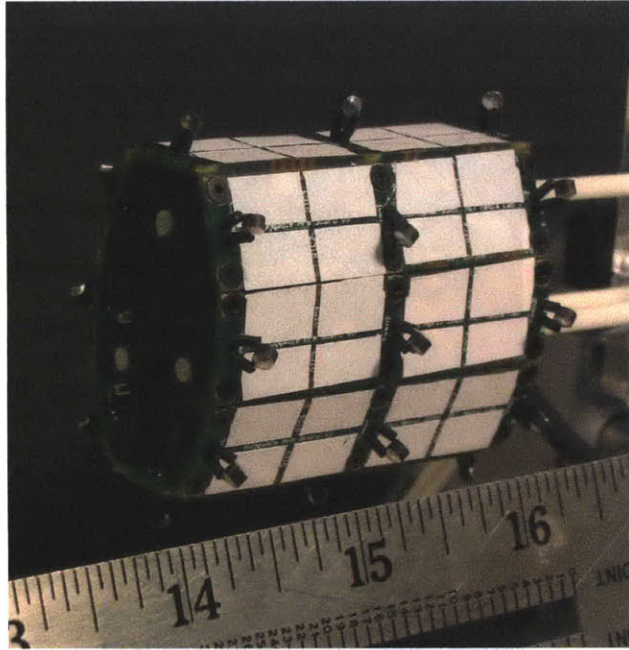


Figure 11-21: The Completed Arm Assembly – Perspective View

12 Electronic Design

12.1 Multi-layered Approach

The “sensitive skin” of the Huggable is based upon the current design for Leonardo. Compared to the Huggable, the design of the hands for Leonardo is a much simpler system. The Huggable features three types of sensors. This mixed sensor design requires more components than could fit on a single board inside the arm section described in the previous chapter. Thus a multilayered approach was used.

12.1.1 Division Into Body Regions

First sensors were combined into body regions. Each arm section has two regions as shown in Figure 12-1. One region encompasses the four sensor circuit boards of the top and left side. The other region is the remaining four circuit board on the bottom and right side.

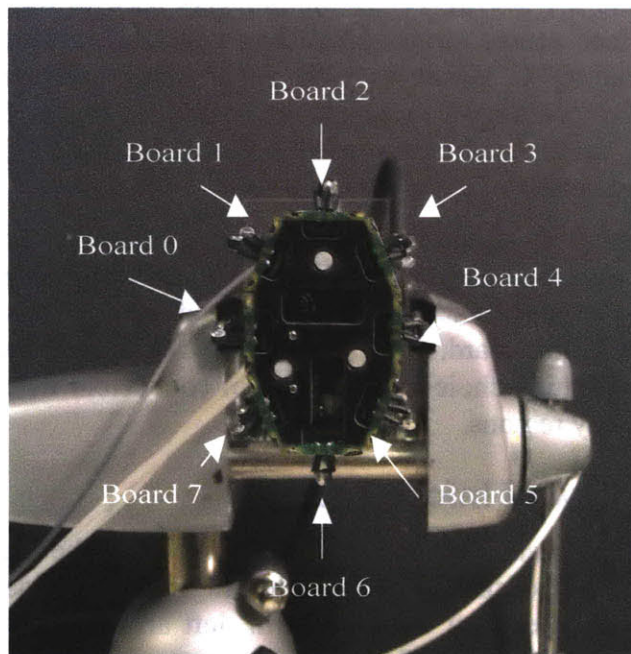


Figure 12-1: The Numbered Sensor Circuit Boards. Boards 0 through 3 are the top/left side region. Boards 4 through 7 are the bottom/right side region.

The electric field sensors necessitated such a division within the arm. The processing time for electric field sensor is much longer, on the order of 4-5msec, compared to the temperature or QTC sensors, on the order of 50 μ s. Thus for issues of speed it was decided to keep the number of capacitive sensors to fewer than 16.

Using the arm solid model of Figure 11-4, we can see that there are four sections of the arm. A fifth section, the front end cap, is not shown in this model. The electric field sensing was selected for its ability to measure proximity, thus it has a wide receptive field, to use the parlance of the somatosensory system. Therefore a single sensor can measure the proximity to the surface of the arm. Fine spatial resolution is not needed for this type of sensing.

In addition to the electric field sensors, the multiplexing capabilities of the mid-plane circuit board also contributed to grouping of sensors into regions. Multiplexers are commonly produced to switch from a selection of channels in multiples of 2, such as the 8:1 SN74LV4051 multiplexers used in the Leonardo hands. Each sensor circuit board has a total of two outputs – a multiplexed QTC signal as well as a multiplexer temperature signal. By combining these circuit boards in groups of four, a single 8:1 multiplexer can be used to output the final signal to the processing board.

The final reason for the grouping was due to the physical size limits of the connectors. As shown in the previous chapter, there were a series of size constraints placed upon the design of the mid-plane circuit board. Thus only two sets of connectors could be used. The natural choice for two sets of connectors would be two separate body regions.

12.1.2 Flow of Information

The current implementation is one part of the much larger “sensitive skin” of the Huggable. The Huggable is divided into six sections (right leg, left leg, right arm, left arm, body, and head) with each section assigned to one somatic processing board, such as the one described later in this chapter. Each somatic processing board outputs to an embedded PC inside the Huggable running a

simplified version of the “Virtual Somatosensory Cortex” software system. Figure 12-2 shows this division.

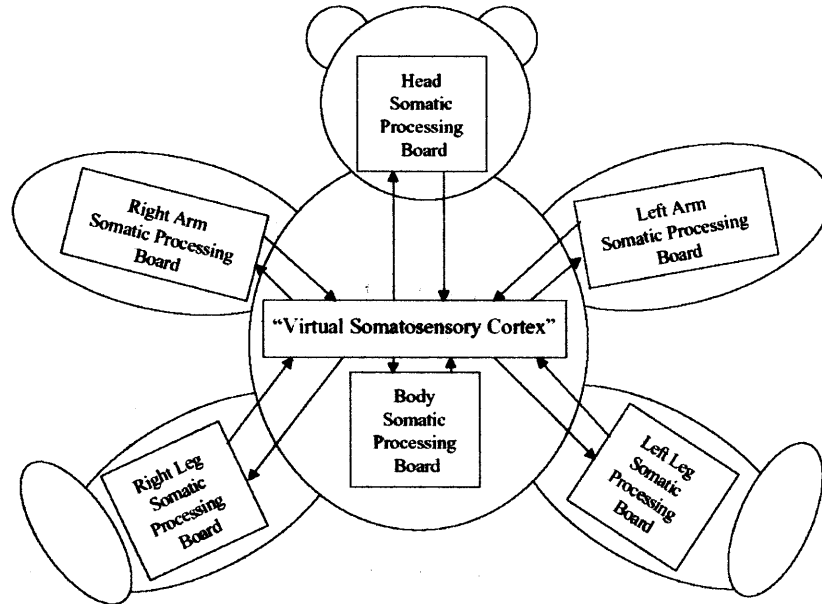


Figure 12-2: The Division of the Huggable into Somatic Processing Board Sections

Each somatic processing circuit board receives data from each of the mid-plane processing boards within that section. For example, the somatic processing board for the left arm would receive input from the current arm section implementation as well as from the other four sections (end cap, elbow, middle arm, and upper arm). As previously mentioned, each mid-plane processing board receives input from each of the arm sensor boards connected to it. Figure 12-3 is a diagram of the flow of information within a somatic processing section.

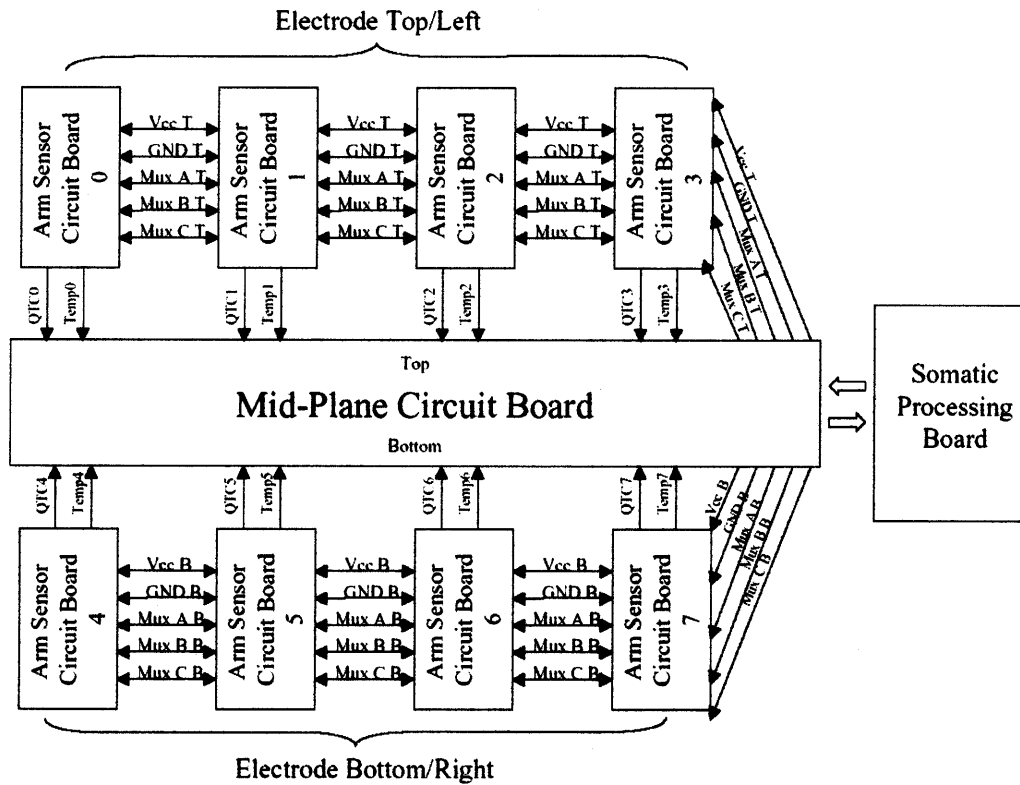


Figure 12-3: The Flow of Sensor Information Within One Somatic Processing Section

The next sections of this chapter detail each part of this information flow from sensor to somatic processing board.

12.2 Sensor Performance

12.2.1 QTC Sensor

A sense of touch is important for both robots and living creatures. In the Leonardo hands described in Section II, Interlink FSRs were used as the robotic analog to this type of somatic sensor. However, these sensors posed a series of drawbacks, mainly in sensitivity and geometry. For the Huggable, Quantum Tunneling Composites (QTC) were chosen for detecting contact pressures.

A Quantum Tunneling Composite is a material which normally acts as an insulator, but when deformed, it becomes highly conductive. This change is due to Quantum Tunneling in which electrons, seen as waves in Quantum Mechanics, encounter a non-conducting barrier. If the exponential decay of the wave has not reached zero by the time the electron emerges on the opposite side of the non-conducting barrier, then there is a chance that electron could be on the opposite side (Peratech. 2004). In the QTC switch substrate, the metal particles of the material come so close together that Quantum Tunneling can occur.

Figure 12-4 is a plot of the sensor resistance change as a function of force. Peratech claims that the switch substrate has a resistance range from over 10M-ohms to less than 1 ohm (Peratech Product Literature). This range is much larger, and thus much more sensitive than that of the Interlink FSRs used in the Leonardo hands. More information on QTC can be found at the Peratech website: <http://www.peratech.co.uk/>

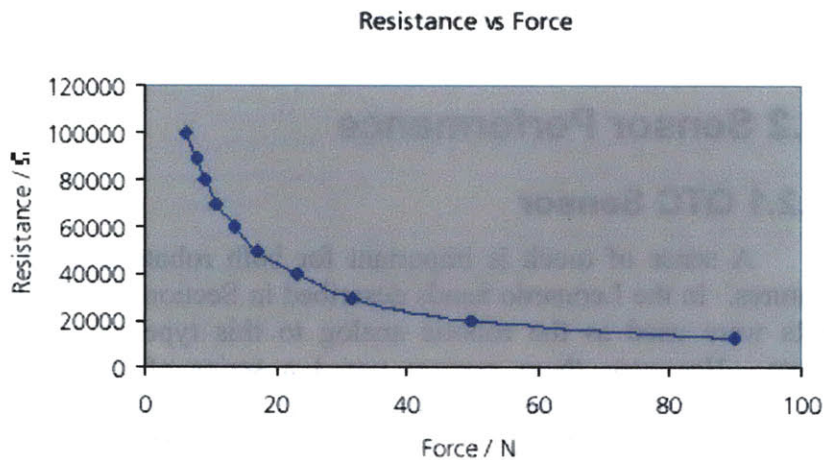


Figure 12-4: The Plot of the Resistance vs. Force for the QTC Switch Substrate. (Peratech Product Literature)

12.2.2 Electric Field Sensor

The QTC sensors are great for contact, but there are times when sensing contact force is not enough, especially for a soft, furry robot such as the Huggable. In nature, an entire class of receptors has emerged to detect the motion of hair on the skin. These hair receptors can detect such things as stroking or fluttering.

The Huggable should be able to detect when it is lightly petted; thus, some form of hair receptor is necessary. One implementation would be to use a form of whisker sensor such as the sensors used in the Tribble (Lifton, Broxton et al. 2003) or the Paro (Shibata and Tanie 2001). Such a sensor is created by gluing a whisker material to a piezoelectric cantilever. One problem with such an implementation is that these sensors measure only transients, or in the parlance of the somatic system act as rapidly adapting sensors. The ideal sensor would be able to sense static contact as well as transients, much like the QTC and FSR sensors are able to. Another problem arises in the physical fabrication of such a sensor. The whisker material would need to poke through the silicone rubber and through the fur, which poses a problem in the event that the robot ever needed to be taken apart for repairs or needs maintenance. Additionally, to transmit force to the cantilever, the material would need to be significantly stiffer than

the soft fur of the arm sleeve. Thus the Huggable would no longer feel like a teddy bear.

Electric field sensing was selected as the analog to the hair receptors. This type of sensing measures the distance between an object and an electrode by measuring capacitance. An in-depth discussion of this type of sensing can be found in (Smith 1999). The Motorola/Freescale Semiconductor 33794 electric field sensing integrated circuit, used in the Huggable, is associated to the work of Josh Smith. Another reason for the selection of electric field sensing was that other projects at the Media Lab in recent years have featured various other uses of electric field sensing, and thus a wide body of knowledge was available (Paradiso and Gershenfeld 1997; Smith, White et al. 1998).

The 33794 was chosen for its ability to “black box” the design of an electric field sensor. The main task of the microcontroller on the somatic processing board is to switch between sensors, convert the analog value to a digital value, and finally to output this value via serial communication to the embedded PC. Thus it was important to not spend clock cycles performing an electric field sensing measurement. The 33794 can process one electrode while the microcontroller performs other tasks. The 33794 also has the capability to multiplex between nine electrodes and provides a driven shield. When one electrode is selected, the others are grounded by the 33794 to improve the sensing resolution of the selected electrode.

Measuring the proximity of human contact through electric field sensing offers many useful applications for the Huggable. First, some of the potential populations which the Huggable can benefit are the elderly, young children, and patients in hospitals who do not have much strength. While the QTC sensors can be tuned to detect very light touch, as will be described at the end of this chapter, the electric field sensor guarantees that some sensor signal will be received from even the lightest of contact. The electric field sensor is able to distinguish between contact with people and other objects, when tuned as discussed later in this chapter. Thus this sensor can help with classification of the types of touch as the affective content of touch should be encoded only when the Huggable is sitting on a person’s lap as opposed to sitting alone on a tabletop. Finally the proximity information can be used to detect where the person is in relationship to the robot. If the

robot is gently held in someone's lap, the back of the Huggable may not be in contact to the person's chest, but it will be close to it. Thus, the proximity measurement can allow the robot to interpret that the person is behind the robot as opposed to in front. This information becomes important for look-at and other relation behaviors.

12.2.3 Temperature Sensor

The final modality of the sensitive skin is temperature. There is an entire class of temperature receptors in human and animal skin. Each of these receptors encodes a specific range of temperature, as discussed in Chapter 2. Thermistors were chosen due to their low cost and wide range. The thermistors currently used are 100 K-ohm at 25 degrees Celsius with a negative temperature coefficient (NTC). Figure 12-5 shows a comparison between NTC thermistors and RTDs in resistance-ratio vs. temperature characteristics from (Thermometrics Product Literature.).

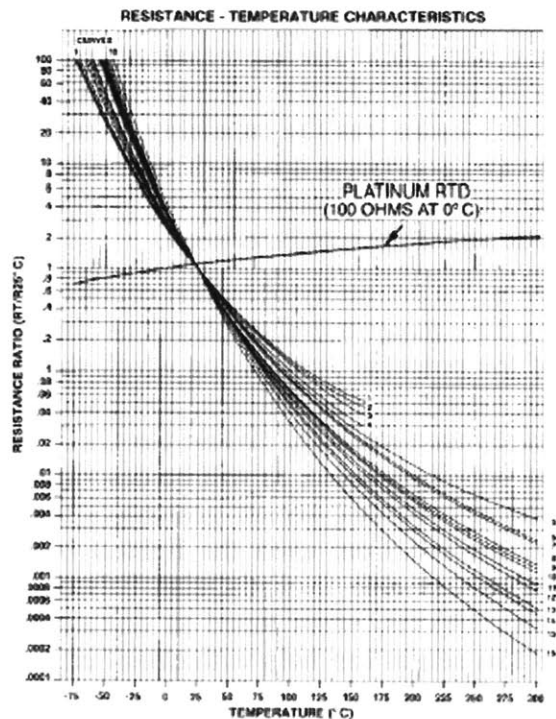


Figure 12-5: Resistance-Ratio vs. Temperature Characteristics for Thermistors and RTDs. (Thermometrics Product Literature.)

As can be shown from Figure 12-5 the thermistors have a very wide range of sensing. Compared to the other sensors of electric field and force, the thermistor has a much slower response rate – on the order of seconds. While this type of delay would not be appropriate if used alone, when combined with the other two types of sensors, the long time constant actually is a benefit. Such types of interactions as hugs and squeezes would max out the other types of sensors, but the continual slow change in temperature can indicate that the person is still there even if the other sensors have not changed. Additionally, because people emit a natural body temperature, this type of sensor can be used as another bit of information in the determination of whether the contact is due to a person or an inanimate object.

12.3 Arm Circuit Boards

The flow of information described at the beginning of the chapter begins with the arm sensor circuit boards. Each of these sensor circuit boards features three types of sensors described in the previous section of this chapter. Figure 12-6 shows the bottom of the arm sensor circuit board.

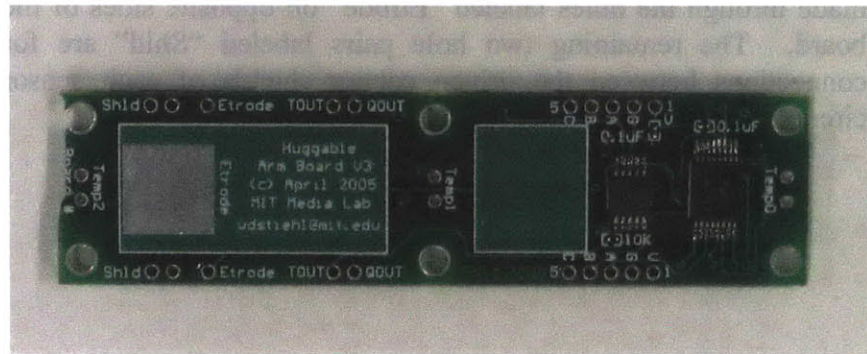


Figure 12-6: The Bottom of the Arm Sensor Circuit Board.

Each of the arm sensor circuit boards is designed to function as part of a group of four circuit boards as described earlier. These regions (top and left side or bottom and right side) are formed by connecting the series of boards as shown in Figure 12-7. Thus the holes shown in Figure 11-6 are connected across the board to allow common input information to pass through from one board to the next. This common information is divided into two sections. The 5 holes labeled “V” (Vcc), “G” (Ground), “A”

(Multiplexer Control A), “B” (Multiplexer Control B), and “C” (Multiplexer Control C) are the common power and control inputs for the on-board multiplexers for the QTC and temperature sensors. The QTC multiplexer is a single SN74LV4051 8:1 analog multiplexer. The temperature multiplexer is a MAX4634 single 4:1 analog multiplexer. Both multiplexers share common A and B control channels to limit the number of wires required.

Just to the left of the midline of the circuit board are two pairs of holes labeled “QOUT” and “TOUT.” These are the output of the QTC and Temperature multiplexers. These signals are connected to the sensor select multiplexer on the mid-plane circuit board, which will be discussed in the next section of the chapter. The holes were placed on opposite sides of the circuit board to allow for flexibility in placement of the wires as some boards will have the holes near the top of the circuit board closer to the mid-plane connectors while others will have the holes at the bottom closer.

The electric field sensor electrode is located on the bottom layer of the sensor circuit board shown by the light green rectangles. Connections between the electrodes in a region are made through the holes labeled “Etrode” on opposite sides of the board. The remaining two hole pairs labeled “Shld” are for connections between the driven copper shields of each sensor circuit board.

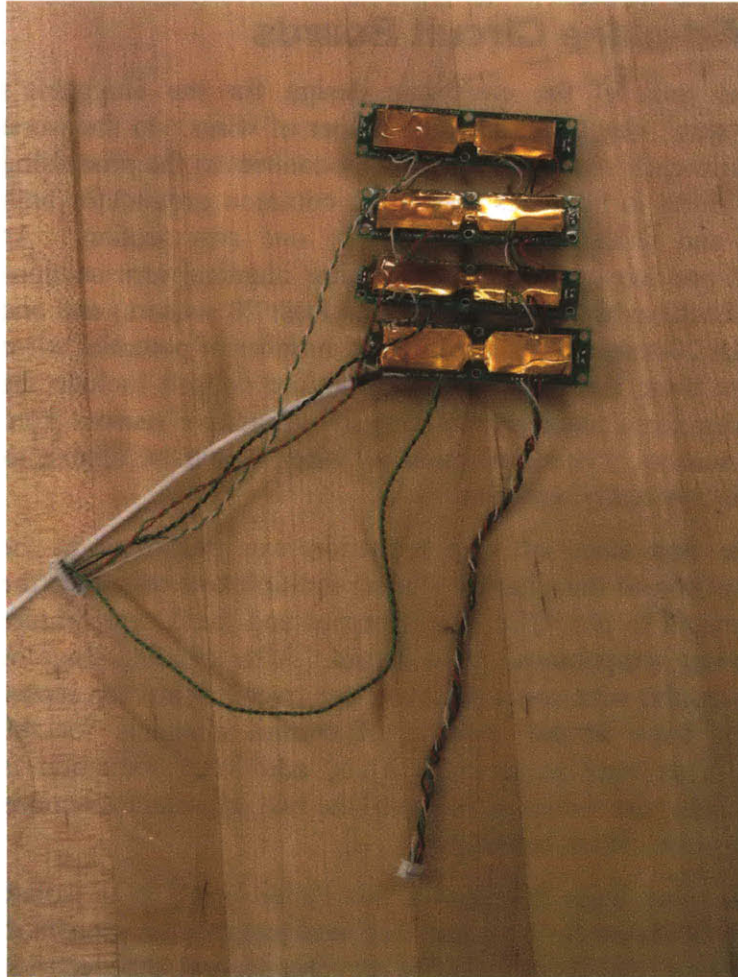


Figure 12-7: The Assembled Top and Left Side Arm Sensor Circuit Boards.

The white coaxial cable is shown at the left of Figure 12-7 connects to the electric field sensing electrode. The shielding of this cable is connected to the driven shield input of the sensor circuit board and is driven by the 33794. The 8-pin connector in the middle of Figure 12-7 connects the QTC and temperature outputs of each of the four sensor circuit boards to the mid-plane circuit board. The 5-pin connector at the right of Figure 12-7 connects to the common multiplexer and power output of the mid-plane circuit board. Each sensor circuit board was connected to its neighbors as shown in the figure to reduce the number of wires going to the mid-plane circuit board.

12.4 Mid-plane Circuit Boards

One goal of the electronic design for the Huggable's "sensitive skin" was to reduce the number of wires. In the worst case scenario each sensor would directly connect to the processing board, resulting in 90 wires (assuming common ground for both the QTC and temperature sensors) for one arm section. As mentioned previously there are two other identical arm sections (90 wires each) as well as the elbow (at least 20 sensors) and end cap (at least 20 sensors). Thus, the total number of potential wires for sensors alone is over 300. This number doesn't include the wires needed for electrically isolating the capacitive sensors from the other sensors. This collection of wires would be almost as thick as the tiny teddy bear arm.

The first stage of wire reduction was described in the previous section of this chapter – using multiplexers to reduce the 8 QTC sensors to one QTC board output and the 3 temperature sensors to one temperature board output. After the first stage of multiplexing, the wire count is now 2 per circuit board for sensor output, but there is the addition of control channels for the multiplexers as well as power. Thus, additional reduction is required. This wire reduction is one of the two important functions of the mid-plane circuit board.

The other main function of this circuit board is to isolate the electric field sensors from the QTC and temperature sensors in the arm section. As discussed in the previous section, the electrode is located on the bottom layer of the arm sensing circuit board with a driven shield below. This driven shield causes the field lines from the sensor to travel up through the other sensors and copper electrical traces above the electrode in the sensor circuit board. Thus, the actual electrode includes the QTC sensors, the temperature sensors, and the traces. Because the traces carry the electric field sensing signal, this signal is also conducted down the wires which connect each sensing board to the other boards in the same region, as well as to the output and input wires connecting to the mid-plane circuit board. This poses a problem as now, through the direct connection of these wires, the electric field sensing signal is coupling into the mid-plane circuit board. This coupling reduces sensor performance. The solution is to place a switch to electrically disconnect these wires connecting to the mid-plane circuit board from the rest of the mid-plane circuit during the

electric field sensing measurement. In the next sections the specifics the methods employed to reduce the wire count will be detailed. Additionally, the methods used to isolate the electric field sensing from the other sensors will be described.

12.4.1 Wire Reduction

Figure 12-8 shows the bottom side of the mid-plane circuit board.

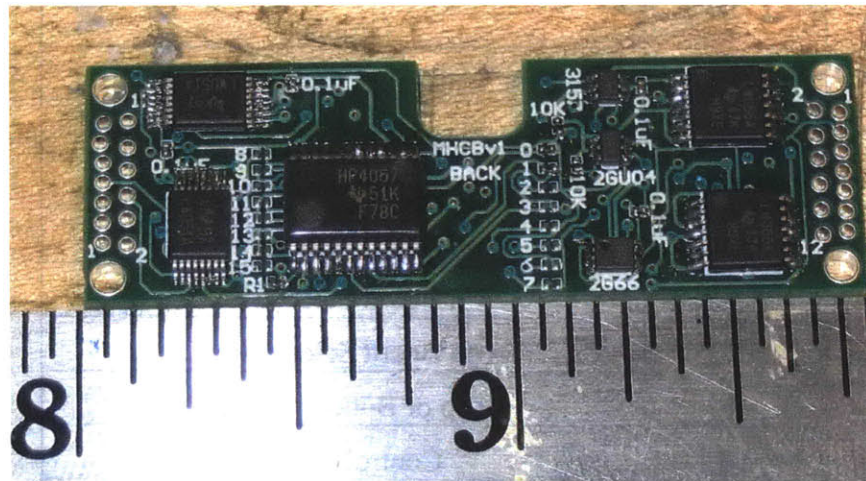


Figure 12-8: The Bottom of the Mid-Plane Circuit Board.

This board is designed to pass common information through the board to the other circuit boards in the region in a similar design as the sensor circuit boards discussed in the previous section of this chapter. Here the 13 holes located on opposite sides of the circuit board carry power and common control signals. Table 12-1 shows the pin assignment for these 13 holes.

Table 12-1: The Pin Assignment for the Common Throughput of the Mid-Plane Circuit Board.

Pin Number	Description
1	Power (Vcc)
2	Ground
3	Arm Sensor Circuit Board Mux A
4	Arm Sensor Circuit Board Mux B
5	Arm Sensor Circuit Board Mux C
6	Arm Board Select Mux A
7	Arm Board Select Mux B
8	Arm Board Select Mux C
9	Top or Bottom Control
10	Control Mux A
11	Control Mux B
12	Control Mux C
13	Control Mux D

The first five pins of Table 12-1 are the same five common input pins for the arm sensor circuit boards. Pins six through eight are for the control of the multiplexers on the mid-plane circuit board to select the arm sensor circuit board output. Pin nine is to select the body region (top and left side or bottom and right side) output. Pins ten through twelve are used to select which of the potential sixteen electric field sensing electrodes is activated.

The mid-plane circuit board is divided into the two regions with a separate SN74LV4051 single channel 8:1 multiplexer and set of switches for each region. The switches will be discussed in the next section of the chapter as they relate to the isolation of the electric field sensors from the other sensors. Each 4051 multiplexer receives two inputs (QTC output and temperature

output) from each of the four arm sensor circuit boards in the region. The output of this multiplexer then passes through a Fairchild Semiconductor NC7SBU3157 SPDT analog switch. The other input to this switch comes from the other region's 4051 multiplexer. The top or bottom control is used to select which region's multiplexer output to connect to the sensor output of the mid-plane circuit board. This output then travels down the length of the arm to the somatic processing board. Thus, by the two stages of multiplexing and single stage of switching the 88 sensors can result in a single wire output for each arm section.

12.4.2 Electric Field Sensor Isolation

As discussed previously, it was important to isolate the electric field sensing electrode from the other sensors through switches. This section details the approach taken to do so.

Each electrode is assigned a number. For example, in the current arm section the electrode for the top and left side is electrode 0, and the electrode for the bottom and right side region is electrode 1. One approach would be to have a separate control wire for each electrode. With the five arm sections and two electrodes for each of three of these five section, a total of 8 wires would be required. Other body regions may have more than just 8 electrodes, and thus would require more wires. One goal of this design was to minimize the number of wires to not only reduce cost, but complexity as well.

The solution chosen requires only four wires to switch between sixteen electrodes. A Texas Instruments CD74HC4067 single channel 16:1 analog multiplexer is used for this task. The control mux signals (Control Mux A through D) are used to select which of the sixteen capacitive sensing electrodes will be active. Each circuit board has two rows of numbered 0201 resistor footprints, as shown in Figure 12-8. A 0201 0.0 K-ohm jumper resistor is placed across the corresponding numbered footprint as the electrodes in the region. For example, in the current arm section jumper resistors are soldered to the 0 and 1 numbered footprints. The even numbered footprints correspond to electrodes in the top region of the arm section, while the odd numbered correspond to the electrodes in the bottom region.

The input of the 4067 is Vcc, or in digital logic a high value 1. The control mux signals select an electrode, such as electrode 0. If there is a jumper resistor present, this high value signal is then passed to the inhibit pin (INH) of the corresponding 4051 multiplexer. If the electrode selected is even, the inhibit pin of the top region multiplexer is pulled high. If odd, the bottom region multiplexer is pulled high. A pull-down resistor is used with both multiplexers to pull the inhibit pin low in the default case. When the inhibit pin is pulled high in the 4051 multiplexer, the input and output channels are disconnected from each other. Thus, the sensor outputs from the corresponding electrode region are now isolated from the rest of the system.

The same high inhibit signal which passed through the jumper resistor is then inverted using a Texas Instruments SN74LVC2GU04 dual inverter gate. The top region uses one of the inverters of the 2GU04, while the other inverter is for the bottom region. The inverted output of the high inhibit signal is now a low value. This low control value is then passed to the switches of the appropriate region for disconnecting the power and the multiplexer control for sensor selection on each sensor circuit board.

In the default case, the control signal for each of the power and sensor selection multiplexer control channels is a high value. This high value is the inverted default low multiplexer inhibit value. Two switches are used. The top region is switched using a Texas Instruments SN74LV4066A quadruple bilateral analog switch for the power (Vcc), ground, Mux A, and Mux B signals, and one channel of the Texas Instruments SN74LVC2G66 dual bilateral analog switch for the remaining Mux C signal. The bottom region is switched with the other channel of the 2G66 as well as an additional 4066A. All switches in the same region are controlled by the same control signal, thus when the control signal is low, that region is disconnected, isolating the capacitive sensor of that region from the rest of the system.

This isolation allows for the QTC and temperature sensors of the other regions to still be read, even though one region is currently in the electric field sensing mode. Such an approach allows for constant processing of sensor information without the long delays of electric field sensing.

12.5 Huggable Somatic Processing Circuit Board

The last stage of this multi-level approach occurs at the somatic processing circuit board. This circuit board outputs control signals and provides power to the mid-plane and arm sensor circuit boards via the 13-conductor flexible control cable as described previously. The somatic processing circuit board receives one combined QTC and temperature sensor output from each of the mid-plane boards in the Huggable section. The processing board also receives the sensor output from and provides a driven shield to each of the electric field sensing electrodes in the Huggable section. Thus in the current implementation of one arm section, there are four electrical cables connecting the somatic processing circuit board to the mid-plane circuit board and sensor circuit boards. These are the 13-conductor control cable, the single conductor QTC and temperature sensor output, and two flexible coaxial cables – one per electrode.

A large development board was created to begin to explore the ways in which the somatic sensors could be processed in an efficient manner. Figure 12-9 is a photo of the Huggable somatic processing circuit board. As can be seen in the photo this large board features a number of jumpers and analog potentiometers which will be removed in the final embedded version. A jumper was placed at every control signal in the circuit design to allow for both microprocessor control as well as manual control of switching. Additionally, the circuit features both a digital potentiometer and analog potentiometer pathway for the signal conditioning of the sensory outputs. A jumper is used to switch between the analog and digital pathways. During development the analog potentiometers are used for tuning, but ultimately the Huggable somatic processing board will feature only digital potentiometers to allow for auto-calibration capabilities, which will be discussed later in this chapter.

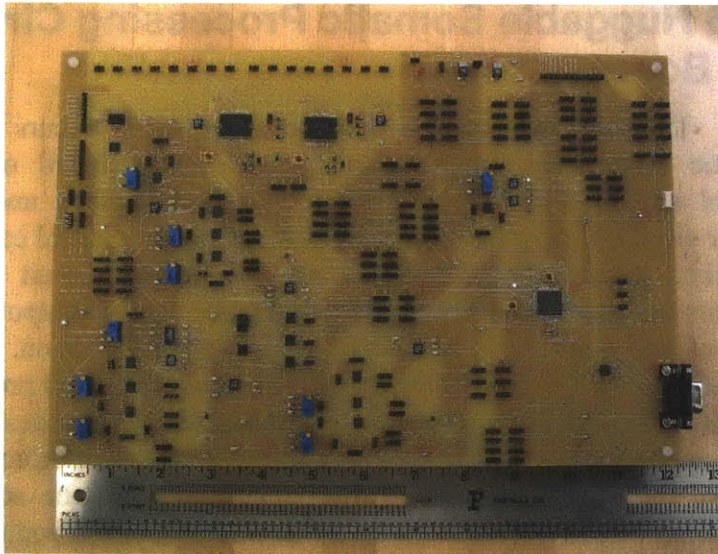


Figure 12-9: The Huggable Somatic Processing Circuit Board.

The somatic processing board uses a Microchip PIC18F8772 microcontroller. This microcontroller was selected because it has 70 I/O pins and a large program and data memory. Additionally, the microcontroller can use a 40-MHz oscillator, which at the 18F8772's slow 4 clock cycles per instruction, means that the PIC can run at up to 10 MHz. Thus, compared to the other available microchip PIC family of products, the 18F8772 is the fastest microcontroller with the greatest number of I/O pins.

In a similar flow of information as the Leonardo mid-hand processing circuit board described in Section II, the inputs from the sensors are first conditioned. Then the conditioned analog sensor value is converted to a 10-bit digital signal using the internal A/D converters of the PIC. This output is then sent to the computer via a MAX3221 RS-232 serial driver/receiver at a baud rate of 57600. This baud rate can probably be doubled in the future.

As discussed previously, the goal of the Huggable “sensitive skin” is to use these three types of sensors to pull out the affective content of how it is being touched. The use of these three sensors together can also differentiate between human contact and contact with an inanimate object. In the next sections the signal conditioning of each sensor input will be described. Because of the large force sensing range of the QTC, the QTC will be processed in three different ways – light touch, moderate touch,

and hard touch. This decision was made because one can imagine many interactions where the type of touch could fall within at least one, if not all, of the sensing regimes. Each type of processing is discussed in the next section. Finally a discussion of the auto-calibration hardware design, currently not implemented, is found at the end of this chapter.

12.5.1 Electric Field Sensing Pathway

The Motorola/Freescale Semiconductor 33794 electric field sensing integrated circuit is used as an analog to the biological hair receptors. Each electrode is paired with a driven shield. The 33794 only has a single shield output. This driven shield output is connected to the input of an Analog Devices ADG408 high-performance single 8-channel analog multiplexer. The driven shield of each electrode's coaxial cable was connected to one of the eight outputs of the ADG408. Since the ADG408 was able to only multiplex 8 channels, only the first eight electrode inputs of the 33794 were used.

The ADG408 was chosen as opposed to the 4051's used elsewhere in the design due to the fact that shield signal's range is greater than the maximum voltage rating of 5V of the 4051. The ADG408's have a maximum voltage rating of 44V, which is much larger than the 12V supply voltage required by the 33794. Thus, the ADG408's would be able to multiplex the entire shield signal.

Two identical ADG408/33794 pairs were used in this circuit so as to allow a maximum of 16 electrodes to be used in a Huggable body section (each arm, each leg, body, or head). The multiplexer control signals for each ADG408 and each 33794, as well as the DIS-SHIELD (disable shield) pin of each 33794, are directly controlled by the PIC. The control multiplexer channels (Control Mux A through D) used to isolate the electrode are also controlled by the PIC. A Fairchild Semiconductor NC7SBU3157 SPDT analog switch is used to switch between the LEVEL outputs of each 33794. This switch is also controlled by the PIC.

The 33794 outputs a 0 to 5V signal based upon the measured capacitance. In the current implementation this value is centered at 1.75 V and shows a 30 mV change between no contact and contact. Because this signal is analog, this small change can be amplified to create a 0 to 5V change which can use the full 10

bits of resolution of the A/D. The remainder of this section describes the signal conditioning used.

First this output is passed through a voltage follower configuration of a Burr-Brown OPA2340 dual channel single supply operational amplifier. Next, the output of the follower is amplified using an OPA2340 in a non-inverting amplifier configuration. This amplified signal then passes through a differential amplifier, again using an OPA2340. A 250K-ohm potentiometer is used to set the threshold value which will be subtracted from the input signal of the differential. Thus, at this stage the change in voltage is now centered near 0V and can be amplified using another OPA2340 in a noninverting amplifier configuration to produce a 0 to 5V change. The output of the amplifier is low-pass filtered using an RC circuit, and this filtered value is connected to the second A/D input of the PIC for conversion.

12.5.2 QTC Light Touch Pathway

The shared QTC and temperature output passes through two multiplexing stages. In the first stage one of the sixteen possible mid-plane shared QTC and temperature outputs is selected using a Texas Instruments CD74HC4067 single 16:1 analog multiplexer. A Texas Instruments SN74LV4052 dual 4:1 multiplexer is used for the second stage. The 4052 is used to select which type of processing is used for that sensor – QTC light touch, QTC moderate touch, QTC hard touch, or temperature. This selection is synchronized with the mid-plane and arm sensor circuit board control channels operated by the PIC. The output of the 4067 multiplexer passes through the first 4:1 multiplexer of the 4052. This signal is then sent to one of the four possible types of signal conditioning. After conditioning, the second 4:1 multiplexer of the 4052 connects the signal conditioning output to the first A/D PIC input. Both the 4067 and the 4052 channel selections are controlled by the PIC. This section describes the signal conditioning employed for light touches detected by the QTC.

The QTC is processed much like the FSRs used in the Leonardo hands described in Section II. A voltage divider, much like that of Figure 8-4 is used. A 1 M-ohm potentiometer in series with an additional 1 M-ohm fixed resistor is used instead of the 50 K-ohm potentiometer used for Leonardo's hands. As will be

discussed in the last section of this chapter, digital potentiometers are also used in an identical pathway for auto-calibration. There currently does not exist a 1 M-ohm digital potentiometer, let alone a 2 M-ohm one. A 1 M-ohm digital potentiometer can be created by placing a set of lower resistance digital potentiometers in series with one another. Thus to limit the number of digital potentiometers required, a 1 M-ohm fixed resistor is used in series with a 1 M-ohm potentiometer. From bench level experimentation, it was determined that light touch could be detected consistently above 1 M-ohm.

The output of this voltage divider then passes through a voltage follower. The output of this follower then passes through a differential amplifier with the threshold voltage set by a 250K potentiometer. This threshold is tuned to allow only light touch to be detected. A non-inverting amplifier is then used to boost this signal to a 5V scale. Finally, a low pass RC filter is used. This conditioned signal is connected to the first input of the second 4:1 multiplexer of the 4052. In all cases, the amplifiers used were the same OPA2340's used in the signal conditioning of the electric field sensors.

12.5.3 QTC Moderate Touch Pathway

The moderate touch pathway is the second of the four input/outputs of the 4052 sensor type select multiplexer. Again, a voltage divider is used as with the touch pathway. Here a 1 M-ohm potentiometer is used instead of the 50 K-ohm potentiometer of Figure 8-4. The output of the divider passes through an OPA2340 voltage follower and finally is low pass filtered using an RC circuit. This conditioned signal is connected to second input of the second 4:1 multiplexer of the 4052.

12.5.4 QTC Hard Touch Pathway

The hard touch pathway is the third of the four input/outputs of the 4052 sensor type select multiplexer. The signal conditioning is exactly the same as for the moderate pathway except a 50 K-ohm potentiometer is used instead of the 1 M-ohm potentiometer of the moderate touch pathway. The conditioned signal is then connected to the third input of the second 4:1 multiplexer of the 4052.

12.5.5 Temperature Pathway

The temperature pathway is the last of the four input/outputs of the 4052 sensor type select multiplexer. The signal conditioning of this pathway is based upon an original circuit design by Louis Basel, an undergraduate working on the Huggable project. The thermistors used were nominally 100 K-ohms at 25 degrees Celsius. A voltage divider, much like those used for both the QTC of the Huggable and the FSRs of the Leonardo hands was used. Instead of a potentiometer, a fixed 100 K-ohm resistor was selected to match the thermistor. The output of this divider is then passed through a voltage follower. A differential amplifier is used with a 250 K-ohm potentiometer for tuning the threshold. The output of the differential is amplified using a non-inverting op-amp. Because the change of the thermistor is slow, a second differential and non-inverting amplifier pair was used to increase the voltage change. The output of the second non-inverting amplifier was low-pass filtered using an RC circuit. The conditioned signal is then connected to the fourth input of the second 4:1 multiplexer of the 4052. An OPA2340 amplifier was used in all amplification stages.

12.5.6 Auto Calibration Function

The Huggable is expected to encompass hundreds of sensors within its “sensitive skin.” With such a high sensor count, calibration of each sensor becomes a concern. The QTC sensors are all hand cut and assembled, and thus, there could be slight differences between sensors. Also the silicone rubber synthetic skin, described in the next chapter, is at different thicknesses in different parts of the bear. Thus, each QTC sensor must be calibrated for all three types of conditioning – light touch, moderate touch, and hard touch – so as to fill the entire 10-bit range.

The temperature sensors will change based upon their environment. It may also be beneficial to have the temperature sensors calibrate not only to the room environment but also to the person as well. If a person has lower body heat than normal it would be ideal to calibrate the Huggable to that person’s natural temperature so that his or her interactions can be sensed as well as someone who has a normal body temperature. Additionally the two stages of amplification cause small perturbations to result in

large changes. Thus even small changes in temperature from day to day may necessitate regular recalibration.

Finally, the electric field sensor also can change depending upon the environment. If there is a lot of metal near the bear, the signal may be attenuated. Due to the high degree of amplification, slight changes from day to day may show large differences in the conditioned signal. For all of these reasons the ability to auto-calibrate is a necessary design feature.

Currently, the software to perform these functions described in the rest of this section has not been implemented, but the hardware currently is in place. As mentioned previously, jumpers are built into the Huggable somatic processing circuit board of Figure 12-9 to select which of two identical pathways are used for signal conditioning. The first of the pathways features the analog potentiometers described in Chapter 12.5.1 through 12.5.5. The other pathway uses digital potentiometers of the same value as the analog potentiometer.

For all the amplification stages, an Analog Devices AD5235BRU dual 250 K-ohm 1024-tap digital potentiometer is used. This potentiometer was selected because it allows for 10-bit resolution in tuning both the gains as well as the thresholds for each amplification compared to the usual 8-bit resolution of most digital potentiometers on the market.

The 1 M-ohm potentiometer used for the QTC light measurement is created by connecting the outputs of the two digital potentiometers together in series. The Analog Devices AD5263 quadruple 200 K-ohm digital potentiometer and the Analog Devices AD5262 dual 200 K-ohm digital potentiometer were selected. Both of these devices have 8-bit resolution. Due to the fact that these potentiometers would be placed in series with each other as well as with a fixed 1 M-ohm resistor, an 8-bit resolution was deemed appropriate.

The 1 M-ohm potentiometer used for the QTC moderate measurement is formed by placing the outputs of two AD5235BRU dual 250 K-ohm potentiometers in series with each other. The 10-bit resolution was desired as it was not clear where within the 1 M-ohm spectrum the potentiometer value should be tuned to. Likewise, for the QTC hard measurement, the outputs of a single AD5235BRU 25 K-ohm digital potentiometer are placed

in series with each other to form one 50 K-ohm digital potentiometer.

Each digital potentiometer uses SPI communication to receive input from the PIC to set its value. The chip select (CS), SPI output (SDO), and SPI clock (SCK) signals are output by the PIC and passed through a series of three 4051 8:1 multiplexers, one multiplexer for each signal. These multiplexers are under PIC control. The decision to multiplex the signals rather than clock the data through each potentiometer from one to another using the SPI output (SDO) pins of each digital potentiometer was made to increase speed and decouple sensor conditioning processes from each other. There will be many cases where the value of a digital potentiometer will need to be changed while another digital potentiometer is in use, such as adjusting the value of a QTC sensor while reading the electric field sensor.

The auto-calibration routine must be able to tune each digital potentiometer of each amplification stage just as a person would tune the analog potentiometers. During the calibration of the amplification stages it is important to be able to disconnect the output of one stage from the input to another and read that output value. A set of three switches are used to isolate portions of the circuit from one another. The switches used are a Maxim MAX4636 dual SPDT CMOS analog switch and a Fairchild Semiconductor NC7SBU3157 SPDT analog switch.

These switches normally connect the output stages to input stages as the PIC sets each switch control to a default low value. If the PIC pulls the switch control high, then the output of that amplification stage is connected to a 4067 16:1 multiplexer and disconnected from the input stage of the next amplifier. The output of the 4067 is connected to the third analog input of the A/D. Due to the fact that there were not enough free pins on the PIC to control the 4067 calibration multiplexer, a Texas Instruments SN74LV393A dual 4-bit binary counter was used. The 393A was under PIC control. The PIC can run an auto-calibration routine by selectively connecting and disconnecting the various op-amp stages and threshold potentiometers and reading the value of each stage using the calibration multiplexer and its internal A/D as described above.

It is important to note that the signal conditioning for the electric field sensors and the temperature sensors described in the

previous sections has been changed from that of the original design, and, as such, additional switches would be needed to fully auto-calibrate as described in this section of this chapter.

13 Synthetic Silicone Skin

13.1 Why Give a Robot Skin?

As was previously described in Chapter 2, our skin is viscoelastic. But should synthetic skins designed for robots be as well? In their article, (Karason, Srinivasan et al. 1999) answer this question with the following:

“By definition, tactile sensing is achieved through direct contact with objects, and therefore a ‘skin’ is necessary to protect the sensors from physical damage. The requirements that the skin should be soft comes from the needs to have (1) regions of contact within which skin surface conforms to the object surface (instead of point or line contact that occurs between two rigid objects), and (2) significant deformation within the medium so that the sensors are activated and have enough resolution. If the substrate material on which the sensors and the skin rest is also soft, then, in addition to the above, better prehension stability can be achieved...Thus, although robotic tactile sensors themselves might differ in their operation...the overall configuration of all the designs is that of mechano-sensitive transducers embedded in a deformable medium.” (Karason, Srinivasan et al. 1999, pgs 131-132)

Thus it becomes clear that a “soft skin” is necessary for tactile sensing. But these requirements are based solely on function. If one is to design either a sociable robot or an anthropomorphic robot that attempts to display the illusion of life, the “skin” has other important design constraints as well. It must be flexible and stretch around joints. It must look lifelike and organic. If the robot and human are to interact together through touch, the skin must have an organic feel as well. Thus, when the external look and movement of the robot are equal to or greater than its function, a whole new set of design constraints for a “sensitive skin” must be employed. Much of the text in Chapter 13.1 and 13.2 has been reproduced from (Stiehl 2003).

But what material should this “skin” be made of? To answer this question one should look to the fields of prosthetics and special effects. The field of prosthetic rehabilitation, more than any other field of medicine, knows how important the exterior “skin” is to a patient who has suffered the loss of a limb, or has lost

portions of his or her face to cancer or other disease. In the words of Keith F. Thomas, a maxillofacial prosthetist, “the mental trauma associated with severe facial deformity must be immense, as the face is the most important non-verbal means of communication” (Thomas 1994, pg 26). In this field, materials and techniques are used in order to create prostheses that can help patients regain some of their dignity. A few examples of some of these realistic prostheses appear in Figure 13-1.

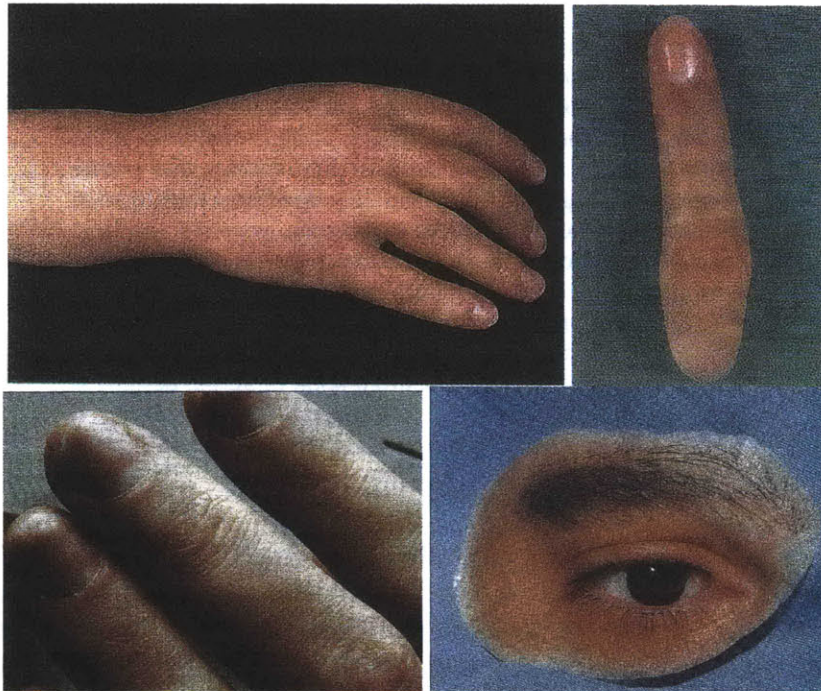


Figure 13-1: Examples of Realistic Prostheses. At top are a silicone rubber hand and fingertip from (Thomas 1994, pg 136). Lower left is a detailed close-up of silicone rubber fingers from (McKinstry 1995, pg 120). Lower right is an ocular prosthesis from (McKinstry 1995, pg 117)

As is clearly evident from these images, each possesses an amazing lifelike quality. The translucency, shown best in the feathered edges of the ocular prosthesis, is key to this quality. In addition, silicone rubber is capable of picking up very minute detail as can be shown in the close-up of the fingers in Figure 13-1. Silicone rubber is “the most popular material to use in this field due to their speed and ease of processing, and their flexibility and durability” (Heller and McKinstry 1995, pg 84).

In many ways the animatronics and special effects industries achieve the illusion of life on a daily basis. Through the puppeteering and design of their creatures, they convince the audience that dinosaurs have come back to life, or that a toy truly can feel. Again, the exterior look of the robot or puppet is intimately related to the audience's perception. It is for this industry that a whole new type of silicone – the special effects silicone has been developed. These silicones are much softer and stretchier than their medical counterparts and are also easier to work with. Even a new series of silicone gel prosthetic appliances is under development, which will allow the actor to further convince the audience that he has aged 40 or 50 years or has transformed into a new fanciful character.

Silicone has begun to enter the world of robotics as well, but still it has a long way to go before it is fully accepted into the field. It has been used as part of an animated face robot as shown in Figure 13-2 (Hara and Kobayashi 1997).



Figure 13-2: Three Different Facial Expressions of Hiroshi Kobayashi's Face Robots from (Aylett 2002, pg 111) At left is shown happiness. Center is anger. At right is sadness.

In the summer of 2002, at SIGGRAPH 2002 in San Antonio, the Robotic Life Group presented "Public Anemone," a large interactive installation of robotic theater in which the main robot, the anemone, was outfitted with a silicone skin. The addition of the silicone skin not only protected the robot from the waterfall and pond nearby but also helped to provide an increased illusion of life as can be seen from the images in Figure 13-3.



Figure 13-3: Public Anemone shown at SIGGRAPH 2002 in San Antonio, Texas.

In addition to providing an exterior to robots, silicone has also been employed as part of the development of a slip sensor (Yamada, Maeno et al. 2002).

The Huggable was designed to be touched, and as such, the way it feels will have a huge effect on the way people interact with it. If the Huggable feels like a hard plastic shell, it is not something that people would like to pet. A silicone skin provides a soft life-like feel to the robot, which encourages people to pet it in the same ways as they would an animal.

In the next section of this chapter a general overview of silicone will be provided. Next, a discussion of the formulations of different silicones and the effect each formulation has on durometer will be discussed. Finally, the design of the silicone skin for the Huggable arm section will be detailed.

13.2 Types of Silicone

There are two main types of silicone which are used in the special effects industry and have applications in the field of robotics and tactile sensing. The first type is condensation cure, also referred to as “tin cure” or simply “tin”. These silicones need both air and moisture in order to cure but will set up against a wide variety of materials (McLaughlin 1999). They are room temperature vulcanizing (RTV), which means that these silicones do not require an oven to cure. Thus tin cure silicones are appropriate for use in robotics or other research as, unlike with foam latex, another popular skin material in the special effects industry, there is no need for the upfront cost of a large oven. Tin silicones are available as either a 2-part kit, consisting of the base and the catalyst which when combined will form the rubber, or a 1-part silicone, such as caulk, which will begin to set once it is exposed to the air. There are also two types of 1-part tin silicones. Acetoxy silicones give off acetic acid (vinegar) as they cure (McLaughlin 1999, pg 3). Oxime cure silicones, also known as neutral cure silicones, do not have the strong odor of acetoxy silicones. The most common applications for tin silicones are for mold making and robotic/animatronic skins, due to the fact they will set up against a wide variety of materials.

The second type of silicone cure type is the platinum addition cure, also known as “platinum cure” or simply “platinum.” Unlike tin silicones, where there is a negligible amount of shrinkage, platinum silicones show practically no shrinkage and are capable of curing in a vacuum. However, these silicones are much more difficult to work with and have usually been employed for use in the field of prosthetics where the environments are very clean. Platinum silicones will not set up in the presence of amines, ammonia, tin, nitrogen oxide, carbon monoxide, sulfur and materials containing sulfur such as some modeling clays (like Roma Plastilina), natural and synthetic rubbers, latex, and foamed latex (McLaughlin 1999, pg 4). These silicones are available as RTV or HTC (High Temperature Cure). High Temperature Cure platinum silicones will not cure unless heat is applied to them, but they will cure at a much faster rate – some in a matter of minutes. All platinum silicones are sold in 2-part kits – base and catalyst. Due to the high purity of these silicones, they are often used for medical applications and many of them have

FDA approval. Some of these silicones are also optically clear. It is important to note that while tin silicones will cure in a platinum mold, a platinum silicone will not cure in a tin mold.

Silicones of either type can be colored using a wide variety of methods. Because of the translucency of silicone, it is possible to emulate the layers of skin in a three-dimensional painting fashion. For a further description of ways of coloring silicone see (Thomas 1994, ch 10; McLaughlin 1999). It is also possible to change the properties of the rubber with the addition of rapid catalysts or silicone fluid. The normal overnight cure time can be lowered to a period of minutes with the addition of rapid catalysts such as Silicone's Inc Ultrafast Catalyst or XT-177A. However, there is a trade-off between the amount of catalyst used and the physical properties of the rubber, such as tear strength. A further discussion can be found in (McLaughlin 1999).

It is also possible to lower the durometer of the rubber, i.e., increase the softness, using silicone fluids. Two common silicone fluids which can be used for plasticizing are Dow Corning's DC200 fluid and Shinetsu's DM-50. Each fluid has a viscosity of 200 and 50 centastokes respectively. The lower the viscosity, the thinner the fluid becomes. Similar to the addition of rapid catalyst, there is a trade-off by plasticizing the rubber. The softer the rubber becomes due to the addition of fluid, the lower the tear strength will be but the elongation will increase. In the considerations of how much fluid to add, it is best to first determine the application. Skins which must be driven by less powerful motors should be softer. Skins which are static and are not expected to move can be firmer. Generally, silicone rubber should never be plasticized more than 50% (McLaughlin 1999).

Those readers who are interested in learning more about silicones are highly encouraged to read *Silicone Art* (McLaughlin 1999) available from Burman Industries, www.burmanfoam.com. In this book are discussions of ways to repair silicone as well as how to attach silicone to metal and other surfaces, which usually poses difficulty due to the reluctance of silicone to stick to anything but itself.

13.3 Silicone Selection

The Huggable poses a set of design constraints in the creation of the synthetic silicone skin. First, the Huggable must feel soft. The fact that the Huggable must be able to be picked up and held by the elderly and young children requires that the weight of the silicone skin be minimized. Additionally, the sensor performance under that silicone skin should have a wide range and resolution. Thus the skin formulation should maximize the softness and sensor performance while minimizing the weight.

In the next section the creation of the set of silicone samples for testing will be described. These samples will then be compared to each other in terms of durometer (a measurement of hardness), mass, and sensor performance in the next sections of this chapter.

13.3.1 Sample Preparation

Four different commercially available brands of special effects silicone were selected for experimentation. These brands were the Walco V-1082, the Factor II FX-308T, the Silicone's Inc XT-298, and the Silicone's Inc GI-245. Each of these samples was varied along the dimensions of thickness (1/16", 1/8", 3/16", and 1/4") and percentage of silicone fluid (0%, 20%, and 40%).

A set of acrylic molds were laser cut. Each mold was designed to be an assembly of three layers. The bottom layer was the uniform clamping plate with which the other two layers would screw into. The middle layer was the thickness spacer – the thickness of this layer determined the thickness of the sample. Finally the top plate features a series of air vent holes to prevent air bubbles from being trapped inside the rubber. The mold created samples that were 6" x 6" in surface area with thickness determined by the middle spacer layer.

Table 13-1: Silicone Formulas used in Experiments. Information about the working time and cure time was taken from (Burman Industries 2000) for the V-1082 and (Silicones Inc. Product Literature) for the XT-298. The use of the Hi Pro catalyst with the GI-245 base was recommended by an industry expert after consultations regarding the problems with using the GI-245 catalyst. Dual batches of each mixture listed in the table were run at the same time to fill all the molds. All samples were vacuumed under 28 mmHg for 2 minutes. Abbreviations used as: trans. = translucent; S.I. = Silicone's Inc.

Sample #	1	2	3	4	5	6	7	8	9	10	11	12
Silicone Base	Walco V-1082	Walco V-1082	Walco V-1082	Factor II FX-308T	Factor II FX-308T	Factor II FX-308T	S. I. XT-298	S. I. XT-298	S. I. XT-298	S. I. GI-245	S. I. GI-245	S. I. GI-245
Mass of Silicone Base	220.0 g	250.0 g	200.0 g	250.0 g	220.0 g	200.0 g	250.0 g	250.0 g	220.0 g	250.0 g	220.0 g	220.0 g
Silicone Catalyst	Walco V-1082	Walco V-1082	Walco V-1082	Factor II FX-308T	Factor II FX-308T	Factor II FX-308T	S. I. XT-298	S. I. XT-298	S. I. XT-298	Walco V-1082	Walco V-1082	Walco V-1082
Mass of Silicone Catalyst	22.0 g	25.0 g	20.0 g	25.0 g	22.0 g	20.0 g	25.0 g	25.0 g	22.0 g	25.0 g	22.0 g	22.0 g
Silicone Fluid	DM-50	DM-50	DM-50	DM-50	DM-50	DM-50	DM-50	DM-50	DM-50	DM-50	DM-50	DM-50
Mass of Silicone Fluid (% of Base)	0.0 g (0%)	50.0 g (20%)	80.0 g (40%)	0.0 g (0%)	22.0 g (20%)	80.0 g (40%)	0.0 g (0%)	50.0 g (20%)	88.0 g (40%)	0.0 g (0%)	44.0 g (20%)	88.0 g (40%)
Working Time (hrs)	4	4	4	unknown	unknown	unknown	1 to 1.5	1 to 1.5	1 to 1.5	un- known	un- known	un- known
Cure Time (hrs)	16	16	16	overnight	overnight	overnight	18 to 24	18 to 24	18 to 24	over- night	over- night	over- night
Color	trans. blue	trans. yellow	trans. pink	opaque black	none	opaque blue	opaque green	opaque purple	opaque orange	opaque red	opaque yellow	opaque grey

Each sample was prepared according to Table 13-1. A thin coat of ZIP ME-301NS spray Vaseline release was applied to both the inside and outside of each mold. The formulation of each rubber was first vacuumed for 2 minutes at 28 mmHg, and then poured into each of the four molds of varying thickness. The top plate was carefully placed on top to close the mold, being sure to not trap any air inside the mold. A set of four socket head cap screws were used to clamp the mold. The samples were allowed to cure overnight. Figure 13-4 shows one set of samples curing inside the acrylic molds.

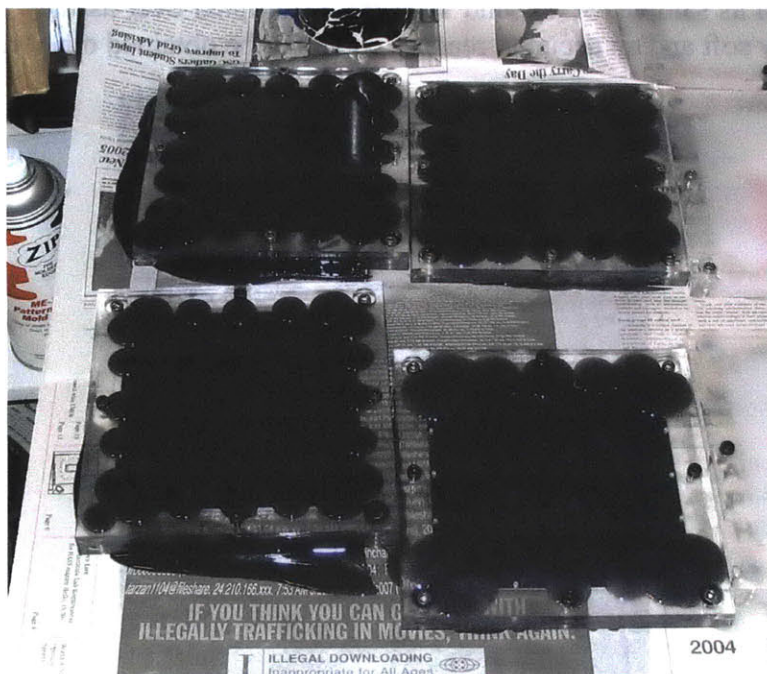


Figure 13-4: The Acrylic Silicone Sample Molds.

Each sample was removed from the mold, trimmed, and washed in a solution of dish soap and water to clean the surfaces of the silicone rubber. To remove the additional tackiness of the surface of the silicone rubber, TS-100 matting powder, was brushed onto the surface of each sample. Samples were then placed in labeled zip-lock bags for storage until further testing.

13.3.2 Hardness Measurement

The durometer, a measure of hardness, of a silicone rubber decreases as more silicone fluid is added to the mixture. Each of the twelve samples prepared in Table 13-1 was then tested using the ASTM D 2240 standard for durometer testing (ASTM 2000). Each measurement is conducted using a Shore OO durometer gauge as shown in Figure 13-5. The ¼" silicone samples used for testing were doubled over for accurate readings, per the ASTM standard, as they were less than ¼" thick due to the fact that the acrylic used was actually 0.236" thick. Some very soft samples, such as samples 9, 11, and 12 were quadrupled over as they were very soft and an accurate reading could not be obtained otherwise.

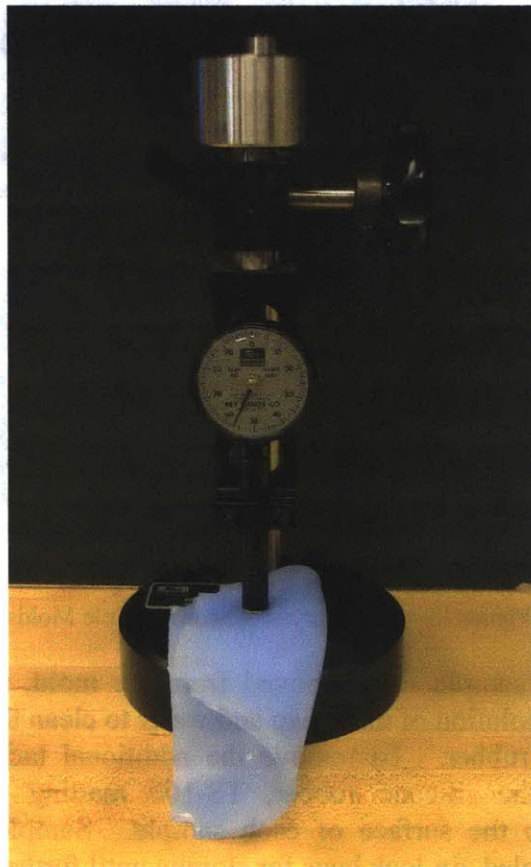


Figure 13-5: The Measurement of the Durometer of the Silicone Samples.

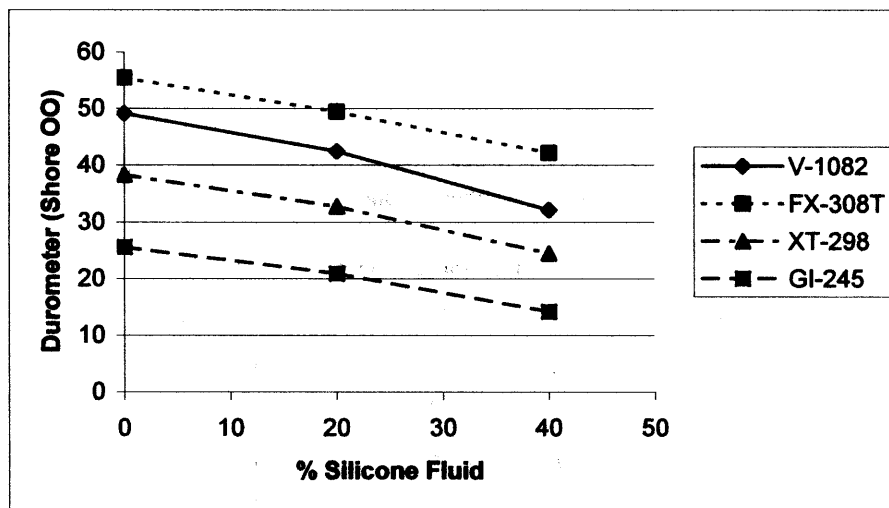


Figure 13-6: The Plot of Durometer as a Function of Silicone Fluid Percentage.

The results of these measurements are shown in Figure 13-6. These results confirm that increasing the percentage of silicone fluid does lower the durometer of the silicone rubber in a nearly linear fashion. The softness of these silicone rubbers can be compared against human skin using the Durometer Conversion Chart shown in Table 13-2.

Table 13-2: The Durometer Conversion Chart from (Custom Seal & Rubber Products website)

▲ Hardness Value						
Durometer Scale:	A	B	C	D	O	OO
	100	85	77	58		
	95	81	70	46		
	90	76	59	39		
	85	71	52	33		
	80	66	47	29	84	98
	75	62	42	25	79	97
	70	56	37	22	75	95
	65	51	32	19	72	95
	60	47	28	16	69	93
	55	42	24	14	65	91
	50	37	20	12	61	90
	45	32	17	10	57	88
	40	27	14	8	53	86
	35	22	12	7	48	83
	30	17	9	6	42	80
	25	12			35	76
	20	6			28	70
	15				21	62
	10				14	55
	5				8	45

From this chart a Shore OO value of 55 corresponds to a Shore A value of 10. Human skin has been measured to be softer than a Shore A of 10 (Custom Seal & Rubber Products website).

Thus the majority of the silicone samples tested are as soft as, if not softer than, human skin.

For purposes of comparison, Figure 13-7 shows a graph of the varying durometers of common medical silicones used in prosthetics.

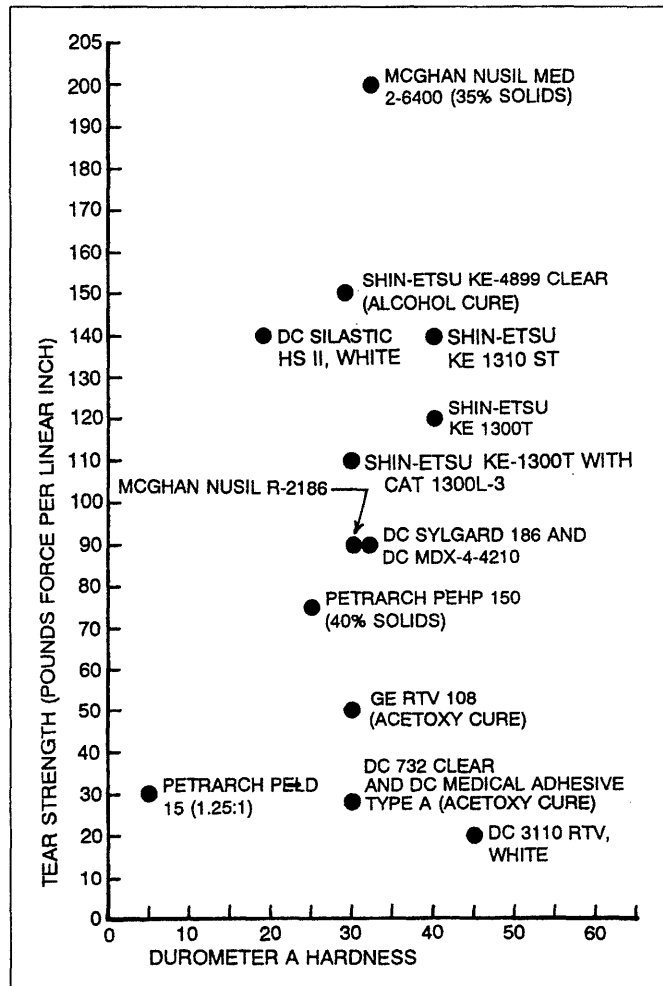


Figure 13-7: Common Medical Grade Silicones Used in Prosthetic Work from (Heller and McKinstry 1995, pg 93).

This graph does show that the silicones used in the medical industry are generally harder than those of the special effects industry. One potential explanation for this fact is that the majority of these applications are cosmetic and, thus, do not have any motion underneath the skin in the sense of motors or other

actuators which is inherent in the fields of special effects, animatronics, and robotics. From a survey of a recent maxillofacial prosthetic catalog (Factor II Inc. Product Catalog 2002) many of the Medical grade and other Platinum silicones are still in the range of 20-30 durometer Shore A.

One final discussion of softness is that thickness of the rubber does play an effect in how soft the rubber feels. In the design of the Huggable, a set of circuit boards is placed underneath the silicone rubber. Thus, if the thickness of the synthetic skin is very thin, such as 1/16" the hard circuit boards will be felt underneath the material, thus increasing the apparent hardness of the rubber. So thinner synthetic skins must use softer silicone rubbers.

13.3.3 Silicone Mass Considerations

The Huggable must be light enough to be picked up and carried. Silicone rubber is more dense than foam rubber; thus, the weight of the synthetic skin is a design concern. The density of each silicone sample was determined for each sample using Equation 13-1.

$$Density = \frac{Mass}{(Width \times Length \times Thickness)} \quad (13-1)$$

The mass of each sample was measured. The width and length were each roughly 6". The thickness of the sample was varied from 1/16" to 1/4" by 1/16". The thicknesses of acrylic used in the sample molds, described previously, was actually slightly less than these thicknesses; thus, the actual thicknesses of the silicone samples were 0.0560", 0.1215", 0.1775", and 0.236". Table 13-3 shows the average density, across the four thicknesses of sample, of each of the twelve silicone samples.

Table 13-3: The Density of Each of the Twelve Silicone Samples

Sample #	Material	% Fluid	Density (oz/in ³)
1	V-1082	0	0.486
2	V-1082	20	0.485
3	V-1082	40	0.483
4	FX-308T	0	0.501
5	FX-308T	20	0.482
6	FX-308T	40	0.482
7	XT-298	0	0.485
8	XT-298	20	0.462
9	XT-298	40	0.500
10	GI-245	0	0.508
11	GI-245	20	0.454
12	GI-245	40	0.464

From comparing the densities among the 12 samples it becomes clear that the amount of fluid or the type of silicone used has little effect. Equation 13-1 can be rearranged to calculate the mass of each sample:

$$Mass = Density \times Width \times Length \times Thickness \quad (13-2)$$

In Equation 13-2, the density is a constant, and the width and length of the silicone samples are fixed by the geometry of the Huggable. Thus, the only variable which can be adjusted to influence the mass of the synthetic skin is the thickness of the rubber. Thus, doubling the thickness of the silicone equates to a doubling of the mass of the skin.

13.3.4 Sensor Performance

The last consideration in the selection of silicone rubber for a synthetic skin is how it affects the performance of the sensors underneath. To test each of the twelve samples of silicone rubber, a QTC sensor array was created as shown in Figure 13-8. The

sensors were 0.75" square and arranged in a 5 x 5 grid. Kapton tape was used to secure the sensors to the circuit board.



Figure 13-8: The QTC 5x5 Sensor Array for Silicone Sample Testing.

A two-axis xy-stage was designed and built by Danny Hilton, another undergraduate working with the Robotic Life Group. The stage features encoders to detect position. A Shimpo FGV-100 digital force gauge is placed on this stage and can be raised and lowered by hand. The output of the force gauge is amplified so as to be calibrated to a 0 to 5V scale for a range of 0 to 5 kg. These x and y positions as well as the force are displayed on both an LCD screen, mounted to the rear of the apparatus, and output via serial to a computer for data collection. The QTC sensor array of Figure 13-8 is mounted to 1/2" thick acrylic plate to prevent the board from flexing during data collection. Figure 13-9 shows the xy-stage with the QTC sensor array mounted.

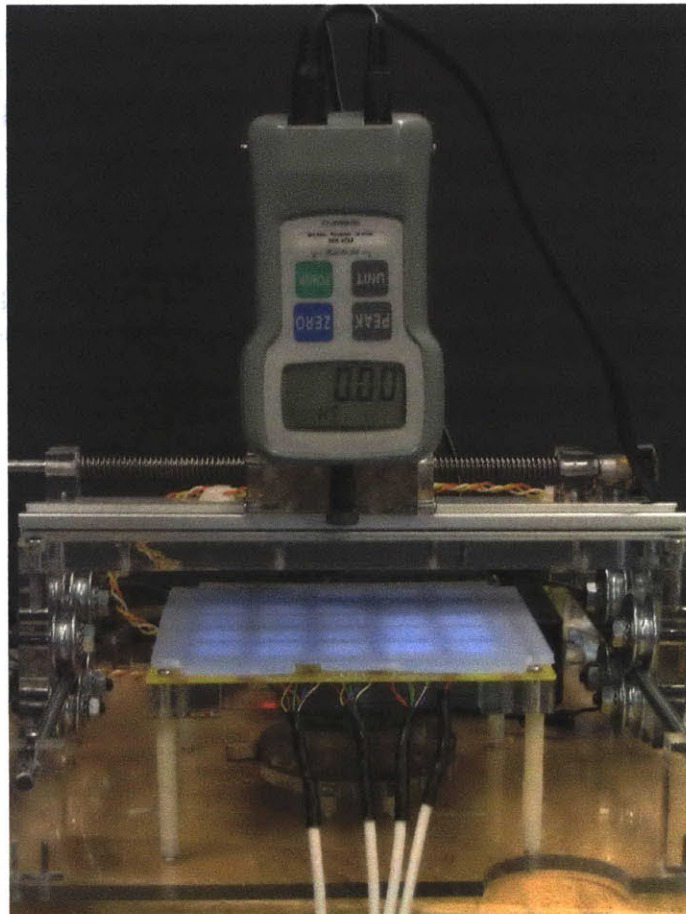


Figure 13-9: The XY-Stage with the 25 Sensor QTC Array Attached. This device was designed and built by Danny Hilton.

Each silicone sample was placed on the array, and data were collected from both the array and the xy-stage as the force gauge was pressed into the center of the middle QTC electrode. The force gauge was pressed until a reading of over 5 kg was made and then slowly raised by hand. The process was repeated ten times for each sample at each thickness.

Figure 13-10 shows the result of this indentation for the 1/8" thick silicone sample created from skin formulation number eight of Table 13-1. Two force profiles emerge from these tests as shown in the figure. The release condition shows a much steeper slope than the applied condition. There are two explanations for this difference. The first is that the rubber may show different

properties for an indentation and release. Many rubbers show such hysteresis, so it is a fair explanation. Another explanation may be due to experimental design. The top surface of each sample still has a slight tack to it even after powdering with TS-100 as described previously in this chapter. Thus when the force gauge is lifted up, it may be lifting the skin off the sensors and thus resulting in the very steep slope. Further testing would need to be done by placing saran wrap, or another material that would prevent the indenter from sticking to the soft surface. Dish soap could also be used for this purpose.

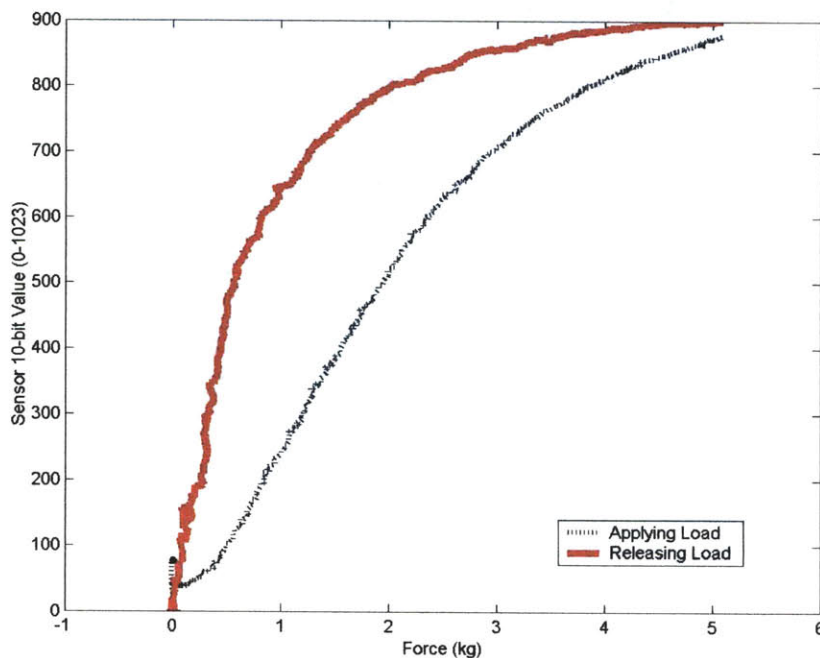


Figure 13-10: The Plot of Applied Force vs Sensor reading. The dotted thin black line is the plot of the sensor response for when the force is being applied to the skin. The solid thick red line is the sensor response for when the applied load is released.

With the softest silicones another interesting behavior is seen as shown in Figure 13-11. At greater applied forces the rubber actually ripples. This rippling lifts the surrounding rubber off of the sensors.



Figure 13-11: The Rippling of Very Soft Silicones with Large Applied Forces. In the figure the silicone sample used was sample #12 – the softest of all the samples. The applied load was 5.4 kg.

13.3.5 Viscosity

The silicone rubber will be injected into the various molds of the Huggable body sections. Thus, the ability to flow through the mold becomes important. The addition of silicone fluid allows the silicone to be injected into the molds in a much easier fashion, especially for the very viscous GI-245 Base with a viscosity of 80,000-90,000 cps. While the catalyst does soften the material and allow it to flow, the addition of fluid helps not only to inject the material into the mold but also to lower the risk of trapping air bubbles in the skin. The lower the viscosity of the rubber, the greater the chance that air bubbles will rise to the surface and out through the air vents of the mold.

13.3.6 Sensor Selection

For all of the reasons mentioned in this section of the chapter, the synthetic skin chosen was sample #8, the Silicone's Inc XT-298, in a thickness of 1/8". This formulation was chosen primarily for its feel. When placed under the fur of the Huggable, it has a very natural animal softness. It also showed a good range and sensitivity in sensing the applied forces. It has a low viscosity and is easy to inject into molds. Finally, the 1/8" was chosen as a

compromise between softness and weight. Also this thickness allowed more room for sensor boards, than a ¼” thick skin due to the fact that the external envelope of the bear is defined by the fur.

13.4 Silicone Mold Design

The electromechanical design described in Chapter 11 is covered by a synthetic silicone skin. There are different ways to create this skin. The skin can be cut from a sheet and wrapped around the sensor boards. This approach poses problems, however, as the Huggable has complex geometry that a skin of uniform thickness would not adequately cover. A uniform thickness skin wrapped over the sensor boards of Chapter 11 would result in a rounded octagonal shape – a very unnatural shape for the arms of a teddy bear. A better approach would be to mold the silicone rubber into a shape that fills the cavity between the sensor boards and the underside of the fur arm sleeve. This is the approach taken in this thesis.

As discussed in the previous chapters, the Huggable fabric of fur defined the envelope of what could fit inside the bear. Both the mechanical and electrical circuit board designs exist in a digital format. Ideally, the molds would be able to be designed digitally as well to assure a high tolerance between the mechanical, electrical, and skin designs.

In traditional molding and casting, such as those employed for Leonardo’s foam hands, the process begins with a sculpture. A mold of this sculpture is made. When the thickness of the cast object must be controlled, a core mold is made as well. The core mold is formed by laying in thicknesses of clay or wax inside the molds of the exterior of the object. This thickness is equal to the thickness of finished cast piece. Finally, the core mold is made by assembling the exterior molds with the thickness of clay or wax inside and making a mold of this interior cavity. Thus, when disassembled and the clay is removed, a cavity between the core mold and the exterior molds exists. This cavity is the thickness of the clay or wax. The mold can then be filled with silicone, foam latex, or other material.

The process of sculpting and molding described above takes a long time. Additionally if the sculpture is slightly larger than what is desired, the whole process must start from the

beginning. If the core mold is a little too small or too large, it must be sanded down or built up before another cast can be made. This iterative process takes time and skill in order to produce the correct casts.

The Media Lab and the Center for Bits and Atoms at MIT share a Z Corporation Z510 3-dimensional printer. This device is capable of printing parts with a 600 x 540 dpi resolution and a bed size of 10" x 14" x 8" (Z Corporation Press Release, 2005). With this machine the traditional molding cycle can be drastically sped up with much finer tolerances than would be possible otherwise.

A solid model of the mold design for the silicone skin of the Huggable arm section is shown in Figure 13-12. The mold consists of three parts. The outer mold is created by placing the teddy bear arm solid model of Figure 11-1 inside a solid and using the mold functions of Solidworks to create a two-part mold with the interior section equal to the exterior section of the arm solid model. The core mold is created directly from the solid model of the arm sensor circuit board assembly of Figure 11-14. Additional features such as pry points, registration keys, vent holes, and the inject port are also created in the solid model of each mold part.

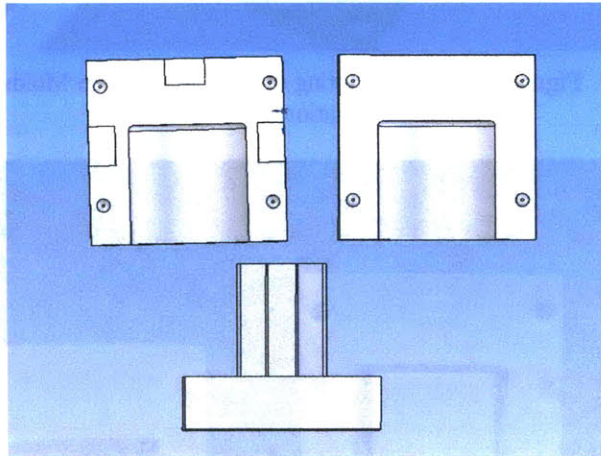


Figure 13-12: The Solid Model of the Silicone Arm Molds.
Note the core mold at the bottom does not show the registration keys on the final part.

Each part of the solid model was printed with the Z Corporation Z510 3D printer. Figure 13-13 shows a photo of the molds being printed. Once removed from the printer, the unused material was removed and super glue was dripped over each mold

part to increase the strength of the part. Once the super glue cured, the parts were sanded down to a smooth finish. Two coats of Mequiar's Mold Release Wax were applied with a brush to each mold part. Figure 13-14 shows the final finished mold printed parts.

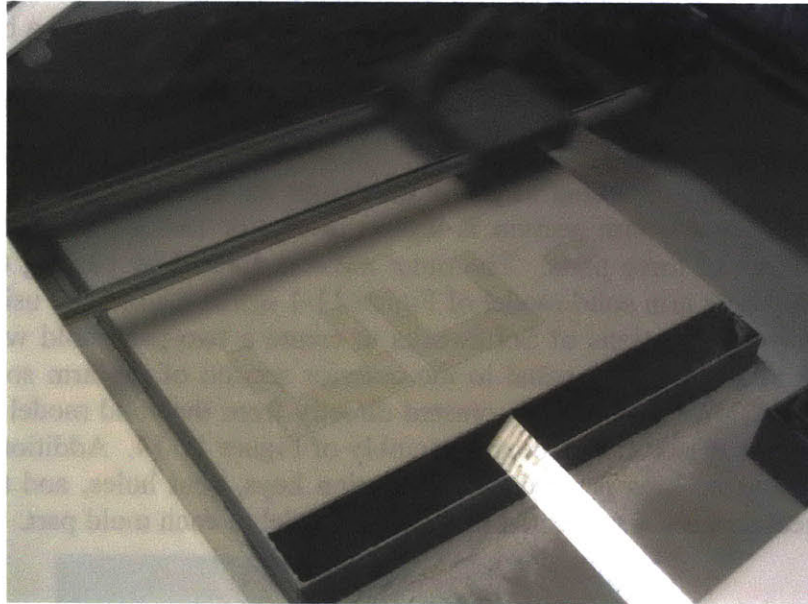


Figure 13-13: The Printing of the Silicone Arm Molds on a Z Corporation Z510 3D printer.

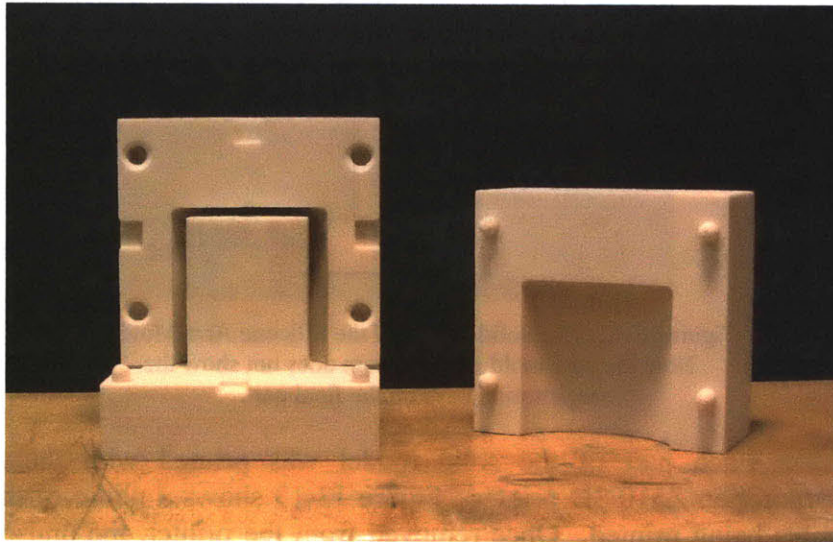


Figure 13-14: The Finished Silicone Arm Molds.

Prior to the casting of silicone, ZIP ME301-NS spray Vaseline release was applied to all surfaces of the mold. The mold was assembled and clamped together. Silicone formulation #8 was injected into the mold using a syringe as shown in Figure 13-15. The silicone was allowed to cure overnight inside the mold. Figure 13-16 shows the finished silicone skin.

The Silicone sample was then trimmed, washed, and powdered with TS-100 matting agent. A set of slits were made in the silicone skin at the location of each thermistor as shown in Figure 13-17. These slits allowed the thermistors to pass through the silicone skin for better sensing. The silicone skin was then unrolled onto the arm assembly as shown in Figure 13-18. Finally the fur sleeve is placed around the silicone skin as shown in Figures 13-19 and 13-20.



Figure 13-15: Injecting the Silicone into the Arm Silicone Molds

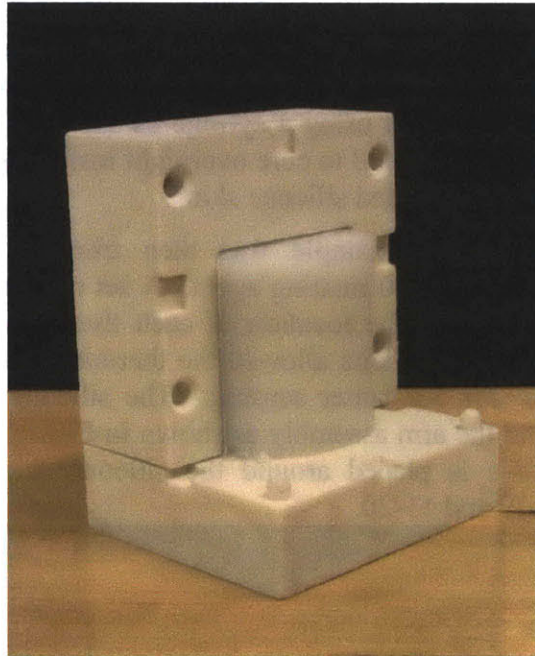


Figure 13-16: The Arm Silicone Skin.

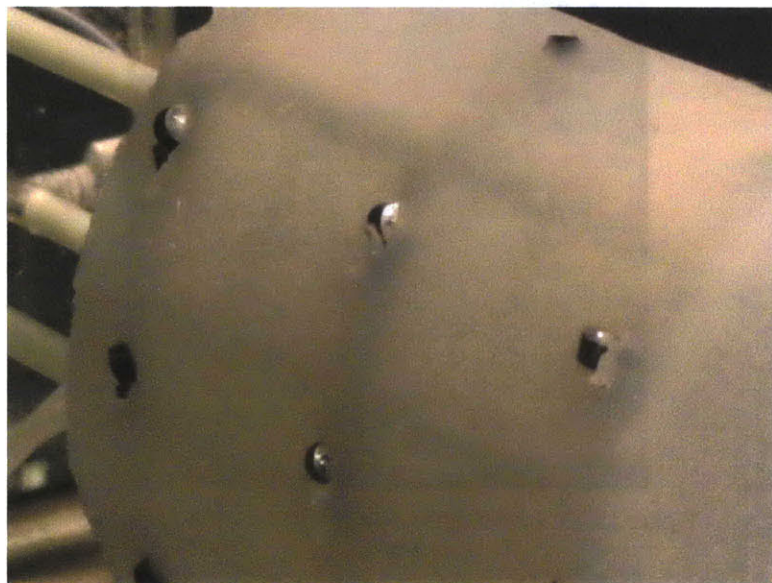


Figure 13-17: Close-up of the Holes in the Silicone Skin to allow the Thermistors to Pass Through.

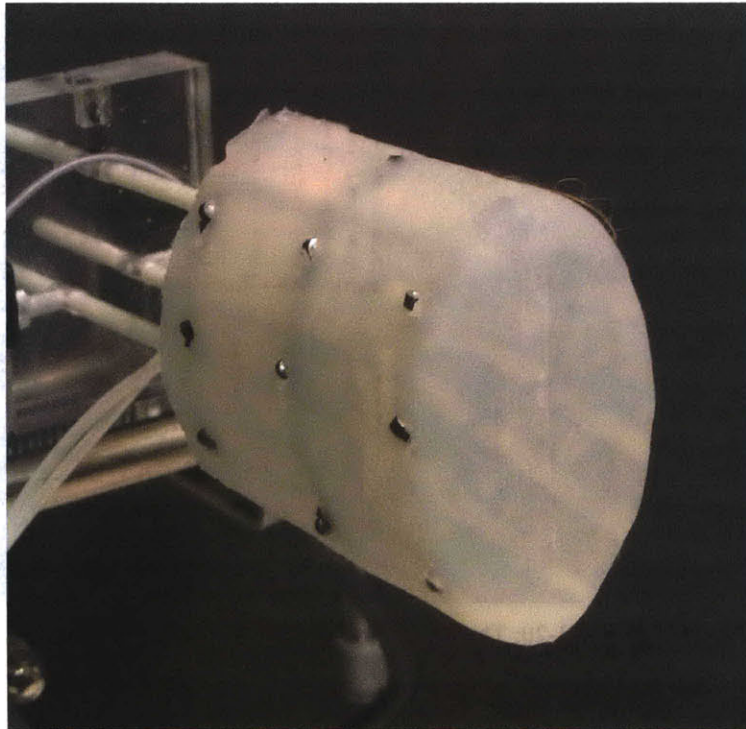


Figure 13-18: The Completed Arm Assembly with Silicone Skin



Figure 13-19: The Completed Arm Assemble with Silicone and Fur

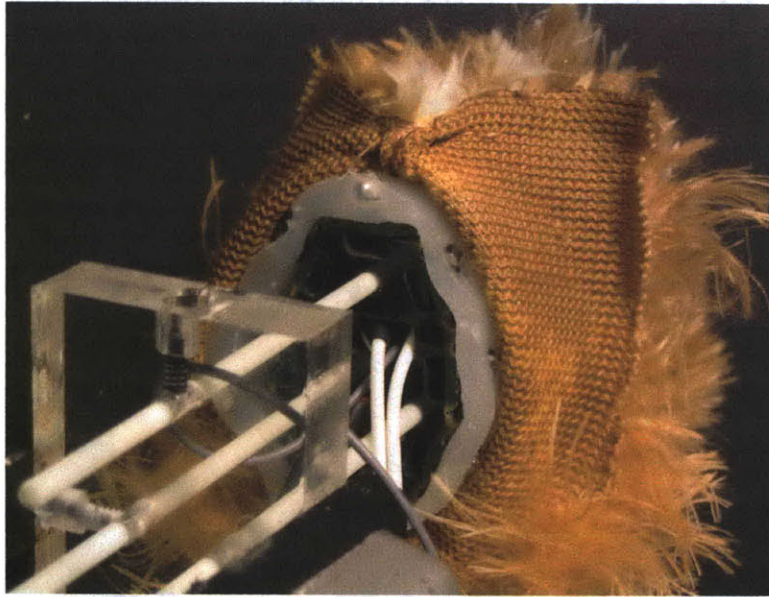


Figure 13-20: The Layered Structure of the Huggable "Sensitive Skin." The outer layer is the fur arm sleeve. The middle layer is the silicone skin. The inner layer is the electromechanical arm assembly described in Chapters 11 and 12.

14 Affective Processing

14.1 Overview

One important design feature that distinguishes the Huggable from other robotic companions is the emphasis placed upon affective touch. Most current platforms only feature a handful of touch sensors. Many of these systems also do not feature full body coverage. Finally, touch sensing is often only limited to the modality of pressure information.

The Huggable will feature a high spatial resolution, full-body, multi-modal “sensitive skin” and thus will be able to classify and distinguish between many different types of affective interactions such as petting, patting, or tickling. This chapter describes the next extension of the “Virtual Somatosensory Cortex” described in Chapter 9.

Much like Leonardo’s somatic architecture, the Huggable features levels of processing. At the lowest level is the peripheral output of each sensor. In Chapter 14.2 the output of each sensor will be discussed. Chapter 14.3 will discuss some initial feature extractors which have been developed to pull out information from the receptive field grouping of sensors. Finally some preliminary results of classification using a neural network will be described in Chapter 14.4.

14.2 Peripheral Sensory Output

As discussed in Chapter 9, the “Virtual Somatosensory Cortex”, much like its biological counterpart, does not process the world by itself. Rather it receives inputs from the sensors in the periphery that encode this somatic information about the external world in a form that the cortex can decode – in the virtual version this is the binary format of digital communication; in the biological version this is action potentials.

In this section of the chapter the inputs to the “Virtual Somatosensory Cortex” of the Huggable, or “letters” of the somatic alphabet, will be described.

14.2.1 Response of Electric Field Sensor to touch by a human and inanimate objects

As discussed previously in Chapter 12, the electric field sensor measures the capacitance between the electrode and surrounding objects. In many ways this is a proximity measurement. Figure 14-1 shows a plot of the capacitive sensor signal as a hand is moved closer to and farther away from the top surface of the arm section of Figure 13-19. Thus, the capacitive sensor is a good proximity detector.

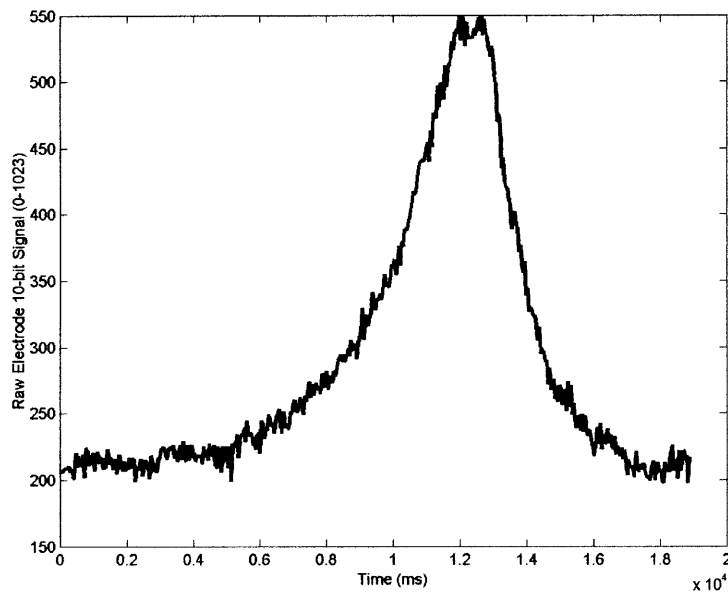


Figure 14-1: The Response of the Electric Field Sensor to the Human Hand Moving towards and Away from the Electrode. The unfiltered, uncalibrated, raw value is shown.

An experiment was conducted to see how well the capacitive sensor could distinguish between contact with humans and inanimate objects. Three different objects (a wooden bar, a delrin bar, and an aluminum bar) in addition to the human hand were placed in contact with the top of the bear palm. Figure 14-2 shows photos of the objects and hand used in this experiment.

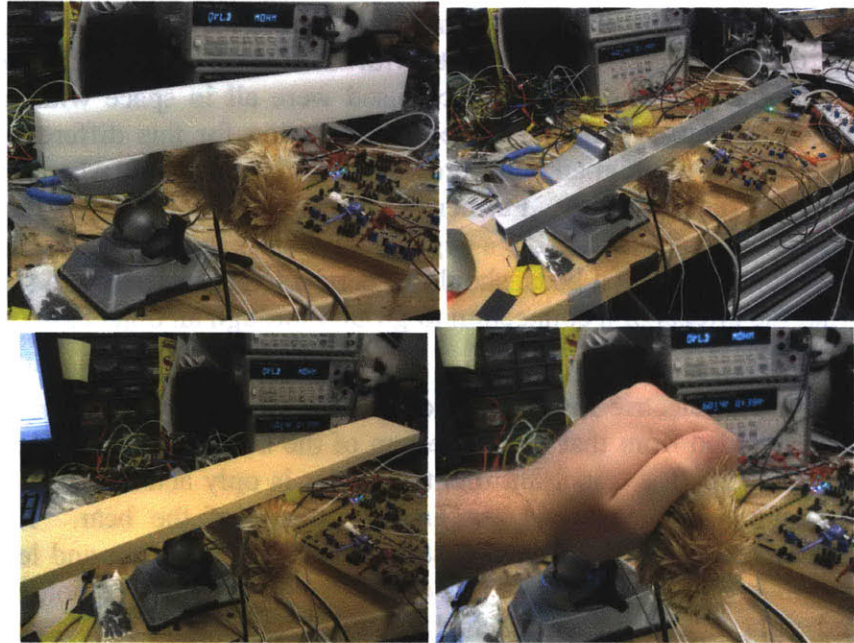


Figure 14-2: Top Region Electrode in Contact with Three Objects and a Human Hand. The upper left is the white delrin bar. The upper right is the aluminum bar. The lower left is a wooden bar. The lower right is contact with a human hand.

Data was collected in each case of the experiment and the 10-bit electric field sensing value for each object is shown in Figure 14-3.

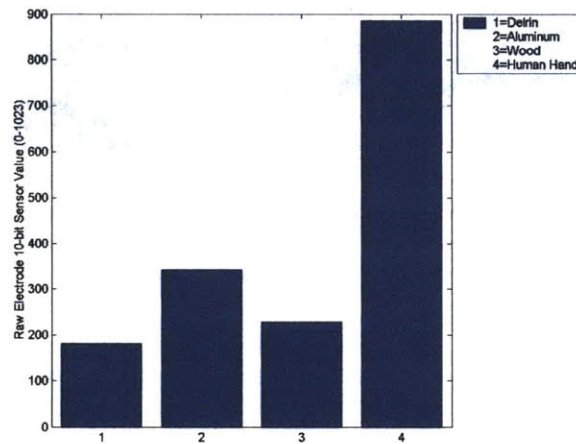


Figure 14-3: The Electric Field Sensor Signal in Contact with the Objects of Figure 14-2. In the figure: 1 = the Delrin Bar, 2 = Aluminum Bar, 3 = Wood Bar, 4 = Human Hand

As can be clearly shown in this figure, human contact can be distinguished from contact with inanimate objects. One important note is that the objects used were all in space without any contact to ground. Thus one explanation for this difference may be that the human hand provides a path to ground, whereas the other objects do not. Further experimentation with objects that would be in the Huggable's regular environment, such as metal table tops or hospital beds, should be conducted in the future to see what the effects of a connection to ground through an object are on the signal.

The electric field sensor on the top of the circuit board is well shielded from that on the bottom of the board as discussed in Chapter 12. It is important that the sensor is only activated when touching that sensor and not another region of the bear. An experiment was conducted to test this shielding. The top and left electrode was touched while this electrode was active. The bottom and right electrode was touched while the top and left electrode was active. Measurements were recorded from the top and left electrode in both cases. Figure 14-4 shows the experiment. Figure 14-5 shows the result.

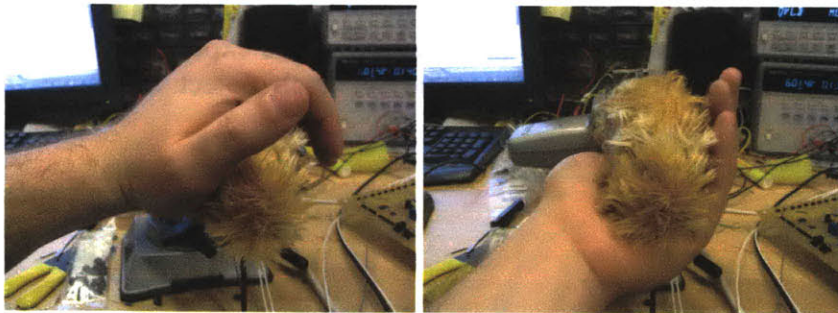


Figure 14-4: The Contact Points for the Shielding Experiment.

At left shows the contact with the top and left electrode. At right shows the contact with the bottom and right electrode. In both cases, measurements were recorded from the top and left electrode

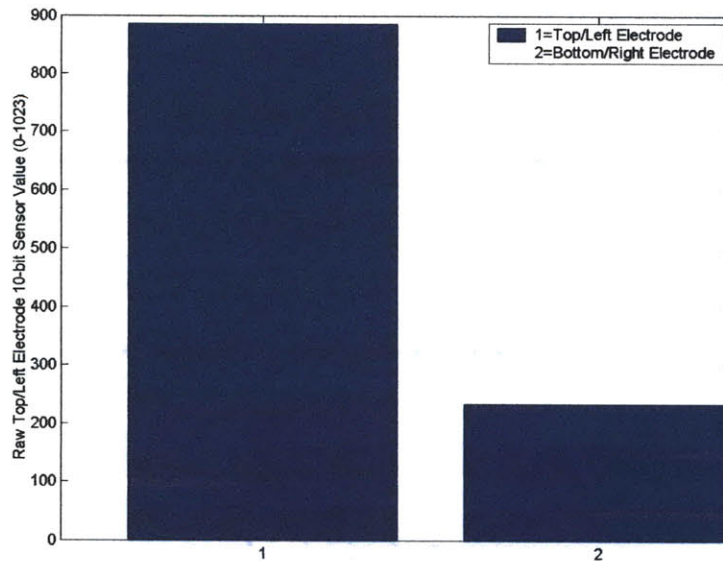


Figure 14-5: The Electric Field Sensor Signal from the Top and Left Electrode for Contact with the Top and Left Electrode and the Bottom and Right Electrode. In the figure: 1 = Hand covering the Top/Left Electrode, 2 = Hand covering the Bottom/Right Electrode

As shown in Figure 14-5, there is a clear distinction between contact with the sensed electrode and contact with the non-sensed electrode. This is due to the fact that the 33794 grounds the unused electrodes as discussed in Chapter 12. Each electrode is thus isolated from one another. Thus, such affective classes of touch like petting and rubbing which span more than one electrode can be detected using the electrode signal.

14.2.2 Performance of three levels of QTC processing

As discussed in Chapter 12, the QTC signal was conditioned in three different ways to detect three different ranges of force – light touch, moderate touch, and hard touch. Figure 14-6 shows the result of the three types of processing on the same input signal.

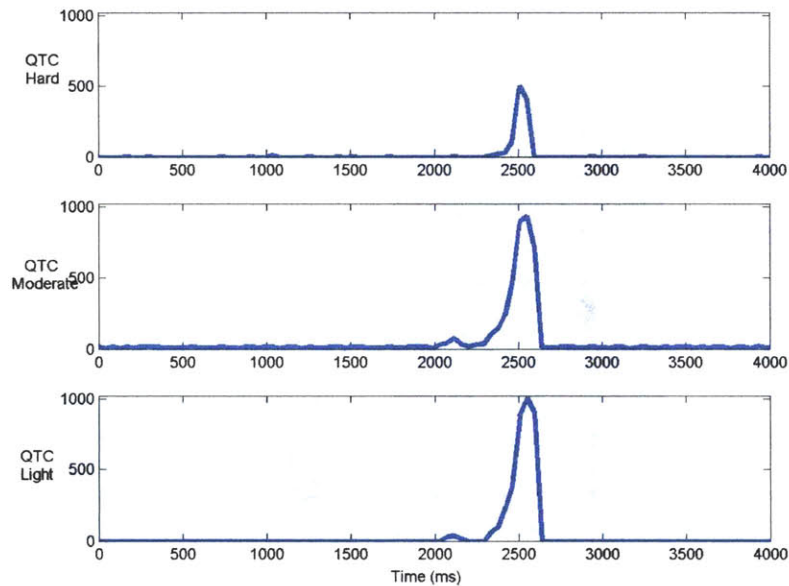


Figure 14-6: The Processing of the QTC Signal for Light, Moderate, and Hard Touch. At top is the QTC hard signal. In the middle is the QTC moderate signal. At bottom is the QTC light signal.

As can be shown in the figure, each type of processing results in a different value with light touch have the largest signal amplitude and hard touch having the smallest. In Figure 14-6, the difference between the moderate and light value is not very much. This small change is due primarily to the fact that each type of processing was tuned differently. Thus the moderate tuning was a little higher than it should have been. The auto calibration routine described in Chapter 12 would help to distinguish these values in the future.

Currently this processing is done simultaneously with a light touch, a moderate touch, and a hard touch all being done one after another. A more efficient form of processing would be to first process the light touch signal. When this value fell below a threshold the PIC would switch the QTC signal for moderate touch processing. The same would occur in switching between moderate and hard touch.

14.2.3 Temperature Sensor Response

The temperature sensors show a slow time response, as discussed in Chapter 12. Figure 14-7 is a plot of this response to pressing into the skin with a moderate level of force.

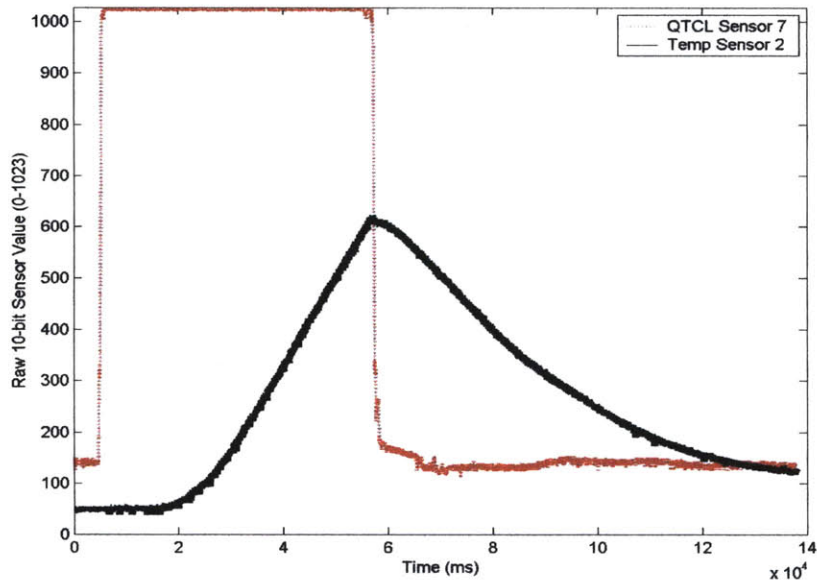


Figure 14-7: The Response of the Temperature Signal. The red, thin, dotted line is the QTC light signal from sensor 7. The thick, black, solid line is the temperature signal from sensor 2. All displayed time information is $\times 10^4$.

As shown in Figure 14-7, the QTC light sensor signals when the contact was applied. The 7th QTC sensor and the 2nd temperature sensors are located right next to each other. Thus we can calculate the time it takes for the temperature signal to change from applied contact. From the figure there is an initial delay of between 10 to 15 seconds. However, once the sensor is released the temperature sensor shows a change in less than 5 seconds. Thus these sensors have a very slow response rate. Some of the initial onset time could be due to calibration, as the plot does not show the calibrated values. Thus the sensor value may be changing, but it is below one of the differential amplifier thresholds and thus not amplified. It would be interesting to explore a more dynamic response, such as repeatedly making contact and then releasing keeping the same time interval. It may

be that once initial contact is made the sensor heats up and thus is more sensitive to slight changes around that temperature.

14.2.4 Combined Response across multiple sensors

The sensors can be combined to reveal more information. Figure 14-8 shows the response of the sensors to patting hard for the active receptive field. A patting data set was a series of 10 pats.

As shown in the figure, the 10 pats can be clearly seen. This data was not filtered or calibrated, as such; some of the sensors are not baselined at 0. Even with this fact, QTCL17 and 18 replicate this signal. The capacitive sensor provides the best image of the interaction as it peaks for each of the 10 pats. A sense of size is shown by the number of sensors which are active.

The electric field sensor is the first and last sensor to activated as shown in the figure. Thus it can act as anticipation of touch sensor. The temperature sensors show very little response due to the short time period of contact during a pat. However over a longer time period such as a squeeze shown in Figure 14-9, they show a visible change.

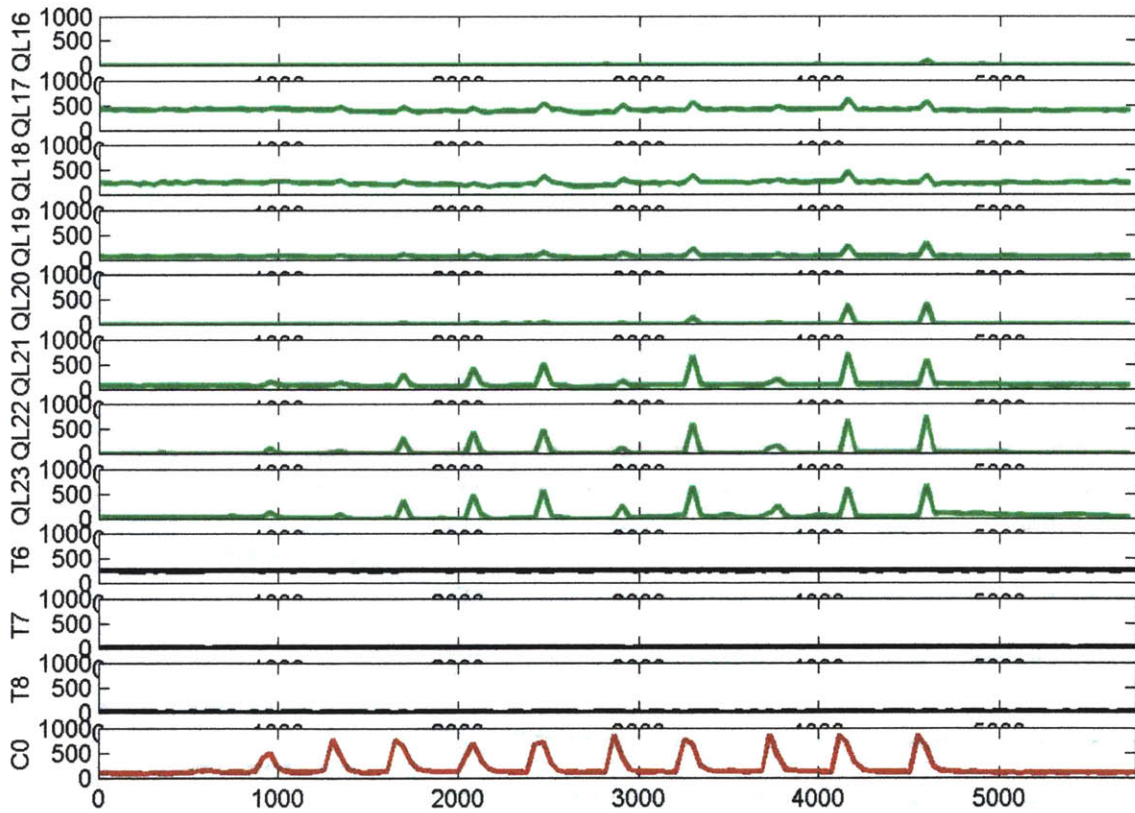


Figure 14-8: The Response of the Electric Field, QTC, and Temperature Sensors to Patting. QL = QTC sensor with light touch signal conditioning (green), T = Temperature (black), C = Capacitive sensor (red). The number is the sensor number. Only the active receptive field is shown

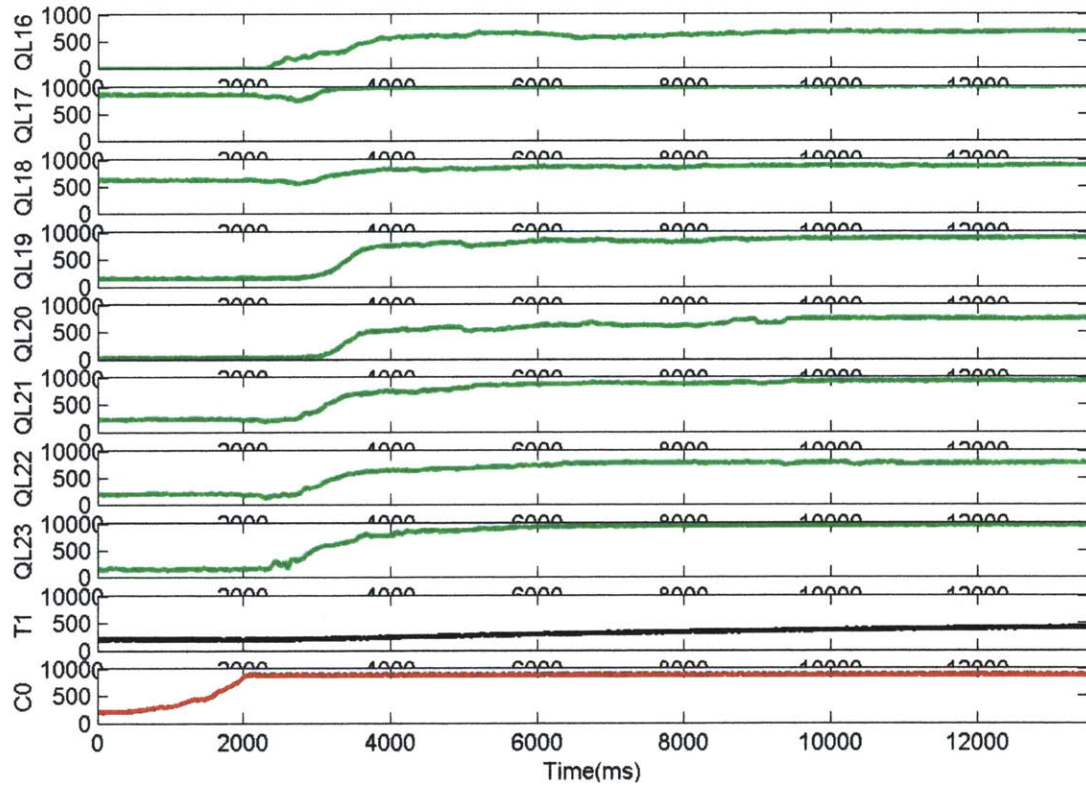


Figure 14-9: The Response of the Electric Field, QTC, and Temperature Sensors to Squeezing. QL = QTC sensor with light touch signal conditioning (green), T = Temperature (black), C = Capacitive sensor (red). The number is the sensor number. Only one of the active receptive fields is shown

With squeezing, most of the sensors in the receptive field are near or at their maximum value. Thus there is a lot of contact between the surface of the Huggable arm section and the person's hand, which in turn results in the transference of a lot of body heat to the thermistors as shown in Figure 14-9 for T0. The ability of the capacitive sensor to precede the QTC sensors, previously discussed, is also clearly shown. With a squeeze the QTC and capacitive sensors should be at their maximum values. Again, the sensors were not calibrated which is why some sensor outputs do not reach the maximum 1023 value.

Figure 14-10 shows the response of these sensors to petting.

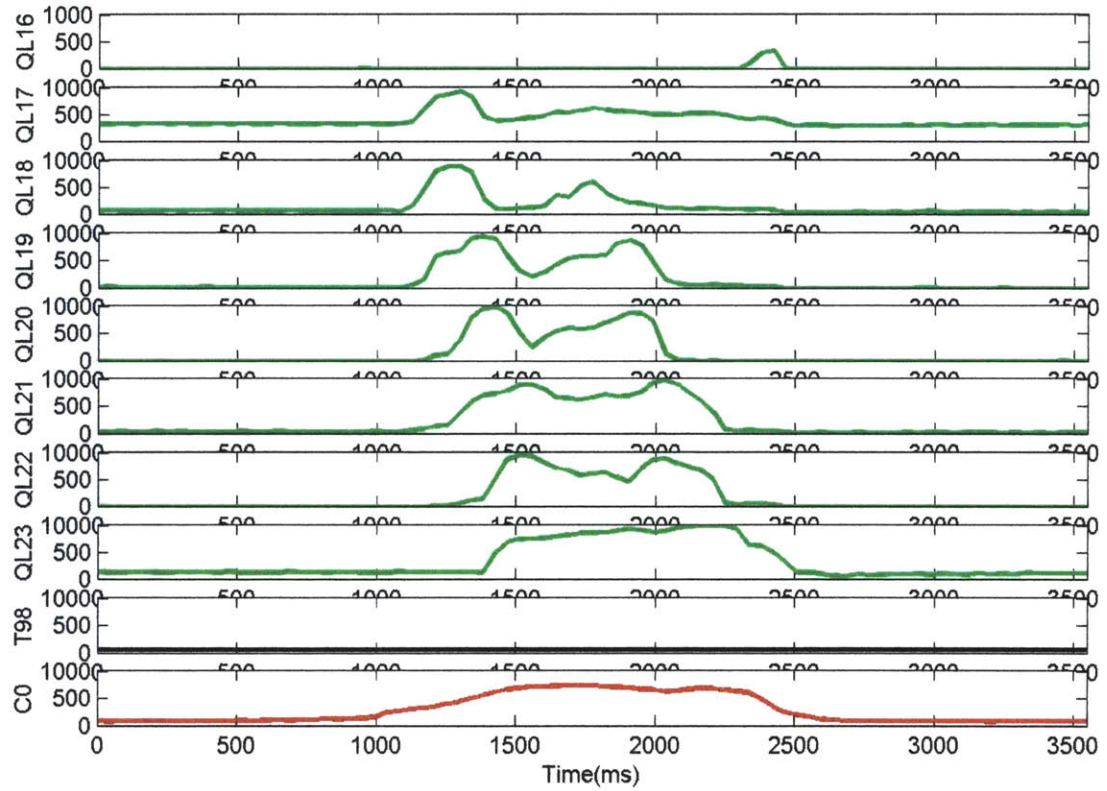


Figure 14-10: The Response of the Electric Field, QTC, and Temperature Sensors to Petting. QL = QTC sensor with light touch signal conditioning (green), T = Temperature (black), C = Capacitive sensor (red). The number is the sensor number. Only the active receptive fields is shown.

The direction of motion can be seen in the order that the QTC sensors are activated. The close spacing of the QTC as compared to the spacing of the FSRs in the Leonardo hands described in Section II results in a better sense of direction of motion as there is more overlap between the sensors. The peaks that emerge could be from the gaps between the person's fingers as it slides across the surface of the skin. The temperature sensors do not convey much information in this interaction.

14.3 Feature Extraction

As previously discussed in Chapter 9, the peripheral sensor values are combined into receptive fields. Features, or the "words," from these receptive fields are then extracted. These features include the direction of motion, centroid location, and orientation processing discussed in Chapter 9. This chapter describes the additional features calculated at each time step in preparation for the Neural Networks (NN) described in the next chapter.

In the current implementation, digital potentiometers are not used. Thus, each sensor's baseline is not at the same value. The sensors are normalized in the following manner. First, the first 50 data points at the start of every data set are averaged together. This is only done for cases in which there is no contact with the sensors at the beginning of the data set. Some data sets like "contact" or "squeeze" were started while there was contact with the arm section. For these data sets, the baseline used is a "baseline" data set in which more than 1000 samples made without contact were averaged for each sensor.

Once a baseline is determined, the sensor can be normalized to this baseline using Equation 14-1:

$$\text{NormalizedSensorValue} = \frac{\text{SensorValue} - \text{baseline}}{1023 - \text{baseline}} \quad (14-1)$$

This baseline value is then filtered and negative sensor values are set to zero. Next the number of active sensors in a given receptive field is calculated. A sensor is considered to be active if its sensor value is above a threshold. The number of active sensors within a receptive field is then normalized by the number of sensors in that receptive field. Thus, if the normalized active sensor feature for the QTC sensors on the top circuit board is 1.0,

then all eight QTC sensors are have some sensory value which is above a threshold.

Another feature calculates the normalized sensor value sum by dividing the sum of all of the sensor values in a receptive field and dividing this number the number of sensors in that receptive field. Thus, a value of 1.0 would occur if all eight QTC sensors in the top sensor circuit board were at their maximum value.

The normalized average sensor value sum is calculated by dividing the sensor value sum by the number of active sensors in a receptive field. A value of 1.0 would occur if all of the active sensors in a receptive field were at their maximum value and the inactive sensors were 0.

Another feature calculates the change in sensor value sum between each time step by subtracting the last normalized sensor value sum from the current normalized sensor value sum. Two additional binary features are use to indicate the direction of the change. The sensor value increasing feature is true (1) if the sign of the change in normalized sensor value sum is positive. The sensor value decreasing feature is true (1) if the sign is negative.

There is a set of features used to signify the degree of activity within a receptive field. One feature is a 1 if the current sensor was active at the last time step and still is. Another feature is 1 if the sensor was not active at the last time step and still is inactive. Finally, one other feature is 1 only if there was no change in sensor value, i.e., the sensor was inactive and still is or was active and still is.

The number of time steps since there was a change in activity for a sensor is recorded by a feature. This value is normalized at 1 if it has been 100 samples or more since there was a change in activity (i.e., changing from active to inactive or vice versa). This feature can encode the periodicity of a signal by counting the number of times the sensor stays active or inactive.

The centroid and direction of motion are calculated as described in Chapter 9. The direction of motion is then broken up into 8 45-degree regions – up, upper left, left, lower left, down, lower right, right, and upper right. If the direction of motion falls within one of these regions, a corresponding binary value is 1. Thus if the centroid is moving from towards the right, the right direction binary value will be 1 and all other values will be 0.

Once the direction of motion is divided into the 8 regions the same feature detection done with sensor activity can be done with changes in direction. Thus there are features which are 1 if there is a change in motion. Another features counts how long it has been since a direction change.

The set of features described in this section can be applied at the various levels of the Huggable. For example, a feature can be used to see how long it has been since there was a change of direction in a specific board, or in the entire arm.

14.4 Neural Network

Once a set of features are created, as described in Chapter 14.3, pattern recognition algorithms can be used to classify these features into labeled categories. Neural Networks (NN) were selected because of their influence from the biological system.

The data presented in this section is from a single early attempt at classification. As such there are few important things to mention at the beginning. First, the sensor values have not been calibrated in hardware or software. Only the normalization method of Equation 14-1 was used. For sensors which have a very high baseline to begin with, there is not much range and thus they will show less resolution than a sensor with the full range. Second, the optimization of polling the QTC and temperature sensors while a different electric field sensing electrode is read was not implemented. Thus there is a 4 ms delay between the set of QTC and temperature sensors while the electric field sensor was read. Finally, the QTC sensors were processed in all three ways – light touch, moderate touch, and hard touch – one after another. This increased the timing between each sample.

14.4.1 Data Collection Methods

As an early exploration into the classification of the affective content of touch a set of 199 data sets were created. All of the data sets were taken using the Huggable arm section of Figure 13-19. Only the top and left region was activated and all interactions were located in that region of the arm section. Table 14-1 lists each data set as well as the labels used for classification.

Table 14-1: The Data Sets Used for the Classification of Affective Touch

Type	# of Data Sets	Class	Response
Tickle Softly, Fingers Only	10	Tickle	Tease Pleasant
Tickle Hard, Fingers Only	10	Tickle	Tease Painful
Poking Softly	20	Poking	Tease Pleasant
Poking Hard	20	Poking	Tease Painful
Scratching One Finger Softly	20	Scratching	Touch Pleasant
Scratching One Finger Hard	20	Scratching	Touch Painful
Slapping Fingers Only Softly	10	Slapping	Punishment Light
Slapping Fingers and Palm Softly	10	Slapping	Punishment Light
Slapping Fingers Only Hard	10	Slapping	Punishment Painful
Petting Softly	10	Petting	Touch Pleasant
Petting Hard	10	Petting	Touch Painful
Patting Softly	10	Patting	Touch Pleasant
Patting Hard	10	Patting	Touch Painful
Rubbing	10	Rubbing	Touch Pleasant
Squeezing	10	Squeeze	Touch Painful
Contact	10	Contact	Touch Pleasant

These data sets were organized into types, classes, and responses. The types were the kind of tactile interaction applied to the arm section, such as tickling softly. There were a total of 16 types. Each type was assigned to one of nine classes. These classes were the canonical type of interaction, such as tickling or petting. Finally, the types were assigned to six response groups. A response was the highest level of classification such as pleasant teasing or light punishment. These responses would be used by the behavior system to initiate a reaction or influence the behavior. The types were assigned to each response category based upon what the author believed would be the best classification.

14.4.2 Training of the Neural Network

All of the feature detection and neural network training and evaluation was done using MATLAB. The features were first extracted for each data set. A total of 421 features were extracted. The reason for such a large number of features was that features were calculated for each sensor circuit board, all the QTC light touch sensors, all the QTC moderate touch sensors, all the QTC hard touch sensors, all the temperature sensors, as well as the combinations of sensors on each board. In the future, other methods will be used to reduce the size of this feature set. The feature extractor also labeled the data with the appropriate type, class, and response for validation. In all cases, data was labeled “no contact” if none of the sensors in the top region were active.

The outputs of the feature extractor were then randomly assigned into training and validation sets. There were a total of 100 training data sets and 99 validation data sets. The missing data set was due to a corrupted file.

A three layer neural network was trained with 100 inner layer nodes. The number of output nodes was 16 for the type neural network classifier, 9 for the class neural network classifier, and 6 for the response neural network classifier. The “logsig” transfer function was used with the “trainrp” transfer function for all three neural networks. The learning rate was 0.001. The maximum number of epochs was 1000. The error tolerance was $1e-3$. Due to time constraints, only one neural network was trained for each of the type, class, and response classifiers.

14.4.3 Results

Tests of Neural Network Performance

The trained neural networks were then simulated using the validation data to observe the performance of the classifier. There were a high number of times in each data set when a “no contact” situation occurred. Thus, a simple measure of accuracy would not reveal much information as the true negatives would dominate the effect of the true positives. The equation for accuracy is shown below:

$$Accuracy = \frac{TruePositive + TrueNegative}{TruePositive + TrueNegative + FalsePositive + FalseNegative} \quad (14-2)$$

It is much better to use the specificity, the sensitivity, the positive predictive value, and the negative predictive value (rapid-diagnostics.org). The specificity is the probability that an interaction will be classified as not occurring when that interaction did not occur. The equation for specificity is shown below:

$$Specificity = \frac{TrueNegative}{TrueNegative + FalsePositive} \quad (14-3)$$

The sensitivity is the probability that an interaction will be classified as having occurred when it did occur. Equation 14-4 is the equation used to calculate sensitivity.

$$Sensitivity = \frac{TruePositive}{TruePositive + FalseNegative} \quad (14-4)$$

The positive predictive value (ppv) is the probability that the classified interaction did happen. The equation used to calculate the positive predictive value is shown below:

$$ppv = \frac{TruePositive}{TruePositive + FalsePositive} \quad (14-5)$$

The negative predictive value (npv) is the probability that an interaction did not occur when it is classified as not happening. The equation used is shown in Equation 14-6:

$$npv = \frac{TrueNegative}{TrueNegative + FalseNegative} \quad (14-6)$$

Performance of Neural Network Classifier: Type

The specificity and negative predictive values are shown in Figures 14-11 and 14-12. In both cases, the high probabilities are due to the fact that the majority of the time that type was not the form of interaction.

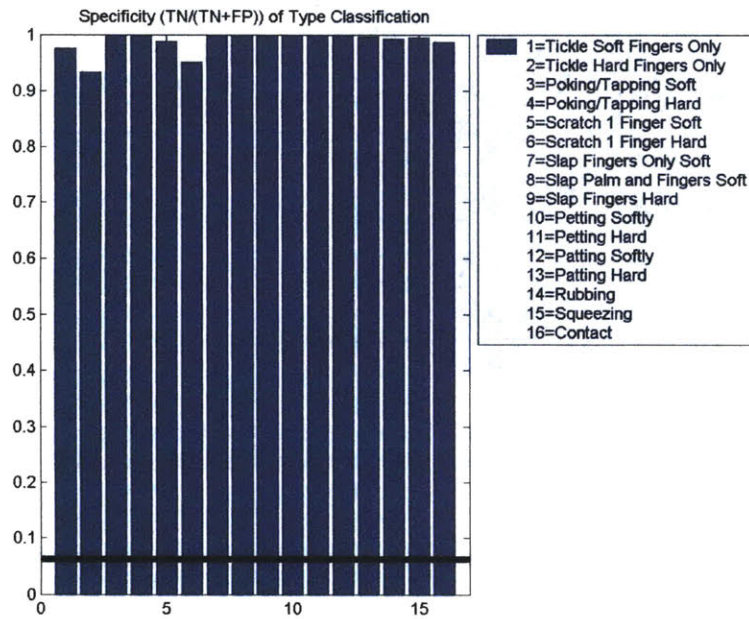


Figure 14-11: The Specificity of the Classification of Type. The black line at the bottom of the figure indicates chance - 1 out of 16.

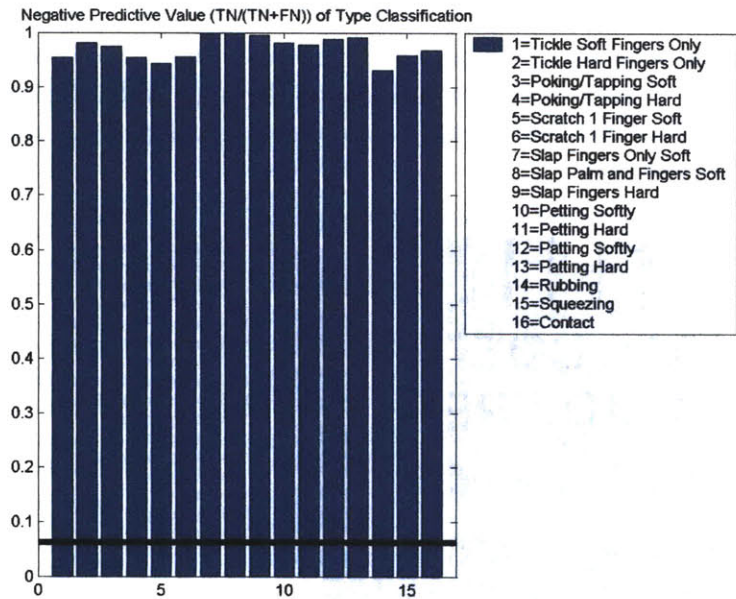


Figure 14-12: The Negative Predictive Value of Type Classification. The black line at the bottom indicates chance – 1 out of 16.

The sensitivity and positive predictive value are shown in Figures 14-13 and 14-14.

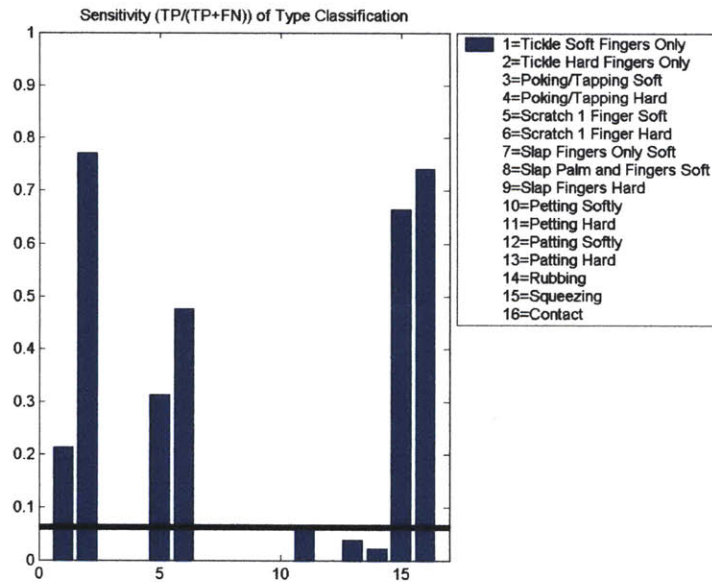


Figure 14-13: The Sensitivity of Type Classification. The black line at the bottom of the figure indicates chance.

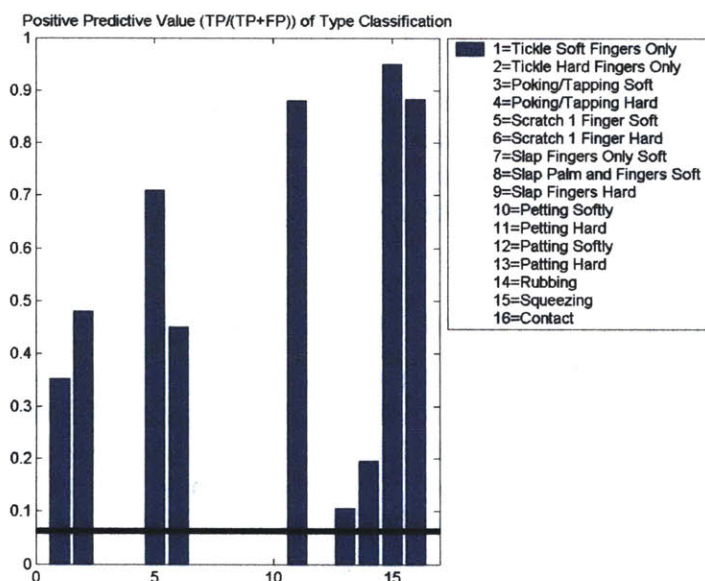


Figure 14-14: The Positive Predictive Value of Type Classification. The black line at the bottom of the figure indicates chance.

From Figures 14-3 and 14-4 it appears that the poking and slapping interactions were not classified well. This could be due to the fact that each interaction is very short compared to the other types. Another factor could be that a hard poke and a soft poke may look so similar to each other that they cancel each other out. One other explanation is that a poke may look similar to a slap due to the fact that the sensor circuit boards are so small that a quick indentation with a finger for a poke is very similar to the quick indentation with a knuckle during a slap. Further exploration into the results of the feature extractor may reveal that pokes and slaps are too similar to each other with the current feature set and new ones must be developed.

Another interesting result is shown in that interactions with more force (i.e., “Hard”) are classified better than the “Soft” version of the same interaction. This could be because each QTC sensor is processed for both light touch, moderate touch, and hard touch all within one data collection loop. Thus, there is more data available for the increased applied forces as they will be detected by the moderate and hard touch conditioning circuits. The applied forces were not controlled during the collection of data. Thus, it

may be the case that data sets classified as “Hard” may actually contain some “Soft” touch information, and vice versa.

Finally, the sensors were not calibrated to begin with, but instead normalized to an initial baseline. It may also be the case that the resolution of the sensors, due to the fact that they were not calibrated, may not be enough to distinguish between hard and soft contact.

Performance of Neural Network Classifier: Class

The specificity and negative predictive values are shown in Figures 14-15 and 14-16. As seen with the type classification, the high probabilities are due to the fact that the majority of the time that class was not the form of interaction. Thus, the true negative value was much greater than the false positive or false negative.

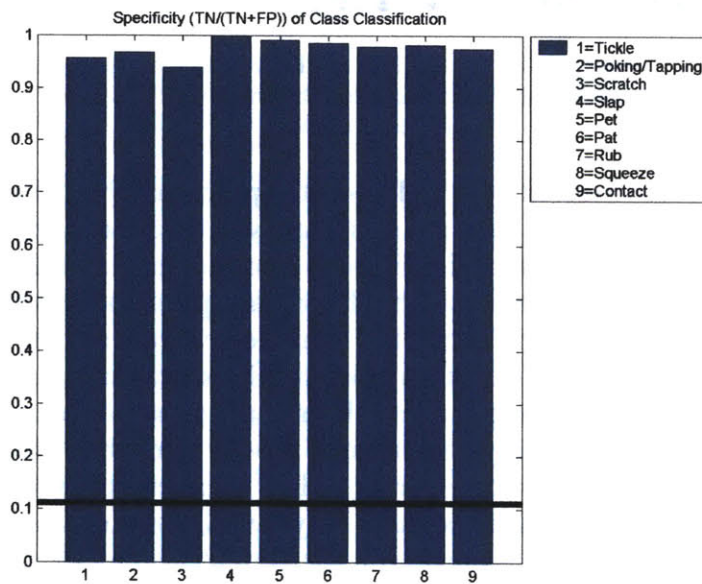


Figure 14-15: The Specificity of Class Classification. The black line at the bottom of the figure indicates chance – 1 out of 9.

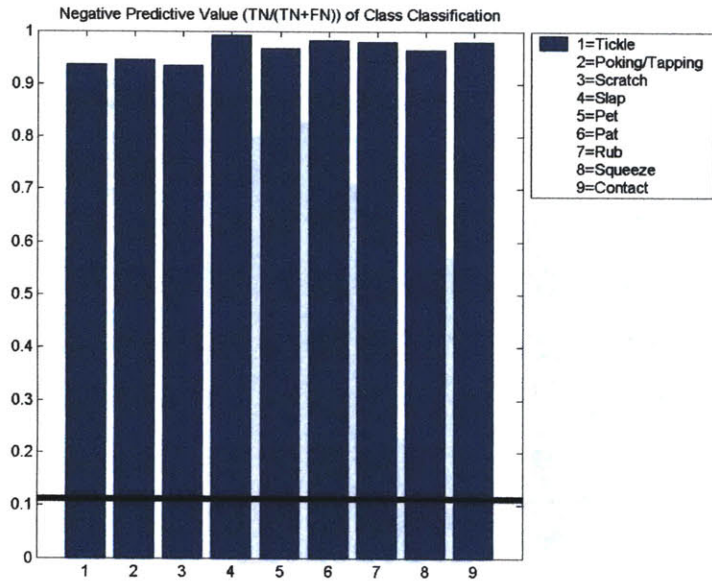


Figure 14-16: The Negative Predictive Value of Class Classification. The black line at the bottom of the figure indicates chance.

Figures 14-17 and 14-18 show the sensitivity and positive predictive value of the class classification.

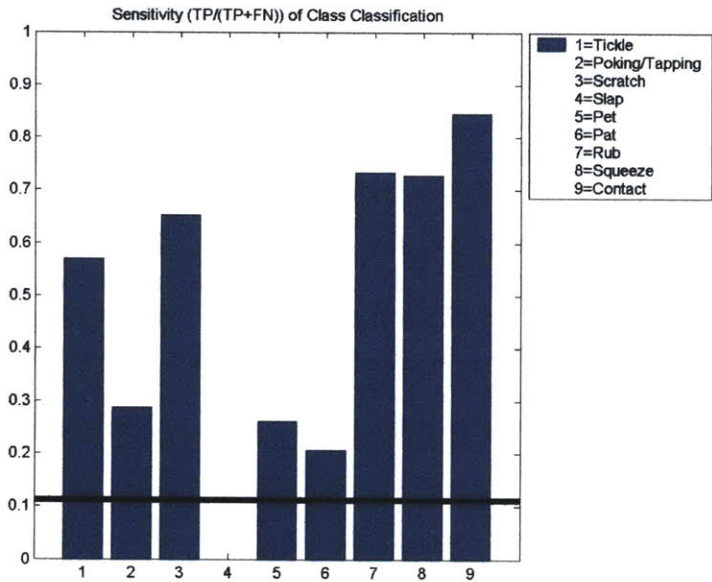


Figure 14-17: The Sensitivity of Class Classification. The black line at the bottom of the figure indicates chance.

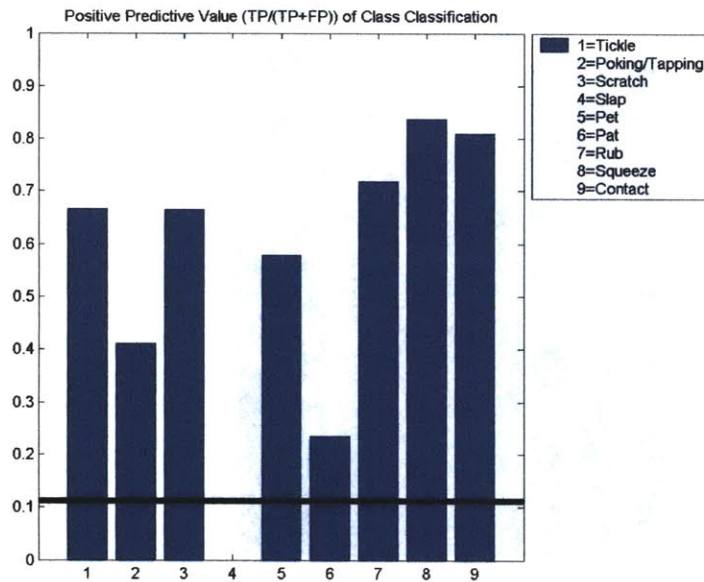


Figure 14-18: The Positive Predictive Value of Class Classification. The black line at the bottom of the figure indicates chance.

The performance for classification by class is much better in general than that of type. This could be due to the fact that similar types who may have been hard to distinguish from each other are now combined. The poking class when split into the poking hard and poking soft types was not classified well at all. However, the class performance is much better indicating that it was hard to distinguish between the hard and soft version of the same interaction.

The slap class appears to not be classified at all. Thus, there may be a problem with the design of the feature detector, or there may have been very few slap data sets in the training set. A slap happens very quickly compared to the other interactions such as scratching or rubbing. As such, the amount of slap data on which the neural network could be trained is much less than the other types of interactions.

Performance of Neural Network Classifier: Response

The specificity and negative predictive values for response are shown in Figures 14-19 and 14-20. As with the type and class cases, these values are high. The touch pleasant and touch painful values are lower than the specificity and negative predictive value of type and class. One explanation is that the grouping of data sets into these responses was subjective. It may be that some of the touch pleasant and touch painful data would be better classified as a different response.

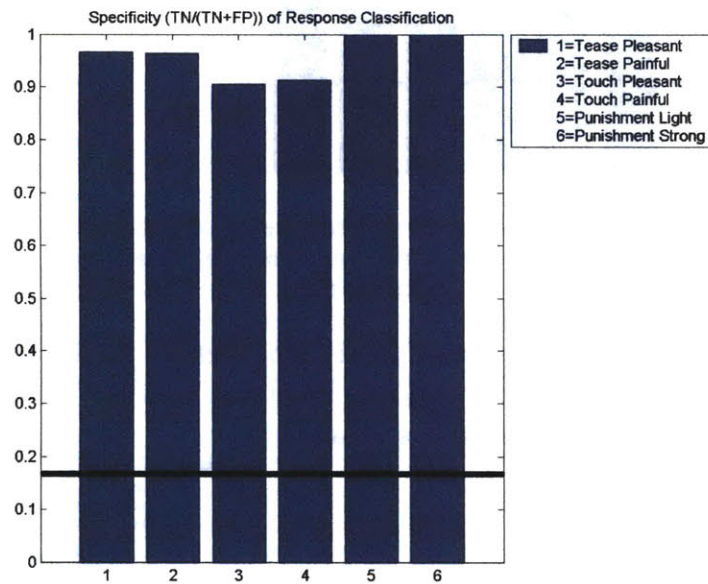


Figure 14-19: The Specificity of the Response Classification. The black line at the bottom of the figure indicates chance – 1 out of 6.

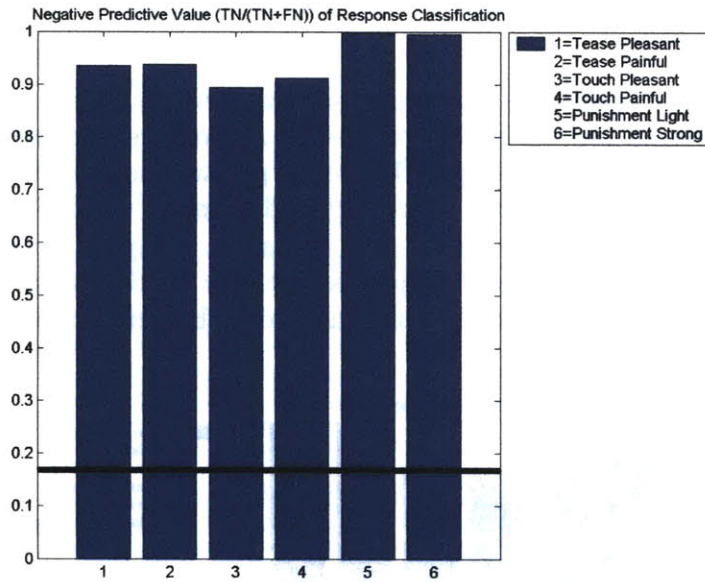


Figure 14-20: The Negative Predictive Value of Response Classification. The black line at the bottom of the figure indicates chance.

The sensitivity and positive predictive values for the response type are shown in Figures 14-21 and 14-22.

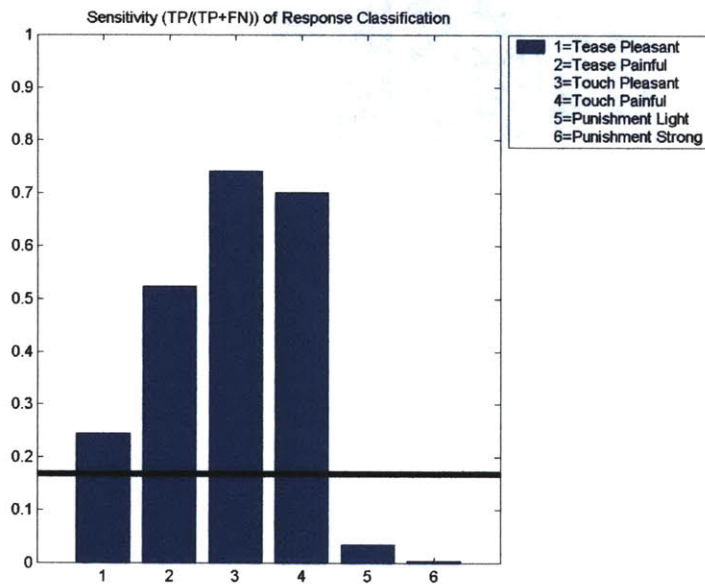


Figure 14-21: The Sensitivity of Response Classification. The black line at the bottom of the figure indicates chance.

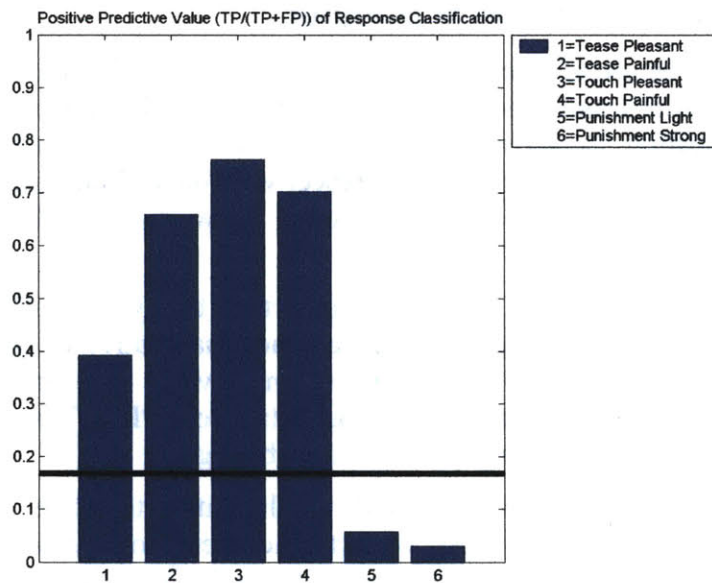


Figure 14-22: The Positive Predictive Value of Response Classification. The black line at the bottom of the figure indicates chance.

In general, the performance of the response classifier appears to be worse than the performance of the class classifier. The low sensitivity and positive predictive value are most likely due to the failure to correctly classify the slap data. As discussed previously, the grouping of types into responses was done subjectively. As such, there may be a better response grouping of types that would yield better results.

Another interesting pattern emerges from looking at the grouping of the types into responses shown in Table 14-1. The touch pleasant has five types. The touch painful has four types. The tease pleasant, tease painful, and punishment light each have two types. The punishment strong only has one type. There is a strong relationship between the order of positive predictive value and sensitivity to the number of types within one response. Thus it appears that the amount of data within the training set is having an effect on the classification result. In the future the responses should be better balanced in terms of quantity of data for each response in the training set.

14.4.4 Discussion of Results

The use of a neural network to classify the affective content of touch does show good results. In general, the class and response classification showed good results for a preliminary data set that was not calibrated. One would expect with better initial data, the performance of each of these neural networks would greatly improve.

In the future, it will be important to try to distinguish “Hard” and “Soft” touch from one another quantitatively. Another approach would be to threshold the sensor value sum or another feature and automatically place that data into a “Hard” or “Soft” grouping without relying upon human labeling.

It will be important to balance the data sets better. Slaps, which were active for only a short time, were dominated by the other data sets with longer activity and thus showed poor performance.

Finally, the response grouping should be done more quantitatively with attention paid to balancing the data sets. The touch pleasant response had more than twice the number of types than all the other responses except for touch painful.

Section IV: Conclusion

15 Conclusions and Future Work

15.1 Conclusions

In this thesis the “sensitive skin” design for two robotic platforms, Leonardo and the Huggable, was detailed. While this skin is not yet fully implemented, the initial framework for large sensor networks is in place – specifically with the levels of processing and design of the “Virtual Somatosensory Cortex.”

The multi-modal sensing approach of the Huggable was based upon the sense of touch in human and animals. The Huggable featured a soft silicone skin selected to minimize weight and hardness while maximizing the sensor performance. The design of the arm section described in this thesis resulted in a low wire count while still allowing the ability to process a high number of sensors. The neural networks described at the end of this thesis show promise for being able to pull out the affective content of touch from the sensor data.

15.2 Future Work: Leonardo

Leonardo will soon move into the realm of active touch – in which the tactile information from his hands will be combined with the kinesthetic information from his potentiometers and encoders at each degree of freedom. The sense of touch will not only prevent Leonardo from damaging his hands if he encounters an obstacle, but also be able to interact with objects through two handed manipulation or single handed pushing.

Vision can be combined with the tactile information from the hands to allow Leonardo to reach out and touch objects. Currently, with the additional degrees of freedom in the hand for independent finger control, Leonardo can point. The next steps will be to allow Leonardo to reach for an object and use the tactile information as feedback to allow him to know when he is touching that object.

The “skin” will soon be expanded to the rest of the body of Leonardo. New geometries of sensors will be created for the arms based upon the QTC material used in the Huggable. Additionally, the sensor circuit boards of the hands on the palm, side, and back

of hand will be remade with QTC replacing the FSRs to increase the sensor density and coverage.

The ability to shield the electric field sensors from one another shows promise that it might be possible to implement an electric field sensor for Leonardo's "skin" as well. One potential challenge is that Leonardo is made entirely of metal and could pose problems for the sensors.

15.3 Future Work: The Huggable

The next step will be to revise the design of the arm region to allow for easier assembly. The hand soldering of each connecting wire between each sensor circuit board as well as from the sensor circuit board to the mid-plane board is much too time intensive if multiple bears were to be created. Additionally, the cables used will be shielded in the next iteration to further prevent coupling between the electrode and the rest of the arm section.

The arms and legs are nearing the final stages of design and will be ready to begin fabrication by the middle of the summer. The legs will also feature additional potentiometers inside the ankles and hips. These sensors will also be processed by the somatic processing board for each leg. Such a posture sensor allows the Huggable to detect when someone is playing with the bear's legs or to detect if the bear is sitting or standing. These pieces of information will help to build even stronger classifiers.

The Stack inertial measurement unit (Morris 2004) will be placed inside the Huggable. This additional sensor will be used to detect the orientation of the bear in space. Thus the Huggable will be able to tell when it is being dangled by its arm as a child walks down the hall with it. The Huggable can know when it is sitting on someone's lap or being held like a baby. When this inertial sensor is combined with the other somatic sensors described in Section III of this thesis, relational touch emerges. The Huggable can combine the knowledge of its orientation with the sense of touch to determine where the person is in relation to itself. For example, when held in someone's arms like a baby, the Huggable can detect the presence of the other person through touch and nuzzle into their chest.

The current work in affective touch classification, described in Chapter 14, will be improved upon by implementing

the auto-calibration routine so that all sensors will be able to use the full voltage range. Additionally, the classification methods used will be designed so as to run in real time on the embedded PC of the Huggable. The ultimate goal of classification is that the Huggable will be able to understand the type of touch and respond in an appropriate manner that conveys meaning. For example, a painful slap should never result in a giggle.

The voice coil actuators, currently being designed by Jeff Lieberman and Mike Wolf, will be installed by early summer. The embedded PC and battery power also will be selected and installed into the bear. The Huggable somatic processing board will be redesigned to fit inside the bear.

As the Huggable moves towards a stand-alone, portable, robotic platform a series of developmental milestones must be completed. One milestone is the reduction of power consumption to allow the Huggable to run on a single battery for a long enough interaction time. Additionally, the Huggable should be designed with easily cleanable, removable skins for the hospital or nursing home environment. Finally, the interactions and behavior must be made very read-able to a wide variety of users.

The ultimate goal of the Huggable project is the deployment of these therapeutic robotic companions to a wide variety of people who have limited or no access to animals. Once the first full-bear prototype is created, it will be shown to area nursing homes and hospitals as part of a series of focus groups. These focus groups will serve a dual purpose. First they will allow those people who will use the Huggable to provide feedback about the design – specifically how it feels, what they wish it could do, etc. Second, these interactions during the focus groups will serve as valuable data gathering opportunities. The ways in which people will interact with the Huggable through touch are different from person to person. Some may simply want to hold it. Other's may very weakly pet it. While others, such as young children, may be a bit rougher with it. In all of these cases it is important that the Huggable be able to interpret this information.

The Huggable also can act as a member of a team that includes the patient or resident and the staff or care providers. The Huggable can be used for data collection and as a monitor of a person's daily activity. The Huggable can be used to call for help

if a person is in distress. A microphone inside the Huggable could relay such a distress signal to the staff over the hospital's network.

The Huggable can also be used as an avatar. In a modified version, sensing and actuation could be tied together with networking to allow a grandmother to play with her granddaughter through the bear. As one can see, The Huggable platform offers a lot of room for future applications.

References

- Allen, P. K. and P. Michelman (1990). "Acquisition and Interpretation of 3-D Sensor Data from Touch." IEEE Transactions on Robotics and Automation **6**(4): 397-404.
- ASTM (2000). "D 2240: Standard Test Method for Rubber Property - Durometer Hardness."
- Aylett, R. (2002). Robots: Bringing Intelligent Machines to Life? Hauppauge, NY, Barron's Educational Series, Inc.
- Ballarini, G. (2003). "Pet Therapy, Animals in Human Therapy." Acta Bio Medica **74**: 97-100.
- Breazeal, C., A. Brooks, et al. (2003). "Humanoid Robots as Cooperative Partners for People." Submitted for review to International Journal of Humanoid Robotics.
- Breazeal, C. L. (2002). Designing Sociable Robots. Cambridge, MA, MIT Press.
- Burman Industries (2000). Product Catalog.
- Cholewiak, R. W. and A. A. Collins (1991). Sensory and Physiological Bases of Touch. The Psychology of Touch. M. A. Heller and W. Schiff. Hillsdale, NJ, Lawrence Erlbaum Associates, Inc.: 23-60.
- Clark, F. J. and K. W. Horch (1986). Kinesthesia. 1986. K. R. Boff, L. Kaufman and J. P. Thomas. New York, Wiley & Sons. **1**: 1-62.
- Connor, C. E., S. S. Hsiao, et al. (1990). "Tactile Roughness: neural codes that account for psychophysical magnitude estimates." Journal of Neuroscience **10**: 3823-3836.
- Connor, C. E. and K. O. Johnson (1992). "Neural coding of tactile texture: comparisons of spatial and temporal mechanisms for roughness perception." Journal of Neuroscience **12**: 3414-3426.
- Craig, J. C. and G. B. Rollman (1999). "Somesthesia." Annual Review Psychology **50**: 305-31.
- Cusack, O. (1988). Pets and Mental Health. New York, Haworth Press.
- Custom Seal & Rubber Products website
<http://www.customsealandrubber.com/charts.html>.
- Dayan, P. and L. F. Abbott (2001). Theoretical Neuroscience: Computational and Mathematical Modeling of Neural Systems. Cambridge, Massachusetts, MIT Press.

- DeRossi, D., F. Carpi, et al. (2002). Electroactive Fabrics for Distributed, Conformable and Interactive Systems. Sensors 2002, Orlando, Florida, IEEE.
- Factor II Inc. Product Catalog (2002).
- Garrity, T. F. and L. Stallones (1998). Effects of Pet Contact on Human Well-Being: Review of Recent Research. Companion Animals in Human Health. C. C. Wilson and D. C. Turner. Thousand Oaks, SAGE Publications.
- Gray, H. (1977). Anatomy, Descriptive and Surgical. New York, Gramercy Books.
- Hakozaki, M., A. Hatori, et al. (2001). A Sensitive Skin Using Wireless Tactile Sensing Elements. 18th Sensor Symposium.
- Hara, F. and H. Kobayashi (1997). "State of the art in component technology for an animated face robot: its component technology development for interactive communication with humans." Advanced Robotics **11**(66): 585-604.
- Haughie, E. (1992). "An Evaluation of Companion Pets with Elderly Psychiatric Patients." Behavioural Psychotherapy **20**: 367-372.
- Heller, H. L. and R. E. McKinstry (1995). Facial Materials. Fundamentals of Facial Prosthetics. R. E. McKinstry. Arlington, VA, ABI Professional Publications: 79-97.
- Hollins, M., R. Faldowski, et al. (1993). "Perpetual dimensions of tactile surface texture: a multidimensional scaling analysis." Perception & Psychophysics **54**: 697-705.
- Howe, R. D. (1994). "Tactile sensing and control of robotic manipulation." Journal of Advanced Robotics **8**(3): 245-261.
- Hyvarinen, J. and A. Poranen (1978). "Movement-sensitive and direction and orientation-selective cutaneous receptive fields in the hand area of the postcentral gyrus in monkeys." Journal of Physiology (London) **283**: 523-537.
- Interlink Electronics product literature. FSR Integration Guide and Evaluation Parts Catalog: www.interlinkelec.com.
- Johnson, K. O. and S. S. Hsiao (1992). "Neural Mechanisms of Tactual Form and Texture Perception." Annual Review of Neuroscience **15**: 227-50.
- Johnson, K. O. and S. S. Hsiao (1994). "Evaluation of the relative roles of slowly and rapidly adapting afferent fibers in

- roughness perception." Canadian Journal of Physiology and Pharmacology **72**: 488-497.
- Johnson, K. O. and G. D. Lamb (1981). "Neural Mechanisms of spatial tactile discrimination: Neural patterns evoked by Braille-like dot patterns in the monkey." Journal of Physiology (London) **310**: 117-44.
- Johnson, K. O., J. R. Phillips, et al. (1991). Tactile pattern recognition. Information Processing in the Somatosensory System. O. Franzen and J. Westman. London, Macmillan: 308-18.
- Kanda, T., H. Ishiguro, et al. (2002). Development and Evaluation of an Interactive Humanoid Robot "Robovie". International Conference on Robotics & Automation, Washington, D.C.
- Kandel, E. R., J. H. Schwartz, et al. (2000). Principles of Neuroscience, 4th Edition. New York, McGraw-Hill Health Professions Division.
- Karason, S. P., M. A. Srinivasan, et al. (1999). "Encoding and Decoding of Static Information in Tactile Sensing Systems." International Journal of Robotics Research **18**(2): 131-151.
- Kongable, L. G., J. M. Stolley, et al. (1990). "Pet Therapy for Alzheimer's Patients: A Survey." The Journal of Long Term Care Administration **18**(3): 17-21.
- Lamb, G. D. (1983). "Tactile discrimination of textured surfaces: peripheral neural coding in the monkey." Journal of Physiology (London) **338**: 567-587.
- LaMotte, R. H. and M. A. Srinivasan (1987). "Tactile Discrimination of Shape: Responses of Rapidly Adapting Mechanoreceptive Afferents to a Step Stroked Across the Monkey Fingerpad." The Journal of Neuroscience **7**(6): 1672-1681.
- LaMotte, R. H. and M. A. Srinivasan (1987). "Tactile Discrimination of Shape: Responses of Slowly Adapting Mechanoreceptive Afferents to a Step Stroked Across the Monkey Fingerpad." The Journal of Neuroscience **7**(6): 1655-1671.
- LaMotte, R. H. and M. A. Srinivasan (1993). "Responses of cutaneous mechanoreceptors to the shape of objects applied to the primate fingerpad." Acta Psychologica **84**: 41-51.
- Lederman, S. J. (1974). "Tactile roughness of grooved surfaces: The touching process and effects of macro- and

- microsurface structure." Perception & Psychophysics **16(2)**: 385-395.
- Libin, A. V. and E. Libin (2004). "Person-Robot Interactions From the Robopsychologists' Point of View: The Robotic Psychology and Rotherapy Approach." Proceedings of the IEEE **92(11)**: 1-15.
- Lifton, J., M. Broxton, et al. (2003). Distributed Sensor Networks as Sensate Skin. IEEE Sensors 2003.
- Lumelsky, V. J., M. S. Shur, et al. (2001). "Sensitive Skin." IEEE Sensors Journal **1(1)**: 41-51.
- Martin, T. B., R. O. Ambrose, et al. (2004). Tactile Gloves for Autonomous Grasping with the NASA/DARPA Robonaut. International Conference on Robotics and Automation (ICRA'04), New Orleans, LA.
- McBean, J. (2004). Design and Control of a Voice Coil Actuated Arm for Human-Robot Interaction. Masters of Science Thesis: Department of Mechanical Engineering, MIT.
- McKinstry, R. E. (1995). Fundamentals of Facial Prosthetics. Arlington, VA, ABI Professional Publications.
- McLaughlin, T. (1999). Silicone Art: Materials, Methods & Techniques for Coloring, Painting, and Finishing Silicone Rubber Version 1.1. Sherman Oaks, California, McLaughlin Productions Publishing.
- Menzel, P. and F. D'Aluisio (2000). Robo-Sapians: Evolution of a New Species. Cambridge, MA, MIT Press.
- Montagu, A. (1986). Touching. The Human Significance of the Skin, 3rd Edition. New York, Harper & Row.
- Morris, S. J. (2004). A Shoe-Integrated Sensor System for Wireless Gait Analysis and Real-Time Therapeutic Feedback. Health Sciences and Technology Sc.D. Thesis. Cambridge, MIT.
- Motorola/Freescale Semiconductor. 33794 Electric Field Imaging Device Product Literature.
- Muschel, I. J. (1984). "Pet Therapy with Terminal Cancer Patients." The Journal of Contemporary Social Work. **65(8)**: 451-458.
- Nolte, J. (2002). The Human Brain: An Introduction to Its Functional Anatomy 5th Edition. St. Louis, Missouri, Mosby Inc.

- Odendaal, J. S. J. (2000). "Animal-Assisted Therapy - Magic or Medicine." Journal of Psychosomatic Research **49**: 275-280.
- Omron Corporation Product Literature NeCoRo website:
<http://www.necoro.com>.
- Paradiso, J. A. and N. Gershenfeld (1997). "Musical Applications of Electric Field Sensing." Computer Music Journal **21**(2): 69-89.
- Paradiso, J. A., J. Lifton, et al. (2004). "Sensate Media - Multimodal Electronic Skins as Dense Sensor Networks." BT Technology Journal **22**(4).
- Paro Product Literature <http://paro.jp/english/index.html>.
- Penfield, W. and T. Rasmussen (1950/1978). The Cerebral Cortex of Man, Macmillan Publishing Co., Inc.
- Peratech Product Literature <http://peratech.co.uk/>.
- Peratech. (2004). The Science of QTC:
<http://www.peratech.co.uk/science.htm>.
- Pohja, S. (1996). Survey of Studies on Tactile Sensing: R96:02. Kista, Sweden, RWCP Neuro SICS Laboratory: 1-13.
- rapid-diagnostics.org Accuracy of Diagnostics Tests:
<http://www.rapid-diagnostics.org/accuracy.htm>.
- Ritter, H., R. Haschke, et al. (2005). A layered control architecture for imitation grasping with a 20-DOF pneumatic anthropomorphic hand. Robotics 2005, Massachusetts Institute of Technology, Cambridge, Massachusetts USA.
- Rollman, G. B. (1991). Pain Responsiveness. The Psychology of Touch. M. A. Heller and W. Schiff. Hillsdale, NJ, Lawrence Erlbaum Associates, Inc.: 91-114.
- Rosenzweig, M. R., S. M. Breedlove, et al. (2002). Biological Psychology, 3rd Edition. Sunderland, Massachusetts, Sinauer Associates.
- Rosheim, M. E. (1994). Robot Evolution: The Development of Anthrorobotics, John Wiley & Sons Inc.
- Sega Toys Product Literature <http://www.segatoys.co.jp/nearme/>.
- Sega Toys Product Literature NearMe website:
<http://www.segatoys.co.jp/nearme/>.
- Sekuler, R. and R. Blake (2002). Perception, 4th Edition. New York, McGraw-Hill.
- Sergio, M., N. Manaresi, et al. (2002). A Textile Based Capacitive Pressure Sensor. Sensors 2002, Orlando, Florida, IEEE.

- Shadow Robot Company. Shadow Robot Hand Product website:
<http://www.shadow.org.uk/products/newhand.shtml>.
- Sherrick, C. and R. W. Cholewiak (1986). Cutaneous Sensitivity. Handbook of Perception and Human Performance. K. R. Boff, L. Kaufman and J. P. Thomas, Wiley-Interscience. **1**: 12-1 - 12-58.
- Shibata, T., T. Mitsui, et al. (2001). Mental Commit Robot and its Application to Therapy of Children. International Conference on Advanced Intelligent Mechatronics, Como, Italy.
- Shibata, T. and K. Tanie (2001). Physical and Affective Interaction between Human and Mental Commit Robot. International Conference on Robotics and Automation (ICRA), South Korea.
- Shibata, T., K. Wada, et al. (2003). Subjective Evaluation of a Seal Robot at the National Museum of Science and Technology in Stockholm. IEEE International Workshop on Robot and Human Interactive Communication, Millbrae, CA, USA.
- Shigematsu, S., H. Morimura, et al. (1999). "A Single-Chip Fingerprint Sensor and Identifier." IEEE Journal of Solid-State Circuits **34**(12): 1852-1859.
- Silicones Inc. Product Literature.
- Smith, J. R. (1999). Electric Field Imaging. MIT Media Lab Ph. D Thesis. Cambridge, MIT Media Lab.
- Smith, J. R., T. White, et al. (1998). "Electric Field Sensing for Graphical Interfaces." IEEE Computer Graphics and Applications **18**(3): 54-60.
- Sony Product Literature "AIBO ERS-7M2 website:
http://www.sonystyle.com/is-bin/INTERSHOP.enfinity/eCS/Store/en/-/USD/LC_BrowseCatalog-Start;sid=5PwkGv1dhiQk1b8nCd8uEbJRgVs-2uQV4R0=?CategoryName=lc_AIBO."
- Srinivasan, M. A. and R. H. LaMotte (1987). "Tactile Discrimination of Shape: Responses of Slowly and Rapidly Adapting Mechanoreceptive Afferents to a Step Indented into the Monkey Fingerpad." The Journal of Neuroscience **7**(6): 1682-1697.
- Srinivasan, M. A. and R. H. LaMotte (1995). "Tactual discrimination of softness." Journal of Neurophysiology **73**: 88-101.

- Stevens, J. C. (1991). Thermal Sensibility. The Psychology of Touch. M. A. Heller and W. Schiff. Hillsdale, NJ, Lawrence Erlbaum Associates, Inc.: 61-90.
- Stiehl, W. D. (2003). Tactile Perception in Robots: From the Somatic Alphabet to the Realization of a Fully "Sensitive Skin". MIT Mechanical Engineering Bachelor's Thesis. Cambridge, MIT: 174.
- Stiehl, W. D. and C. Breazeal (2004). Applying a "Somatic Alphabet" Approach to Inferring Orientation, Motion, and Direction in Clusters of Force Sensing Resistors. IROS.
- Stiehl, W. D., L. Lalla, et al. (2004). A "Somatic Alphabet" Approach to "Sensitive Skin". International Conference on Robotics and Automation, New Orleans, Louisiana, IEEE.
- Tamura, T., S. Yonemitsu, et al. (2004). "Is an Entertainment Robot Useful in the Care of Elderly People with Severe Dementia?" The Journals of Gerontology **59A**(1): 83-85.
- Thermometrics Product Literature. NTC Thermistors:
<http://www.thermometrics.com/assets/images/ntcnotes.pdf>.
- Thomas, K. F. (1994). Prosthetic Rehabilitation. Quintessence Publishing Co., Ltd., London.
- Thomas, W. H. (1996). Life Worth Living: How Someone You Love Can Still Enjoy Life in a Nursing Home. Acton, Massachusetts, VanderWyk & Burham.
- Vega-Bermudez, F., K. O. Johnson, et al. (1991). "Human tactile pattern recognition: Active versus passive touch, velocity effects and patterns of confusion." Journal of Neurophysiology **65**: 531-46.
- Wada, K., T. Shibata, et al. (2002). Effects of Robot Assisted Activity for Elderly People at Day Service Center and Analysis of Its Factors. 4th World Congress on Intelligent Control and Automation, Shanghai, P.R. China.
- Xu, Y., Y.-C. Tai, et al. (2002). IC-Integrated Flexible Shear-Stress Sensor Skin. Solid-State Sensor, Actuator and Microsystems Workshop, Hilton Head Island, South Carolina.
- Yamada, K., K. Goto, et al. (2002). A Sensor Skin Using Wire-Free Tactile Sensing Elements Based on Optical Connection. SICE 2002, Osaka.
- Yamada, Y., T. Maeno, et al. (2002). Identification of Incipient Slip Phenomena Based on the Circuit Output Signals of

PVDF Film Strips Embedded in Artificial Finger Ridges.

SICE 2002, Osaka.

Z Corporation Press Release. (2005). First High-Definition, Color
3D Printer a Breakthrough in Prototype Model Quality.